UNIVERSITAT POLITÈCNICA
DE CATALUNYA

Ph.D. Dissertation

Coherent and Non-Coherent Ultra-Wideband Communications

Author: José A. López-Salcedo

Advisor: Prof. Gregori Vázquez Grau

Department of Signal Theory and Communications
Universitat Politècnica de Catalunya

Barcelona, March 28th, 2007

Abstract

Short-range wireless communication has become an essential part of everyday life thanks to the enormous growth in the deployment of wireless local and personal area networks. However, traditional wireless technology cannot meet the requirements of upcoming wireless services that demand high-data rates to operate. This issue has motivated an unprecedented resurgence of ultra-wideband (UWB) technology, a transmission technique that is based on the emission of sub-nanosecond pulses with a very low transmitted power. Because of the particular characteristics of UWB signals, very high data rates can be provided with multipath immunity and high penetration capabilities.

Nevertheless, formidable challenges must be faced in order to fulfill the expectations of UWB technology. One of the most important challenges is to cope with the overwhelming distortion introduced by the intricate propagation physics of UWB signals. In addition to this, UWB antennas behave like direction-sensitive filters such that the signal driving the transmit antenna, the electric far field, and the signal across the receiver load, they all may differ considerably in wave shape. As a result, the well-known and popular concept of matched filter correlation cannot be implemented unless high computational complexity is available for perfect waveform estimation.

The lack of knowledge about the received waveform leads UWB receivers to be implemented under a *coherent* or *non-coherent* approach depending on a tradeoff between waveform estimation complexity and system performance. On the one hand, coherent receivers provide the reference benchmark in the sense that they have ideally perfect knowledge of the end-to-end channel response and thus, optimal performance is achieved. On the other hand, non-coherent receivers appear as a low-cost and low-power consumption alternative since channel estimation is not considered and thus, suboptimal performance is expected.

In the present dissertation, both coherent and non-coherent receivers for UWB communications are analyzed from a twofold perspective. In the first part of the thesis, an information theoretic approach is adopted to understand the implications of coherent and non-coherent reception. This is done by analyzing the achievable data rates for which reliable communication is possible in the presence and in the absence of channel state information. The simulation results

show a different behavior when evaluating spectral efficiency of coherent and non-coherent receivers under the wideband regime. For this reason, and in order to shed some light on this issue, closed-form expressions are derived to allow an analytical study of the asymptotic behavior of constellation-constrained capacity.

In the second part of the thesis, the emphasis is placed on the design of signal processing techniques for carrying out the basic tasks of an UWB receiver. For the case of coherent receivers, a maximum likelihood waveform estimation technique is proposed based on the exploitation of second-order statistics. One of the key features of the proposed technique is that it establishes a clear link between maximum likelihood waveform estimation and correlation matching techniques. Moreover, the proposed method can be understood as a principal component analysis that compresses the likelihood function with information regarding the signal subspace of the received signal. As a result, significant reduction in the computational burden is obtained through a tradeoff between bias and variance.

For the case of non-coherent receivers, the problems of symbol detection and signal synchronization are addressed from a waveform-independent perspective. The framework of waveform-independent symbol detection is derived for the case of correlated and uncorrelated scenarios, and low-complexity implementations are proposed based on the maximization of the Jeffreys divergence measure. As for the synchronization problem, a nondata-aided and waveform-independent technique is proposed for the frame-timing acquisition of the received signal. Next, a low-complexity implementation is proposed based on the multifamily likelihood ratio testing by understanding the frame-timing acquisition of UWB signals as a problem of model order detection.

Resumen

Las comunicaciones inalámbricas de corto alcance se han convertido en una parte imprescindible de la vida diaria gracias a la extraordinaria expansión de las redes inalámbricas de área local y personal. Sin embargo, la tecnología inalámbrica actual no es capaz de satisfacer los requisitos de alta velocidad que demandan los servicios de nueva generación. Este problema ha motivado la reaparición de la tecnología de banda ultra-ancha o *ultra-wideband* (UWB), una tecnología basada en la emisión de pulsos de baja potencia cuya duración temporal es inferior al nanosegundo. Debido a las particulares características de las señales UWB, es posible conseguir velocidades de transmisión muy elevadas con inmunidad al efecto multicamino y alta penetrabilidad en materiales.

A pesar de ello, existen formidables desafíos que han de afrontarse si se pretende cumplir con las expectativas que la tecnología UWB ha generado. En concreto, uno de los desafíos más importantes es el relacionado con la severa distorsión que introduce la propagación de señales de banda ultra-ancha. En este sentido, se ha comprobado que la señal que alimenta la antena de UWB, la señal del campo eléctrico lejano y la señal recibida en la carga de la antena receptora, todas ellas suelen diferir de manera considerable en su forma de onda. Como consecuencia, el tradicional concepto de filtrado adaptado se hace inviable a no ser que se disponga de una gran capacidad de cálculo y complejidad hardware para llevar a cabo una estimación precisa de la forma de onda recibida.

El desconocimiento de la forma de onda recibida conduce a la implementación de receptores de UWB bajo una perspectiva coherente o no-coherente, dependiendo de un compromiso entre complejidad hardware y prestaciones del sistema. Por un lado, los receptores coherentes implementan estimación de forma de onda y por lo tanto proporcionan las mejores prestaciones al asumir un conocimiento preciso de las condiciones de propagación. Por otro lado, los receptores no-coherentes aparecen como una alternativa sub-óptima de bajo coste y bajo consumo al no implementar estimación de canal.

En la presente tesis, los receptores coherentes y no-coherentes para señales de UWB son analizados desde una doble perspectiva. En la primera parte de la tesis se adopta un planteamiento de teoría de la información con el objetivo de comprender las implicaciones de la detección coher-

ente y no-coherente. Ello se consigue mediante el análisis de los límites teóricos para los cuales es posible una comunicación fiable sin errores en presencia y en ausencia de información acerca del estado del canal. Los resultados de simulación muestran un comportamiento diferente entre los receptores coherentes y no-coherentes cuando ambos son evaluados en términos de su eficiencia espectral bajo el régimen de banda ancha. Por esta razón, y con el objetivo con profundizar en este problema, se proponen expresiones cerradas para el análisis teórico del comportamiento asintótico de la capacidad de canal sujeta a una constelación discreta de entrada.

En la segunda parte de la tesis, el énfasis se centra en el diseño de técnicas de procesado de señal para llevar a cabo las tareas básicas de un receptor de UWB. Para el caso de receptores coherentes, se propone una técnica de estimación de forma de onda basada en estadísticos de segundo orden. Una de las características principales de la técnica propuesta es que establece una relación clara entre el criterio de máxima verosimilitud y las técnicas de *correlation matching*. Además de ello, el método propuesto puede ser entendido como una técnica de análisis de componentes principales (PCA) que comprime la función de máxima verosimilitud con la información disponible acerca del subespacio de señal. Como resultado, se obtiene una significativa reducción de complejidad mediante un compromiso entre sesgo y varianza.

Para el caso de receptores no-coherentes, se plantean los problemas de detección no-coherente y sincronización no asistida. Por lo que respecta al problema de detección, se ha desarrollado un marco teórico para implementar de manera óptima la decisión de símbolo en escenarios con *scattering* correlado o incorrelado. Se propone una implementación de baja complejidad basada en la maximización de la divergencia de Jeffreys. Por lo que respecta al problema de sincronización, se propone una técnica de adquisición de timing de trama no asistida por datos e independiente de la forma de onda recibida. En este caso se propone también una implementación de baja complejidad basada en el criterio de *multifamily likelihood ratio testing* mediante la interpretación de la adquisición de timing como un problema de detección de orden del modelo.

Agradecimientos

Estas primeras líneas ponen punto y final a mis años de doctorado, un antes y un después en una de las etapas de mi vida que sin duda recordaré con más cariño. Una vez llegados al final, es de justicia volver la vista atrás para mostrar mi más sincero agradecimiento y admiración a todos aquellos que han hecho posible que recorriera este largo pero apasionante camino.

Mi primer agradecimiento no puede ser para otra persona más que para Gregori, copartícipe de esta tesis y persona excepcional allá donde las haya. Una persona de la que sigo aprendiendo cada día y de la que agradezco el apoyo y confianza que ha tenido en mí tanto a nivel personal como a nivel profesional. Mi agradecimiento también para Jaume por su inestimable ayuda y su particular sentido de la intuición. Una gran persona en el sentido más literal de la palabra. De manera similar, no puedo olvidar tampoco el tiempo que estuve trabajando con Xell al comienzo de mi etapa de doctorado. De ella guardo un recuerdo muy especial y a ella le debo todo lo que aprendí sobre codificación. Francesc Rey y Xavi Villares también merecen una mención especial. Ellos han sido de alguna manera mis hermanos mayores durante todo este tiempo y en ellos siempre he encontrado consejos y ánimos en los momentos difíciles.

Cómo no, quisiera también mostrar mi agradecimiento a los becarios de doctorado con los que he tenido el placer de compartir esta experiencia. A los que todavía están ahí y a los que ya se han ido. A todos ellos mi agradecimiento por todo lo que hemos compartido juntos. Nombrarlos a todos sería excesivo, pero ellos saben quiénes son y por qué los admiro.

Finalmente, agradecer también el apoyo que me han brindado siempre mi familia y Ester. Después de mi dedicación a la carrera, quiero expresar mi gratitud por su compresión y paciencia a lo largo de este nuevo ciclo de otros cinco años de doctorado que ahora termina. Espero poderles devolver pronto el tiempo que no les he podido dedicar durante estos casi diez años de estudios.

José A. López-Salcedo
7 de febrero de 2007

Este trabajo ha sido parcialmente financiado por el Ministerio de Educación y Ciencia a través del programa de Formación de Personal Investigador (F.P.I.) mediante la beca FP-2001-2639.

Contents

List of Figures

List of Tables

Notation

In the sequel, matrices are indicated by uppercase boldface letters, vectors are indicated by lowercase boldface letters, and scalars are indicated by italics letters. Other specific notation has been introduced as follows:

$\lvert a \rvert$	Absolute value of a.
$\approx$	Approximately equal to.
$\mathbf{A}^*$, $\mathbf{A}^T$, $\mathbf{A}^H$	Complex conjugate, transpose, and conjugate transpose (Hermitian) of matrix $\mathbf{A}$, respectively.
δ_{ij}	Kronecker delta. That is, $\delta_{ij} = \begin{cases} 1, & i = j \\ 0, & \text{otherwise.} \end{cases}$
$f'(x_0)$	Derivative of function $f(x)$ evaluated at $x = x_0$.
$L'(\mathbf{r})$	Simplified version of the log-likelihood $L(\mathbf{r})$ where all irrelevant constant terms have been removed.
$\doteq$	Defined as.
$\det(\mathbf{A})$	Determinant of matrix $\mathbf{A}$.
$\text{diag}(\mathbf{x})$	Returns a diagonal matrix formed from the elements of vector $\mathbf{x}$.
$\text{diag}(\mathbf{X})$	Returns a vector formed from the elements in the main diagonal of matrix $\mathbf{X}$.
$[\mathbf{A}]_{i,j}$	The (i, j) entry of matrix $\mathbf{A}$.
$=$	Equal to.
$\neq$	Not equal to.
$\propto$	Equal up to a constant factor.
$\widehat{\mathbf{a}}$	Estimate of vector $\mathbf{a}$.

$\mathrm{E}[\cdot]$	Statistical expectation. A subscript may be used to indicate the random variable considered in the expectation.
$\exp(x)$	Exponential function. That is, e^x.
$\nabla_{\mathbf{a}} f(\mathbf{a})$	The gradient of function $f(\mathbf{a})$ with respect to vector $\mathbf{a}$.
$\nabla^2_{\mathbf{a}} f(\mathbf{a})$	The Hessian of function $f(\mathbf{a})$ with respect to vector $\mathbf{a}$.
$\Leftrightarrow$	If and only if.
$\max\{a, b\}$	The largest of a and b.
$\min\{a, b\}$	The smallest of a and b.
$\log(\cdot)$	Natural logarithm.
$\log_2(\cdot)$	Logarithm in base 2.
$\|\mathbf{a}\|$	Euclidean norm of vector $\mathbf{a}$. That is, $\|\mathbf{a}\| = \sqrt{\mathbf{a}^H \mathbf{a}}$.
$\|\mathbf{A}\|_F$	Frobenius norm of the $m \times n$ matrix $\mathbf{A}$. That is, $\|\mathbf{A}\|_F = \sqrt{\sum_{i=1}^{m} \sum_{j=1}^{n} [\mathbf{A}]_{i,j}}$.
$\mathcal{N}(\mathbf{m}, \mathbf{C})$	Multivariate Normal (i.e. Gaussian) distribution with mean $\mathbf{m}$ and covariance matrix $\mathbf{C}$.
$\mathbf{A} \bullet \mathbf{B}$	Inner product of matrices. That is, $\mathbf{A} \bullet \mathbf{B} = Tr\left(\mathbf{A}^T \mathbf{B}\right)$
$\mathbf{A} \otimes \mathbf{B}$	Kronecker product of matrices. That is, $$\mathbf{A} \otimes \mathbf{B} = \begin{bmatrix} [\mathbf{A}]_{1,1}\mathbf{B} & \cdots & [\mathbf{A}]_{1,n}\mathbf{B} \\ \vdots & & \vdots \\ [\mathbf{A}]_{m,1}\mathbf{B} & \cdots & [\mathbf{A}]_{m,n}\mathbf{B} \end{bmatrix} \quad (1)$$ where $\mathbf{A}$ is a $m \times n$ matrix.
$\mathbf{A} \odot \mathbf{B}$	Schur-Hadamard (i.e. element-wise) product of matrices. That is, $[\mathbf{A} \odot \mathbf{B}]_{i,j} = [\mathbf{A}]_{i,j} [\mathbf{B}]_{i,j}$.
$a < b$	a smaller than b.
$a > b$	a greater than b.
$a \ll b$	a much smaller than b.
$a \gg b$	a much greater than b.
$a \leq b$	a smaller or equal to b.

$a \geq b$	a greater or equal to b.
$\mathbb{R}^{m\times n}, \mathbb{C}^{m\times n}$	The set of $m \times n$ matrices with real and complex valued entries, respectively
$\mathrm{Re}\left[\cdot\right], \mathrm{Im}\left[\cdot\right]$	Real and imaginary parts, respectively.
$Tr\left(A\right)$	Trace of matrix $\mathbf{A}$.
$\breve{\mathbf{A}}$	Truncated matrix obtained by removing some of the first rows and some of the last rows of matrix $\mathbf{A}$.
$\mathrm{vec}\left(\mathbf{A}\right)$	Vec operator or column-wise stacking of matrix $\mathbf{A}$.
$\mathrm{vech}\left(\mathbf{A}\right)$	Vech operator or column-wise stacking of matrix $\mathbf{A}$ by removing the terms above the main diagonal of $\mathbf{A}$.

Acronyms

ADC	Analog-to-Digital Converter
APPM	Amplitude Pulse Position Modulation
ASK	Amplitude Shift Keying
AWGN	Additive White Gaussian Noise
BAN	Body Area Network
BER	Bit Error Rate
BPSK	Binary Phase Shift Keying
CDMA	Code Division Multiple Access
CDF	Cumulative Density Function
CEPT	European Conference of Postal and Telecommunications Administrations
CM	Correlation Matching
CMA	Constant Modulus Algorithm
CS	Correlated Scattering
DA	Data-aided
DARPA	Defense Advanced Research Projects Agency
DPPM	Differential PPM
DSL	Digital Subscriber Line
DT	Dirty Template
$\mathbf{E_b/N_0}$	Energy-per-bit to noise spectral density
$\mathbf{E_f/N_0}$	Energy-per-frame to noise spectral density
ECC	Electronics Communication Committe
ED	Energy Detector
ETSI	European Telecommunications Standards Institute

EU	European Union
FCC	Federal Communications Commission
GLRT	Generalized Likelihood Ratio Test
GPS	Global Positioning System
GTD	General Theory of Diffraction
IEEE	Institute of Electrical and Electronics Engineers
LAN	Local Area Network
LNA	Low Noise Amplifier
LOS	Line-Of-Sight
LPF	Low-Pass Filter
MB-OFDM	Multiband OFDM
MF	Matched Filter
ML	Maximum Likelihood
MLRP	Maximum Likelihood Receiver with Partial channel knowledge
MLRT	Multifamily Likelihood Ratio Test
MPPM	Multipulse PPM
NDA	Nondata-aided
NLOS	Non-Line-Of-Sight
NMSE	Normalized Mean Square Error
OFDM	Orthogonal Frequency Division Multiplex
OOK	On-Off Keying
OPPM	Overlapping PPM
PAM	Pulse Amplitude Modulation
PCA	Principal Component Analysis
PCB	Printed Circuit Board
PDP	Power Delay Profile
PPM	Pulse Position Modulation
PSK	Phase Shift Keying
QAM	Quadrature Amplitude Modulation
QPSK	Quadrature Phase Shift Keying

RQI	Rayleigh Quotient Iteration
Rx	Receiver
SCPC	Single Channel Per Carrier
SNR	Signal-to-Noise-Ratio
SOCC	Synchronous Overlapped Cross-Correlation
SS	Subspace
S-V	Saleh-Valenzuela
TDMA	Time Division Multiple Access
TH	Time Hopping
TR	Transmitted Reference
Tx	Transmitter
UML	Unconditional Maximum Likelihood
USB	Universal Serial Bus
UTD	Uniform Theory of Diffraction
US	Uncorrelated Scattering
UWB	Ultra-wideband
WLAN	Wireless Local Area Network
WPAN	Wireless Personal Area Network
WSS	Wide Sense Stationary

Chapter 1

Introduction

In the recent years, both the wireless and the wired transmissions have experienced an amazing growth due to the rapid advances in semiconductor research and the increasingly demand for high-data rate services. This fact has paved the way for the advent of the so-called *next generation* communication systems, among which, future short-range wireless systems are experiencing an unprecedented transformation.

Short-range wireless connectivity has become an essential part of everyday life thanks to the enormous growth in the deployment of wireless local area networks (WLAN) and wireless personal area networks (WPAN). However, today's WLAN and WPAN cannot meet the requirements of upcoming wireless services that demand high-data rates to operate. This issue has motivated the resurgence of ultra-wideband (UWB) technology, certainly the oldest form of radio communication ever created, whose origins date back to the late 19th century.

Ultra-wideband technology is based on the emission of extremely-short pulses with a spectral occupancy on the order of several GHz. This is in contrast with traditional narrowband and wideband communication systems, whose transmitted bandwidth is on the order of some kHz and some MHz, respectively. As a result of this huge spectral occupancy, UWB technology can provide unique and attractive features. For instance, this accounts for ultra-high-speed data rates, ultra-fine time resolution for precise positioning and ranging, multipath immunity and low probability of interception due to the low power spectral density. Because of this great potential, UWB technology is being considered for the physical layer of next generation short-range wireless communications, radar, ad-hoc networking, sounding and positioning systems.

Nevertheless, formidable challenges must be faced in order to fulfill the expectations of UWB technology. One of the most important challenges is to cope with the overwhelming distortion introduced by the intricate propagation physics of UWB signals. This will be the central part of the present dissertation. In particular, special attention will be devoted to the design of

robust receivers for UWB communications both in the presence and in the absence of channel state information. In the sequel, this will lead to the consideration of *coherent* and *non-coherent* receivers, respectively.

1.1 Motivation and Objectives

So far, little attention has been paid to the actual propagation conditions of UWB signals. As a result, this ignorance has led to the design of UWB communication systems that are just a straightforward extension of traditional spread-spectrum systems. Reality, however, is rather different, and recent measurement campaigns show that the unconventional propagation physics of UWB signals must be taken into consideration in the receiver design.

In this context, the basic motivation of this dissertation is to optimally design the basic tasks of a digital UWB receiver by taking into consideration the physical constraints of actual UWB received signals. As it will be discussed later on in Section 2.4, unknown signal distortion and very low signal-to-noise ratios are certainly the two major issues encountered at the receiver. These impairments are the key elements in the present dissertation and they lead to the following research lines:

- Evaluation of the incurred performance loss when the received waveform is unknown to the receiver.
- Design of waveform estimation techniques to resolve the uncertainty about the unknown received signal.
- Design of robust non-coherent receivers to cope with the absence of instantaneous waveform state information.
- Design of non-coherent and non-assisted timing synchronization techniques.

An individual chapter is dedicated to each of the above research lines and a brief summary of these chapters is presented in Section 1.2.

1.2 Thesis Outline

This section provides an outline of the present dissertation with a brief summary of the material presented in each chapter. A schematic presentation is also depicted in Figure 1.1.

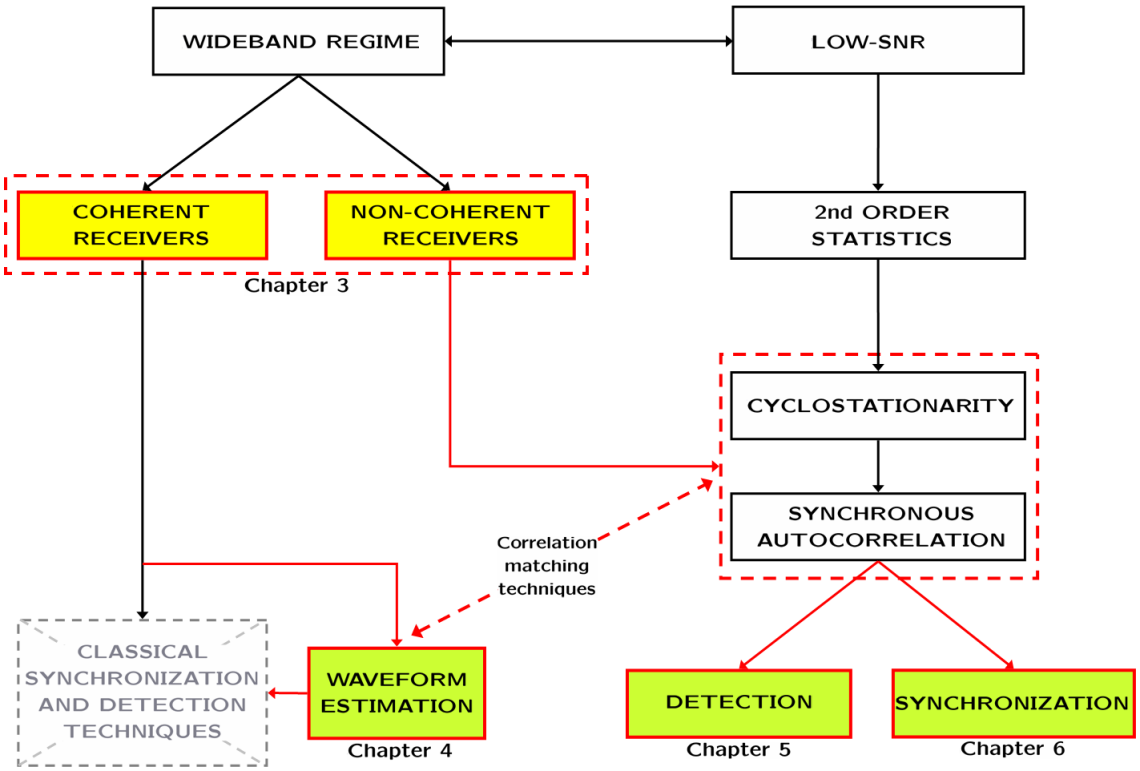

Figure 1.1: Schematic overview of the topics covered within the present dissertation.

Chapter 2

This chapter presents a general overview of UWB technology from both a historical and a technical point of view. First of all, this section investigates the origins of UWB technology through a historical review of the most relevant contributions in the field of *impulse radio*. Next, the evolution of UWB technology until the present day is reviewed and some aspects related to current spectral regulations are discussed. However, the main purpose of this section is to understand the fundamentals of UWB technology. To this end, the key features of UWB signals are presented. This includes a review of the mostly adopted modulation formats, some important remarks about the propagation physics of UWB signals, and the impact they have onto the receiver design. Finally, this chapter also provides a brief presentation on the open challenges in the design of UWB receivers for reliable communication.

Chapter 3

This chapter analyzes the performance limits of UWB technology from an information theoretic point of view. The emphasis is placed on understanding the conditions for which reliable communication is possible with UWB systems. To this end, the notion of constellation-constrained capacity is adopted all through this chapter as an upper bound on the achievable data rate of any

UWB system. Two different approaches are distinguished in this chapter depending on whether channel state information is perfectly known at the receiver or not. As a result, this leads to the analysis of *coherent* and *non-coherent* receivers, respectively. Both approaches result in a tradeoff between implementation complexity and achievable performance, and both theoretical and numerical results are provided to illustrate this issue.

Chapter 4

This chapter concentrates on the recovery of channel state information for enabling the implementation of coherent UWB receivers. This is a very important problem in UWB communications since the shape of the propagating pulse cannot be a-priori known at the receiver. This is due to the intricate propagation physics of UWB signals that cause a severe frequency-selective behavior but also a path- and angle-dependent distortion in the received signal. As a result, a single transmitted pulse arrives in the form of a series of delayed and distorted waveforms that cannot be properly represented by the traditional tapped-delay line model. Because of the unconventional propagation physics of UWB signals, this chapter proposes a waveform estimation framework where the aggregated channel response, and not the individual paths and amplitudes, is estimated. The proposed waveform estimation technique is derived under the unconditional maximum likelihood criterion and, similarly to previous chapters, special emphasis is devoted to application in the low-SNR regime. Finally, a nondata-aided approach is considered where no training nor pilot symbols are required for the waveform estimation.

Chapter 5

This chapter focuses on the problem of non-coherent detection of random UWB signals. The problem of non-coherent detection arises in those working scenarios with random and rapid fluctuations of the propagation environment. In these circumstances, it is unfeasible to obtain instantaneous channel state information for implementing a coherent receiver. Therefore, there is no choice but to resort to non-coherent receivers in order to exploit the statistical characterization of the propagation channel. Based on the above premise, this chapter formulates the optimal decision metrics for the non-coherent detection of random UWB signals. Both correlated and uncorrelated scattering scenarios are considered, and a low-complexity implementation of non-coherent receivers is proposed.

Chapter 6

This chapter deals with the problem of frame-timing acquisition for non-coherent UWB receivers. Frame-timing acquisition is an important topic in UWB communication systems since both co-

herent and non-coherent receivers require frame-timing acquisition to determine the starting point of each information-bearing symbol. For the case of coherent receivers, timing acquisition is rather simple and it is based on correlating the incoming signal with the available reference waveform, similarly to what occurs with traditional spread-spectrum communication systems. However, timing acquisition for non-coherent receivers is much more difficult because no reference waveform is available at the receiver. This chapter sheds lights on this topic by formulating the optimal frame-timing acquisition method when neither the received waveform nor the transmitted symbols are available at the receiver. The mathematical derivation is based on the unconditional maximum likelihood criterion and a low-complexity implementation is proposed based on the multifamily likelihood ratio test.

1.3 Research Contributions

The work conducted within the present thesis resulted in the publication of several contributions in technical journals and international conferences. These contributions are listed herein and they are related to the corresponding chapter of the dissertation.

Chapter 3

The main result of this chapter is the analysis of the performance limits of UWB communications when either coherent or non-coherent receivers are adopted. The results in this chapter are summarized in the following papers:

- J. A. López-Salcedo and G. Vázquez, "Closed-Form Upper Bounds for the Constellation-Constrained Capacity of UWB Communications", *IEEE International Conference on Acoustics, Speech and Signal Processing (ICASSP), Honolulu, Hawaii, USA, 15-20 April 2007.*

- J. A. López-Salcedo and G. Vázquez, "Performance Limits for Coherent and Non-Coherent UWB Communications", *submitted to IEEE Journal of Selected Topics in Signal Processing, special issue on Performance Limits of Ultra-Wideband.*

Chapter 4

The main result of this chapter is the formulation of a unified framework for the waveform estimation problem under the unconditional maximum likelihood criterion. Special emphasis is devoted to obtain a closed-form solution for application to the low-SNR scenarios where UWB

communication systems are likely to operate. The results in this chapter have been published in one conference paper and are currently under review in one journal paper:

- J. A. López-Salcedo and G. Vázquez, "NDA Waveform Estimation in the Low-SNR Regime", *submitted to IEEE Transactions on Signal Processing*, January 2007.
- J. A. López-Salcedo and G. Vázquez, "NDA Maximum-Likelihood Waveform Identification by Model Order Selection in Digital Modulations", *Proc. 6th IEEE International Workshop on Signal Processing Advances in Wireless Communications (SPAWC)*, pags. 385-389, New York City, NY, USA, 5-8 June 2005.

Preliminary results in the topic of waveform estimation were initially obtained based on an iterative algorithm in the frequency domain. This algorithm is not included in the present dissertation but the resulting contribution can be found in two conference papers:

- J. A. López-Salcedo and G. Vázquez, "Frequency Domain Iterative Pulse Shape Estimation Based on Second-Order Statistics", *Proc. 5th IEEE International Workshop on Signal Processing Advances in Wireless Communications (SPAWC)*, pags. 92-96, Lisbon, Portugal, 11-14 July 2004.
- J. A. López-Salcedo and G. Vázquez, "Stochastic Approach to NDA Synchronization and Pulse Shape Estimation", *Proc. 8th International Workshop on Signal Processing for Space Communications (SPSC), European Space Agency (ESA)*, Calabria, Italy, September 2003.

Chapter 5

The main result of this chapter is the formulation of the optimal decision metrics for the detection of random UWB signals with non-coherent receivers. The results in this chapter are summarized in one submitted journal paper:

- J. A. López-Salcedo and G. Vázquez, "Detection of UWB Random Signals", *submitted to IEEE Transactions on Signal Processing*, May 2006.

Chapter 6

The main result of this chapter is the derivation of an optimal frame-timing acquisition method for the low-SNR regime. The material of this chapter has been published in the form of one journal paper and two conference papers:

- J. A. López-Salcedo and G. Vázquez, "Waveform-Independent Frame-Timing Acquisition for UWB Signals", *IEEE Transactions on Signal Processing*, vol. 55, no. 1, pags. 279-289, January 2007.
- J. A. López-Salcedo and G. Vázquez, "Frame-Timing Acquisition for UWB Signals via the Multifamily Likelihood Ratio Test", *Proc. 7th IEEE International Workshop on Signal Processing Advances in Wireless Communications (SPAWC)*, Cannes, France, 2-5 July 2006.
- J. A. López-Salcedo and G. Vázquez, "NDA Maximum-Likelihood Acquisition of UWB Signals", *Proc. 6th IEEE International Workshop on Signal Processing Advances in Wireless Communications (SPAWC)*, pags. 206-210, New York City, NY, USA, 5-8 June 2005.

Other contributions not directly related with this dissertation

Apart from the topic of UWB communications, other research topics have been addressed during the period of PhD studies. Some of these topics were related with research projects for private industry and public administrations, and the most relevant publications are listed below.

⋆ **Research in synchronization for digital receivers:**

- J. A. López-Salcedo and G. Vázquez, "Asymptotic Equivalence Between the Unconditional Maximum-Likelihood and the Square-Law Nonlinearity Symbol Timing Estimation", *IEEE Transactions on Signal Processing*, vol. 54, no. 1, pags. 244-257, January 2006.
- J. A. López-Salcedo and G. Vázquez, "Cyclostationary Joint Phase and Timing Estimation for Staggered Modulations", *Proc. IEEE International Conference on Acoustics, Speech and Signal Processing (ICASSP)*, vol. 4, pags. 833-836, Montreal, Canada, 17-21 May 2004.
- J. A. López-Salcedo and G. Vázquez, "Stochastic Approach to Square Timing Estimation with Frequency Uncertainty", *Proc. IEEE International Conference on Communications (ICC)*, vol. 5, pags. 3555-3559, Anchorage, AK, USA, 11-15 May 2003.
- J. A. López-Salcedo and G. Vázquez, "Second-order Cyclostationary Approach to NDA ML Square Timing Estimation with Frequency Uncertainty", *Proc. IEEE International Conference on on Acoustics, Speech and Signal Processing (ICASSP)*, vol. 4, pags. 572-575, Hong Kong, China, 6-10 April 2003.

⋆ **Research in space-time turbo decoding:**

- J. A. López-Salcedo and M. Lamarca, "A New Metric for BER Evaluation in APP Decoders with Space Diversity", *Proc. 5th IEEE International Workshop on Signal Processing Advances in Wireless Communications (SPAWC)*, pags. 54-58, Lisbon, Portugal, 11-14 July 2004.
- M. Lamarca and J. A. López-Salcedo, "Decoding Algorithms for Reconfigurable Space-Time Turbo Codes", *Proc. IEEE International Conference on on Acoustics, Speech and Signal Processing (ICASSP)*, vol. 5, pags. 129-132, Hong Kong, China, 6-10 April 2003.

Chapter 2

Overview of UWB Technology

2.1 Introduction

The purpose of this chapter is to present a general overview from the very first steps of ultra-wideband (UWB) technology to the most recent advances, applications and regulatory issues. To this end, Section 2.2 presents a brief historical review with the most significant events in the development of UWB technology. Since recent advances in UWB technology are closely related with the advent of spectral regulations, Section 2.3 presents the current requirements that regulatory bodies demand for the safe operation of commercial UWB devices. Next, the fundamentals of UWB technology are introduced in Section 2.4. Special emphasis is devoted to the signaling format, channel modeling and pulse distortion at the receiver. Finally, applications of UWB technology are listed in Section 2.5 and current challenges in UWB technology are discussed in Section 2.6.

2.2 A Brief Historical Review

The concept of ultra-wideband communication (also known as *impulse radio*) dates back from the early days of radio communications, in the transition from the 19th to the 20th century. Probably the first experiments on impulse radio were conducted by Heinrich Hertz in 1887, who used spark gaps and arc discharges between carbon electrodes to generate impulsive electromagnetic waves. Seven years later, while vacationing in the Alps, Guglielmo Marconi read a journal article by Hertz and abruptly came to his mind the vision of applying impulse radio for wireless telegraphy. Some time later, the Marconi spark gap Morse transmitter was found to succeed and it established the beginning of wireless radio communications and the widely adoption of spark gap technology.

However, one of the major drawbacks of spark gap transmissions was that the instantaneous bandwidth of the radiated signals vastly exceeded their information rate. As a result, there was a huge spectrum occupancy for a single user transmission, and multiple access to other users could not be efficiently managed. Since the impulse radio technology of that time did not offer a practical answer to the problem of spectral sharing, research efforts were conducted toward the development of modulated sinusoidal carriers, more suitable for the government regulation. Carrier-based communications were successfully introduced at the beginning of the 20th century and they were proven to be better for voice communication than the rudimentary spark gap technology of Hertz and Marconi. The successful deployment of carrier-based communications and the interfering issues of impulsive radio made the communications world to abandon wideband in favor of narrowband transmissions. In fact, the adoption of narrowband technology has been so dominating until the recent days that the viability of short-pulse systems often has been greeted with skepticism.

Impulse radios were forbidden in amateur radio bands by 1924 due to their unregulated emissions that were disruptive to narrowband, carrier-based radios. However, sparks continued to be used in the maritime service and during the World War II [Bel94]. Indeed, military applications were the ones that kept UWB communications alive. In the 1940s, several pulse communication systems were developed for military purposes with the aim of reducing interference or jamming and enhancing the secrecy of communications. Later on, some patents appeared for the application of UWB technology to non-communication systems such as radar or ground penetrating sounding. In that sense, probably the very first reference to an UWB system can be found from the patent that De Rosa obtained in 1954 for an early UWB system [Ros54]. However, by some years later when Hoeppner patented a representation of its pulsed communications system [Hoe61], there were no secrets about UWB technology and all the essential elements of an impulse radio transmission system were already known to the scientific community.

Contributions to the modern development of UWB systems started in the 1960s with the pioneering work by Harmuth at the Catholic University of America, who published the basic design rules for UWB transmitters and receivers. The contributions by Harmuth were focused on the carrier-free nature and the huge spectral occupancy of UWB signals. His work culminated with many publications on the topic of nonsinusoidal functions for communication systems [Har69b], [Har68], [Har69a]. This topic led to confrontations with many researchers of that time which were very skeptical about the use of carrier-free signals and very large bandwidths. The arguments can be found in a series of comments and replies to many publications in that topic. See for instance [Dav79] and [Har79], but also [Bar00] and [And05] for a historical perspective.

Almost simultaneously to Harmuth, Ross and Robins at the Sperry Rand Co. obtained the patents for the use of UWB in communications and radar applications with coding schemes [Ros73]. Later on, Van Etten at the United States Air Force (USAF) Rome Air Development

Center provided some empirical testing of UWB radar systems which resulted in the development of basic system design and antenna concepts [Ett77]. Notwithstanding, it is interesting to note that, apart from radar applications, UWB technology was also applied to geoscience for ground characterization by penetrating sounding, which became a commercial success [Mof76].

One of the most important issues of UWB techniques has always been its relatively simple implementation. The fact that UWB was initially a carrierless modulation scheme rapidly promoted the construction of low-cost commercial hand-held radar receivers. As an example, a simple UWB receiver could be built at 1978 by purchasing the basic parts from the Tektronix Inc. catalogs, and using the published schematics for a UWB radar design by Benett & Ross [Ben78]. The generation of extremely short pulses (also known as *monopulses*) was produced by means of solid state devices such as avalanche transistors [Mor74], [Ros86] or tunnel diodes, providing a minimum rise time of approximately 25 picoseconds. Once the implementation of UWB systems was not a problem, the emphasis was placed on the improvement of existent technology, and understanding the implications of transmitting wideband pulses in a world plenty of non-interfering radio-frequency communications.

The step forward from radar and point-to-point communications to wireless multi-user networks was established by Scholtz in a landmark paper where each user was assigned a unique time-hopping code for transmission [Sch93]. With a viable way of introducing multiple access, UWB technology became a promising candidate for future wireless networks. Significant research efforts started to be dedicated and many small companies were set up in the mid 1990s to develop commercial UWB systems. For instance, Multi-Spectral Solutions, Time Domain Co., AetherWire, X-treme Spectrum, Pulse-Link Inc, Fantasma Networks and many others, were the pioneers in developing high-data rate and carrierless commercial products. However, no regulations on the emission limits of UWB signals were available at that moment. The definite push into the commercial deployment of UWB technology was due to the American Federal Communication Commission (FCC) in 2002, which for the first time, established the emission limits for the safe operation of UWB devices [FCC02].

2.3 Regulation and Standardization of UWB Technology

Many terms have been adopted for ultra-wideband communications since the very first experiments by Hertz and Marconi. For instance, this includes "impulse", "short-pulse", "nonsinusoidal", "carrierless", "monopulse" or "baseband" communications. However, the first to have started to use the unifying term *ultra-wideband* is believed to be the United States Department of Defense through its Defense Advanced Research Projects Agency (DARPA) [Gha04]. This is an example on how official and governmental bodies have played a major role in the development, unification and regulation of UWB technology during the recent years. In this section,

this issue is reviewed. Special emphasis is placed on spectral regulations and current approaches within industry for the deployment of UWB technology.

2.3.1 Regulations on the emission limits of UWB signals

2.3.1.1 Regulations in the United States of America

The first definition for a signal to be qualified as *ultra-wideband* is due to the United States DARPA in 1990 which adopted the measure of fractional bandwidth for this purpose [DAR90]. The fractional bandwidth of a signal can be determined as

$$W_{\text{frac}} = 2\frac{f_{\text{H}} - f_{\text{L}}}{f_{\text{H}} + f_{\text{L}}} \tag{2.1}$$

with f_{H} and f_{L} the upper and the lower frequency, respectively, measured at the -3dB spectrum. This first definition of UWB signal stated that a signal can be classified as UWB when the fractional bandwidth W_{frac} is greater than 0.25.

The DARPA definition of UWB signals led to the development of purely carrierless communications systems, and several companies such as AetherWire, Time Domain Co., Multi-Spectral Solutions Inc., X-treme Spectrum or Pulse-Link Inc. were the pioneers in developing high-data rate and carrierless commercial products. No spectral regulations on the UWB emission limits were available at that moment, although the carrierless nature of UWB technology was later demonstrated to produce potential interference to GPS positioning systems [Luo00], [Car01], [hop01]. Thus, a specific regulation for UWB emission was required by the industry for a successful coexistence with existing spectrum allocation.

After discussion of more than 1000 comments, studies and analysis, the expected regulation came out in February 2002 when the Federal Communications Commission (FCC) issued the preliminary *First Report and Order* (R&O) on UWB technology. Taking into consideration the potential interference with existing governmental systems such as GPS, navigation radars and emergency services, the FCC R&O on UWB technology restricted the unlicensed use of UWB systems to the frequency band within 3.1 GHz to 10.6 GHz. The final report was issued in April 2002 and it introduced four different categories for the allowed UWB applications as well as a set of spectral masks to be accomplished [FCC02]. The masks for communication and measurement applications are shown in Figure 2.1 for the case of indoor and outdoor emissions.

Apart from emission restrictions, the final report of the FCC R&O introduced a slight modification in the definition of UWB signals from the one originally adopted by the DARPA. In particular, the required fractional bandwidth was reduced to 0.20 and the upper and lower frequencies were now placed at the -10 dB spectrum. In addition to this, a signal was also considered to be UWB if the signal bandwidth is equal or greater than 500 MHz.

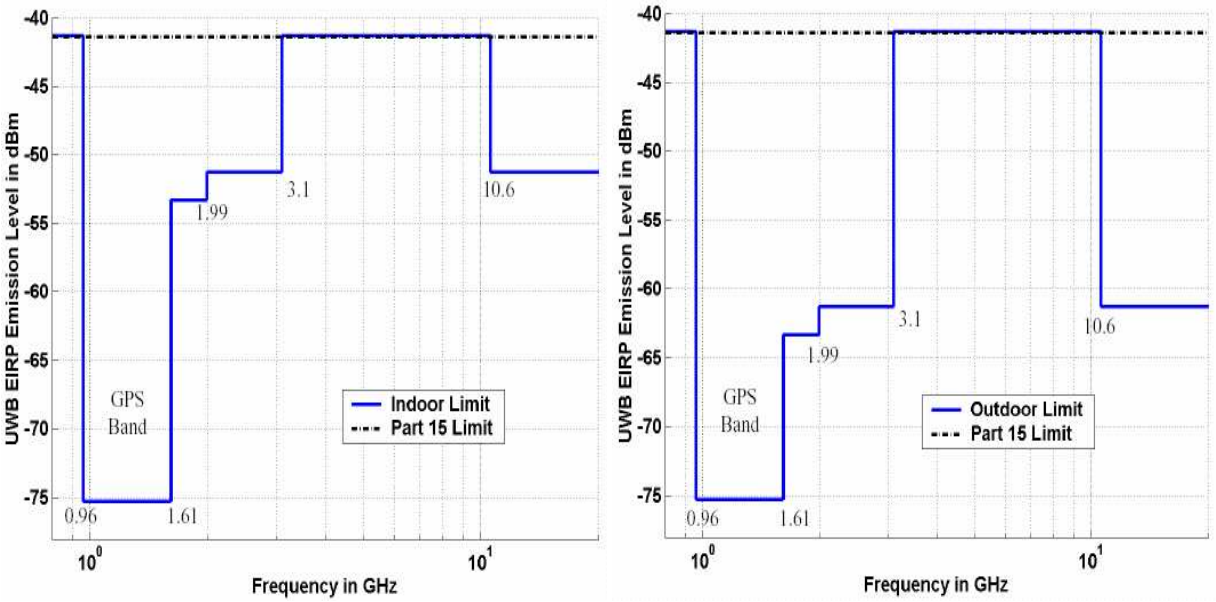

Figure 2.1: FCC UWB spectral masks corresponding to indoor (left) and outdoor (right) emissions for communication and measurement equipments.

An important issue to be taken into consideration is that the FCC R&O provides spectral masks to be accomplished but does not restrict users to adopt any specific modulation format. As a result, there are currently a plenty of proposals both from industry and academia that promote different modulation schemes for future UWB systems. This topic will be discussed later on in Section 2.3.3 and Section 2.4.2.

2.3.1.2 Regulations in Europe

The European Commission is the responsible for adopting technical measures to ensure harmonised conditions with regard to the availability and efficient use of the radio spectrum in the European Union internal market. In order to develop the technical requirements of such measures, in March 2004 the Commission required the European Conference of Postal and Telecommunications Administrations (CEPT) to identify the technical and operational criteria for the harmonised introduction of UWB-based applications. Similarly, the European Telecommunications Standards Institute (ETSI) established the Task Group ERM TG31 to develop a set of standards for short-range devices using UWB technology.

In February 2005, the Electronics Communication Committee (ECC) of the CEPT issued the Report 64 with the proposed technical recommendations for the safe operation of UWB devices in the EU [ECC05]. The main results stated that at least 10 or 20 dB more of attenuation were required in some bands in comparison with the American FCC regulation. The reason was claimed to be the avoidance of harmful interference of unlicensed UWB devices to sensitive

equipments such as meteorological and military radars, according to European experimental tests.

Later on, in March 2006, some minor changes were introduced to Report 64 and a decision was made to permit unlicensed UWB operation within the band from 6 to 8.5 GHz, in contrast with the 3.1 to 10.6 GHz in the American regulation [CEP06]. The reason is claimed to be the reservation of the band below 5 GHz for the future development of cellular networks and to preserve military radars operating in the band from 8.5 to 9 GHz. This regulation has created significant controversy in industry and is now under revision after a call for comments in April 2006. Therefore, some changes may still be introduced until a definite regulation is issued.

2.3.2 Standardization within the IEEE

Without any doubt, one of the leading developers of technology standardization is the Institute of Electrical and Electronics Engineers Standards Association (IEEE-SA), with nearly 1300 standards in both traditional and emerging fields. This accounts for telecommunications, information technology, power generation and biomedical and healthcare. In addition to producing the prominent 802® standards for local and metropolitan area network wireless and wired, IEEE-SA is also undertaking the definition of a new physical layer concept for short-range, high data rate communication applications. To this end, two different working groups have been created:

- The **IEEE 802.15.3a** study group is working to define a higher speed physical layer for applications which involve imaging and multimedia in wireless personal area networks (WPAN). The minimum data rate is set to 100 Mbps within a range of 10 meters and 480 Mbps within 2 meters. Although not specifically intended to be an UWB standards group, the technical requirements lend themselves to the use of UWB technology. In this sense, the work of this group includes the analysis of the radio channel model to be used in the evaluation of UWB systems [Foe03].

- The **IEEE 802.15.4** study group is working to define a new physical layer for low-complexity and low-data rate applications. It is intended to operate in unlicensed, international frequency bands. One of the main objectives is to address new applications that require not only moderate data throughput, but also long battery life. For this reason, this working group is focusing upon low data rate WPAN, sensor networks, interactive toys, smart badges, remote controls and home automation. The work of this group also includes the analysis of the radio channel model to be used in the proposed UWB system evaluation, with special emphasis on the particular issues and working conditions of low data rate devices [Mol04].

2.3.3 Standardization controversy within industry

Despite the standardization efforts within the IEEE, it has been unable to reach consensus with industrial partners to adopt a common specification for UWB technology. The reason can be found in the fact that IEEE began its standardization attempt when companies had already begun serious design work for chips based on proprietary UWB technology. Now, an agreement is almost impossible since most vendors are currently preparing to release commercial products by the end of 2006. According to some analysts [Sch06], global UWB hardware shipments will reach 300 millions by 2011 and thus, being the first to be in the market will make the difference. A change in the underlying specifications of each vendor's UWB technology would incur in significant financial losses for all the engineering work already done in nearly the last decade.

Currently, there are two different approaches to UWB technology within industry:

- A **DS-UWB** approach (i.e direct-sequence UWB) is being adopted by the UWB Forum, originally led by Freescale (former Motorola Semiconductor) with 220 members amongst international telecommunication vendors and service providers such as Fujitsu, Siemens or Vodafone. The Forum promotes a purely impulse radio scheme where multiple access is achieved by binary amplitude modulating the transmitted pulses, similarly to traditional CDMA spread spectrum systems. In April 2006, Freescale abandoned the UWB Forum to concentrate on *Cable-Free*, its own proposal for the next generation of wireless universal serial bus (USB) and wireless IEEE 1394 (FireWire).

- An **MB-OFDM** approach (i.e. multiband OFDM) is being adopted by the WiMedia Alliance, led by Intel Corporation with 214 members amongst PC and consumer electronics vendors such as Hewlett-Packard, Sony, Nokia, Texas Instruments or Microsoft. The Alliance promotes a carrier-based multiband scheme where the available bandwidth is split into many bands with a minimum bandwidth of 500 MHz, as shown in Figure 2.2. The multiband approach is similar to traditional OFDM techniques widely adopted in xDSL and high data rate WLAN systems such as the IEEE 802.11g. The Alliance is focused on using UWB for computer, consumer electronics and mobile-phone connectivity as a common physical layer for supporting next generation USB, IEEE 1394 and Bluetooth applications [Int04], [Int05a], [Int05b].

Proponents of each approach are trying to get as many manufacturers as possible to use their technology and thus, establish a strong market position so that a *de facto* standard is finally

reached. However, this is still unclear, and probably, both approaches will coexist in different kind of applications [Gee06]. In this dissertation, however, we will focus on the original flavor of UWB technology. Thus, the carrierless implementation will be adopted and purely impulse radio will be considered.

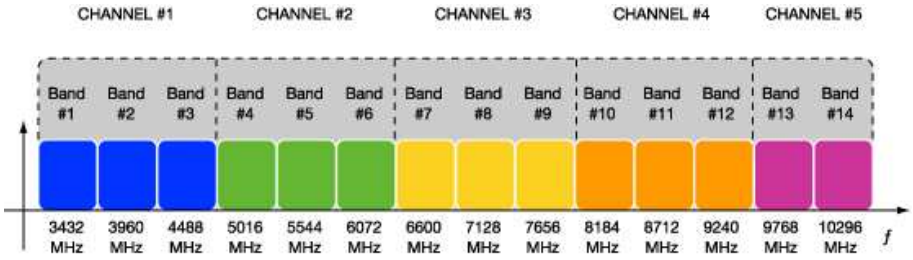

Figure 2.2: The WiMedia Alliance multiband-OFDM frequency plan [Kol04].

2.4 Fundamentals of UWB Technology

Apart from the different industrial approaches to UWB technology, there are many features that are common to the UWB nature of the transmitted signal. These features are presented in Section 2.4.1 and they are the ones that make UWB technology a unique candidate for future wireless short range applications. Next, Section 2.4.2 discusses the mostly adopted modulation formats for enabling UWB signals to convey information from transmitter to receiver. Finally, since transmitted signals are sent over a rather hostile propagation environment, Section 2.4.3 introduces the major impairments that UWB signals suffer in their way to the receiver end. Moreover, the proposed channel models by the standardization bodies are also overviewed.

2.4.1 Key features of UWB technology

UWB technology is based on the emission of extremely-short pulses on the order of subnanoseconds with a very low power spectral density. As a result of these particular characteristics, UWB has several features that differentiate it from conventional narrowband systems. Some of these key features are the following:

- **High data rate for short- and medium-range**. This is achieved by transmitting extremely-short pulses on the order of sub-nanoseconds (also known as *monocycles*) and by using fast switching and precise synchronization at the receiver.
- **Low-complexity and low-cost equipment**. For the original flavor of UWB technology, baseband impulse radio is considered by directly modulating onto the antenna without any prior RF mixing stage [Yao04]. Apart from not requiring any RF mixing stage, impulse

radio systems can be implemented in CMOS platforms that are superior in both power consumption and cost to SiGe platforms adopted in implementations with RF elements [Yan04b]. As a result, carrierless UWB allows simple and cheap transceivers for application to sensor, tracking or positioning networks [Rab04b], [Sto04].

- **Low transmit power and noise-like spectrum**. The very low power spectral density, the very large spectral occupancy, and the pseudo-random time-position of the transmitted pulses, they all make UWB to appear as a noise-like signal to narrowband systems. Consequently, UWB signals provide a low probability of interception. That was one of the main reasons for which UWB technology was widely adopted for military applications during the last five decades [Tay94].

- **Multipath and interference immunity.** Because of the very large bandwidth of the transmitted signal, very high multipath resolution is achieved. In addition, the large bandwidth also provides a large frequency diversity that, together with low duty cycle transmissions, makes UWB signals to be resilient to multipath and interference or jamming.

- **High penetration capability.** Since UWB signals expand over a very wide range of frequencies, low material penetration losses are incurred. This is particularly true for the low frequencies of UWB signals, which have good penetration properties through different materials and improve the coverage of UWB systems [Lee04].

- **Unique pulse distortion.** Unlike traditional narrowband communications systems, UWB signals suffer from significant degradations in their way from transmitter to receiver. The main reason is that the end-to-end channel response exhibits a severe frequency- and path-dependent distortion due to the unique propagation physics of UWB signals [Qiu02], [Kon05]. Moreover, antennas are also found to introduce pulse dispersion that may change with elevation and azimuth angles [Ben06], [And05]. In particular, antennas behave like direction-sensitive filters such that the signal driving the transmitting antenna, the electric far field, and the signal across the receiver load may differ considerably in waveshape and spectral content. As a result, matched filter correlation is difficult to be implemented at the receiver unless high computational complexity is dedicated for obtaining perfect waveshape estimation [Sch05a]. Thus, UWB receivers can be implemented under a coherent or non-coherent approach depending on a tradeoff between complexity and performance.

It is interesting to note that, among the above key features of UWB technology, this dissertation focuses on the last topic, the one related with the pulse distortion at the receiver. The reason is that, although an important issue in the design and implementation of UWB receivers, little attention has been devoted to the problem of not knowing the shape of the received waveform. Indeed, there are many contributions in the recent literature that still formulate the UWB receiver in terms of the traditional matched filter correlation (see for instance [Gez04], [Chu04],

[Oh05] or [Tan05a] among many other). Contrary to this unrealistic approach, the present work pretends to analyze the problem of unknown received waveform and the impact it has on the symbol detection and signal synchronization at the receiver.

2.4.2 Signaling formats

The mostly adopted modulation formats for UWB technology are the following:

- **Pulse-amplitude modulation (PAM).** This is a modulation scheme where the information is conveyed by the amplitude of the transmitted pulse. While PAM is widely adopted in many narrowband communication systems, it has not been until the recent years that PAM has been used with UWB signals. So far, the major problem was related with the difficulty in manipulating the amplitude of the transmitted subnanosecond pulses. However, the recent advances in low-cost and high-speed CMOS and SiGe integrated circuits have paved the way for an easier implementation of PAM UWB transceivers. Similarly to direct-sequence spread-spectrum, the amplitude modulation of UWB pulses is usually restricted to binary signaling leading to a binary-phase shift keying (BPSK) scheme.

  A major drawback of PAM modulation is that channel state information (CSI) is required for resolving the ambiguity introduced by the fading multipath channel. Accurate CSI can be obtained by using optimal or near-optimal channel estimation techniques for UWB signals. Alternatively, noisy CSI can be obtained by using transmitted reference (TR) signaling, an old concept which is based on the transmission of a reference pulse prior to each data modulated pulse [Rus64], [Hoc02]. The efficiency loss caused by unmodulated pulses comes at the expense of avoiding channel estimation at the receiver. Then, since the reference pulse is an unmodulated pulse, the receiver can implement a coherent detection by taking this reference pulse as a noisy estimate or *template* of the end-to-end channel response [Yan04c]. However, irrespective of the quality of CSI (i.e. either perfect CSI or noisy templates), coherent receivers are always required for demodulating PAM.

- **Pulse-position modulation (PPM).** This is a classical modulation scheme where the information is conveyed by the time interval in which the pulse is transmitted. For the case of P-ary PPM, with $P = 2^b$ and b the number of bits per symbol, the symbol duration T is typically divided into P disjoint (i.e. orthogonal) time-slots where the transmitted pulse can be located[1]. It is important to note that, historically, PPM was adopted because of the difficulty in implementing polarity inversion of transmitted pulses. However, PPM is still adopted today in many UWB systems because its orthogonal implementation can achieve an arbitrarily small bit error probability provided that $P \to \infty$ [Pro94, p.498], and

[1] Overlap between time slots provides a higher data rate at the expense of a performance degradation.

it allows non-coherent detection. A detailed and rigorous analysis of PPM modulation can be found in [Woz65, p.623] as well as an interesting discussion on the PPM threshold.

Depending on the single-band or multi-band implementation of UWB communication systems, a given modulation format is preferred. For the case of single-band UWB (e.g. impulse radio adopted by the UWB Forum), the real-valued baseband nature of the carrierless transmission is exploited for implementing either binary-PAM or PPM modulation. Moreover, this is done by directly modulating onto the transmit antenna. Multiple access is usually achieved in single-band UWB by using traditional concepts of time-hopping (TH) and pseudorandom direct-sequence (DS) spread spectrum.

For the case of multi-band UWB (e.g. MB-OFDM adopted by the WiMedia Alliance), the information is modulated onto a carrier and thus, the low-pass equivalent signal is found to be complex. In this case, PAM modulation is considered with complex information-bearing symbols, and usually, QPSK constellation is adopted [Aie03]. Multiple access in multi-band UWB is achieved by allocating each user a group of carriers. This is feasible because, unlike traditional OFDM techniques, the multi-band UWB spectrum is allowed to have gaps between carriers.

2.4.3 Standardized channel modeling

The propagation physics of UWB signals are rather intricate and many in-depth contributions have been published in the recent years about this topic. It is not the purpose of this section to provide a detailed analysis on the characterization of UWB channels, since the reader may find valuable references in the literature. For instance, this accounts for the IEEE 802.15.3a channel models in [Foe03], the IEEE 802.15.4 channel models in [Mol04], and some important papers such as [Cra02], [Qiu02], [Qiu05], [Kon05] and [Sch05a], among many other. A very detailed and complete review of UWB propagation channels can also be found in [Ben06, Ch. 2].

In particular, the IEEE 802.15.3a/4 channel models are widely adopted in the UWB engineering community when trying to simulate realistic propagation conditions. The first to be released was the IEEE 802.15.3a channel characterization for high data rate applications. This channel analysis is based on the tapped-delay line model introduced by Saleh and Valenzuela (S-V) [Sal87] with some minor modifications. For instance, the IEEE 802.15.3a recommends to substitute the Rayleigh distribution for the multipath gain magnitudes in the S-V model by a lognormal distribution. In addition, independent fading is assumed for each cluster and for each ray within the cluster. Depending on the particular values assigned to each of the different parameters of the IEEE 802.15.3a channel characterization (e.g. cluster arrival rate, ray decay factor, standard deviation for lognormal fading, etc.), a total of four different scenarios can be simulated for line-of-sight (LOS) and non-line-of-sight (NLOS) conditions [Foe03]. A summary

of these models is briefly presented in Table 2.1.

Channel model	LOS / NLOS	Distance between Tx and Rx (meters)
CM1	LOS	$0 - 4$
CM2	NLOS	$0 - 4$
CM3	NLOS	$4 - 10$
CM4	NLOS	not specified, but causing very dense multipath

Table 2.1: Channel models for different propagation scenarios within the IEEE 802.15.3a.

Later on, standardization activities began for low data rate applications within the IEEE 802.15.4 working group. As a part of the studies undertaken within this group, the UWB channel was characterized for the particular working scenarios of low data rate devices. This included factories, storage halls, rural environments and so forth. The proposed channel models were also based on the S-V model, but instead of the lognormal distribution in the IEEE 802.15.3a, the Nakagami distribution was found to fit better for low data rate applications. A very interesting point was that dense multipath was experienced in industrial environments which, according to some contributions, allowed the multipath gain magnitudes to be modeled by a Rayleigh distribution as in traditional narrowband communications [Kar04], [Sch05b], [Sch05c]. This fact opens up the opportunity to assume a Gaussian distribution for the multipath gain amplitudes, which significantly simplifies the mathematical analysis of the receiver design. A summary of the channel models within the IEEE 802.15.4 working group is briefly presented in Table 2.2.

Finally, there is an important remark to be made regarding the tapped-delay line model of the above mentioned channel characterizations. As recognized in [Mol04, p. 35], the traditional tapped-delay line model is an easy and tractable way of representing the impulse response of a propagation channel. Indeed, it is adopted in the above mentioned channel models within the IEEE 802.15.3a/4 working groups, and in most of the existing contributions on UWB technology in the recent literature. However, this simple channel model does not really represent the exact propagation physics of UWB signals. In particular, the tapped-delay line model assumes that the received signal is the sum of a finite number of scaled and delayed versions of the transmitted signal. That is, the received signal is the superposition of a number of undistorted versions of the transmitted pulse. However, as indicated in [Cra02] and [Qiu05], the transmitted UWB pulse experiences different frequency-dependent distortion on a per-path basis. Consequently, different distortion is experienced by the same transmitted pulse when propagating through different paths.

The standardized channel models presented before cannot explicitly take into account this

Channel model	LOS / NLOS	Propagation environment
CM1	LOS	Residential
CM2	NLOS	Residential
CM3	LOS	Office
CM4	NLOS	Office
CM5	LOS	Outdoor
CM6	NLOS	Outdoor
CM7	LOS	Industrial
CM8	NLOS	Industrial
BAN	NLOS[†]	Body-Area-Networks

[†] Because of the diffraction around the body [For06].

Table 2.2: Channel models for different propagation scenarios within the IEEE 802.15.4.

path-dependent distortion because they are all based on a tapped-delay line model. However, they do reflect this path-dependent distortion in an implicit manner by introducing *phantom* paths [Ben06]. These paths are not real but just an artifact to represent the different pulse distortion among real paths. Consequently, care must be taken when interpreting the proposed models. This is because each path in the model does not necessarily represent a separate independent path in reality, so that the fading coefficients of different delay bins need not be independent.

As a result of the above considerations, the main conclusion is that the channel model for UWB signals must be regarded more as a black box than as a real representation of the propagation physics. Therefore, the proposed channel models are intended to evaluate the performance of UWB systems in terms of statistical parameters such as delay spread, temporal correlation, etc. rather than in terms of detailed temporal characteristics such as, for instance, the required number of fingers in a Rake receiver.

2.4.4 Pulse distortion

Pulse distortion is certainly the major reason of this dissertation. Contrary to traditional narrowband communication systems, pulse distortion is one of the unique characteristics of UWB systems and it requires a completely different approach for the receiver design. Consequently, new opportunities arise for developing a theoretical framework in which one of the key elements is the lack of knowledge about the received wave shape.

Pulse distortion has been under investigation since the early 1900s in the context of diffraction at a half-plane for sound pulses [Som01], [Lam10]. Later on, military investigations were carried out for transient wave pulses originated from nuclear detonations. However, it was not until the 1990s that initial studies for the pulse distortion of UWB signals started to be developed [Sch93]. Up to now, there are many important contributions on this topic. In particular, special emphasis should be given to the work by R. C. Qiu, one of the major contributors to the pulse distortion theory of UWB signals [Qiu95], [Qiu96], [Qiu02], [Qiu04], [Qiu05]. The work by Qiu is based on the geometric and the uniform theories of diffraction (GTD/UTD), which can be viewed as an asymptotic theory (i.e. frequency $f \rightarrow \infty$) of the solution to Maxwell's equations. As a result of the studies by Qiu, a clear conclusion can be drawn. For the case of UWB channels, diffraction and dispersion leads to different frequency-dependent distortion for each echo. In that sense, exact and approximate formulations based on GTD/UTD allow a modification of the classical tapped-delay line model such that the impulsive response in a multipath environment can be expressed as the sum of differently distorted, scaled and delayed pulses (for details, see [Ben06, Section 2.3]). However this is still a rather complex model and the state of the art in approximating per-path impulse responses is very primitive. For this reason the modeling of the per-path distortion is usually combined in a statistical manner with the traditional tapped-delay line. This is the case, for instance, of the phantom paths already mentioned in Section 2.4.3.

Apart from diffraction and reflection, the radiating antenna is another important cause of pulse distortion. Basically, this is due to frequency-dependent variations in the antenna impedance and radiation pattern [Kon05]. As a result of the impedance variation, the spectrum of the radiated signal is modified and signal distortion is experienced. In turn, the radiation pattern variation causes radiation at a given frequency to be concentrated on a certain part of the antenna. This causes the antenna frequency response to vary for different angles in both elevation and azimuth. An important point to be highlighted is that, since the pulse shape produced by the antenna is different for different angles, the notion of a single pulse shape channel modeling is again problematic. Detailed measurements on this topic have been carried out by [Bue04]. Finally, signal distortion is also introduced because different signal frequency components may travel different distances and thus, all frequency components do not reach the receiver at the same time [Har04].

In front of this complex scenario where the received pulse shape may vary from different paths and different angles, a typical approximation in practice is to assume that the line-of-sight pulse is the transmitted pulse shape. This pulse shape is often adopted for matched filter correlation or to create the discrete tap impulse response channel when analyzing experimental data. However, care must be taken when making this assumption. On the one hand, matched filtering with the incorrect pulse shape leads to a significant loss in correlation energy. On the other hand, using a single pulse for channel modeling will require the generation of additional

multipath components for representing the pulse distortion of actual paths. Clearly, this is a rather loose approximation, and one of the main objectives of this dissertation is to address the problem of random and time varying pulse shape in a more rigorous manner.

2.5 Applications of UWB Technology

During the last five decades, the unprecedented large bandwidth of UWB signals has been mainly exploited for radar and ground penetrating sounding [Tay94]. However, the release of the DARPA report on UWB technology in 1990 and the FCC R&O in 2002 have attracted significant research efforts for extending UWB technology to commercial applications. This fact has also been accelerated when the research community realized that UWB systems could be almost inexpensively implemented with standard CMOS technology.

As already mentioned in Section 2.3.2, two working groups have been created within the IEEE for defining new physical layers for next generation wireless personal area networks. This includes both high and low data rate applications, some of which are indicated below:

- **High data rate applications:**
  - Wireless Personal Area Networks (WPAN) for ad-hoc networking between computers, peripherals and wearable computing. This includes the next generation wireless universal serial bus (USB) for which both the UWB Forum and the WiMedia Alliance are almost to release the first products. Moreover, UWB technology is being considered as the universal physical layer to support the next generation of Bluetooth and IEEE 1394 FireWire [Int04], [Int05a], [Int05b].
  - Home and professional media networking (digital cameras, DVDs, digital TV, etc.).
  - Fourth generation (4G) wireless systems [Chu05].
  - Search and rescue imaging systems. This application is intended for police, fire and rescue services to locate persons hidden behind a wall or under debris in building collapses.
  - Medical applications such as radar monitoring of physiologic functions. Because of the extremely time resolution of UWB signals, a low-cost and effective monitoring of internal organs is possible without the need for direct skin contact. Moreover, ongoing research projects are being conducted for analyzing the backscattered signal from UWB pulses to detect cancer [Li05], [Con06].
- **Low data rate applications:**
  - Sensor networks with tracking and positioning capabilities [Gez05].

- Identification tags for mobile inventory, personnel and asset tracking.
- Location-aware communication systems, a hybrid of radar and data communications that uses UWB pulses to precisely track the 2-D and 3-D position of an item as well as transmitting information about the item to a centralized database system.
- Vehicular radar systems for avoiding front and rear collisions.
- Positioning systems for providing real time indoor and outdoor precision tracking. Some potential uses include locator beacons for emergency services and precision navigation capabilities for vehicles, industrial and agricultural equipment.

2.6 Challenges in UWB Technology

The most important challenges in UWB technology can be classified into two major groups. On the one hand, the very large bandwidth of UWB signals results in serious hardware difficulties for transmitting, receiving and digitally representing such signals. On the other hand, advanced signal processing techniques must be devised both at the transmitter and receiver in order to cope with the unique features of UWB signals. For instance, this includes optimal pulse shaping for fulfilling the FCC spectral masks, data detection in the presence of pulse distortion and robust synchronization to handle the extremely high time resolution of UWB signals. In this section, the most challenging issues of these two groups will be discussed.

2.6.1 Hardware implementation challenges

The very large bandwidth of UWB signals poses many difficulties in the implementation of practical and low-cost UWB devices. The two major hardware implementation problems are related with the pulse distortion introduced by the radiating antennas and the performance of ultra-high speed analog-to-digital converters (ADC).

- **Antenna distortion.** One of the major challenges in the implementation of UWB systems is the development of suitable antennas that provide minimum pulse distortion at the receiver. Antennas for UWB signals require to cover a signal bandwidth on the order of several GHz and current research efforts are being pursued in achieving antenna impedances and radiation patterns that are constant for such a range of frequencies. In addition, this must be done by using simple manufacturing procedures, low-cost materials and small geometrical antenna structures for easy integration into small devices.

  Since traditional wideband antennas cannot be adopted for UWB applications, specific designs for UWB antennas are required. Some UWB antennas have been already proposed in the existing literature. See for instance the planar antenna proposed in [Yaz04], [Yaz05]

or [Brz06], the low-cost Cobra antenna in [Yin04] or the printed-circuit board (PCB) antennas proposed in [Low05] and [Gué05]. However, all the above proposals provide a constant behavior just for a portion of the UWB spectrum specified by the FCC. Further research is still required to provide a more stable behavior for the whole spectrum.

- **Analog-to-digital conversion**. Another important challenge in the hardware implementation of UWB systems is related with the analog-to-digital conversion at the receiver. Because of the very large bandwidth of UWB signals, a sampling rate on the order of a few gigasamples per second (Gsps) is required, according to the Nyquist criterion. Certainly, this is an ultra-high speed requirement for the analog-to-digital converter (ADC) and it becomes the bottleneck of fully digital implementations of UWB receivers.

  Currently, there are several approaches to overcome the ultra-high speed requirements of ADCs for UWB applications. For instance, some authors propose to reduce the sampling rate by dividing the whole bandwidth into several sub-bands and adopting a parallel architecture where each ADC operates with a fraction of the required sampling frequency [Nam03], [Hoy04]. However, the major drawback of this approach is that there appear many issues related with mismatches between different sub-bands and it requires extra complexity for integrating multiple signals.

  Another very popular alternative is to reduce the sampling rate down to frame-rate or symbol-rate. This is done by implementing the matched filter operation in the analog domain and then sampling its output at the desired rate (see for instance, [Gez04], [Tan05b], [Tia02] or [Tia05a], among many other). Unfortunately, there are two major drawbacks for this popular approach. First, the correlation required in the matched filter operation must be performed in the analog domain. Consequently, many circuit mismatches and instabilities may be encountered in the analog implementation. Second, the received signal must be perfectly known for implementing the matched filter, and this is not a realistic assumption in practical UWB receivers.

  Finally, a simple approach is being proposed by some authors based on a single ADC for digitizing the whole bandwidth of the received UWB signal. This is done by taking advantage of the tradeoff between sampling rate and number of bits per sample [Wal99]. In this sense, high sampling rates can be achieved by ADCs at the expense of reducing the number of bits per sample. For instance, high-speed single-bit ADCs are proposed in [Hoy03] and [Hoy05] to implement fully digital UWB receivers. This single-bit approach seems reasonable since the noise-like spectrum of UWB signals is similar to the one claimed in traditional spread-spectrum systems for adopting just one bit for the analog-to-digital conversion at the receiver. However, there is a significant degradation loss in single-bit receivers when the input signal has a large dynamic range (e.g. because of the presence of a strong interfering signal). In that case, more bits per sample are required and the

available sampling rate dramatically falls down [Le05].

This last approach based on a single ADC for covering the whole UWB frequency range is the most flexible and appropriate for a fully digital implementation of the signal processing techniques at the receiver. Commercial ADCs with sampling rates on the order of $1-3$ Gsps are already available. Moreover, the rapid advances in VLSI technology are making possible the commercial release of ADCs with sampling rates over 20 Gsps in the short-term [Nos04]. Therefore, the adoption of ultra-high speed ADCs for implementing a fully digital UWB receiver is now possible, and this will be the approach assumed in this dissertation.

2.6.2 Signal processing challenges

Current challenges in signal processing techniques for UWB systems are related to the accomplishment of the severe spectral regulations and how to reliably detect the transmitted information in the presence of unknown pulse distortion at the receiver. Some of the ongoing research efforts are briefly summarized herein.

- **Optimal pulse shaping.** The carrierless nature of original UWB signals is a key feature that allows simple and low-cost hardware implementation. However, this comes at the expense of limiting the emissions in order to avoid any possible harmful interference with existing wireless services. To this end, spectral regulations have been issued and the result is a set of spectral masks that any UWB device must accomplish for safe operation with neighboring narrowband equipments.

  Spontaneously generated UWB pulses do not in general accomplish the required spectral masks unless some kind of pre-processing is applied. As a result, it turns out that optimal pulse shapes for UWB signals must be carefully designed to achieve two basic objectives. First, to accomplish the required spectral masks. Second, to maximize the signal-to-noise ratio at the receiver. To this end, several proposals can be found in the literature. For instance, pulses satisfying the FCC spectral mask are presented in [Par03]. However, these proposed pulses do not optimally exploit the allowable bandwidth and transmit power. Another alternative is the adoption of orthogonal pulses as proposed in [Wu04] which satisfy the FCC spectral mask and allow multiple sub-band allocation.

- **Channel estimation.** The unique features of UWB signals make channel estimation to significantly differ from the approaches adopted in traditional narrowband and/or spread spectrum communication systems.

  On the one hand, most of the known channel estimation techniques for narrowband communications are based on deterministic properties of cyclostationary modulations (see for instance, [Liu94], [Ton94], [Hua96b], [Mou95], [Lou00]). As a result, high signal-to-noise

ratios are required for these techniques to succeed. However, the very low-power of UWB signals results in a very low signal-to-noise ratio (SNR) at the receiver. Thus, specific channel estimation techniques are required for UWB signals by taking into consideration the very low SNR of practical UWB working scenarios.

On the other hand, traditional channel estimation techniques focus on the estimation of the impulse response of the propagation channel. For the case of UWB signals, this may involve hundreds of delays and amplitudes to be estimated requiring an incredible sampling rate for resolving independent multipaths. Some contributions based on this approach can be found in the literature, for instance, the iterative method proposed in [Lot00]. However, it is always recommended to avoid such a huge computational complexity. To this end, research efforts in channel estimation for UWB systems should be directed toward the estimation of the aggregate channel response given by the transmitted pulse and the propagation channel itself. This is an unstructured approach in which the paths of the propagation channel are completely disregarded and the received waveform is just considered as a whole [Car03]. In addition, a closed-form solution is also appreciated to avoid iterative solutions that may require high computational complexity and may suffer from divergence issues in the presence of low-SNR abnormals. A solution to these issues is proposed in Chapter 4.

- **Timing synchronization.** Timing synchronization has received significant attention in the last decades in the context of narrowband carrier-based linear modulations [Gar88], [Men97], [Váz00]. However, the carrierless nature of UWB signals, their very low duty cycle operation, and the pulse distortion caused by the propagation channel and radiating elements, they all make the timing synchronization a completely different problem for the case of UWB systems. In addition to this, UWB systems employ extremely-short pulses with very low-power. Consequently, timing requirements are stringent because even minor timing misalignments result in lack of energy capture which may render symbol detection impossible [Tia05b], [Tia05c].

  The most challenging issue in the timing synchronization of UWB signals is concerned with the pulse distortion of the received signal. The reason is that the unknown shape of the received pulses prevents the implementation of traditional correlation-based timing detectors. Some methods have been proposed in the recent literature to cope with this problem. For instance, data-aided techniques for the timing recovery of UWB signals have been proposed in [Tia05d], [Tia05e] based on the generalized likelihood ratio test. In [Yan03b], a data-aided technique is also proposed to recover the timing error by correlation with successive pieces of received signal and data-aided joint timing and channel estimation is proposed in [Car06b].

  Although data-aided techniques provide the best possible performance, a significant drawback is that they require some kind of pre-alignment to match the incoming data with the

local replica of the training sequence. Therefore, some kind of prior pre-synchronization is required and this involves extra complexity to the system design. In order to avoid this problem, nondata-aided techniques for the timing recovery of UWB signals are being pursued. The advantage is that no prior pre-alignment is required and thus timing synchronization can be switched on at any time. Moreover, since no training sequence is transmitted, the effective throughput is maximized and the mean transmitted power is minimized.

Many nondata-aided timing recovery techniques have been proposed in the literature based on the concept of dirty template [Yan04a], [Yan05]. The idea behind dirty templates is to use part of the received signal as the correlation template. This is similar to the transmitted-reference (TR) approach where an unmodulated pulse is transmitted prior to each modulated pulse. In that way, the receiver can always take the unmodulated pulse as the reference pulse for correlation [Rus64], [Hoc02], [Cha03]. However, the major drawback of timing recovery based on dirty templates is that a relatively high-SNR is required. Therefore, optimal nondata-aided timing recovery for low-SNR scenarios is still a pending issue in the timing synchronization of UWB signals. This problem will be addressed in Chapter 6.

- **Data detection in the absence of CSI.** Because of the unknown pulse distortion at the receiver, reliable data detection for UWB systems becomes a challenging task. When no channel state information is available at the receiver, noncoherent receivers are the simplest and most cost-effective alternative to the much more complex approach of estimating the channel and then implementing a coherent receiver. Noncoherent receivers for UWB signals have been proposed in [Yan04c] and [Yan06], again, based on the concept of dirty template, and in [Car06a] for the case of orthogonal PPM modulation. However, further research is still required to determine the optimal data detection strategy. Two major issues are of special interest. First, the case in which there is waveform overlapping because of the excessive delay spread of the multipath channel. Second, the case in which the received waveform exhibits random time variations because of the path-dependent distortion introduced by relative movements between transmitter and receiver or by moving objects in-between. These issues will be addressed in Chapter 5.

Chapter 3

Performance Limits of Coherent and Non-coherent Ultra-Wideband Communications

3.1 Introduction

In this chapter, the asymptotic performance of UWB communication systems is analyzed from an information theoretic point of view. To this end, the conditions for which an arbitrarily small error probability can be achieved are evaluated, and the emphasis is placed on both coherent and non-coherent receivers operating over multipath fading channels.

On the one hand, coherent receivers are optimal in the sense that they exploit the perfect knowledge of the end-to-end channel response. This channel state information is usually obtained by using some kind of channel estimation technique prior to the symbol detection stage. With proper channel knowledge, coherent receivers consist of a traditional correlator-based architecture where a replica of the transmitted pulse is used to implement a matched filtering or Rake receiver [Win98], [Zha03]. On the other hand, non-coherent receivers do not perform channel estimation and thus, they can be seen as a low-cost and low-power alternative to the more complex and computationally demanding coherent receivers [Car06a]. The save in hardware complexity is especially important because channel estimation is usually found to require about 60 % of the total number of gates in the hardware implementation of an UWB coherent receiver [Yan04b].

A fair decision on whether to use coherent or non-coherent receivers is a question that basically depends on the signal-to-noise ratio, the transmitted bandwidth and the modulation format. The interplay between these parameters will be analyzed in this chapter and some

performance metrics will be provided to shed light on the decision to be made.

The structure of this chapter is the following. The mostly adopted modulation formats for UWB communication systems are first presented in Section 3.2. This is an important topic because the ultimate performance of any communication system directly depends on the way the information is conveyed by the transmitted signal. Next, Section 3.3 reviews some information theoretic aspects related to the channel capacity and the achievable data rates in the wideband regime. Note that the wideband regime is of interest for the case under study due to the very large spectral occupancy of UWB signals. The limits for reliable communication are presented in Sections 3.4 and 3.5 for coherent and non-coherent UWB receivers, respectively. Finally, a comparison between these two approaches is presented in Section 3.6.

3.2 Modulation Formats for UWB Communication Systems

3.2.1 PAM or PPM modulation?

The achievable data rate of any communication system is intimately related to the way the information is conveyed by the transmitted signal. For this reason, before addressing the performance evaluation of UWB communication systems, it is first mandatory to analyze the most convenient modulation format for reliable communication with UWB signals.

As already mentioned in Section 2.4, the mostly adopted modulation formats for UWB signals are pulse-amplitude modulation (PAM) and pulse-position modulation (PPM). PAM modulation requires perfect channel state information in order to resolve the ambiguity introduced by the channel in the amplitude of the received signal. In contrast, PPM modulation can be either adopted in the presence or in the absence of channel state information. That is, PPM modulation can be adopted by either coherent or non-coherent receivers. This is a very important issue because non-coherent detection is essential in most realistic UWB systems. This is due to the severe distortion experienced by transmitted pulses when propagating through the UWB multipath channel. It is found that the received pulses have very little resemblance with the transmitted ones [Qiu02], [Qiu05], but most importantly, the pulse distortion is found to be direction-dependent so that it varies when the receiver looks at the transmit antenna from different directions [Cra02], [Sch05a]. In addition to this, the very large multipath resolution of UWB signals makes the computation of fast and accurate channel estimates a challenging and computationally demanding task. Consequently, the possibility of avoiding channel estimation, and thus implementing low-complexity and non-coherent detection, is certainly appreciated.

Apart from traditional PPM modulation, there are several variations including multipulse PPM (MPPM), overlapping PPM (OPPM) and differential PPM (DPPM), among other. Interestingly, they all can be regarded as a constrained version of a more general pulse modulation

method called on-off keying (OOK) modulation. In OOK modulation a single bit is transmitted per channel use. That is, a pulse is transmitted within the symbol duration for representing "1" and no pulse is transmitted for representing "0". An important point to be taken into consideration is that, since PPM, MPPM, OPPM and DPPM are each a constrained version of OOK modulation, the capacity of unconstrained OOK becomes the upper bound on the capacity of these pulse-position modulation formats. As it is shown in [Ham04], the capacity of PPM is found to be near that of OOK for the low-SNR regime. Consequently, and for the low-SNR regime, no other constrained version of OOK modulation (e.g. MPPM, OPPM or DPPM) can offer a significant improvement over traditional PPM. Since one of the emphases of this work is to focus on the low-SNR regime, we will not consider MPPM, OPPM nor DPPM hereafter but only the standard and traditional PPM modulation as a reference benchmark.

In the sequel, only PPM modulation will be considered for analyzing the performance limits of UWB communication systems. The reason to focus on PPM modulation is that it allows either coherent or non-coherent reception so that a more general overview of UWB communications can be obtained. On the contrary, PAM modulation is only of interest when perfect channel state information is available and thus, the potential interest of PAM in hostile propagation environments is very limited.

3.2.2 Signal model for PPM modulation

Since the performance analysis of UWB systems will be based on PPM modulation, the signal model for this modulation format is presented herein. Let us consider the following discrete-time model for the received signal corresponding to a single transmitted PPM symbol,

$$\mathbf{y} = \mathbf{H}\mathbf{x}_i + \mathbf{w} \tag{3.1}$$

where $\mathbf{y} \in \mathbb{R}^{N_{ss}\times 1}$ is the vector of received samples with N_{ss} the number of samples per symbol. The vector $\mathbf{w} \in \mathbb{R}^{N_{ss}\times 1}$ incorporates the Gaussian contribution from both the thermal noise and possible multiple access interference with $\mathbf{C}_w \doteq \mathrm{E}\left[\mathbf{w}\mathbf{w}^T\right]$. The $(P \times 1)$ vector $\mathbf{x}_i$ corresponds to the i-th PPM symbol from the PPM codebook $\mathcal{X} : \{\mathbf{x}_0, \mathbf{x}_1, \ldots, \mathbf{x}_{P-1}\}$. Only the i-th entry in $\mathbf{x}_i$ is active. That is, $[\mathbf{x}_i]_i = 1$ and $[\mathbf{x}_i]_j = 0$ for all $j \neq i$. Thus, a PPM modulator can be understood as an encoder producing $P = 2^b$ codewords of a $(2^b, b)$ orthogonal code. The shaping matrix $\mathbf{H} \in \mathbb{R}^{N_{ss}\times P}$ incorporates the end-to-end channel response between transmitter and receiver. The columns of the shaping matrix $\mathbf{H}$ are indicated by $\mathbf{h}_i$ with $\mathbf{H} = [\mathbf{h}_0, \mathbf{h}_1, \ldots, \mathbf{h}_{P-1}]$ and they contain time-shifted replicas of the end-to-end channel response with the time-shift equal to N_Δ samples, as illustrated in Figure 3.1.

From the observation of Figure 3.1, the end-to-end channel response has a maximum length of N_g samples. Then, by taking into consideration the maximum delay spread of the channel and the maximum PPM time-shift, a guard interval is introduced in order to avoid intersymbol

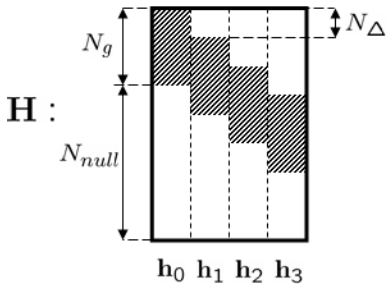

Figure 3.1: Schematic representation of the shaping matrix $\mathbf{H}$ for the case of $P = 4$.

interference with the next received symbol. Since no time-hopping is assumed here for the sake of simplicity, the condition for avoiding intersymbol interference is

$$N_{ss} \geq N_g + (P-1)N_\Delta. \tag{3.2}$$

Later on, it will be useful to incorporate the N_g samples of the channel response into a vector indicated herein by $\mathbf{g}$, with $\mathbf{g} \in \mathbb{R}^{N_g \times 1}$. Indeed, the effective channel response $\mathbf{g}$ is included in the columns of the shaping matrix $\mathbf{H}$ as follows,

$$\mathbf{h}_i = \Big[\underbrace{0,0,\ldots,0,0}_{iN_\Delta}, \mathbf{g}^T, \underbrace{0,0,\ldots,0,0}_{N_{ss}-iN_\Delta-N_g}\Big]^T. \tag{3.3}$$

Finally, an important remark must be made with respect to the statistical properties of the end-to-end channel response. Two different approaches are considered in this dissertation depending on whether coherent or non-coherent receivers are considered.

- **Coherent receiver:** In this case, the end-to-end channel response is assumed to be perfectly known at the receiver side. Therefore, the only nuisance parameter is the Gaussian contribution from the noise. As a result, the probability density function of the received signal $\mathbf{y}$ conditioned on the transmission of the PPM codeword $\mathbf{x}_i$ and a given channel response $\mathbf{g}$ becomes

$$f_{\text{coh}}\left(\mathbf{y}|\mathbf{x}_i, \mathbf{g}\right) = \frac{1}{(2\pi)^{N_{ss}/2}\det^{1/2}\left(\mathbf{C}_w\right)} \exp\left(-\frac{1}{2}\left(\mathbf{y}-\mathbf{h}_i\right)^T \mathbf{C}_w^{-1}\left(\mathbf{y}-\mathbf{h}_i\right)\right). \tag{3.4}$$

- **Non-coherent receiver:** In this case, the end-to-end channel response is assumed to be an unknown random Gaussian process. Since the unknown end-to-end channel response and the noise are statistically independent, the probability density function of the received signal $\mathbf{y}$ conditioned on the transmission of the PPM codeword $\mathbf{x}_i$ is

$$f_{\text{non-coh}}\left(\mathbf{y}|\mathbf{x}_i\right) = \frac{1}{(2\pi)^{N_{ss}/2}\det^{1/2}\left(\mathbf{C}_w + \mathbf{C}_{\mathbf{h}_i}\right)} \exp\left(-\frac{1}{2}\mathbf{y}^T\left(\mathbf{C}_w + \mathbf{C}_{\mathbf{h}_i}\right)^{-1}\mathbf{y}\right) \tag{3.5}$$

with $\mathbf{C}_{\mathbf{h}_i} \doteq \mathrm{E}\left[\mathbf{h}_i\mathbf{h}_i^T\right]$ the covariance matrix for the received waveform under the hypothesis $\mathcal{H}_i : \mathbf{x} = \mathbf{x}_i$. That is, the covariance matrix for the i-th column of the shaping matrix $\mathbf{H}$.

In the sequel, the probability density functions presented in (3.4) and (3.5) will be adopted for obtaining the performance limits of both coherent and non-coherent communication.

3.3 Review of Information Theoretic Results for Wideband Communications

3.3.1 Power efficiency in the wideband regime

Power efficiency is, without any doubt, the most important issue in the design of communication systems where power consumption is the limiting factor. An example of these communication systems can be found in wireless, deep space and sensor networks devices, among other. In particular, UWB systems can also be incorporated into this group of low power operating devices. The reason for the low power operation of UWB systems is not only power consumption but also coexistence and interference avoidance with other systems. In this sense, the Federal Communications Commission restricts the radiation emissions of UWB systems in order to avoid possible interference with existing wireless services. For instance, the power spectral density of UWB signals must be smaller than -41 dBm/Mhz in the $[3.1 - 10.6]$ GHz band and smaller than -75 dBm/Mhz in the GPS band [FCC02].

Related with the above considerations, a topic that will receive significant attention within this chapter is the interplay between the low signal-to-noise ratio (SNR) regime and the wideband regime. The relationship can be found in the fact that the limit of zero SNR is equivalent to the limit of infinite bandwidth, assuming the transmitted power to be constant. The proof is straightforward from the definition of the signal-to-noise ratio,

$$\mathsf{SNR} \doteq \frac{P_{\mathrm{S}}}{P_{\mathrm{N}}} = \frac{P_{\mathrm{S}}}{N_0 W} \tag{3.6}$$

with P_{S} the signal power, P_{N} the noise power, $\frac{N_0}{2}$ the double-sided noise spectral density and W the transmitted bandwidth. Then, for constant signal power, the limit of zero signal-to-noise ratio can be driven by the limit of infinite bandwidth. That is,

$$\lim_{W\to\infty} \mathsf{SNR} = \lim_{W\to\infty} \frac{P_{\mathrm{S}}}{N_0 W} = 0. \tag{3.7}$$

For this reason, the low-SNR regime and the infinite-bandwidth regime are often used indistinguishably in many contributions in the field of information theory [Por05].

Coming back to the power efficiency requirement, it is interesting to note that a measure for power efficiency can be obtained from the notion of channel capacity. For a given signal-to-noise ratio, channel capacity indicates the maximum data rate for which reliable communication is possible, understanding *reliable* as having an arbitrarily small error probability. Thus, achieving

capacity can be understood as the optimal use of the available power resources. In [Sha48], Shannon showed that the capacity of an ideal bandlimited additive white Gaussian noise (AWGN) channel is given by

$$\mathsf{C} = W \log_2 \left(1 + \frac{P_S}{W N_0}\right) \quad \text{(bits/s)}. \tag{3.8}$$

For the case of the infinite-bandwidth, i.e. $W \to \infty$, the capacity results in

$$\mathsf{C}_\infty \doteq \lim_{W\to\infty} \mathsf{C} = \frac{P_S}{N_0} \log_2 e \quad \text{(bits/s)}. \tag{3.9}$$

That is, the channel capacity depends linearly on the signal power P_S when operating under the wideband (i.e. low-SNR) regime. This is an important feature of the wideband or low-SNR regime, and it is in contrast with the behavior exhibited for limited bandwidth or medium to high SNR, where the capacity depends much more slowly on the signal power because of the logarithmic function in (3.8).

An important issue to be taken into consideration is that channel capacity is a theoretical upper bound on the error-free performance of a communication system. In that sense, two major remarks should be made. First, the upper bound behavior implies that no reliable communication is possible for a data rate greater than capacity. Second, capacity is a theoretical bound and thus, no specific guidelines are provided on how to design capacity achieving communication systems. However, it is a known result that the AWGN wideband capacity in (3.9) can be achieved by certain communication systems. For instance, [Gol49] showed that wideband capacity can be achieved by using PPM modulation with vanishing duty cycle. That is, when the fraction of time used for transmission tends to zero. Equivalently this means that wideband capacity can be achieved by using M-ary orthogonal signaling as long as $M \to \infty$ [Tur59]. Consequently, there is not much to worry about since achieving capacity is found to be a feasible goal.

3.3.2 Asymptotic performance over fading channels

A step forward can be done by considering fading communication channels. Here, a striking result was noted by [Ken69] in the sense that channel capacity for the AWGN is not affected by the presence of fading as long as the bandwidth is large enough. That is,

$$\mathsf{C}_\infty^{\text{AWGN}} = \mathsf{C}_\infty^{\text{fading}}. \tag{3.10}$$

The result in (3.10) was also noted by [Gal68] and it was initially conceived for the case of Rayleigh fading channels. However, an extension was presented by [Tel00] to show that wideband capacity for the AWGN channel is indeed a rather general result that coincides with wideband capacity for a general class of fading channel models. In addition, the result in (3.10) assumes the absence of channel state information at the transmitter, but it holds regardless of whether channel state information is available at the receiver or not.

The wideband capacity identity in (3.10) has important consequences in our study of coherent and non-coherent UWB communications. In particular, the result in (3.10) claims that the same achievable data rates can be achieved in the presence of fading regardless of whether coherent or non-coherent receivers are adopted. However, this is a rather daring assumption and some fine analysis will be required in order to determine the conditions for this to occur. In any case, it is interesting to question ourselves how the wideband capacity can be achieved by practical communication systems over fading channels. Some answers can be found in [Jac63] and [Pie66], where the wideband capacity over Rayleigh fading was found to be achieved by using M-ary orthogonal frequency shift keying (FSK) with vanishing duty cycle and non-coherent detection. This result was extended by [Luo02] to show that FSK with vanishing duty cycle can achieve capacity on ultra-wideband channels even with limits on bandwidth and peak power.

Among all the results for capacity achieving communication systems, a common characteristic is the *peakiness* of the transmitted signals either in time or frequency. This fact is confirmed in [Ver02b] where a formal proof is presented to show that *peaky*- or *flash*-signaling on-off schemes are required to achieve capacity when there is no channel knowledge at the receiver. Consequently the impulsive nature of UWB signals seems to be inherently designed to achieve capacity with non-coherent receivers. However there are some drawbacks associated with peaky signaling. The optimal input signals for non-coherent receivers are increasingly peaky as the SNR diminishes and thus, communication systems with some kind of peakiness constraint (i.e. peak-to-average power) experience a severe degradation in the low-SNR regime. Peakiness constraints and their impact on second and fourth order moments of the input signal are addressed in [Gur05a]. The results in [Gur05a] show that communication systems with average power and peak-to-average power constraints require infinite energy per bit in the limit of infinite bandwidth when no channel state information is available at the receiver.

Unfortunately, the conclusion from the above statement is that practical peaky signaling schemes are not likely to achieve wideband capacity when peakiness constraints are imposed due to spectral regulations. Thus, we now see that achieving wideband capacity may not be an attainable goal for certain communication systems. Even though, a pending issue is to determine how close the ultimate performance can be to that limit.

3.3.3 Wideband optimality and minimum E_b/N_0

Most information theoretic studies for wideband channels are based on extrapolating the results obtained under the hypothesis of infinite bandwidth. Based on this assumption, the following statements are usually claimed,

- Wideband capacity is not affected by fading.

- Channel state information does not alter wideband capacity.
- On-off signaling is wideband optimal.

However, the above claims suffer from some inaccuracies when ignoring the real effect of finite bandwidth and peakiness constraints on the behavior of channel capacity. Indeed, little attention is usually paid to the convergence rate at which wideband capacity is achieved as a function of bandwidth. In that case, it would be found that on-off signaling is no longer optimal since it requires six times the minimum bandwidth to achieve capacity [Ver02a]. This example illustrates the importance of considering the convergence rate of spectral efficiency as a crucial measure for determining optimality.

In the analysis of capacity, one of the most important parameters to be considered is the convergence rate as a function of energy-per-bit to noise spectral density, E_b/N_0, where

$$\frac{E_b}{N_0} = \frac{W}{R}\mathsf{SNR} = \frac{\mathsf{SNR}}{\frac{R}{W}} \tag{3.11}$$

with R the data rate in bits/s. In particular, it is found that achieving capacity with infinite bandwidth is equivalent to achieving minimum E_b/N_0. That is,

$$\left(\frac{E_b}{N_0}\right)_{\min} \equiv \left(\frac{E_b}{N_0}\right)_{|R=\mathsf{C}_\infty} = \frac{\mathsf{SNR}}{\frac{\mathsf{C}_\infty}{W}} = \log 2 = -1.59 \text{ dB}. \tag{3.12}$$

Consequently, achieving the minimum energy per bit has also been adopted as a synonym of asymptotic optimality in the wideband regime. Due to the interplay between wideband regime (i.e. $W \to \infty$) and vanishing SNR (i.e $\mathsf{SNR} \to 0$), the minimum energy per bit in (3.12) can also be expressed as

$$\left(\frac{E_b}{N_0}\right)_{\min} = \lim_{W\to\infty} \frac{\mathsf{SNR}}{\frac{R}{W}} = \lim_{\mathsf{SNR}\to 0} \frac{\mathsf{SNR}}{\mathsf{C}(\mathsf{SNR})} \tag{3.13}$$

where $\mathsf{C}(\mathsf{SNR}) = \frac{R}{W}$ is now the capacity in bits/s/Hz.

The identity in (3.13) is particularly interesting because it clearly indicates that minimum energy per bit is defined in the limit of $\mathsf{SNR} \to 0$. Since capacity is a positive concave and monotically decreasing function for decreasing SNR, we have that $\lim_{\mathsf{SNR}\to 0} \mathsf{C}(\mathsf{SNR}) = 0$. Then, minimum energy per bit is indeed defined in the limit of $\mathsf{C} \to 0$. This is a very subtle aspect now, but it will become a key issue in the convergence analysis of wideband capacity to be presented later on.

3.3.4 First and second order analysis of spectral efficiency

The topic of spectral efficiency, that is, the capacity behavior as a function of E_b/N_0, is analyzed in [Ver02b] based on the second order Taylor expansion of the channel capacity,

$$\mathsf{C}(\mathsf{SNR}) = \mathsf{C}'(0)\mathsf{SNR} + \frac{1}{2}\mathsf{C}''(0)\mathsf{SNR}^2 + o\left(\mathsf{SNR}^2\right) \tag{3.14}$$

with $\mathsf{C}'(0)$ and $\mathsf{C}''(0)$ the first and the second derivatives of the channel capacity evaluated at $\mathsf{SNR} = 0$. One of major contributions of [Ver02b] is that it establishes a clear link between spectral efficiency and the derivatives of the channel capacity in the wideband regime.

- **Role of $\mathsf{C}'(0)$:** The first derivative of channel capacity at $\mathsf{SNR} = 0$, $\mathsf{C}'(0)$, is intimately related with the minimum required bit energy for reliable communication. In particular, [Ver02b] shows that

$$\left(\frac{E_b}{N_0}\right)_{\min} = \frac{1}{\mathsf{C}'(0)}. \tag{3.15}$$

  The result in (3.15) can easily be proved by substituting the Taylor expansion (3.14) into (3.13). For the AWGN and Rayleigh or Rice fading channels with channel state information, the first derivative results in $\mathsf{C}'(0) = \frac{1}{\log 2}$ so that the minimum required (E_b/N_0) for reliable communication becomes the well-known value of $(E_b/N_0)_{\min} = \log 2 = -1.59$ dB.

  Furthermore, communication systems achieving the limit of $(E_b/N_0)_{\min}$ are defined as *first order optimal*. First order optimality is ensured for coherent receivers and it is also achieved by non-coherent receivers as long as unconstrained peaky signaling is allowed in the wideband regime.

- **Role of $\mathsf{C}''(0)$:** The second derivative of channel capacity at $\mathsf{SNR} = 0$, $\mathsf{C}''(0)$, is related with the rate of convergence at which $(E_b/N_0)_{\min}$ is achieved. That is, $\mathsf{C}''(0)$ is related with the slope of the channel capacity versus E_b/N_0 curve at $\mathsf{SNR} = 0$. This slope is indicated by $\mathcal{S}_0$ and it is referred to as the *wideband slope*. In [Ver02b], the wideband slope is expressed as

$$\mathcal{S}_0 = -2\frac{[\mathsf{C}'(0)]^2}{\mathsf{C}''(0)} \quad \text{(bits/s/Hz/3 dB)} \tag{3.16}$$

  and it is defined as the increase in bits/s/Hz that is experienced when increasing 3 dB in the energy per bit from $(E_b/N_0)_{\min}$.

  It is interesting to note that the wideband slope depends crucially on the receiver knowledge of the channel. For a general class of fading channels, the second derivative $\mathsf{C}''(0)$ is a finite nonzero value when channel state information is available at the receiver. Consequently, a finite nonzero value is obtained for the wideband slope of coherent receivers. However, $\mathsf{C}''(0) = -\infty$ when the channel is unknown to the receiver. Thus, the wideband slope for non-coherent receivers is found to be $\mathcal{S}_0 = 0$ and wideband capacity is achieved much more slowly than for the coherent case.

  Finally, communication systems achieving both the wideband slope and $(E_b/N_0)_{\min}$ are defined as *second order optimal*.

From the above considerations, the convergence rate analysis of capacity is intimately related with channel knowledge at the receiver and peakiness constraints. For the sake of clarity, some examples of capacity curves with first and second order optimality are depicted in Figure 3.2.

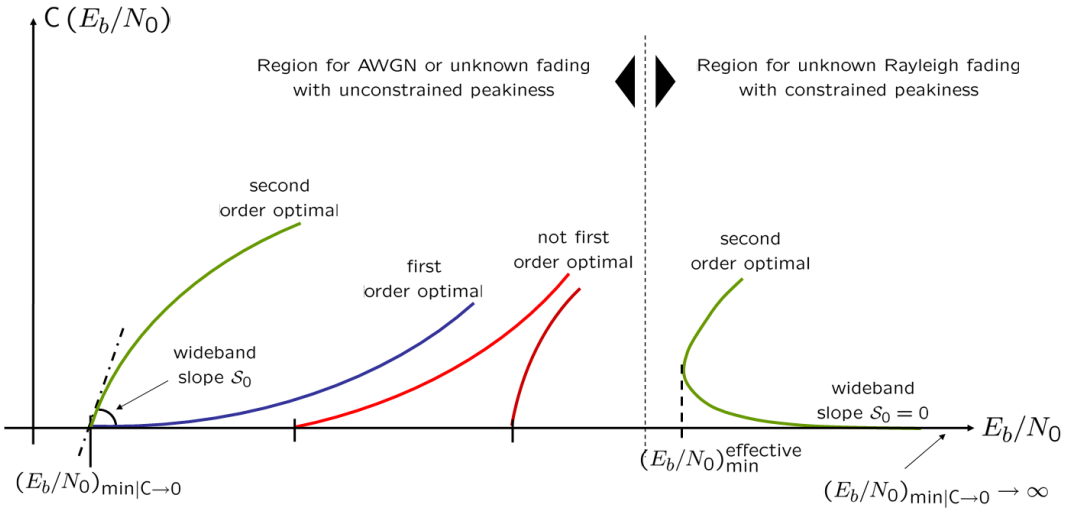

Figure 3.2: Examples of different capacity curves for illustrating the concepts of first and second order optimality.

A brief presentation of the different working scenarios to be considered is presented in Table 3.1. The most important conclusion to be drawn from this table is that the absence of channel knowledge (i.e. non-coherent receivers) results in the wideband slope to be $\mathcal{S}_0 = 0$. This is in contrast with AWGN channels (i.e. coherent receivers) where the wideband slope is $\mathcal{S}_0 = 2$. As a result, non-coherent receivers can be seen to be trapped in the region of $\mathsf{C} \to 0$ because a large increase in bit energy is required to achieve the non-null capacity region when departing from the limit of $\mathsf{C} \to 0$. That is, a zero wideband slope indicates that even when the bit energy is increased in 3 dB, the resulting capacity is still zero. In contrast, a 3 dB increase in bit energy for coherent receivers results in capacity to move from $\mathsf{C} = 0$ to $\mathsf{C} = 2$ bits/s/Hz, as observed in Figure 3.3 for the AWGN channel when optimal Gaussian inputs are considered.

Another important remark to be made is the one regarding the infinite minimum bit energy required by non-coherent receivers under peakiness constraints. As shown in [Gur05b], when the channel is unknown but no peaky-signaling is allowed because of peak constraints, then $\mathsf{C}'(0) = 0$ and infinite minimum bit energy is required when $\mathsf{C} \to 0$. That is, non-coherent receivers converge much more slowly to the wideband capacity because of the difficulty in escaping from the $\mathsf{C} \to 0$ region. This also means that operating at very low SNR (i.e. $\mathsf{SNR} \to 0$ and thus, $\mathsf{C} \to 0$) is power inefficient and the practical (i.e. the effective) minimum bit energy is achieved for a nonzero value of capacity. This is in contrast with traditional AWGN channels, where minimum bit energy is always achieved at $\mathsf{C} = 0$.

		$(E_b/N_0)_{\min}$	$\mathcal{S}_0$
Unconstrained peakiness	AWGN	$\log 2$	2
	Unknown Rayleigh or Rice fading	$\log 2$	0
Constrained peakiness	AWGN	$\log 2$	2
	Unknown Rayleigh fading	∞	0
	Unknown Rice fading†	$\left(1+\frac{1}{K}\right)\log 2$	$\frac{2K^2}{(1+K)^2-\kappa}$

† Assuming a finite and known specular component. The Ricean factor is indicated by K and κ stands for the peak-to-average constraint.

Table 3.1: Convergence rate analysis of capacity as a function of the channel knowledge and peakiness constraints.

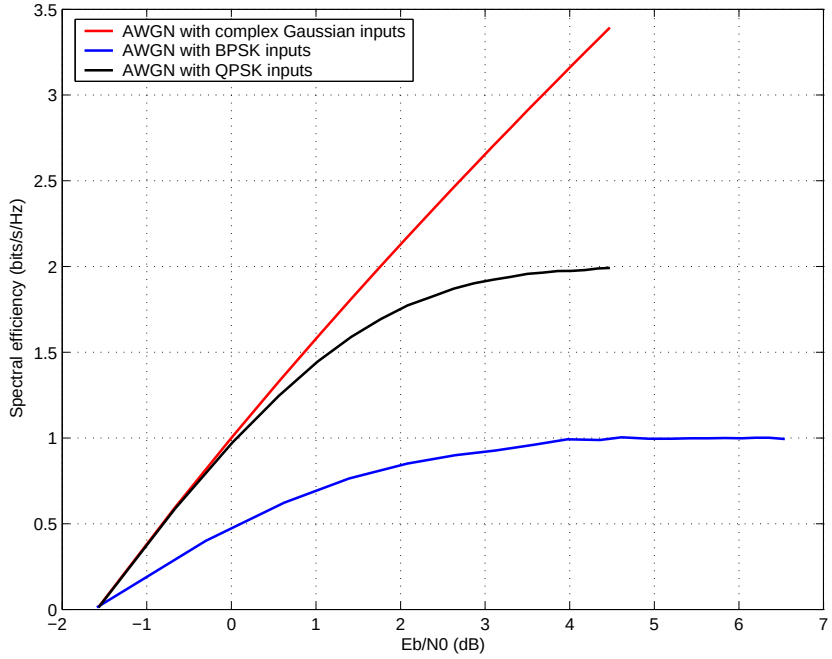

Figure 3.3: Spectral efficiency (i.e. capacity as a function of E_b/N_0) for the AWGN channel with Gaussian inputs, BPSK and QPSK modulation.

From the above considerations, the purpose of this chapter is to evaluate in a quantitative manner the loss incurred by the slow rate of convergence of practical non-coherent receivers. To this end, Section 3.4 and Section 3.5 analyze the exact channel capacity for practical coherent and non-coherent UWB receivers, respectively.

3.3.5 Constellation-Constrained Capacity

It is important to remark that channel capacity as presented so far is just a particular case of a more general definition of channel capacity. In particular, channel capacity is defined as the maximum of the mutual information between the channel input $\mathbf{x}$ and channel output $\mathbf{y}$ over all distributions of the input $f(\mathbf{x})$ that satisfy a given power constraint $\mathrm{P_c}$. That is,

$$\mathsf{C} \doteq \max_{f(\mathbf{x}):\mathrm{P_c}} I(\mathbf{x};\mathbf{y}) \tag{3.17}$$

where the mutual information $I(\mathbf{x};\mathbf{y})$ is the relative entropy between the joint distribution $f(\mathbf{x},\mathbf{y})$ and the product distribution $f(\mathbf{x})f(\mathbf{y})$ [Cov91],

$$I(\mathbf{x};\mathbf{y}) \doteq \int_{\mathbf{x}}\int_{\mathbf{y}} f(\mathbf{x},\mathbf{y}) \log_2 \frac{f(\mathbf{x},\mathbf{y})}{f(\mathbf{x})f(\mathbf{y})} d\mathbf{x}d\mathbf{y}. \tag{3.18}$$

For the AWGN channel, the optimal input distribution is Gaussian and the capacity results in the compact expression presented in (3.8) due to [Sha48]. However, this result is usually taken for granted and little attention is paid to the fact that (3.8) can only be achieved when the input distribution is Gaussian. Clearly, this cannot happen when dealing with digital communication systems. The reason is that digital communications are based on the transmission of information symbols from a finite alphabet and thus, the input distribution is not continuous but discrete. Indeed, the AWGN channel capacity in (3.8) can also be achieved with discrete input distributions, but this requires an asymptotically large alphabet with equiprobable symbols [Sun93]. Practical communication systems usually operate with a reduced alphabet so that the capacity achieving assumption in [Sun93] cannot be applied. As a result, a redefinition of channel capacity is required for digital transmissions.

For the case of digital communication systems, the so-called *constellation-constrained capacity* establishes a benchmark on the best rate it can be achieved with a given discrete input distribution [Ung82], [Bla87]. Constellation constrained capacity is indicated herein by $\mathsf{C_c}$. It follows the definition in (3.17) by omitting the maximization over the input distribution, and substituting the integral over $\mathbf{x}$ in (3.18) by a discrete summation,

$$\mathsf{C_c} \doteq \sum_{\mathbf{x}} \int_{\mathbf{y}} f(\mathbf{x},\mathbf{y}) \log_2 \frac{f(\mathbf{x},\mathbf{y})}{f(\mathbf{x})f(\mathbf{y})} d\mathbf{y} \quad \text{(bits/channel use)}. \tag{3.19}$$

In the sequel, the units of capacity will be (bits/channel use) unless otherwise specified.

For the case of P-ary modulation with equiprobable transmitted symbols, we have that $p(\mathbf{x}=\mathbf{x}_i) = \frac{1}{P}$. In that case, a relatively simple expression can be derived for the constellation-

constrained capacity. That is,

$$\begin{aligned}
\mathsf{C_c} &= \sum_{\mathbf{x}_i} \int_{\mathbf{y}} f(\mathbf{y}|\mathbf{x}=\mathbf{x}_i)\, p(\mathbf{x}=\mathbf{x}_i) \log_2 \frac{f(\mathbf{y}|\mathbf{x}=\mathbf{x}_i)}{\sum_{\mathbf{x}_j} f(\mathbf{y}|\mathbf{x}=\mathbf{x}_j)\, p(\mathbf{x}=\mathbf{x}_j)} d\mathbf{y} && (3.20)\\
&= \frac{1}{P} \sum_{\mathbf{x}_i} \int_{\mathbf{y}} f(\mathbf{y}|\mathbf{x}=\mathbf{x}_i) \log_2 \frac{f(\mathbf{y}|\mathbf{x}=\mathbf{x}_i)}{\frac{1}{P}\sum_{\mathbf{x}_j} f(\mathbf{y}|\mathbf{x}=\mathbf{x}_j)} d\mathbf{y} && (3.21)\\
&= \frac{1}{P} \sum_{\mathbf{x}_i} \int_{\mathbf{y}} f(\mathbf{y}|\mathbf{x}=\mathbf{x}_i) \log_2 P d\mathbf{y} - \frac{1}{P} \sum_{\mathbf{x}_i} \int_{\mathbf{y}} f(\mathbf{y}|\mathbf{x}=\mathbf{x}_i) \log_2 \frac{\sum_{\mathbf{x}_j} f(\mathbf{y}|\mathbf{x}=\mathbf{x}_j)}{f(\mathbf{y}|\mathbf{x}=\mathbf{x}_i)} d\mathbf{y}\\
&= \log_2 P - \frac{1}{P} \sum_{\mathbf{x}_i} \int_{\mathbf{y}} f(\mathbf{y}|\mathbf{x}=\mathbf{x}_i) \log_2 \frac{\sum_{\mathbf{x}_j} f(\mathbf{y}|\mathbf{x}=\mathbf{x}_j)}{f(\mathbf{y}|\mathbf{x}=\mathbf{x}_i)} d\mathbf{y} && (3.22)
\end{aligned}$$

so that the constellation-capacity can be expressed as

$$\mathsf{C_c} = \log_2 P - \frac{1}{P} \sum_{i=0}^{P-1} \mathrm{E}_{\mathbf{y}|\mathbf{x}_i} \left[\log_2 \sum_{j=0}^{P-1} \frac{f(\mathbf{y}|\mathbf{x}=\mathbf{x}_j)}{f(\mathbf{y}|\mathbf{x}=\mathbf{x}_i)} \right]. \tag{3.23}$$

The final result in (3.23) provides a valuable interpretation of the notion of channel capacity. In particular, note that the argument of the $\log_2(\cdot)$ operator is indeed a sum of likelihood ratios. That is, the quotient $\frac{f(\mathbf{y}|\mathbf{x}=\mathbf{x}_j)}{f(\mathbf{y}|\mathbf{x}=\mathbf{x}_i)}$ in the right hand side of (3.23) is the likelihood ratio for deciding between the hypothesis $\mathcal{H}_i : \mathbf{x} = \mathbf{x}_i$ and the hypothesis $\mathcal{H}_j : \mathbf{x} = \mathbf{x}_j$. Let us indicate the likelihood ratio by $\Lambda_{j,i}(\mathbf{y})$ as follows,

$$\Lambda_{j,i}(\mathbf{y}) \doteq \frac{f(\mathbf{y}|\mathbf{x}=\mathbf{x}_j)}{f(\mathbf{y}|\mathbf{x}=\mathbf{x}_i)}. \tag{3.24}$$

In this way, the constellation-constrained capacity for equiprobable discrete inputs can be expressed in a more insightful manner as

$$\mathsf{C_c} = \log_2 P - \frac{1}{P} \sum_{i=0}^{P-1} \mathrm{E}_{\mathbf{y}|\mathbf{x}_i} \left[\log_2 \sum_{j=0}^{P-1} \Lambda_{j,i}(\mathbf{y}) \right]. \tag{3.25}$$

In the sequel, the constellation-constrained capacity in (3.25) will be evaluated for coherent and non-coherent UWB receivers. PPM modulation will be adopted since it is widely adopted in UWB communication systems and it allows for both coherent and non-coherent reception. Special emphasis will be devoted to spectral efficiency in the wideband regime, where coherent and non-coherent receivers are expected to exhibit rather different convergence rates.

3.4 Constellation-Constrained Capacity for Coherent PPM

In order to evaluate the constellation-constrained capacity in (3.25), let us first concentrate on the expression of the likelihood ratio $\Lambda_{j,i}$ defined in (3.24). For the case of coherent communication, channel state information is available at the receiver. Therefore the input distribution

conditioned on a given transmitted symbol $\mathbf{x}_i$ corresponds to the probability density function presented in (3.4). With the above considerations, the likelihood ratio $\Lambda_{j,i}(\mathbf{y})$ in (3.25) can be further manipulated to result in

$$\Lambda_{j,i}(\mathbf{y},\mathbf{g}) = \frac{\exp\left(-\frac{1}{2}\left(\mathbf{y}-\mathbf{h}_j\right)^T \mathbf{C}_w^{-1}\left(\mathbf{y}-\mathbf{h}_j\right)\right)}{\exp\left(-\frac{1}{2}\left(\mathbf{y}-\mathbf{h}_i\right)^T \mathbf{C}_w^{-1}\left(\mathbf{y}-\mathbf{h}_i\right)\right)} \tag{3.26}$$

$$= \exp\left(\frac{1}{2} Tr\left(\mathbf{C}_w^{-1}\left[2\mathbf{y}\left(\mathbf{h}_j-\mathbf{h}_i\right)^T + \mathbf{h}_i\mathbf{h}_i^T - \mathbf{h}_j\mathbf{h}_j^T\right]\right)\right). \tag{3.27}$$

According to the signal model in Section 3.2.2, the likelihood ratio for coherent detection depends on the particular realization of the end-to-end channel response $\mathbf{g}$ within $\mathbf{h}_i$, the i-th column of the channel shaping matrix. The fact is that the channel response is perfectly known for a given transmission but due to the specific propagation physics of UWB signals, the channel response may vary from transmission to transmission, and so does the capacity. As a result, capacity becomes random in the presence of unknown fading variations between consecutive symbol transmissions. In this situation a meaningful measure for channel capacity must resort to the expectation of the mutual information $I(\mathbf{x};\mathbf{y})$ over the channel statistics. To this end the so-called *ergodic* capacity is defined as

$$\mathsf{C}_{\mathsf{c}\,|\,\mathrm{coh}} = \mathrm{E}_{\mathbf{g}}\left[I\left(\mathbf{x};\mathbf{y}\right)\right]. \tag{3.28}$$

For the sake of simplicity, the noise contribution is assumed to be white herein. Despite of the very large bandwidth of UWB signals and the coexistence with many existing narrowband wireless systems, the white assumption for the noise contribution is commonly adopted in most of the analysis for UWB communications (see for instance [Ben06] and the references therein). This assumption is well justified by the low duty cycle of UWB transmissions and the adoption of time hopping mechanisms for multiple access. In that case,

$$\mathsf{C}_{\mathsf{c}\,|\,\mathrm{coh}} = \tag{3.29}$$
$$\log_2 P - \frac{1}{P}\sum_{i=0}^{P-1} \mathrm{E}_{\mathbf{g},\,\mathbf{y}|\mathbf{x}_i}\left[\log_2 \sum_{j=0}^{P-1} \exp\left(\frac{1}{2\sigma_w^2} Tr\left(2\mathbf{y}\left(\mathbf{h}_j-\mathbf{h}_i\right)^T + \mathbf{h}_i\mathbf{h}_i^T - \mathbf{h}_j\mathbf{h}_j^T\right)\right)\right].$$

In order to further simplify the expression in (3.29), let us substitute the received signal $\mathbf{y}$ by the model $\mathbf{y} = \mathbf{h}_i + \mathbf{w}$. This can be done because the conditioned expectation $\mathrm{E}_{\mathbf{y}|\mathbf{x}_i}[\cdot]$ is to be performed, and this assumes the transmission of the codeword $\mathbf{x} = \mathbf{x}_i$ and thus the reception

of the waveform $\mathbf{h}_i$. By doing so, we have

$$\mathsf{C}_{\mathsf{c}\,|\,\mathrm{coh}} = \tag{3.30}$$

$$\log_2 P - \frac{1}{P}\sum_{i=0}^{P-1} \mathrm{E}_{\mathbf{g},\,\mathbf{w}}\left[\log_2 \sum_{j=0}^{P-1} \exp\left(\frac{1}{2\sigma_w^2} Tr\left(2\left(\mathbf{h}_i+\mathbf{w}\right)\left(\mathbf{h}_j-\mathbf{h}_i\right)^T + \mathbf{h}_i\mathbf{h}_i^T - \mathbf{h}_j\mathbf{h}_j^T\right)\right)\right]$$

$$= \log_2 P - \frac{1}{P}\sum_{i=0}^{P-1} \mathrm{E}_{\mathbf{g},\,\mathbf{w}}\left[\log_2 \sum_{j=0}^{P-1} \exp\left(\frac{-1}{2\sigma_w^2}\left[\mathbf{h}_i^T\mathbf{h}_i - 2\mathbf{h}_i^T\mathbf{h}_j + \mathbf{h}_j^T\mathbf{h}_j\right]\right)\exp\left(\frac{1}{\sigma_w^2}\left(\mathbf{h}_i-\mathbf{h}_j\right)^T\mathbf{w}\right)\right]$$

$$= \log_2 P - \frac{1}{P}\sum_{i=0}^{P-1} \mathrm{E}_{\mathbf{g},\,\mathbf{w}}\left[\log_2 \sum_{j=0}^{P-1} \exp\left(-\frac{1}{2\sigma_w^2}\|\mathbf{h}_i-\mathbf{h}_j\|^2\right)\exp\left(\frac{1}{\sigma_w^2}\left(\mathbf{h}_i-\mathbf{h}_j\right)^T\mathbf{w}\right)\right]. \tag{3.31}$$

A closed-form expression for (3.31) is still very difficult to find. One of the main difficulties is due to the discrete nature of the input alphabet. Discrete input alphabets make the argument of the $\log_2(\cdot)$ operator to consist on the sum of likelihood ratios, and this makes difficult to approximate the nonlinear behavior of the $\log_2(\cdot)$ with simple linear expansions. The problem of finding a simple expression for the logarithm of a sum of exponential terms is also a recurrent problem, for instance, in the field of turbo decoding. In particular, the so-called *max-log MAP* algorithm for turbo decoding is based on the approximation $\log\left(\sum_i \exp z_i\right) \approx \max_i x_i$ [Woo00]. However, the max operator is still a nonlinear operator which does not help in providing a closed-form expression for (3.31).

Since a closed-form expression for (3.31) is still an open problem, Section 3.4.1 provides some mathematical derivations with the aim of upper bounding the constellation-constrained capacity in (3.31). To this end, orthogonal signaling is assumed. Once the upper bound is presented, the goodness of this bound is evaluated by computer simulations.

3.4.1 Closed-form upper bound for orthogonal signaling

Interestingly, a closed-form upper bound for the constellation-constrained capacity in (3.31) can be obtained when orthogonal PPM signaling is considered. Orthogonal signaling can directly be obtained by properly designing the transmitted signal such that non-overlapping time intervals are assigned to different PPM symbols. However, even when some overlapping exists, the randomness of the propagation channel makes the cross-correlation between received waveforms for different PPM symbols to be almost negligible. That is, the noise-like structure of the received waveforms contributes to reasonably validate the orthogonal signaling assumption, as confirmed by the simulation results to be presented later on.

The first important consequence of assuming orthogonal signaling is that the Euclidean distance in (3.31) turns out to depend on the energy of the received waveform only. That is, $\|\mathbf{h}_i-\mathbf{h}_j\|^2 = 2E_s$ for $i \neq j$ with $E_s = \|\mathbf{g}\|^2$ the energy of the received waveform or, equivalently,

the energy-per-symbol[1]. Then, the constellation-constrained capacity in (3.31) can be simplified as follows,

$$\mathsf{C}_{\mathsf{c}\,|\,\mathrm{coh+orthog}} = \tag{3.32}$$

$$\log_2 P - \frac{1}{P}\sum_{i=0}^{P-1} \mathrm{E}_{\mathbf{g},\mathbf{w}}\left[\log_2\left(1+\exp\left(-\rho\right)\sum_{j\neq i}\exp\left(\frac{1}{\sigma_w^2}\left(\mathbf{h}_i-\mathbf{h}_j\right)^T\mathbf{w}\right)\right)\right]$$

$$= \log_2 P - \frac{1}{P}\sum_{i=0}^{P-1} \mathrm{E}_{\mathbf{g},\mathbf{w}}\left[\log_2\left(1+\exp\left(-\rho\right)\exp\left(\frac{1}{\sigma_w^2}\mathbf{h}_i^T\mathbf{w}\right)\sum_{j\neq i}\exp\left(-\frac{1}{\sigma_w^2}\mathbf{h}_j^T\mathbf{w}\right)\right)\right] \tag{3.33}$$

where the symbol-SNR ρ is defined as in [Dol00],

$$\rho \doteq \frac{E_s}{\sigma_w^2} = 2\frac{E_s}{N_0}. \tag{3.34}$$

The rationale behind the definition of symbol-SNR is the following. Let us consider the traditional SNR as the quotient between the signal and noise powers denoted by P_S and P_N, respectively. Then,

$$\mathsf{SNR} = \frac{P_S}{P_N} = \frac{\frac{E_s}{T}}{\frac{N_0}{2}2W} = 2\frac{E_s}{N_0}\frac{1}{2TW} \tag{3.35}$$

with E_s the energy per PPM symbol, $\frac{N_0}{2}$ the double-sided noise spectral density, T the symbol period and W the signal bandwidth. According to the Nyquist signaling theorem, no more than $2W$ samples can be transmitted per second when a bandwidth W is available. Therefore, no more than $2TW$ samples per second can be introduced to the channel within a symbol period T. According to this reasoning, *symbol-SNR* can be defined as

$$\rho \doteq \mathsf{SNR}\cdot 2TW = 2\frac{E_s}{N_0}. \tag{3.36}$$

Regarding the noise power σ_w^2, it represents the noise variance per sample in the received signal. Since the symbol period is T and no more than $2TW$ samples per symbol can be introduced to the channel,

$$\sigma_w^2 = \frac{N_0 W\cdot T}{2TW} = \frac{N_0}{2}. \tag{3.37}$$

Consequently, the symbol-SNR defined in (3.36) can also be expressed as

$$\rho = \frac{E_s}{\sigma_w^2} \tag{3.38}$$

as initially defined in (3.34).

Next, we can proceed with the simplification of the constellation-constrained capacity in (3.33). To this end, let us first consider the law of large numbers. Then, the summation of

[1]Notice that, for the sake of simplicity, frame repetition is not considered in this theoretical study on the performance limits of UWB communications.

exponentials in (3.33) can be assumed to converge to the sum of individual mean values. That is,

$$\sum_{j\neq i}\exp\left(-\frac{1}{\sigma_w^2}\mathbf{h}_j^T\mathbf{w}\right)\rightarrow(P-1)\mathrm{E}_{\mathbf{w}}\left[\exp\left(-\frac{1}{\sigma_w^2}\mathbf{h}_j^T\mathbf{w}\right)\right]. \tag{3.39}$$

The assumption above can be reasonably adopted provided that P is sufficiently large and taking into consideration that the product $\mathbf{h}_j^T\mathbf{w}$ does not vary significantly for different $j=\{0,1,\ldots,P-1\}$. Moreover, the reason for the expectation in the right hand side of (3.39) to be carried out over the noise $\mathbf{w}$ is the following. The length of waveform $\mathbf{g}$ within $\mathbf{h}_j$ is usually very short compared to the total length of $\mathbf{h}_j$. That is, $\mathbf{h}_j$ is usually sparse. Then, it is reasonable to assume that moving j makes the short waveform $\mathbf{g}$ to correlate with different samples of noise. Equivalently, the summation in the left hand side of (3.39) is indeed generating different noise realizations for different values of j.

According to the mathematical derivations in Appendix 3.A, the required expectation is given by

$$\mathrm{E}_{\mathbf{w}}\left[\exp\left(-\frac{1}{\sigma_w^2}\mathbf{h}_j^T\mathbf{w}\right)\right]=\exp\left(\frac{1}{2\sigma_w^2}\|\mathbf{h}_j\|^2\right)=\exp\left(\frac{1}{2}\rho\right). \tag{3.40}$$

Note that the result in (3.40) is indeed an exact result. No approximations were made at this point. Then, by substituting the result in (3.40) into the constellation-constrained capacity in (3.33) the result is

$$\mathsf{C}_{\mathsf{c}\,|\,\mathrm{coh+orthog}}\approx\log_2 P-\frac{1}{P}\sum_{i=0}^{P-1}\mathrm{E}_{\mathbf{g},\mathbf{w}}\left[\log_2\left(1+(P-1)\exp\left(-\frac{1}{2}\rho\right)\exp\left(\frac{1}{\sigma_w^2}\mathbf{h}_i^T\mathbf{w}\right)\right)\right]. \tag{3.41}$$

The expression in (3.41) is an approximation of the true constellation-constrained capacity since the partial result in (3.39) required P to be sufficiently large. Moreover, numerical evaluation is still required. However, a simple and closed-form expression can be obtained by introducing the Jensen's inequality. To this end, let us define the function

$$g\left(\mathbf{h}_i,\mathbf{w}\right)\doteq\log_2\left(1+(P-1)\exp\left(-\frac{1}{2}\rho\right)\exp\left(\frac{1}{\sigma_w^2}\mathbf{h}_i^T\mathbf{w}\right)\right). \tag{3.42}$$

The function $g(\mathbf{h}_i,\mathbf{w})$ is a convex $\cup$ function. Consequently, the Jensen's inequality results in

$$\mathrm{E}_{\mathbf{w}}\left[g\left(\mathbf{h}_i,\mathbf{w}\right)\right]\;\geq\;g\left(\mathbf{h}_i,\mathrm{E}_{\mathbf{w}}\left[\mathbf{w}\right]\right)=\log_2\left(1+(P-1)\exp\left(-\frac{1}{2}\rho\right)\right) \tag{3.43}$$

because of the zero mean of the Gaussian noise contribution, $\mathrm{E}_{\mathbf{w}}\left[\mathbf{w}\right]=\mathbf{0}$.

Finally, substitution of the Jensen's inequality results in the following closed-form upper-bound for the constellation-constrained capacity of orthogonal PPM signaling with coherent reception,

$$\mathsf{C}_{\mathsf{c}\,|\,\mathrm{coh+orthog}}\leq\log_2 P-\log_2\left(1+(P-1)\exp\left(-\frac{1}{2}\rho\right)\right). \tag{3.44}$$

3.4.2 Numerical results

In this section, the exact constellation-constrained capacity in (3.31) is evaluated for UWB signals propagating through the IEEE 802.15.3a and the IEEE 802.15.4a channel models in [Foe03] and [Mol04], respectively. Since an exact and closed-form expression for (3.31) is very difficult to be obtained, there is no choice but to evaluate (3.31) in a numerical manner via Monte-Carlo simulations. These numerical results will be compared with the analytical results obtained with the closed-form upper bound proposed in (3.44). The advantage of (3.44) is that it provides a simple and closed-form expression to upper bound capacity. However, (3.44) was derived assuming orthogonal PPM and thus, it is just a particular case of the more general result in (3.31).

In order to identify how close we are to the real capacity of orthogonal signaling, and thus, how valid the proposed upper bound in (3.44) can be, the capacity for coherent orthogonal signaling is also considered in this study. This expression was derived in [Dol00] and it is revisited here for the sake of clarity,

$$\mathsf{C}_{\mathsf{c}\,|\,\mathrm{coh+orthog}} \approx \log_2 P - \mathrm{E}_{v_1|\mathbf{x}_1}\Big[\log_2\left(1+(P-1)\exp\left(\rho/2\right)\exp\left(-\sqrt{\rho}v_1\right)\right)\Big] \tag{3.45}$$

with $v_1 \sim \mathcal{N}\left(\sqrt{\rho},1\right)$. Note that the expression (3.45) derived in [Dol00] requires numerical evaluation, similarly to what happens with our exact result in (3.31). However, the result in (3.31) is more general because it encompasses both orthogonal and non-orthogonal coherent PPM. It is also interesting to point out that the expression in (3.45) was also adopted in [Zha01] to show the superior performance of UWB PPM systems in comparison with traditional direct-sequence spread spectrum (DS-SS) for $P > 4$ in the wideband regime.

Coming back to the simulation results to be presented in this section, the channel models CM1 and CM2 from the IEEE 802.15.3a working group and the channel model CM8 from the IEEE802.15.4a working group are considered here. On the one hand, both the CM1 and CM2 channel models assume a distance between transmitter and receiver from 0 to 4 meters. However, the channel model CM1 considers line-of-sight (LOS) propagation whereas the channel model CM2 considers non line-of-sight (NLOS) propagation. On the other hand, the CM8 channel model assumes a distance between transmitter and receiver from 2 to 8 meters with NLOS propagation in an industrial environment.

The sampling time is set here to $T_s = 0.5$ ns. The symbol interval is $T = 1.5$ μs and for the sake of simplicity, there is only one transmitted pulse per symbol. That is, there is no pulse repetition within the symbol interval. The PPM time-shift is equal to $T_\Delta = 15$ ns. The delay spread is approximately 25 ns for the CM1 channel model, 50 ns for the CM2 channel model and 100 ns for the CM8 channel model. Since the PPM time-shift is just 15 ns, there is overlapping between the received waveforms for adjacent hypothesis.

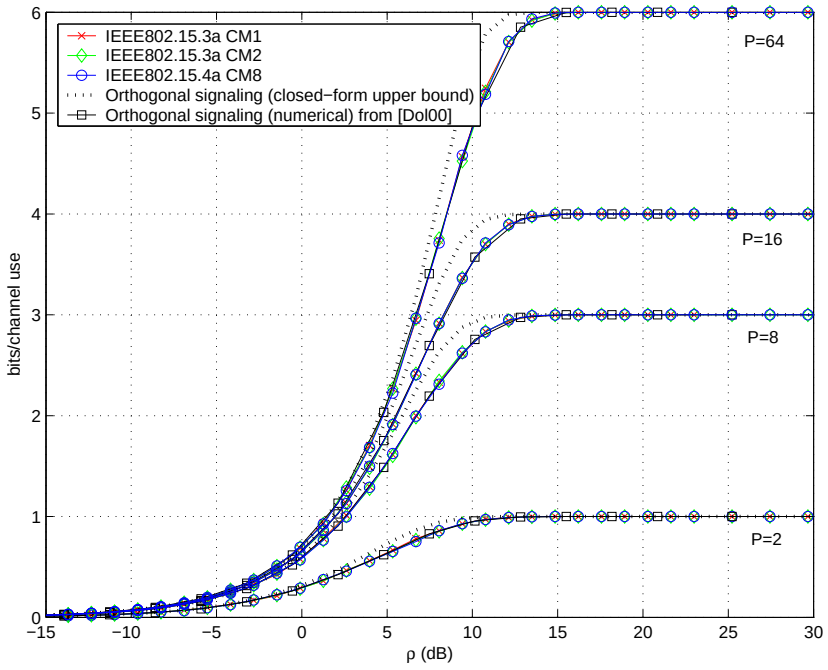

Figure 3.4: Constellation-constrained capacity for UWB PPM coherent receivers.

From the observation of the results in Figure 3.4 two important conclusions can be drawn:

1. In theory, there is a different amount of overlapping when propagating through the CM1, CM2 and CM8 channel models. The reason is that the time-shift is $T_\Delta = 15$ ns for all channel models but the delay spread is 25 ns, 50 ns and 100 ns, respectively. Thus, the received waveforms corresponding to adjacent hypothesis do overlap. However, this does not seem to affect the capacity of the system. Note that capacity curves for all the channel models do coincide. This indicates that overlapping caused by the delay spread is not significant enough so as to degrade capacity. The reason can be found in the fact that the shape of the received waveforms is random enough so as to guarantee that the cross-correlation is approximately zero for any time-shift different from 0. In particular, it can be verified that for the simulated channel responses, $\mathbf{h}_i^T \mathbf{h}_j \approx 0$ for $i \neq j$. Even though there is overlapping in adjacent hypothesis, the randomness of the propagation channel allows the system to operate almost like an orthogonal pseudo-random signaling scheme. This is confirmed by noting that the curves for the exact capacity of orthogonal PPM given by (3.45) in [Dol00] coincide with that of the simulated CM1, CM2 and CM8 channel models with overlapping. Thus, we are virtually dealing with an orthogonal PPM signaling despite of the waveform overlapping.

2. The closed-form upper bound for the constellation-constrained capacity of orthogonal signaling in (3.44) is a reasonable tight upper bound, as shown in Figure 3.4. This is especially important when taking into consideration that it provides a closed-form expression and

thus, no numerical evaluation is required.

Apart from the analysis of capacity versus symbol-SNR presented so far, another interesting approach is to evaluate spectral efficiency in terms of the minimum required E_b/N_0 for reliable communication. According to [Ver02b], the minimum required E_b/N_0 is related with the first derivative of the channel capacity at $\mathsf{SNR} = 0$, as already mentioned in Section 3.3. Moreover, a coherent signaling scheme is first order optimal when the minimum E_b/N_0 coincides with $(E_b/N_0)_{\min} = -1.59$ dB when $\mathsf{SNR} \to 0$. For the case under consideration, the E_b/N_0 parameter can be easily recovered from the symbol-SNR ρ by noting that $\rho = 2E_s/N_0$ and $E_s/N_0 = bE_b/N_0$ with b the number of bits per symbol. Then we have that

$$\frac{E_b}{N_0} = \frac{\rho}{2b}. \tag{3.46}$$

For a given constant value of ρ, $(E_b/N_0)_{\min}$ is achieved when the maximum number of bits are allocated per symbol. Consequently, b in (3.46) must be substituted with the channel capacity in bits per channel use,

$$\left(\frac{E_b}{N_0}\right)_{\min} = \frac{\rho}{2\mathsf{C}}. \tag{3.47}$$

The results in Figure 3.4 are now depicted in Figure 3.5 as a function of the minimum required E_b/N_0 according to (3.47). Capacity is found to be rapidly achieved by using large PPM alphabets so that a brickwall effect can be observed at $(E_b/N_0)_{\min} = -1.59$ dB. Since $(E_b/N_0)_{\min}$ is achieved, coherent PPM signaling is first order optimal for $P \to \infty$. Moreover, the asymptotic brickwall effect also indicates that the wideband slope for infinite bandwidth is achieved and thus, coherent PPM is indeed second order optimal.

For low PPM alphabets (e.g. $P = 2$) there is a penalty due to the orthogonal behavior of the received waveforms. It is well known that orthogonal signaling incurs in a power penalty when compared to the more efficient simplex signaling. Indeed, simplex signals achieve capacity for the low-SNR regime [Mas76] and they can be obtained from orthogonal signals just by substracting the mean. The result is a signaling set with the same cross-correlation between all the elements of the alphabet and an average symbol energy that is lower than for the orthogonal case [Pro01, p.179]. In particular,

$$E_s^{\text{simplex}} = \left(\frac{P-1}{P}\right) E_s^{\text{orthog}} \tag{3.48}$$

with P the constellation order. Therefore the penalty in terms of the minimum required E_b/N_0 is $10\log_{10}\left(\frac{P}{P-1}\right)$ dB. For 2-PPM, this penalty is equal to 3 dB, as confirmed in Figure 3.5.

Finally, it is also worth noting that the proposed approximation for the constellation-constrained capacity in (3.44) performs reasonably well for most E_b/N_0 values. The difference between the proposed approximation and the exact result turns out to be more significant at two different points: for the case of decreasing values of E_b/N_0, and prior to the saturation of

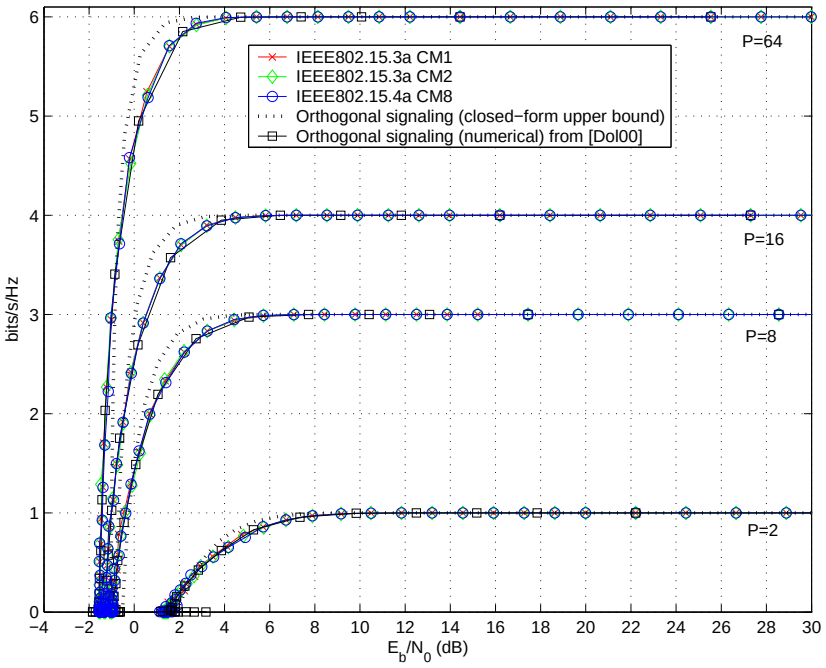

Figure 3.5: Spectral efficiency for UWB PPM coherent receivers.

spectral efficiency to the value $\log_2 P$. The proposed approximation still performs reasonably well for the rest of E_b/N_0 values providing a valuable and simple result for approximating the constellation-constrained capacity of orthogonal PPM signaling with coherent reception.

3.5 Constellation-Constrained Capacity for Non-Coherent PPM

Similarly to the coherent case, the core of constellation-constrained capacity for non-coherent receivers is based on the evaluation of the likelihood ratio

$$\Lambda_{j,i}(\mathbf{y}) \doteq \frac{f\left(\mathbf{y}|\mathbf{x}=\mathbf{x}_j\right)}{f\left(\mathbf{y}|\mathbf{x}=\mathbf{x}_i\right)}. \tag{3.49}$$

For the case of non-coherent receivers, however, the end-to-end channel response is assumed to be a random Gaussian process driven by a given covariance matrix $\mathbf{C_g} = \mathrm{E}\left[\mathbf{g}\mathbf{g}^T\right]$. When the pulse-position modulation comes into action, the received waveform $\mathbf{g}$ creates a set of time-shifted replicas $\{\mathbf{h}_0, \mathbf{h}_1, \ldots, \mathbf{h}_{P-1}\}$ as indicated in the signal model in Section 3.2.2. These received waveforms $\mathbf{h}_k$ for $k = 0, 1, \ldots, P-1$ are characterized by the multivariate Gaussian probability density function in (3.5) so that the likelihood ratio $\Lambda_{j,i}(\mathbf{y})$ becomes,

$$\Lambda_{j,i}(\mathbf{y}) \quad = \quad \frac{\det^{1/2}\left(\mathbf{C}_w + \mathbf{C}_{\mathbf{h}_i}\right)}{\det^{1/2}\left(\mathbf{C}_w + \mathbf{C}_{\mathbf{h}_j}\right)} \frac{\exp\left(-\frac{1}{2}\mathbf{y}^T\left(\mathbf{C}_w + \mathbf{C}_{\mathbf{h}_j}\right)^{-1}\mathbf{y}\right)}{\exp\left(-\frac{1}{2}\mathbf{y}\left(\mathbf{C}_w + \mathbf{C}_{\mathbf{h}_i}\right)^{-1}\mathbf{y}\right)}. \tag{3.50}$$

The expression above can be simplified for the case of AWGN noise, $\mathbf{C}_w = \sigma_w^2\mathbf{I}$. In this case, the determinant $\det(\mathbf{C}_w + \mathbf{C}_{\mathbf{h}_i})$ in (3.50) turns out to be independent of i and thus

$$\det(\mathbf{C}_w + \mathbf{C}_{\mathbf{h}_i}) = \det\left(\mathbf{C}_w + \mathbf{C}_{\mathbf{h}_j}\right) \tag{3.51}$$

for any $\{i, j\}$. This statement can easily be proved by noting that $\sigma_w^2\mathbf{I} + \mathbf{C}_{\mathbf{h}_i}$ can be understood as a block partitioned matrix. According to the properties of block partitioned matrices [Har00, p.185],

$$\det\left(\sigma_w^2\mathbf{I} + \mathbf{C}_{\mathbf{h}_i}\right) = \det\left(\begin{bmatrix} \sigma_w^2\mathbf{I}_{N_g} + \mathbf{C}_{\mathbf{g}} & \mathbf{0} \\ \mathbf{0} & \sigma_w^2\mathbf{I}_{N_{ss}-N_g} \end{bmatrix}\right) = \det\left(\sigma_w^2\mathbf{I}_{N_g} + \mathbf{C}_{\mathbf{g}}\right)\sigma_w^{2(N_{ss}-N_g)}. \tag{3.52}$$

Since the right hand side of (3.52) does not depend on the time position of the transmitted PPM symbol, the likelihood ratio simplifies to

$$\Lambda_{j,i}(\mathbf{y}) = \exp\left(\frac{1}{2}\mathbf{y}^T\left[\left(\sigma_w^2\mathbf{I} + \mathbf{C}_{\mathbf{h}_i}\right)^{-1} - \left(\sigma_w^2\mathbf{I} + \mathbf{C}_{\mathbf{h}_j}\right)^{-1}\right]\mathbf{y}\right) \tag{3.53}$$

and constellation-constrained capacity becomes

$$\mathsf{C}_{\mathsf{c}\,|\,\mathrm{no-coh}} = \tag{3.54}$$
$$\log_2 P - \frac{1}{P}\sum_{i=0}^{P-1}\mathrm{E}_{\mathbf{g},\,\mathbf{y}|\mathbf{x}_i}\left[\log_2\sum_{j=0}^{P-1}\exp\left(\frac{1}{2}\mathbf{y}^T\left[\left(\sigma_w^2\mathbf{I} + \mathbf{C}_{\mathbf{h}_i}\right)^{-1} - \left(\sigma_w^2\mathbf{I} + \mathbf{C}_{\mathbf{h}_j}\right)^{-1}\right]\mathbf{y}\right)\right].$$

It is interesting to note that constellation-constrained capacity for non-coherent receivers in (3.54) depends on the second-order moments of the received signal. This is in contrast with the constellation-constrained capacity for coherent receivers in (3.31), where just the first order moment of the received signal was required. Second-order moments are required for non-coherent receivers because the absence of channel state information makes the received waveform to be considered an unknown random Gaussian process with zero-mean. Therefore, the detection process must resort to second-order statistics in order to distinguish the received signal from the background noise. The shift from first to second order moments is an important difference in the constellation-constrained capacity for coherent and non-coherent receivers, and it is the responsible for the different rate of convergence of spectral efficiency in the wideband regime. This issue will be discussed in more detail in Section 3.6.

3.5.1 Upper bound for uncorrelated scattering

Similarly to what occurred in Section 3.4 for the case of coherent receivers, the resulting likelihood ratio for non-coherent receivers makes very difficult to obtain a closed-form expression for capacity in (3.54). In order to circumvent this limitation, a closed-form upper bound will be

derived herein based on the Jensen's inequality already applied in Section 3.4.1. By doing so, the following upper bound is obtained,

$$\mathsf{C}_{\mathsf{c}\,|\,\mathrm{no-coh}} = \tag{3.55}$$

$$\log_2 P - \frac{1}{P}\sum_{i=0}^{P-1} \mathrm{E}_{\mathbf{g},\,\mathbf{y}|\mathbf{x}_i}\left[\log_2 \sum_{j=0}^{P-1} \exp\left(\frac{1}{2} Tr\left(\left[\left(\sigma_w^2\mathbf{I}+\mathbf{C}_{\mathbf{h}_i}\right)^{-1} - \left(\sigma_w^2\mathbf{I}+\mathbf{C}_{\mathbf{h}_j}\right)^{-1}\right]\mathbf{y}\mathbf{y}^T\right)\right)\right]$$

$$\leq \log_2 P - \frac{1}{P}\sum_{i=0}^{P-1} \log_2 \sum_{j=0}^{P-1} \exp\left(\frac{1}{2} Tr\left(\left[\left(\sigma_w^2\mathbf{I}+\mathbf{C}_{\mathbf{h}_i}\right)^{-1} - \left(\sigma_w^2\mathbf{I}+\mathbf{C}_{\mathbf{h}_j}\right)^{-1}\right]\left(\sigma_w^2\mathbf{I}+\mathbf{C}_{\mathbf{h}_i}\right)\right)\right) \tag{3.56}$$

$$= \log_2 P - \frac{1}{P}\sum_{i=0}^{P-1} \log_2 \sum_{j=0}^{P-1} \exp\left(\frac{1}{2}\left[N_{ss} - Tr\left(\left(\sigma_w^2\mathbf{I}+\mathbf{C}_{\mathbf{h}_j}\right)^{-1}\left(\sigma_w^2\mathbf{I}+\mathbf{C}_{\mathbf{h}_i}\right)\right)\right]\right) \tag{3.57}$$

with $\mathbf{y}\mathbf{y}^T$ the random variable where the Jensen's inequality is applied. That is,

$$\mathrm{E}_{\mathbf{g},\,\mathbf{y}|\mathbf{x}_i}\left[\mathsf{C}_{\mathsf{c}\,|\,\mathrm{no-coh}}\left(\mathbf{y}\mathbf{y}^T\right)\right] \leq \mathsf{C}_{\mathsf{c}\,|\,\mathrm{no-coh}}\left(\mathrm{E}_{\mathbf{g},\,\mathbf{y}|\mathbf{x}_i}\left[\mathbf{y}\mathbf{y}^T\right]\right) \tag{3.58}$$

$$= \mathsf{C}_{\mathsf{c}\,|\,\mathrm{no-coh}}\left(\sigma_w^2\mathbf{I}+\mathbf{C}_{\mathbf{h}_i}\right). \tag{3.59}$$

Received waveforms with uncorrelated scattering (US) are obtained when adopting most of the channel models in the IEEE802.15.3a/4a specifications. In these situations, the covariance matrices $\mathbf{C}_{\mathbf{h}_i}$ for the received waveforms turn out to be diagonal and significant simplifications can be done in (3.57). After some straightforward manipulations, the upper bound for the constellation-constrained capacity of non-coherent receivers with uncorrelated received samples is given by

$$C_{c\,|\,\mathrm{no-coh}}^{\mathrm{US}} \leq \log_2 P - \frac{1}{P}\sum_{i=0}^{P-1} \log_2 \sum_{j=0}^{P-1} \exp\left(-\frac{1}{2}\sum_{k=0}^{N_{ss}-1} \frac{\gamma_i(k)-\gamma_j(k)}{\sigma_w^2+\gamma_j(k)}\right) \tag{3.60}$$

with $\gamma_i(k) = [\mathbf{C}_{\mathbf{h}_i}]_{k,k}$ the k-th entry of the power delay profile (PDP) of the received waveform under the hypothesis $\mathcal{H}_i : \mathbf{x} = \mathbf{x}_i$.

3.5.2 Numerical results

In this section, the exact constellation-constrained capacity in (3.54) is evaluated for UWB signals propagating through the IEEE 802.15.4a channel model CM8 [Mol04]. The reason to focus on this channel model is that it assumes an industrial environment with NLOS propagation where the small-scale fading statistics are found to be modeled by the traditional Rayleigh distribution [Kar04], [Sch05b], [Sch05c]. This is in contrast with the IEEE 802.15.3a channel models, where the small-scale fading statistics were found to be closer to Nakagami and lognormal distributions, and thus, a rather intricate mathematical treatment is required. For the case of the Rayleigh distribution encountered in the IEEE 802.15.4a CM8 channel model, a simple

mathematical treatment is possible. This is because a Rayleigh distribution in the fading statistics involves a Gaussian distribution in the amplitudes of the received waveform. Consequently, the Gaussian signal model in Section 3.2.2 can be adopted.

The simulation parameters are the same as in Section 3.4.2. That is, the sampling time is $T_s = 0.5$ ns, the symbol interval is $T = 1.5$ μs and the PPM time-shift is $T_\Delta = 15$ ns. Since the delay spread for the IEEE 802.15.4a CM8 channel model is 100 ns, there is certain overlapping between received waveforms corresponding to neighboring hypothesis. However, this just incurs in a minor performance loss as discussed later on in Section 3.6.

Constellation-constrained capacity as a function of the symbol-SNR ρ is shown in Figure 3.6 for non-coherent UWB receivers. Two important remarks can be done. First, the upper bound in (3.60) is found to provide a close match to the exact performance. Second, the performance for non-coherent receivers suffers an important penalty in terms of symbol-SNR. That is, the ρ values at which the limit capacity is achieved for coherent receivers in Figure 3.4 are about 8 to 10 dB lower than the ones required now for non-coherent receivers.

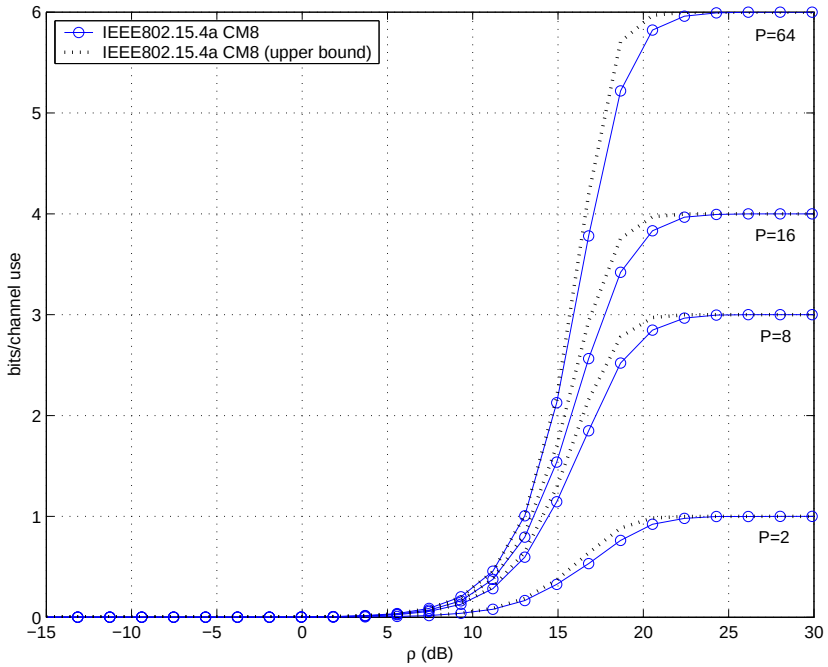

Figure 3.6: Constellation-constrained capacity for UWB PPM non-coherent receivers.

The power inefficiency of non-coherent PPM is also confirmed when analyzing spectral efficiency and the minimum required energy per bit. As introduced in Section 3.3, the wideband slope for non-coherent receivers is $\mathcal{S}_0 = 0$ in the limit of zero spectral efficiency. This issue is confirmed in Figure 3.7 and it is also found that the value of null wideband slope is achieved from the left hand side of 0. As a result, infinite E_b/N_0 is required in the limit of zero spectral efficiency.

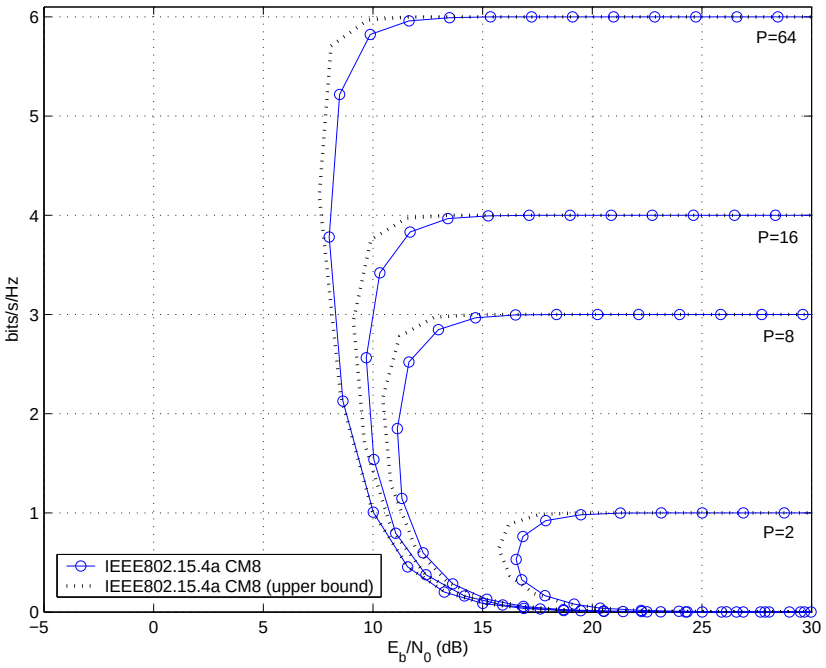

Figure 3.7: Spectral efficiency for UWB PPM non-coherent receivers.

The power inefficiency of non-coherent receivers is an important result that will receive further attention in Section 3.6.

3.6 Comparison of coherent and non-coherent performance

The numerical results obtained in Section 3.4 and Section 3.5 will be compared herein for the case of coherent and non-coherent communication through the IEEE 802.15.4a CM8 channel model. The comparison will be made for three different information theoretic measures:

- Constellation-constrained capacity.
- Spectral efficiency.
- Achievable data rates for a given transmission bandwidth.

First, exact constellation-constrained capacity as a function of symbol-SNR ρ is depicted in Figure 3.8. For the non-coherent case, capacity is also evaluated for the case of using a PPM time-shift with $T_\Delta = 75$ ns. This value of T_Δ for the CM8 channel model avoids the possible performance loss caused by overlapping of received waveforms. With $T_\Delta = 75$ ns almost 96 % of the received energy is captured without overlapping. With this parameter, the results indicate that there is almost an 8 dB loss in terms of signal-to-noise ratio due to the adoption of a non-coherent receiver.

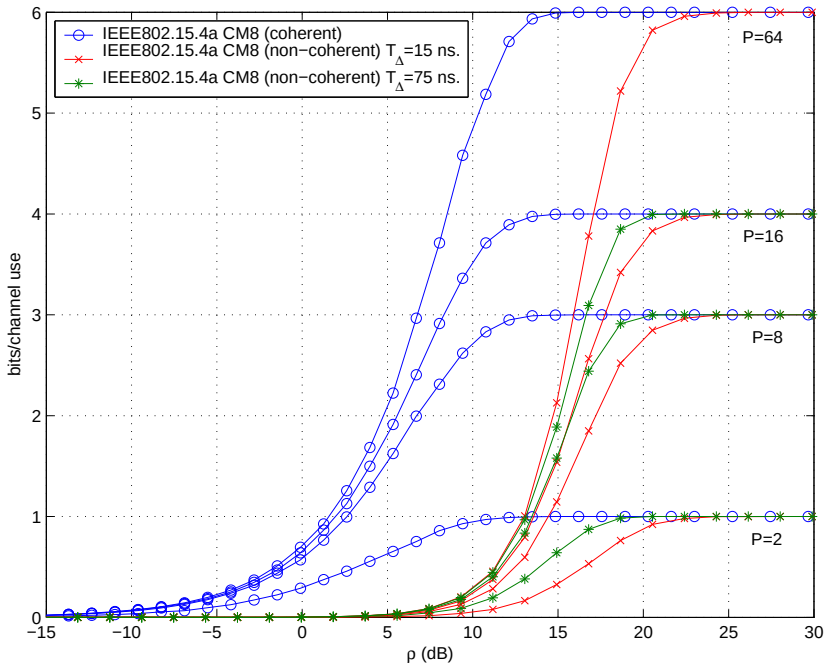

Figure 3.8: Constellation-constrained capacity for UWB PPM coherent and non-coherent receivers.

Spectral efficiency, that is, constellation-constrained capacity as a function of E_b/N_0, is depicted in Figure 3.9. From the observation of this figure, two important conclusions can be drawn.

1. Coherent PPM is second order optimal for increasing constellation P. However, special care must be taken when analyzing the results for non-coherent PPM. First of all, it should be noted that no peaky signaling is simulated herein. Thus, the simulated signal can be understood to be generated in the presence of peakiness constraints. With this remark in mind, note that the results for the simulated non-coherent PPM achieve second order optimality. That is, $(E_b/N_0)_{\min} \to \infty$ and $\mathcal{S}_0 = 0$ as indicated in Table 3.1 for the case of non-coherent receivers with peakiness constraints. However, this notion of second-order optimality is not practical in the sense that the required minimum E_b/N_0 tends to infinity. For practical purposes, the effective minimum E_b/N_0 can be defined as the true minimum value of E_b/N_0. For the results in Fig. 3.9, this effective minimum E_b/N_0 is approximately equal to 8 dB for the case of non-coherent PPM with $P = 64$, and it is still far away from the optimal value of $(E_b/N_0)_{\min} = -1.59$ dB for the case of non-coherent PPM with unconstrained peakiness.

2. The difference between $(E_b/N_0)_{\min}$ for coherent and non-coherent PPM is on the order of 9 to 10 dB for practical constellation orders. This confirms that in the absence of peaky signaling, non-coherent PPM is power inefficient from the spectral efficiency point of view.

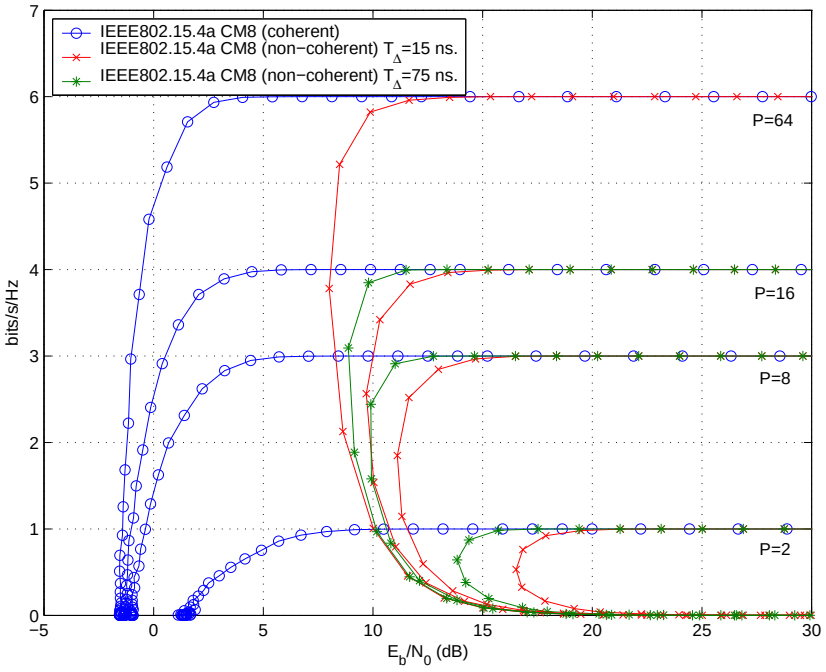

Figure 3.9: Spectral efficiency for UWB PPM coherent and non-coherent receivers.

However, this penalty can be compensated by the very large bandwidth of UWB signals which still can provide reasonably high data rates for the low-SNR regime, as shown next in Figure 3.10.

Achievable data rates for coherent and non-coherent UWB receivers are analyzed for the symbol period $T = 1.5$ μs considered in previous simulation results. Then, achievable data rates in (bits/s) are obtained as

$$\mathsf{C}_c(\text{bits/s}) = \frac{1}{T} \cdot \mathsf{C}_c(\text{bits/channel use}) \tag{3.61}$$

since one channel use or transmission corresponds to one symbol period of T seconds. The results for the achievable data rates in (bits/s) are depicted in Figure 3.10 for coherent and non-coherent UWB receivers under the IEEE 802.15.4a channel model CM8. Figure 3.10 also incorporates the achievable data rates for the infinite-bandwidth regime C_∞ presented in (3.9). The latter capacity is indeed an upper bound on the achievable data rate of practical coherent and non-coherent receiver.

The main conclusion by observing Figure 3.10 is that coherent PPM with increasing constellation order is optimal in the sense that it achieves the infinite-bandwidth capacity. This issue was already pointed out in Figure 3.9 where coherent PPM receivers were found to be second order optimal. For the case of non-coherent PPM receivers, their power inefficiency in the low-SNR regime creates a significant gap between their achievable data rates and that of

coherent receivers [Sou03]. Coherent receivers rapidly converge to the optimal performance of infinite bandwidth but non-coherent receivers slowly converge because of their null wideband slope, $\mathcal{S}_0 = 0$.

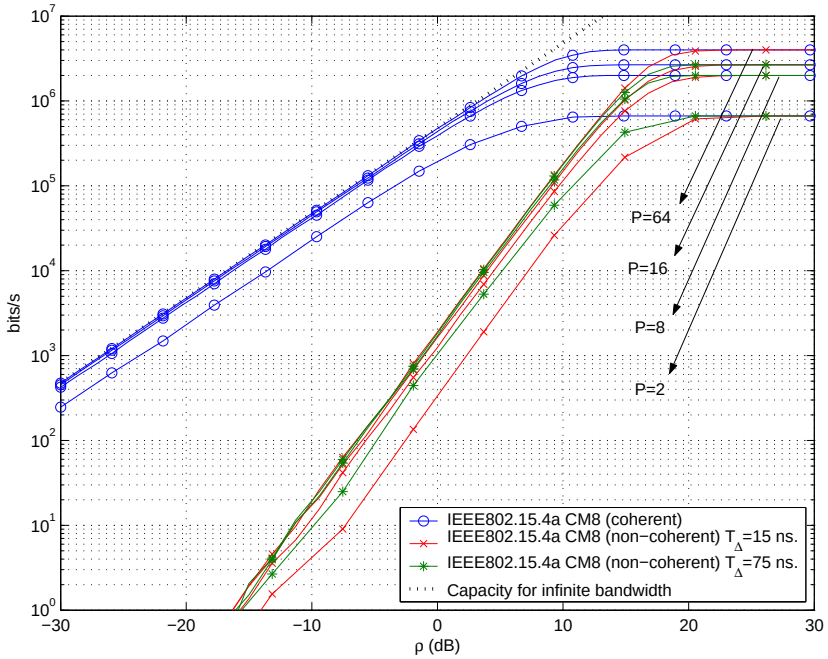

Figure 3.10: Achievable data rates for coherent and non-coherent communications with $W = 1$ GHz.

As a result of the above considerations, very high data rates for a given fixed bandwidth can only be achieved in the low-SNR regime with coherent receivers. In contrast, non-coherent receivers should be preferably considered for low data rate applications where low cost receivers are required.

At this point there exists a tradeoff between system complexity and ultimate performance. The performance for coherent receivers is optimal, but this involves having perfect channel state information at the receiver which may not be an easy requirement to be fulfilled. Obtaining channel state information in hostile environments requires significant complexity and possibly the transmission of pilot symbols. When this is the case, it should be noted that sending training symbols leads to a rate reduction in proportion to the fraction of training duration so that it probably turns out that it is best not to perform training [Rao04]. A detailed analysis must be done for each particular working scenario to determine whether coherent or non-coherent receivers are most suitable. In the next chapter, a channel estimation technique will be provided so that the cost of providing channel state information to the receiver will be revisited.

Appendix 3.A Derivation of the expectation on the form $\mathbf{E}_{\mathbf{w}}\left[\exp\left(\beta\mathbf{u}^T\mathbf{w}\right)\right]$

The purpose of this Appendix is to derive the expectation on the form $\mathrm{E}_{\mathbf{w}}\left[\exp\left(\beta\mathbf{u}^T\mathbf{w}\right)\right]$ with β a constant scalar, $\mathbf{u}\in\mathbb{R}^{N_{ss}\times 1}$ a constant vector, and $\mathbf{w}\in\mathbb{R}^{N_{ss}\times 1}\sim\mathcal{N}\left(\mathbf{0},\sigma_w^2\mathbf{I}\right)$. That is, $\mathbf{w}$ is a zero-mean random Gaussian vector with covariance matrix $\mathrm{E}_{\mathbf{w}}\left[\mathbf{w}\mathbf{w}^T\right]=\sigma_w^2\mathbf{I}$ and probability density function

$$f_{\mathbf{w}}\left(\mathbf{w}\right)=\frac{1}{\left(2\pi\sigma_w^2\right)^{N_{ss}/2}}\exp\left(-\frac{1}{2\sigma_w^2}\|\mathbf{w}\|^2\right). \tag{3.62}$$

The first step is to expand the expectation operator into its integral form,

$$\begin{aligned}
&\mathrm{E}_{\mathbf{w}}\left[\exp\left(\beta\mathbf{u}^T\mathbf{w}\right)\right]\\
&\quad=\int_{\mathbf{w}}\exp\left(\beta\mathbf{u}^T\mathbf{w}\right)f_{\mathbf{w}}\left(\mathbf{w}\right)d\mathbf{w} &(3.63)\\
&\quad=\int_{\mathbf{w}}\exp\left(\beta\mathbf{u}^T\mathbf{w}\right)\frac{1}{\left(2\pi\sigma_w^2\right)^{N_{ss}/2}}\exp\left(-\frac{1}{2\sigma_w^2}\|\mathbf{w}\|^2\right)d\mathbf{w} &(3.64)\\
&\quad=\int_{\mathbf{w}}\frac{1}{\left(2\pi\sigma_w^2\right)^{N_{ss}/2}}\prod_{m=0}^{N_{ss}-1}\exp\left(\beta\left[\mathbf{u}\right]_m\left[\mathbf{w}\right]_m\right)\exp\left(-\frac{1}{2\sigma_w^2}\left[\mathbf{w}\right]_m^2\right)d\mathbf{w} &(3.65)\\
&\quad=\int_{\mathbf{w}}\frac{1}{\left(2\pi\sigma_w^2\right)^{N_{ss}/2}}\prod_{m=0}^{N_{ss}-1}\exp\left(-\frac{1}{2\sigma_w^2}\left[\left[\mathbf{w}\right]_m^2-2\sigma_w^2\beta\left[\mathbf{u}\right]_m\left[\mathbf{w}\right]_m\right]\right)d\mathbf{w}. &(3.66)
\end{aligned}$$

Next, it is interesting to complete the quadratic argument of the exponential in (3.66) so as to make appear the probability density function of a Gaussian distributed vector with some non-zero mean. To this end note that

$$\begin{aligned}
&\exp\left(-\frac{1}{2\sigma_w^2}\left[\left[\mathbf{w}\right]_m^2-2\sigma_w^2\beta\left[\mathbf{u}\right]_m\left[\mathbf{w}\right]_m\right]\right)\\
&\quad=\exp\left(-\frac{1}{2\sigma_w^2}\left[\left[\mathbf{w}\right]_m^2-2\sigma_w^2\beta\left[\mathbf{u}\right]_m\left[\mathbf{w}\right]_m+\sigma_w^4\beta^2\left[\mathbf{u}\right]_m^2\right]\right)\exp\left(\frac{1}{2\sigma_w^2}\sigma_w^4\beta^2\left[\mathbf{u}\right]_m^2\right). &(3.67)
\end{aligned}$$

Therefore, by substituting (3.67) into (3.66) we have,

$$\begin{aligned}
&\mathrm{E}_{\mathbf{w}}\left[\exp\left(\beta\mathbf{u}^T\mathbf{w}\right)\right] &(3.68)\\
&\quad=\prod_{m=0}^{N_{ss}-1}\exp\left(\frac{\sigma_w^2}{2}\beta^2\left[\mathbf{u}\right]_m^2\right)\times\\
&\qquad\int_{\mathbf{w}}\frac{1}{\left(2\pi\sigma_w^2\right)^{N_{ss}/2}}\prod_{m=0}^{N_{ss}-1}\exp\left(-\frac{1}{2\sigma_w^2}\left[\left[\mathbf{w}\right]_m^2-2\sigma_w^2\beta\left[\mathbf{u}\right]_m\left[\mathbf{w}\right]_m+\sigma_w^4\beta^2\left[\mathbf{u}\right]_m^2\right]\right)d\mathbf{w}\\
&\quad=\prod_{m=0}^{N_{ss}-1}\exp\left(\frac{\sigma_w^2}{2}\beta^2\left[\mathbf{u}\right]_m^2\right)\int_{\mathbf{w}}\frac{1}{\left(2\pi\sigma_w^2\right)^{N_{ss}/2}}\prod_{m=0}^{N_{ss}-1}\exp\left(-\frac{1}{2\sigma_w^2}\left(\left[\mathbf{w}\right]_m-\sigma_w^2\beta\left[\mathbf{u}\right]_m\right)^2\right)d\mathbf{w} &(3.69)\\
&\quad=\exp\left(\frac{\sigma_w^2}{2}\beta^2\|\mathbf{u}\|^2\right)\int_{\mathbf{w}}\frac{1}{\left(2\pi\sigma_w^2\right)^{N_{ss}/2}}\exp\left(-\frac{1}{2\sigma_w^2}\|\mathbf{w}-\sigma_w^2\beta\mathbf{u}\|^2\right)d\mathbf{w}. &(3.70)
\end{aligned}$$

Note that the argument of the integral in (3.70) is indeed the probability density function of a Gaussian random vector with non-zero mean. Then, since a probability density function is to be integrated, the result of this integral is found to be equal to 1.

Finally, and with the above considerations, the expectation we are looking for is given by

$$\mathrm{E}_{\mathbf{w}}\left[\exp\left(\beta \mathbf{u}^T \mathbf{w}\right)\right] = \exp\left(\frac{\sigma_w^2}{2}\beta^2 \|\mathbf{u}\|^2\right). \tag{3.71}$$

Chapter 4

Waveform Estimation for the Coherent Detection of UWB Signals

4.1 Introduction

Coherent detection in digital communication systems aims at inferring the presence of a known deterministic signal and deciding the most probable transmitted message from an a-priori known set. In the above statement, it is very important to remark that coherent detection assumes the received signals to be *a-priori* known at the receiver. As a result, the detection problem is rather simple and the optimal solution in the presence of white Gaussian noise leads to the well-known *matched filter* detector [Kay98, Ch. 4]. Even for the case of correlated Gaussian noise, the matched filter optimality can be preserved by whitening the received data with the inverse covariance matrix of the noise.

The popular matched filter detector is based on correlating the incoming data with the expected and a-priori known signal. For this reason, the matched filter detector is also referred to as the *replica-correlator* or the *correlator-based receiver*. This architecture has been widely adopted in a vast range of narrowband and spread-spectrum communication systems. For instance, this was the case of the landmark paper by Scholtz [Sch93] where the basis for multiuser UWB communication systems was established. In [Sch93], a simple correlation architecture was adopted since the UWB received pulse was assumed to be a-priori known and to be equal to the pulse radiated by the transmitter.

In practice, however, the UWB received signal hardly ever resembles the original transmitted pulse. This was already noticed by Scholtz in [Win00], where the received pulses were also assumed to be known at the receiver but this time they were explicitly recognized to be different from the transmitted ones. This issue was confirmed in the channel measurements conducted

by [Cra98a], [Cra98b], [Cra02] and [Cas02a], among many others, where the UWB propagation channel was found to exhibit a severe frequency-selective behavior with both angle- and path-dependent distortion. According to these measurement campaigns, the major conclusion is that coherent detection of UWB signals cannot be implemented by itself unless precise channel state information is available at the receiver. That is, channel estimation is indispensable for enabling the coherent detection of UWB signals, and this constitutes the main motivation of this Chapter.

Channel estimation techniques for UWB signals usually adopt a tapped-delay line model for representing the impulse response of the propagation channel. As a result, the received signal is modeled by a set of replicas of a single distorted pulse with different time delays and different amplitude values. However, it is important to note that this is a rather simplified and not realistic model. The reason is that a tapped-delay line model assumes that the same pulse is replicated in time. Therefore, it does not take into account the path-dependent distortion observed in experimental measurements with UWB signals. Nevertheless, this simplified approach has been widely adopted in the literature and many contributions have been proposed in this direction. See for instance [Win97], [Cas02b], [She03] or [Mie03]. The above references are all based on the Rake receiver, that is, the extension of the matched filter principle for the case of multiple and resolvable replicas of a deterministic signal [Pri58], [Pro94, p. 840]. The Rake architecture is composed by a bank of correlators with different time delays for capturing the energy of the known signal over different propagation paths. Finally, all the correlation outputs are conveniently weighted before symbol decision.

When adopting the traditional Rake approach for the coherent detection of UWB signals, another major drawback is that the assumed tapped-delay line model may require hundreds of delays and amplitudes to be estimated. This involves an incredible computational and hardware complexity for resolving such a huge amount of paths and for implementing the corresponding correlators. For this reason, several approaches have emerged to reduce this computational burden. Most authors propose to reduce the total number of paths to just a small set that includes the most dominant ones. For instance, the contribution in [Car04b] proposes to localize clusters of received pulses in order to reduce the search time for finding the most dominant paths. Similarly, [Ara03] proposes a method for choosing the most dominant paths by taking into consideration the distortion of the received pulse.

Without resorting to the traditional Rake architecture, the main goal of this chapter is to solve the two major problems encountered in channel estimation for UWB receivers.

- First, a simple receiver architecture is envisaged where the aggregated channel response, and not the individual paths and amplitudes, is estimated. This constitutes an *unstructured* approach where the paths of the propagation channel are completely disregarded and the received waveform for a single transmitted pulse is considered as a whole. As a result,

it must be remarked that the focus is placed on the *waveform* estimation problem instead of the traditional *channel* estimation problem. That is, the whole received waveform is now the parameter of interest. By doing so a single correlator is required at the receiver. Moreover the intricate path-dependent pulse distortions are inherently incorporated in the estimated waveform and thus, a more realistic representation of the real propagation conditions is achieved.

- Second, special attention is devoted to the very low-SNR working conditions of UWB signals. To this end the low-SNR formulation is adopted herein as an optimizing criterion exhibiting a robust behavior in front of the noise [Váz00]. This is an important issue since most of the existing channel estimation techniques require a medium- to high-SNR to operate. For instance, about 20 to 30 dB are required in many popular channel estimation techniques such as the ones in [Ton94], [Mou95] or [Xu95]. Consequently, their application in the context of UWB communications is doubtful.

Finally, a nondata-aided approach is adopted which avoids the insertion of training symbols. As a result, the effective throughput is maximized, the mean transmitted power is minimized, and hardware complexity is reduced since no pre-alignment with the incoming signal is required.

Based on the above considerations, the structure of this chapter is the following. The signal model for the waveform estimation problem is introduced in Section 4.2. Different modulation formats are considered in a general signal model that it is not intended to be exclusively restricted to UWB systems. As a result, the proposed waveform estimator is derived in a general manner such that it can also be applied to traditional carrier-based narrowband systems. Next, the waveform estimation framework is presented in Section 4.3 where the unconditional maximum likelihood approach is considered. Based on the low-SNR approximation, an optimal waveform estimation technique is proposed in Section 4.4 allowing for both closed-form and iterative implementations. Finally, simulation results are discussed in Section 4.5 and conclusions are drawn in Section 4.6.

4.2 Signal Model

The signal model to be considered in this chapter encompasses different modulation schemes such as pulse-amplitude modulation (PAM), pulse-position modulation (PPM) and amplitude-pulse-position modulation (APPM). Both the families of PAM and A/PPM modulations can be jointly considered because PPM can always be expressed as a sum of parallel independent PAM signals [Mar00]. As a result, the waveform estimation framework for PAM modulation can easily be extended to cover PPM and APPM modulations in a simple manner, and vice versa.

It is important to remark that the signal model considered in this chapter is rather general

and it is not exclusively intended for UWB systems. That is, the proposed waveform estimation technique can be applied to a wide range of communication systems other than UWB. The only requirement is the system to be based on one of the above mentioned modulation formats. In this way, the waveform estimation framework will be derived herein in a general manner. At the end, the results will be particularized to the case of interest of UWB receivers and simulation results will be provided for this case.

4.2.1 General signal model in scalar notation

The signal model is based on a received waveform that suffers from an unknown distortion caused by the radiating elements and/or the frequency-selective and dispersive behavior of the propagation channel. In discrete-time representation, this end-to-end unknown received waveform is denoted by $g(k)$, and in general, it is assumed to be a complex-valued waveform[1]. Furthermore, the unknown waveform $g(k)$ has a maximum time support of N_g samples with $k \in [0, N_g - 1]$, and for $N_g > N_{ss}$ (e.g. in PAM modulation), N_g is assumed to be an integer multiple of the number of samples per symbol, N_{ss}. Note that this is a more general condition than the one previously considered in (3.2). Finally, the unknown received waveform $g(k)$ is assumed to remain constant over the whole observation interval.

With the above considerations, the discrete-time baseband received signal becomes,

$$r(k) = \sum_{n=-\infty}^{+\infty} s_n g\left(k - d_n N_\Delta - n N_{ss}\right) + w\left(k\right) \tag{4.1}$$

where the sequence of amplitude modulating symbols is indicated by s_n and the sequence of pulse-position modulating symbols is indicated by d_n. The time resolution of the pulse-position modulation is N_Δ samples and it is assumed that $d_n = \{0, 1, \ldots, P-1\}$. Finally, $w(k)$ is the additive white Gaussian noise with zero mean and variance σ_w^2.

4.2.2 General signal model in matrix notation

Let us consider an observation interval comprising a total of N samples, with N a multiple value of the number of samples per symbol N_{ss}. Then, the received samples $r(k)$ in (4.1) can be stacked in an $(N \times 1)$ vector $\mathbf{r}$ as follows, $\mathbf{r} \doteq [r(0), r(1), \ldots, r(N-1)]^T$. As a result, the signal model in matrix notation can be expressed as[2],

$$\mathbf{r} = \sum_{p=0}^{P-1} \mathbf{A}_p(\mathbf{g})\mathbf{x}_p + \mathbf{w}. \tag{4.2}$$

[1]This assumption corresponds to a general working scenario. For the case of carrierless UWB signals, the received waveform would be assumed to be real-valued.

[2]The output of the communication channel (i.e. the received signal) is denoted by $\mathbf{r}$ hereafter. This is in contrast with Chapter 3, where the notation $\mathbf{y}$ was adopted, as usual in information theory.

The signal model in (4.2) represents the general signal model for a set of P parallel and independent linearly modulated signals. For the p-th signal, the waveform shaping is achieved through the $(N \times L)$ matrix $\mathbf{A}_p(\mathbf{g})$ whose columns are N_{ss}-samples time-shifted replicas of the unknown waveform $\mathbf{g}$, with $\mathbf{g} \doteq [g(0), g(1), \ldots, g(N_g - 1)]^T$. The parameter L is the number of symbols within the observation interval of N samples, and it can be decomposed in a symmetric manner as $L = 2K + 1$ for some positive integer K. Finally, the transmitted symbols for the p-th linear modulation are included in the $(L \times 1)$ vector $\mathbf{x}_p$ and the noise samples are contained within the $(N \times 1)$ vector $\mathbf{w}$.

The signal model in (4.2) is rather general and it serves to either PAM, PPM or APPM modulations. On the one hand, and for the case of transmitting a traditional PAM modulation, the number of parallel independent PAM modulations P must be set to $P = 1$. As a result, there is only one vector of transmitted symbols $\mathbf{x}_0 = [s_0, s_1, \ldots, s_{L-1}]^T$ that may represent in general either ASK, PSK or QAM symbols. By doing so, the traditional linear model $\mathbf{r} = \mathbf{A}(\mathbf{g})\mathbf{x}_0 + \mathbf{w}$ is obtained. On the other hand, and for case of transmitting M-ary PPM or APPM modulation, the number of parallel independent PAM modulations P must be set to $P = \log_2(M)$. In that case, let's assume the transmission of the p-th PPM position during the n-th symbol. Then, since only one pulse-position can be active for a given transmitted symbol, $[\mathbf{x}_p]_i \neq 0$ if and only if $i = n$. In general, the transmitted symbols $\mathbf{x}_p$ are assumed to be zero mean, $\mathrm{E}_{\mathbf{x}}[\mathbf{x}_p] = 0$ for any p, and to have a covariance matrix given by $\mathrm{E}_{\mathbf{x}}\left[\mathbf{x}_p \mathbf{x}_q^T\right] = \frac{1}{P}\mathbf{I}_L \delta_{pq}$, with $\mathbf{I}_n$ the $(n \times n)$ identity matrix and δ_{ij} the Kronecker delta. For PPM modulation, the hypothesis of zero mean symbols implies that polarity randomization codes are adopted. This is consistent with the common approach in many PPM-based UWB systems, where polarity randomization codes are introduced to avoid the existence of spectral lines that may violate spectral regulations [Nak03].

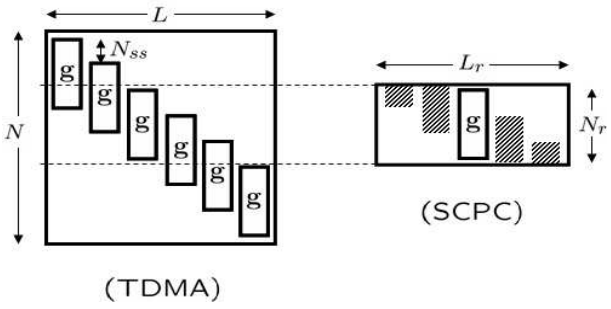

Figure 4.1: Structure of the shaping matrix $\mathbf{A}_p(\mathbf{g})$ with $p = 0$ for both time division multiple access (TDMA) and single-carrier per channel (SCPC) transmissions. Since SCPC involves a continuous transmission, the observation interval at the receiver is always a time-interval of the whole transmission record. Consequently, the shaping matrix becomes truncated (right).

Finally, let us concentrate on the structure of the shaping matrix $\mathbf{A}_p(\mathbf{g})$ since it plays a major role in the problem of waveform identification to be addressed herein. Note that the shaping

matrix $\mathbf{A}_p(\mathbf{g})$ has a particular structure where each column is a N_{ss}-samples time-shifted replica of the unknown waveform $\mathbf{g}$. That is,

$$\mathbf{A}_p(\mathbf{g}) \doteq [\mathbf{a}_{-K,p}(\mathbf{g}), \mathbf{a}_{-K+1,p}(\mathbf{g}), \ldots, \mathbf{a}_{K,p}(\mathbf{g})], \tag{4.3}$$

where the n-th column of $\mathbf{A}_p(\mathbf{g})$ is given by

$$\mathbf{a}_{n,p}(\mathbf{g}) \doteq \mathbf{K}_{n,p}\mathbf{g}, \tag{4.4}$$

with $\mathbf{K}_{n,p}$ an $(N \times N_g)$ N_{ss}-samples shift matrix. The set of time-shift matrices $\mathbf{K}_{n,p}$ is defined from the product of a square $(N \times N)$ N_{ss}-samples shift matrix $\mathbf{J}_{N_{ss}}$, an $(N \times N)$ N_Δ-samples shift matrix $\mathbf{J}_{N_\Delta}$, and an $(N \times N_g)$ zero-padding matrix $\mathbf{\Pi}$ as follows,

$$\mathbf{K}_{n,p} \doteq \mathbf{J}^n_{N_{ss}}\mathbf{J}^p_{N_\Delta}\mathbf{\Pi}. \tag{4.5}$$

The general expression for the set of m-samples shift matrices $\mathbf{J}_m$, for any $0 \leq m \leq N-1$, and for the selection matrix $\mathbf{\Pi}$ is given respectively by

$$[\mathbf{J}_m]_{i,j} = \begin{cases} 1 & : \quad (j-i) = m \\ 0 & : \quad (j-i) \neq m \end{cases}, \tag{4.6}$$

$$\mathbf{\Pi} \doteq \left[\mathbf{0}^T_{(N-N_g)/2\times N_g}, \mathbf{I}_{N_g}, \mathbf{0}^T_{(N-N_g)/2\times N_g}\right]^T. \tag{4.7}$$

Once the signal model for the time-shifted replication of the unknown waveform $\mathbf{g}$ has been defined, the signal model in (4.2) can alternatively be expressed as,

$$\mathbf{r} = \sum_{p=0}^{P-1}\sum_{n=-K}^{K} x_{n,p}\mathbf{K}_{n,p}\mathbf{g} + \mathbf{w} \tag{4.8}$$

with $x_{n,p}$ the n-th entry in $\mathbf{x}_p$. The advantage of the formulation in (4.8) is that it clearly shows the linear dependence of the unknown waveform $\mathbf{g}$ with the received signal $\mathbf{r}$. This linear relationship through the set of matrices $\mathbf{K}_{n,p}$ will be the basis for the derivation of the proposed waveform estimation technique.

4.2.3 Receiver architecture

The system architecture to be considered in this chapter is represented in the block diagram of Figure 4.2. It corresponds to a coherent receiver where the key element to be analyzed is the nondata-aided waveform estimation module. This module is the central part of the coherent receiver and it is the responsible for providing the channel or waveform state information to implement the matched-filtering detection and synchronization

Important attention should be paid to the radiofrequency (RF) front end. This accounts for the low-noise amplifier (LNA), the antialiasing low-pass filtering (LPF) and analog-to-digital

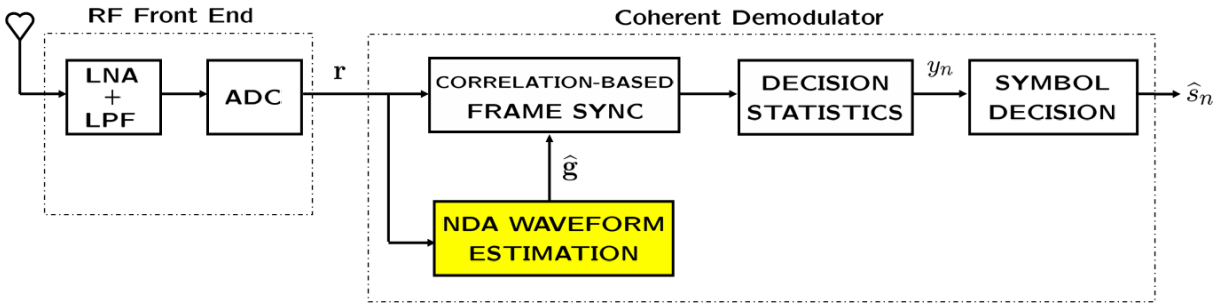

Figure 4.2: Block diagram of the receiver architecture to be considered in this chapter.

conversion (ADC). These are basic elements in any RF front end, and a detailed analysis is out of the scope of this dissertation. For the case of UWB receivers, the interested reader may found valuable the contribution in [Wan05] and the references therein.

The key point in the system architecture of Figure 4.2 is that Nyquist rate sampling is considered. This requires a significant hardware complexity from the ADC point of view, but it allows a fully digital implementation of the whole receiver. Reduced sampling rate receivers have been proposed in the recent literature, but they come at the expense of assuming some kind of a-priori known template for matched filtering in the analog domain. Then, digital conversion is done at the output of the analog correlation at one sample per frame or one sample per symbol. However, when the actual received signal is completely unknown, no realistic template can be assumed for matched filtering and rate reduction. In such a situation, there are two main options. First, implement a transmitted reference (TR) scheme where unmodulated pulses are transmitted to serve as noisy templates at the receiver. Second, adopt a fully digital implementation with Nyquist rate sampling and formulate the optimal detection problem in the digital domain. The latter will be the approach to be considered herein.

Fully digital implementations offer significant advantages over analog and mixed analog/digital implementations. The robustness, accuracy and stability of digital signal processing techniques are important advantages that justify the extra complexity of the required ADC. As indicated in Section 2.6.1, ADC chipsets with sampling rates on the order of 20 Gsps are about to be released to the market. These sampling rates are beyond the minimum requirements for Nyquist rate sampling of UWB signals, and they become a fundamental improvement for the design and implementation of robust UWB receivers.

On the opposite direction, correlation-based receivers can be implemented when the waveform estimate is available. In that case, frame synchronization and decision statistics can be obtained by properly processing of the frame-level matched filter outputs. The tasks of correlation-based synchronization and symbol detection are quite standard in traditional coherent receivers. For this reason, these tasks will not be addressed in the present dissertation since significant information can be found in the literature.

4.3 Waveform Estimation Framework

Channel estimation techniques usually adopt either a *data-aided* (DA) or training-based scheme, or a *nondata-aided* (NDA) or blind[3] approach. When a data-aided approach is adopted, the receiver uses the knowledge of the training symbols to estimate the channel. Data-aided strategies provide the best possible performance, but they require the insertion of training symbols and the pre-alignment of the receiver with the piece of incoming data where the training symbols are located. In contrast, when a nondata-aided approach is adopted, the transmitted symbols are assumed to be unknown at the receiver and channel estimation must rely on the structure and statistical properties of the received signal. Since no training symbols are inserted, nondata-aided techniques maximize the effective throughput and they avoid the requirement of any pre-alignment with the incoming data.

The waveform estimation framework to be developed herein concentrates on the nondata-aided approach and it is based on the seminal work on channel estimation by Tong, Xu and Kailath in [Ton91] and [Ton94]. In their contributions, Tong et al. showed that by sampling at a rate greater than the symbol rate, the received signal becomes cyclostationary and blind channel estimation is possible from second-order statistics[4]. Since the advent of second-order blind channel estimation techniques, several methods have been proposed including subspace decomposition [Lou00], [Mou95], least-squares [Xu95], iterative methods [Hua96a], [Slo94] or moment matching techniques [Gia97]. An excellent review of these methods can be found in [Liu96] and [Ton98], and the analysis of the asymptotic performance and limitations in [Zen97a].

Nevertheless, one the main problems of nondata-aided channel or waveform estimation is the severe impact of the so-called outliers or abnormals when working under practical SNR conditions. This is especially dramatic when dealing with UWB signals, since the stringent emission limits force the receiver to operate near the noise floor. For this reason, the application of traditional channel or waveform estimation techniques is limited in real systems. Basically, this is caused by the deterministic approach in the analytical formulation of these methods, which results in a suboptimal performance in the presence of severe noise.

Because of the high-SNR requirements of existing channel and waveform estimation techniques, the main goal of this section is to provide the mathematical framework for the derivation of optimal waveform estimators to operate in the low-SNR regime. To this end, the low-SNR formulation is adopted herein as an optimizing criterion exhibiting a robust behaviour in front of the noise. Notice that the low-SNR approximation is a classical approach both in estimation and detection theory, and some representative examples can be found in [Kay93], [Men97] or

[3] The terms "nondata-aided" and "blind" are indistinguishably used in this dissertation and they both refer to estimation techniques that do not require the insertion of training symbols.

[4] This is one of the reasons for adopting Nyquist rate sampling in digital UWB receivers.

[Váz00]. However, it is indeed a realistic approach when dealing with UWB systems. Finally, it is also important to remark that the low-SNR assumption does not necessarily imply that the SNR must be particularly low to guarantee that the estimator will work. In fact, most low-SNR techniques still perform quite well for a rather wide range of SNR values.

4.3.1 Low-SNR Unconditional Maximum Likelihood Waveform Estimation

The maximum likelihood (ML) criterion is certainly one of the most popular methods in estimation theory since it provides a systematic way for deriving asymptotically unbiased and efficient estimators [Kay93]. For the problem under consideration, the ML estimate for the waveform $\mathbf{g}$ is the solution to the maximization problem

$$\widehat{\mathbf{g}}_{\mathrm{ML}} = \arg\max_{\mathbf{g}} \Lambda\left(\mathbf{r}|\mathbf{g};\mathbf{x}\right) \tag{4.9}$$

where $\Lambda\left(\mathbf{r}|\mathbf{g};\mathbf{x}\right)$ is the likelihood function of the received data $\mathbf{r}$ conditioned on the unknown waveform $\mathbf{g}$ and the transmitted symbols $\mathbf{x}$.

Clearly, the solution to (4.9) depends on the statistical knowledge of the transmitted symbols $\mathbf{x}$. In the case of data-aided or training-based schemes, this leads to a conventional least squares error (LS) problem. However, a more complex scenario corresponds to the nondata-aided estimation problem. In that case, the transmitted symbols are unknown and they become a nuisance parameter in the ML formulation. To circumvent this limitation, the so-called *stochastic* or *unconditional* maximum likelihood estimation considers the nuisances as unknown random parameters with a known statistical distribution [Ott93]. Then, the marginal likelihood function is evaluated with respect to these unknowns, and the UML estimate becomes

$$\widehat{\mathbf{g}}_{\mathrm{UML}} = \arg\max_{\mathbf{g}} \Lambda\left(\mathbf{r}|\mathbf{g}\right) = \arg\max_{\mathbf{g}} \mathrm{E}_{\mathbf{x}}\left[\Lambda\left(\mathbf{r}|\mathbf{g};\mathbf{x}\right)\right]. \tag{4.10}$$

In general, the expectation $\mathrm{E}_{\mathbf{x}}\left[\cdot\right]$ in (4.10) poses insurmountable obstacles or leads to a complicated cost function. Consequently, a closed-form solution is difficult to be obtained and the maximization problem in (4.10) must be solved in a numerical manner by using either a grid search or iterative/gradient methods [Gia97], [Hua02], [LS04]. In order to circumvent this limitation, the low-SNR approximation is adopted herein as a strategy to reduce the difficulty in obtaining a closed-form solution to the optimization problem in (4.10). In the sequel, most of the mathematical derivations for the low-SNR UML criterion are omitted for clarity reasons. However, they are all given in Appendix 4.A, 4.B and 4.C. The reader is also referred to [Váz00] for a more general presentation about the application of the low-SNR approximation to UML estimation problems.

For the problem at hand, the likelihood function $\Lambda\left(\mathbf{r}|\mathbf{g};\mathbf{x}\right)$ is based on the Gaussian noise

probability density function as follows,

$$\Lambda\left(\mathbf{r}|\mathbf{g};\mathbf{x}\right) = C_0 \exp\left(-\frac{1}{\sigma_w^2}\left\|\mathbf{r} - \sum_{p=0}^{P-1}\mathbf{A}(\mathbf{g})\mathbf{x}_p\right\|^2\right) \tag{4.11}$$

with C_0 an irrelevant positive constant. Then, by expanding the quadratic norm in (4.11) and just taking into consideration those terms which depend on the unknown $\mathbf{g}$, we have

$$\Lambda\left(\mathbf{r}|\mathbf{g};\mathbf{x}\right) = C_1 \exp\left(\frac{2}{\sigma_w^2}\chi\left(\mathbf{r};\mathbf{g};\mathbf{x}\right)\right), \tag{4.12}$$

$$\chi\left(\mathbf{r};\mathbf{g};\mathbf{x}\right) \doteq \sum_{p=0}^{P-1}\mathrm{Re}\left[\mathbf{x}_p^H\mathbf{A}_p^H\mathbf{r}\right] - \frac{1}{2}\sum_{p=0}^{P-1}\sum_{q=0}^{P-1}\mathbf{x}_q^H\mathbf{A}_q^H\mathbf{A}_p\mathbf{x}_p, \tag{4.13}$$

with the constant $C_1 \doteq C_0 \exp\left(-\mathbf{r}^H\mathbf{r}/\sigma_w^2\right)$. Moreover, note that the dependence of $\mathbf{A}$ on $\mathbf{g}$ is omitted for the sake of simplicity.

At this point, the low-SNR approach is considered. Under the low-SNR regime, the approximation $2\chi\left(\mathbf{r};\mathbf{g};\mathbf{x}\right)/\sigma_w^2 \ll 1$ is reasonable and the Taylor series expansion can be applied to (4.12). Then, the problem of performing the expectation $\mathrm{E}_{\mathbf{x}}\left[\Lambda\left(\mathbf{r}|\mathbf{g};\mathbf{x}\right)\right]$ on the Gaussian noise probability density function is now converted into the problem of performing the expectation on a Taylor series expansion.

Proceeding in this way, Appendix 4.A shows that the low-SNR UML cost function is given by

$$L'\left(\mathbf{r}|\mathbf{g}\right) = Tr\left(\breve{\mathbf{M}}\left[\mathbf{R} - \sigma_w^2\mathbf{I}_{N_r}\right]\right) + \frac{1}{2}\|\breve{\mathbf{M}}\|_F^2 \tag{4.14}$$

with $\breve{\mathbf{M}}$ the $(N_r \times N_r)$ matrix given by

$$\breve{\mathbf{M}} \doteq \sum_{p=0}^{L_p-1}\sum_{n=-K_r}^{K_r}\breve{\mathbf{K}}_{n,p}\mathbf{g}\mathbf{g}^H\breve{\mathbf{K}}_{n,p}^H, \tag{4.15}$$

where a truncated observation interval of N_r samples is now considered. In (4.15), K_r stands for the one-sided number of N_{ss}-samples shifted replicas of $\mathbf{g}$ contained within the observation interval of N_r samples. Similarly, L_p stands for the number of N_Δ-samples shifted replicas of $\mathbf{g}$ contained within the same observation interval of N_r samples. Further details will be provided later on for the parameters K_r and L_p. Moreover, the matrix $\breve{\mathbf{K}}_{n,p}$ in (4.15) is the $(N_r \times N_g)$ truncated version of the $(N \times N_g)$ matrix $\mathbf{K}_{n,p}$ defined in (4.5). That is, in Matlab notation, $\breve{\mathbf{K}}_{n,p} \doteq \mathbf{K}_{n,p}\left(1:N_r,:\right)$. Finally, $\mathbf{R}$ is the $(N_r \times N_r)$ synchronous autocorrelation matrix of the received data defined as

$$\mathbf{R} \doteq \lim_{L\to\infty}\frac{1}{L}\sum_{n=0}^{L-1}\mathbf{r}_n\mathbf{r}_n^H \tag{4.16}$$

with $\mathbf{r}_n \doteq \left[r(nN_{ss}), r(nN_{ss}+1), \ldots, r(nN_{ss}+N_r-1)\right]^T$.

It is important to note that the truncated observation interval of N_r samples in (4.14) is fixed according to the rule $N_r = \max\{N_g, N_{ss}\}$. As indicated in Appendix 4.A, the truncation of the observation interval from N samples to N_r samples provides a more intuitive and comprehensive interpretation of the waveform identification problem. In addition, significant computational complexity is saved because the matrices involved in (4.14) do not depend on the length of the observation interval but just on the fixed values of N_g or N_{ss}. Moreover, by choosing $N_r = \max\{N_g, N_{ss}\}$ we always guarantee that at least one of the waveform replicas completely falls within the observation interval of N_r samples (see Fig. 4.1).

Once the low-SNR UML cost function has been introduced in (4.14), two important remarks must be made. First, note that for the observation interval of N_r samples, the signal subspace is now the linear space spanned by $\breve{\mathbf{M}}$. Thus, the first term in (4.14) is projecting the synchronous autocorrelation matrix of the received signal, $\mathbf{R}$, onto the signal subspace. There is an important detail in this projection, and it is that the contribution of the noise must be first removed from $\mathbf{R}$ by substracting the noise covariance $\mathbf{C}_w = \sigma_w^2 \mathbf{I}_{N_r}$, as indicated in (4.14). This implies that the noise power σ_w^2 must be known at the receiver. However, this is not a problem for most modern communication systems since the knowledge of the noise power is also required in other stages of the receiver. For instance, it is required by many synchronization and detection techniques but also by iterative decoding. For this reason it seems reasonable to assume that the noise power will be available. Otherwise it can be estimated from the eigendecomposition of $\mathbf{R}$ to be considered in Section 4.3.2. Nevertheless, the projection of $\mathbf{R}$ onto the signal subspace is one of the major features of the resulting low-SNR UML cost function. Note that this is in contrast with many of the existing blind channel/waveform estimation techniques, which are usually based on the exploitation of the noise subspace [Mou95], [Xu03a], [Zar05]. However, it seems more convenient to exploit the signal subspace of the received signal rather than the noise subspace, especially when working in the low-SNR regime. This is because the signal subspace presents a more robust behavior in front of the noise and possible ill-conditioning than the noise subspace. Therefore, a more robust performance is expected by using the signal subspace.

The second important remark is that the low-SNR UML cost function in (4.14) incorporates in a natural manner a second-order constraint for the waveform estimation problem. This constraint is given by the term $\|\breve{\mathbf{M}}\|_F^2$, and together with the signal subspace projection, both can be thought to be the waveform dependent terms of a correlation matching problem. This will be illustrated in more detail in Section 4.4, where the solution to the low-SNR UML cost function in (4.14) is found to be given by the solution to a least squares problem on the second-order statistics of the received signal.

4.3.2 Subspace-Compressed Approach to the Waveform Estimation Problem

One of the major drawbacks of ML methods is that a closed-form solution is usually difficult to be obtained. In addition, and for the problem of channel or waveform identification, the adoption of ML methods is further complicated by the possible existence of local minima [Ton98]. This is the case of (4.14), where a nonlinear optimization with respect to $\mathbf{g}$ is required. However, a valuable help is given when the information regarding the signal subspace is available. This is because the subspace-constraint helps the ML estimator to restrict the solution space to a neighborhood around the true waveform. Thus, a valid estimate for the unknown channel or waveform is still possible even when close to unidentifiable [Zen97b].

In this sense the purpose of this section is to present a subspace constraint for the low-SNR UML cost function presented in (4.14). To this end, let $\mathbf{R}$ be the $(N_r \times N_r)$ synchronous autocorrelation matrix defined in (4.16). Thus, it is easy to prove that $\mathbf{R}$ is asymptotically given by

$$\mathbf{R} = \breve{\mathbf{M}} + \sigma_w^2 \mathbf{I}_{N_r}. \tag{4.17}$$

Moreover, the synchronous autocorrelation matrix $\mathbf{R}$ can be decomposed as

$$\mathbf{R} = \mathbf{U}_{\mathrm{s}} \mathbf{D}_{\mathrm{s}} \mathbf{U}_{\mathrm{s}}^H + \mathbf{U}_{\mathrm{n}} \mathbf{D}_{\mathrm{n}} \mathbf{U}_{\mathrm{n}}^H, \tag{4.18}$$

where $\mathbf{D}_{\mathrm{s}} = \mathrm{diag}(\lambda_1 + \sigma_w^2, \ldots, \lambda_d + \sigma_w^2)$ contains the d largest signal-subspace eigenvalues of $\mathbf{R}$, with $\lambda_1 \geq \lambda_2 \geq \ldots \geq \lambda_d$, and the $(N_r \times d)$ matrix $\mathbf{U}_{\mathrm{s}}$ contains the corresponding signal-subspace eigenvectors. Similarly, $\mathbf{D}_{\mathrm{n}} = \mathrm{diag}(\lambda_{d+1}, \lambda_{d+2}, \ldots, \lambda_{N_r})$ contains the $N_r - d$ noise-subspace eigenvalues with $\lambda_{d+1} = \lambda_{d+2} = \ldots = \lambda_{N_r} = \sigma_w^2$, and the $(N_r \times (N_r - d))$ matrix $\mathbf{U}_{\mathrm{n}}$ contains the corresponding noise-subspace eigenvectors.

From (4.17) and (4.18), the signal subspace of the synchronous autocorrelation matrix $\mathbf{R}$ is the linear space spanned by the columns of $\breve{\mathbf{M}}$, since $range\left\{\breve{\mathbf{M}}\right\} = range\left\{\mathbf{U}_{\mathrm{s}}\right\}$. Then the dimension of the signal subspace is given by the number of linearly independent columns in $\breve{\mathbf{M}}$. In order to make clear the relationship between the signal subspace dimension and the structure of the received signal, let us define the following parameters. For the case of PAM modulations, let $L_r \doteq 2K_r + 1$, for some positive integer K_r, be the number of replicas with a time-shift of N_{ss} samples contained within the observation interval of N_r samples. Similarly, and for the case of PPM and APPM modulations, let L_p be the number of replicas with a time-shift of N_Δ samples contained within the observation interval of N_r samples. Then, the relationship between the parameters N_r, N_g, L_r, L_p and the signal subspace dimension d, is described in Table 4.1.

From the above considerations, and since $range\left\{\breve{\mathbf{M}}\right\} = range\left\{\mathbf{U}_{\mathrm{s}}\right\}$, the most important point is that the unknown waveform $\mathbf{g}$ must be a linear combination of the signal-subspace eigenvectors. That is,

$$\mathbf{g} = \mathbf{U}_{\mathrm{s}} \boldsymbol{\alpha} \tag{4.19}$$

Observation interval for computing $\mathbf{R}$: $N_r = \max\{N_g, N_{ss}\}$					
	N_r	L_r	K_r	L_p	d
if $N_g \leq N_{ss}$ (with PAM)	N_{ss}	1	0	0	L_r
if $N_g \leq N_{ss}$ (with PPM or APPM)	N_{ss}	1	0	P	L_p
if $N_g > N_{ss}$ (only occurs in PAM)	N_g	$2\left\lceil \frac{N_g}{N_{ss}} \right\rceil - 1$	$\frac{L_r-1}{2}$	0	L_r

Table 4.1: Relationship between the basic signal model parameters.

for some $(d \times 1)$ vector $\boldsymbol{\alpha}$ such that $\boldsymbol{\alpha}^H \boldsymbol{\alpha} = 1$. Note that the vector $\boldsymbol{\alpha}$ contains the coordinates of the unknown waveform with respect to the basis of signal eigenvectors. Moreover, it is important to remark that the unknown waveform $\mathbf{g}$ is an $(N_g \times 1)$ vector whereas the vector of coordinates $\boldsymbol{\alpha}$ in (4.19) is $(d \times 1)$. The key point is that by sampling at a rate equal or greater than twice the symbol rate, the maximum dimension of the signal subspace d is guaranteed to be always smaller than the maximum finite time support of the unknown waveform, N_g. Thus, by projecting the received signal onto the signal subspace, the total number of unknowns is reduced from N_g to just d, for the same amount of received data. This can be seen by noting that for the largest value of d,

$$d_{\max} = L_r = 2\left\lceil \frac{N_r}{N_{ss}} \right\rceil - 1, \tag{4.20}$$

with $N_r \doteq \max\{N_g, N_{ss}\}$, and thus,

$$d_{\max} < N_g \Leftrightarrow N_{ss} \geq 2. \tag{4.21}$$

Since the number of subspace coordinates d is smaller than the number of unknown waveform samples N_g, there is a gain in the effective SNR and a more robust performance in front of the noise is obtained.

4.4 Proposed Waveform Estimation Technique

The key element for the derivation of the proposed waveform estimation technique is the adoption of the *vec* operator. The *vec* operator stacks the columns of any $(M \times N)$ matrix in the form of an $(MN \times 1)$ vector and it is a useful mathematical tool that allows us to obtain a simple and insightful solution to the low-SNR UML cost function in (4.14). An extended version of the *vec* operator, termed *vech* operator, may also be useful. The *vech* operator is especially devoted to dealing with any $(M \times M)$ symmetric matrix and it ignores the elements that are above the diagonal. Consequently, the *vech* operator eliminates the redundancy of symmetric matrices and reduces the overall computational burden. However, for the sake of clarity, only

the standard *vec* operator will be considered henceforth. For more details about the *vec* and the *vech* operator, the reader is referred to [Har00, Ch. 16].

By adopting the *vec* operator, the low-SNR UML cost function in (4.14) is shown in Appendix 4.C to be given by

$$L'(\mathbf{r}|\mathbf{g}) = \boldsymbol{\alpha}_{\mathrm{v}}^H \mathbf{Q}^H \mathring{\mathbf{r}}_{\mathrm{v}} + \frac{1}{2}\boldsymbol{\alpha}_{\mathrm{v}}^H \mathbf{Q}^H \mathbf{Q}\boldsymbol{\alpha}_{\mathrm{v}} \tag{4.22}$$

where

$$\mathring{\mathbf{r}}_{\mathrm{v}} \doteq vec\left(\mathbf{R} - \sigma_w^2 \mathbf{I}_{N_r}\right), \tag{4.23}$$

$$\mathbf{Q} \doteq \sum_{n=-K_r}^{K_r} \sum_{p=0}^{L_p-1} \left(\breve{\mathbf{K}}_{n,p}\mathbf{U}_{\mathrm{s}}^*\right) \otimes \left(\breve{\mathbf{K}}_{n,p}\mathbf{U}_{\mathrm{s}}\right), \tag{4.24}$$

$$\boldsymbol{\alpha}_{\mathrm{v}} \doteq vec\left(\boldsymbol{\alpha}\boldsymbol{\alpha}^H\right). \tag{4.25}$$

The expression in (4.22) is the basis for the proposed waveform estimation approach. Note that by using the *vec* operator a very simple and insightful expression is obtained. In fact the expression in (4.22) is a quadratic equation with a quadratic unknown $\boldsymbol{\alpha}_{\mathrm{v}}$, since $\boldsymbol{\alpha}_{\mathrm{v}} = vec\left(\boldsymbol{\alpha}\boldsymbol{\alpha}^H\right)$ with $\boldsymbol{\alpha}$ the coordinates of the unknown waveform in the basis of the signal eigenvectors. The key point is to notice that the optimization of (4.22) is equivalent to the optimization of a least squares problem. That is,

$$\max_{\boldsymbol{\alpha}_{\mathrm{v}}} L'(\mathbf{r}|\mathbf{g}) = \max_{\boldsymbol{\alpha}_{\mathrm{v}}} \left\{ \boldsymbol{\alpha}_{\mathrm{v}}^H \mathbf{Q}^H \mathring{\mathbf{r}}_{\mathrm{v}} + \frac{1}{2}\boldsymbol{\alpha}_{\mathrm{v}}^H \mathbf{Q}^H \mathbf{Q}\boldsymbol{\alpha}_{\mathrm{v}} \right\} = \min_{\boldsymbol{\alpha}_{\mathrm{v}}} \|\mathring{\mathbf{r}}_{\mathrm{v}} - \mathbf{Q}\boldsymbol{\alpha}_{\mathrm{v}}\|^2. \tag{4.26}$$

Therefore, the low-SNR UML criterion for the waveform estimation problem is equivalent to a least squares problem but on the second-order statistics of the received signal. This is because $\mathring{\mathbf{r}}_{\mathrm{v}} = vec(\mathbf{R})$ contains the samples of the synchronous autocorrelation of the received signal. For this reason, the expression for the low-SNR UML cost function can be understood as a *correlation matching* (CM) method. Based on heuristic reasonings, CM methods have been previously proposed in the literature for channel estimation problems. However, solving this problem involves a nonlinear optimization which usually requires numerical evaluation [Zen97b], [Ton98], [LS04]. In contrast, the low-SNR UML approach presented in this dissertation results in a simple CM problem with a closed-form solution.

4.4.1 Closed-form solution

Based on the equivalence between the low-SNR UML criterion and the least squares problem in (4.26), the optimal solution for this particular correlation matching problem is given by

$$\widehat{\boldsymbol{\alpha}}_{\mathrm{v}} = \gamma \left(\mathbf{Q}^H \mathbf{Q}\right)^{-1} \mathbf{Q}^H \mathring{\mathbf{r}}_{\mathrm{v}} \tag{4.27}$$

with γ an irrelevant constant which is inherent in the solution of any blind channel or waveform estimator based on second-order statistics. The closed-form solution in (4.27) has the same structure as a traditional least squares problem except for the fact that the unknown variables are quadratic. Thus, once $\boldsymbol{\alpha}_{\mathrm{v}}$ is recovered, another step is still required to undo the *vec* operator in $\boldsymbol{\alpha}_{\mathrm{v}} = vec\left(\boldsymbol{\alpha}\boldsymbol{\alpha}^H\right)$. The goal is to recover the vector of signal subspace coordinates $\boldsymbol{\alpha}$, since $\mathbf{g} = \mathbf{U}_{\mathrm{s}}\boldsymbol{\alpha}$. However, when the *vec* operator is undone, noise and possible signal model mismatches may cause the matrix $\boldsymbol{\alpha}\boldsymbol{\alpha}^H$ to be degraded by a perturbation matrix $\boldsymbol{\Delta}$. That is,

$$vec^{-1}\left(\widehat{\boldsymbol{\alpha}}_{\mathrm{v}}\right) = \boldsymbol{\alpha}\boldsymbol{\alpha}^H + \boldsymbol{\Delta} \tag{4.28}$$

with vec^{-1} the inverse *vec* operation. In the absence of any disturbance, the matrix $vec^{-1}\left(\widehat{\boldsymbol{\alpha}}_{\mathrm{v}}\right)$ in (4.28) is a rank one matrix. Therefore an estimate for $\boldsymbol{\alpha}$ can be obtained from the eigendecomposition of $vec^{-1}\left(\widehat{\boldsymbol{\alpha}}_{\mathrm{v}}\right)$ and then taking the eigenvector corresponding to the maximum eigenvalue. That is,

$$vec^{-1}\left(\widehat{\boldsymbol{\alpha}}_{\mathrm{v}}\right)\widehat{\boldsymbol{\alpha}} = \lambda_{max}\widehat{\boldsymbol{\alpha}}, \tag{4.29}$$

where λ_{max} is the maximum eigenvalue of the matrix $vec^{-1}\left(\widehat{\boldsymbol{\alpha}}_{\mathrm{v}}\right)$. This two-step procedure is similar to the one already considered in other contributions such as [Xu01], and recently in [Wu06]. Finally, the waveform estimate is given by

$$\widehat{\mathbf{g}} = \mathbf{U}_{\mathrm{s}}\widehat{\boldsymbol{\alpha}}. \tag{4.30}$$

For clarity, the required steps for the proposed technique are summarized in Table 4.2.

1)	Estimate the $(N_r \times N_r)$ synchronous autocorrelation matrix $\mathbf{R}$ in (4.16).
2)	Determine $\mathbf{U}_{\mathrm{s}}$, the matrix of signal subspace eigenvectors of $\mathbf{R}$ in (4.18).
3)	Construct the vector $\mathring{\mathbf{r}}_{\mathrm{v}}$ in (4.23) and the matrix $\mathbf{Q}$ in (4.24).
4.1)	Solve $\widehat{\boldsymbol{\alpha}}_{\mathrm{v}} = \left(\mathbf{Q}^H\mathbf{Q}\right)^{-1}\mathbf{Q}^H\mathring{\mathbf{r}}_{\mathrm{v}}$ in (4.27).
4.2)	Get $\widehat{\boldsymbol{\alpha}}$, the maximum eigenvector of $vec^{-1}\left(\widehat{\boldsymbol{\alpha}}_{\mathrm{v}}\right)$ in (4.29).
5)	Obtain the waveform estimate as $\widehat{\mathbf{g}} = \mathbf{U}_{\mathrm{s}}\widehat{\boldsymbol{\alpha}}$ in (4.30).

Table 4.2: Description of the proposed low-SNR UML waveform estimation technique.

It has been previously mentioned that the proposed waveform estimation technique can be understood as a CM method. The reason is that it performs a matching between the synchronous autocorrelation of the received signal and the synchronous autocorrelation of the signal model. Indeed, CM methods have been previously proposed in the literature for nondata-aided channel estimation, but the problem is found to be nonlinear and the solution is usually obtained in a rather heuristic manner by numerical evaluation or gradient-based search. In this dissertation, however, we follow a completely different approach. First, the optimal UML formulation is considered. Second, the proposed technique is especially designed to cope with low-SNR scenarios.

Third, the likelihood function is compressed with the information regarding the signal subspace instead of using the noise subspace. Fourth, a closed-form solution is provided.

Apart from the above considerations it is also important to remark that, since the proposed technique can be understood as a CM method, it benefits from the well-known asymptotic performance of these methods. A detailed analysis on the performance of CM methods was presented in [Gia97] and [Zen97a]. One of the main contributions was the derivation of a lower bound for the performance of any CM method, the so-called *asymptotic normalized mean square error* (ANMSE), which showed the superior performance of moment-based estimators (e.g. CM methods) in comparison with traditional eigenstructure-based estimators.

Discussion on the identifiability of the proposed technique

According to the structure of the proposed waveform estimation technique in Table 4.2, the necessary condition for the waveform $\mathbf{g}$ to be uniquely recovered is that the $(N_r^2 \times L_r^2)$ matrix $\mathbf{Q}$ in (4.24) must be a full column rank matrix. The reason is that when $\mathbf{Q}$ is a full column rank matrix, there exists a unique solution to the least squares problem $J(\boldsymbol{\alpha}_{\mathrm{v}}) = \|\mathring{\mathbf{r}}_{\mathrm{v}} - \mathbf{Q}\boldsymbol{\alpha}_{\mathrm{v}}\|^2$. Once the solution to $\boldsymbol{\alpha}_{\mathrm{v}}$ in (4.27) is found to be unique, then the solution to $\boldsymbol{\alpha}$, and thus, the solution to $\mathbf{g}$, are all unique because the relationship between $\boldsymbol{\alpha}_{\mathrm{v}}$, $\boldsymbol{\alpha}$ and $\mathbf{g}$ is linear. However, a formal proof that guarantees the full column rank condition of matrix $\mathbf{Q}$ is difficult to be obtained and it is still under investigation. Meanwhile, it has been heuristically found that the matrix $\mathbf{Q}$ is a full column rank matrix for all the tested waveforms by the authors. This can be seen in the cumulative results shown in Section 4.5 where the robustness of the proposed technique is evaluated for randomly generated unknown waveforms.

4.4.2 Gradient-based solution

Apart from the closed-form solution presented in Section 4.4.1, a gradient-based procedure can also be implemented for obtaining the low-SNR UML estimate for the unknown waveform. At first glance, there should be no interest in deriving a gradient-based or iterative solution for the waveform estimation problem since a systematic and straightforward closed-form solution is available. However, the problem under consideration allows an iterative solution that, in some circumstances, may provide a slightly better performance than the one provided by the proposed closed-form implementation.

The reason for the potential performance gain of a gradient-based solution is the avoidance of the rank one constraint in the recovery of $\boldsymbol{\alpha}$ from the matrix $vec^{-1}(\widehat{\boldsymbol{\alpha}}_{\mathrm{v}}) = \boldsymbol{\alpha}\boldsymbol{\alpha}^H + \boldsymbol{\Delta}$ in (4.28). The matrix $vec^{-1}(\widehat{\boldsymbol{\alpha}}_{\mathrm{v}})$ is virtually a rank one matrix when $\boldsymbol{\Delta} = \mathbf{0}$, and thus, with a single dominant eigenvector. However, noise and possible disturbances result in $\boldsymbol{\Delta} \neq \mathbf{0}$ which

may cause the number of significant eigenvectors to be greater than one. In that case recovering $\boldsymbol{\alpha}$ just by taking the most dominant eigenvector, as proposed in the closed-form implementation of Section 4.4.1, may introduce certain degradation. In order to circumvent this limitation, and taking into consideration the properties of the *vec* operator, a gradient-based solution can be implemented by using the identity

$$\boldsymbol{\alpha}_{\mathrm{v}} = \boldsymbol{\alpha}^* \otimes \boldsymbol{\alpha} \tag{4.31}$$

and solving the waveform estimation problem for $\boldsymbol{\alpha}$ instead of $\boldsymbol{\alpha}_{\mathrm{v}}$. This could not be done in the closed-form approach since the resulting mathematical formulation was extremely intricate.

If $\boldsymbol{\alpha}$ is assumed to be the parameter of interest, the estimate for $\boldsymbol{\alpha}$ can be directly obtained by maximizing the low-SNR UML likelihood cost function in (4.22). That is,

$$\widehat{\boldsymbol{\alpha}} = \arg\max_{\boldsymbol{\alpha}} \; L'\left(\mathbf{r}|\mathbf{g} = \mathbf{U}_{\mathrm{s}}\boldsymbol{\alpha}\right) \tag{4.32}$$

$$= \arg\max_{\boldsymbol{\alpha}} \left\{ \left(\boldsymbol{\alpha}^* \otimes \boldsymbol{\alpha}\right)^H \mathbf{Q}^H \mathring{\mathbf{r}}_{\mathrm{v}} + \frac{1}{2}\left(\boldsymbol{\alpha}^* \otimes \boldsymbol{\alpha}\right)^H \mathbf{Q}^H \mathbf{Q}\left(\boldsymbol{\alpha}^* \otimes \boldsymbol{\alpha}\right) \right\} \tag{4.33}$$

where $\boldsymbol{\alpha}_{\mathrm{v}}$ has been substituted by $(\boldsymbol{\alpha}^* \otimes \boldsymbol{\alpha})$ in (4.33). Then, a gradient-based scheme such as the Newton-Raphson iteration can be implemented as follows,

$$\widehat{\boldsymbol{\alpha}}^{(k+1)} = \widehat{\boldsymbol{\alpha}}^{(k)} - \left[\nabla^2_{\boldsymbol{\alpha}} L'\left(\mathbf{r}|\mathbf{g} = \mathbf{U}_{\mathrm{s}}\boldsymbol{\alpha}\right)\right]^{-1} \left[\nabla_{\boldsymbol{\alpha}} L'\left(\mathbf{r}|\mathbf{g} = \mathbf{U}_{\mathrm{s}}\boldsymbol{\alpha}\right)\right]_{\big|\boldsymbol{\alpha}=\widehat{\boldsymbol{\alpha}}^{(k)}} \tag{4.34}$$

where the gradient of the low-SNR UML cost function and the Hessian are given respectively by

$$\nabla_{\boldsymbol{\alpha}} L'\left(\mathbf{r}|\mathbf{g} = \mathbf{U}_{\mathrm{s}}\boldsymbol{\alpha}\right) = -\left(\boldsymbol{\alpha}^T \otimes \mathbf{I}\right) \mathbf{Q}^H \left(\mathring{\mathbf{r}}_{\mathrm{v}} - \mathbf{Q}\left(\boldsymbol{\alpha}^* \otimes \boldsymbol{\alpha}\right)\right), \tag{4.35}$$

$$\nabla^2_{\boldsymbol{\alpha}} L'\left(\mathbf{r}|\mathbf{g} = \mathbf{U}_{\mathrm{s}}\boldsymbol{\alpha}\right) = \left(\boldsymbol{\alpha}^T \otimes \mathbf{I}\right) \mathbf{Q}^H \mathbf{Q}\left(\boldsymbol{\alpha}^* \otimes \mathbf{I}\right). \tag{4.36}$$

Nevertheless, the performance gain of the proposed iterative implementation is found to be very small for the typical simulation scenarios considered in this dissertation. For instance, this can be seen in Figure 4.3 for a simple simulation scenario of an UWB receiver operating with binary-PAM at $E_s/N_0 = 2$ dB with unknown random Gaussian waveforms. The advantage of the iterative implementation is just about 0.2 dB, in terms of normalized mean square error for the estimated waveform when compared to the result provided by the closed-form solution. Moreover, this small advantage requires about 50 iterations to be appreciated. Since the iterative implementation requires a higher computational complexity than the closed-form solution, the similar results provided by both techniques make the simple closed-form implementation to be preferred. As a result, the closed-form implementation will only be considered in the simulation results to be presented next in Section 4.5.

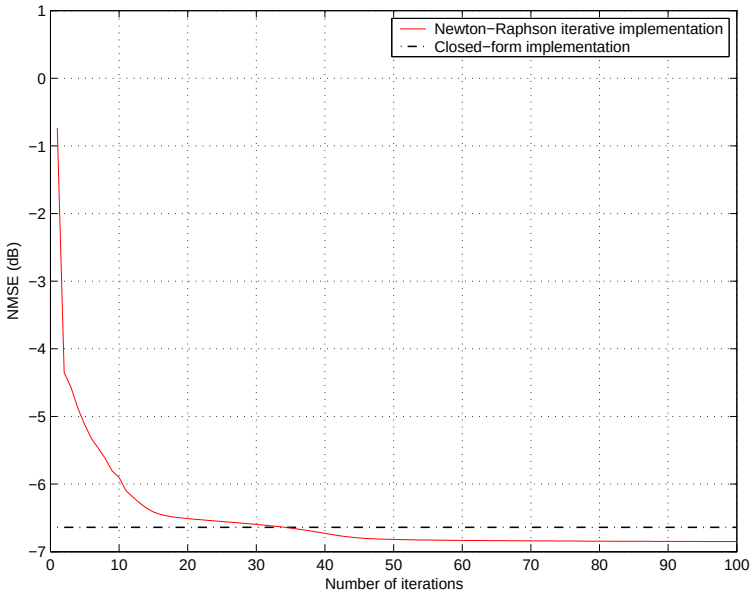

Figure 4.3: Performance comparison between the closed-form and iterative implementations of the proposed waveform estimation technique for a typical simulation scenario with an observation interval of 250 symbols.

4.5 Simulation Results

Computer simulations have been carried out to validate the proposed waveform estimator and to compare the performance with other closed-form and second-order statistics based methods. To this end, the well-known subspace approach (SS) in [Lou00] is considered and the figure of merit for the simulation results is the normalized mean square error (NMSE) which is defined here as,

$$\mathrm{NMSE}(\mathbf{g}) = \frac{1}{N_{\mathrm{sim}}} \sum_{n=1}^{N_{\mathrm{sim}}} \frac{\|\mathbf{g} - \widehat{\mathbf{g}}_n\|^2}{\|\mathbf{g}\|^2} \tag{4.37}$$

with N_{sim} the total number of Monte Carlo runs and $\widehat{\mathbf{g}}_n$ the waveform estimate for the n-th trial run.

The simulation results can be classified into two different groups. First, simulation results for the case of traditional PAM modulation with 16-QAM constellation symbols are considered. In this case, the unknown received waveform is considered to be a particular complex-valued waveform that is selected at random from a multivariate Gaussian distribution. Second, simulations results for UWB signals with binary APPM modulation are presented. In this case, and according to the real nature of carrierless UWB signals, the unknown waveform is considered to be a real-valued waveform obtained from the UWB propagation channel model proposed by Intel [Foe03].

4.5.1 Simulation results for PAM with 16-QAM modulation

The unknown waveform is selected at random from a Gaussian distribution and the maximum finite time support of the waveform is $N_g = 8$ samples. The oversampling factor is $N_{ss} = 2$ and thus, according to Table 4.1, the reduced observation interval is $N_r = N_g$ so that the required $(N_r \times N_r)$ synchronous autocorrelation matrix $\mathbf{R}$ is an (8×8) matrix.

Experiment 1A- NMSE performance as a function of E_s/N_0. The results in Figures 4.4-4.5 show the NMSE as a function of the E_s/N_0 for an observation interval comprising a total of $L = 250$ symbols (left-hand side plots) and $L = 1000$ symbols (right-hand side plots).

The difference between Figure 4.4 and Figure 4.5 is the way the dimension of the signal subspace is determined. It is important to recall that the knowledge of the signal subspace provides a valuable information to the proposed waveform estimation technique, since this knowledge restricts the solution space and concentrates on a neighborhood around the true waveform. However, for the low-SNR regime, it is not trivial to determine which is the optimal signal subspace dimension that provides the minimum NMSE (i.e. the best tradeoff between bias and variance). In Figure 4.4, the dimension of the signal subspace d is determined from three different criteria. The first criterion is indicated by d_{MAX} and it is based on choosing the maximum dimension of the signal subspace, which is given by $d_{MAX} = L_r = 2\lceil \frac{N_r}{N_{ss}} \rceil - 1$. The second criterion is indicated by d_{MAP} and it is based on applying the MAP model order detection rule [Dju98]. For the problem under consideration, the MAP rule is given by

$$d_{MAP} = \arg\min_{m} \|\mathring{\mathbf{r}}_{\mathrm{v}} - \mathbf{Q}^{(m)}\boldsymbol{\alpha}_{\mathrm{v}}^{(m)}\|^2 + \ln|\mathbf{Q}^{(m)^T}\mathbf{Q}^{(m)}|. \tag{4.38}$$

Finally, the last criterion is indicated by d_{opt} and it corresponds to the evaluation of the NMSE for all the signal subspace dimensions $d = \{1, 2, \ldots, L_r\}$ and then selecting the minimum NMSE. This can be considered as a lower bound for the NMSE performance of the proposed waveform estimation technique.

In contrast, the performance results in Figure 4.5 are depicted for each individual signal subspace dimension d. In this sense, Figure 4.5 shows the NMSE when one particular value for d is fixed. Note that for the randomly selected waveform under consideration, there is a significant performance degradation when $d < 4$ because of the large estimation bias. However, for $d = 4$ or $d = 5$, the performance of the proposed technique clearly outperforms the SS approach in [Lou00].

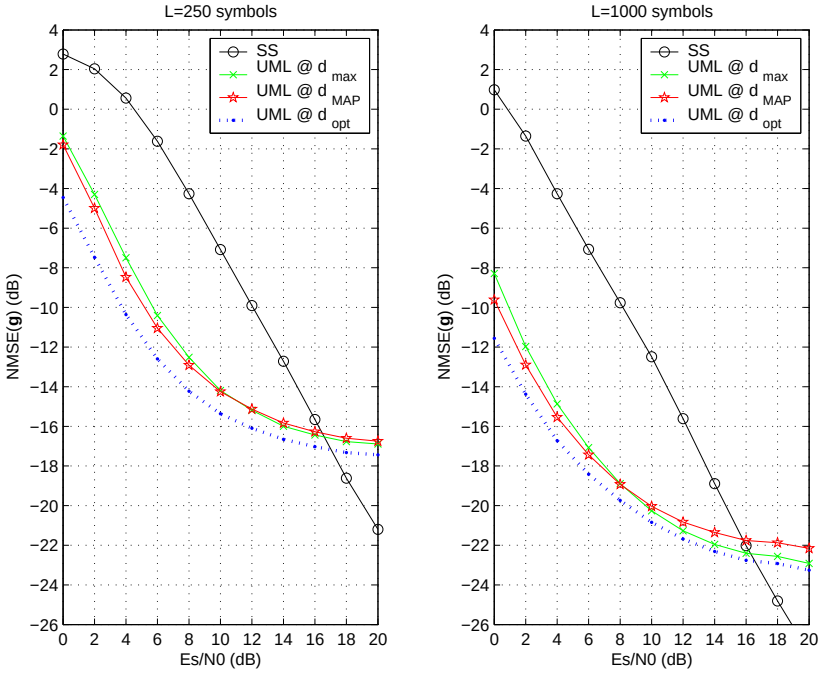

Figure 4.4: NMSE as a function of the E_s/N_0 with different criteria for estimating the dimension of the signal subspace.

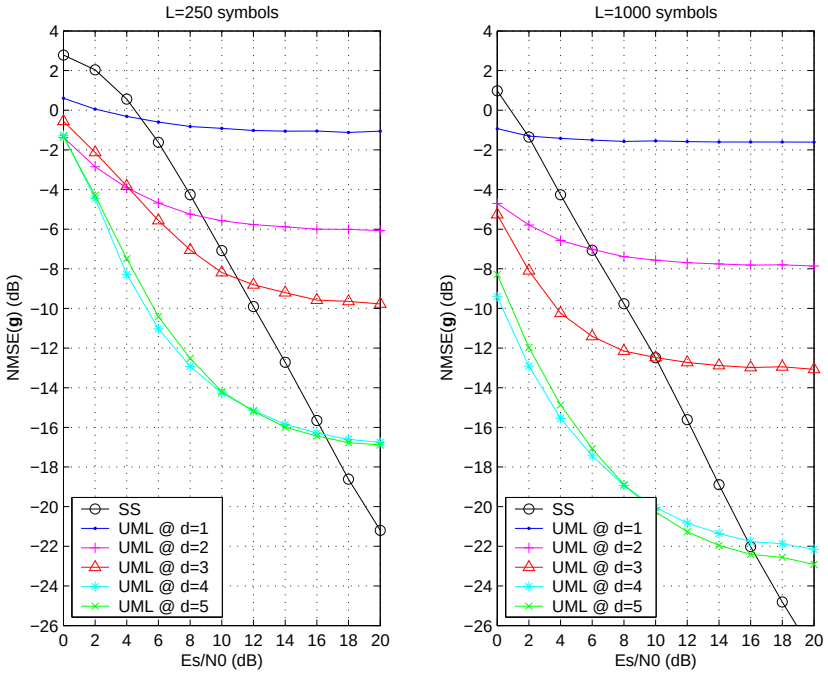

Figure 4.5: NMSE as a function of the E_s/N_0 for all the possible dimensions of the signal subspace.

Several important remarks must be made from the observation of Figures 4.4-4.5. First, note that a large gain is obtained by using the proposed technique for the low-SNR regime. This is especially true for the range from $E_s/N_0 = 0$ dB up to $E_s/N_0 = 10 - 12$ dB. On the contrary, a relatively high E_s/N_0 is required by the SS approach to succeed. This is because the subspace approach in [Lou00] is an eigenstructure technique that exploits the deterministic properties of the shaping matrix. As expected, the SS approach outperforms the proposed low-SNR waveform estimation technique only when the E_s/N_0 is beyond 14 or 18 dB, depending on the observation interval. The second important remark to be made is the floor effect in the proposed method when operating under high E_s/N_0 values. This is a common behavior of most low-SNR estimators, since they are designed for optimal operation under the low-SNR regime and thus, they exhibit self-noise for the high-SNR regime. Finally, note that for the proposed technique, the slope of the NMSE in the low-SNR regime coincides with the slope of the NMSE for the subspace approach in the high-SNR regime. This confirms the optimal behavior of the proposed method for the low-SNR regime.

Experiment 2A- NMSE performance as a function of the observation interval. For the same simulation parameters as in Experiment 1A, the NMSE is now evaluated as a function of the number of symbols in the received data record. The performance evaluation is presented in Figures 4.6-4.7. Clearly, the most remarkable result can be observed in the right-hand side plot of Figure 4.6, where the NMSE is depicted for different observation intervals with $E_s/N_0 = 4$

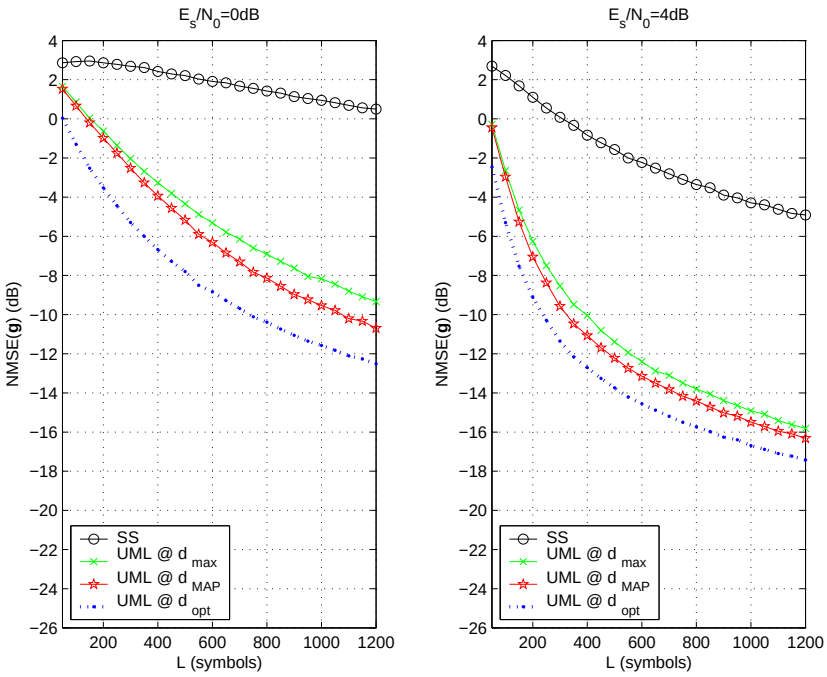

Figure 4.6: NMSE as a function of the observation interval with different criteria for estimating the dimension of the signal subspace.

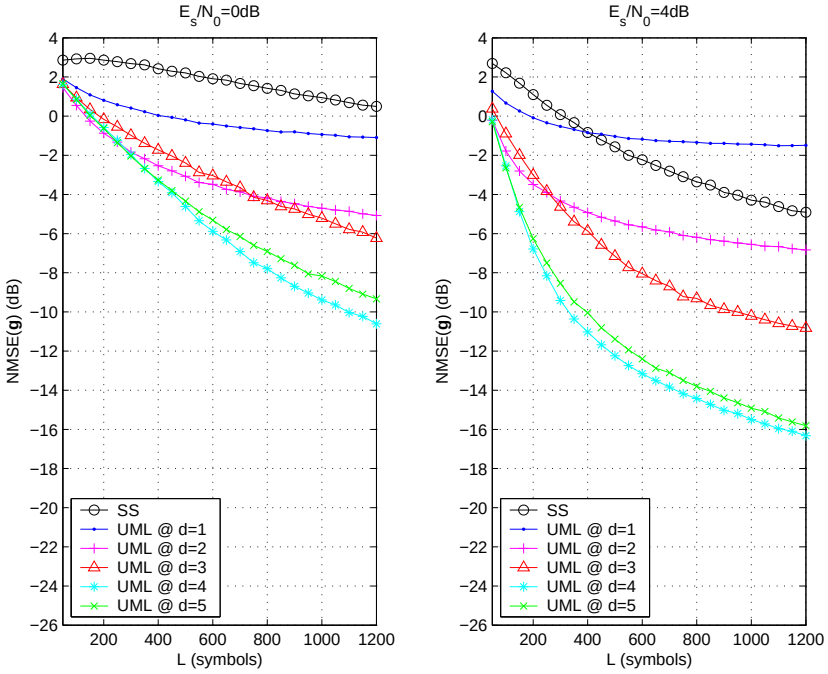

Figure 4.7: NMSE as a function of the E_s/N_0 for all the possible dimensions of the signal subspace.

dB. It can be observed that the difference between the NMSE of the proposed method and the one provided by the SS approach is almost 10 dB when more than 300 symbols are considered.

Experiment 3A- Cumulative probability of the NMSE. The purpose of this experiment is to analyze the robustness of the proposed technique in front of identifiability issues and possible ill-conditioning under the low-SNR regime. For this reason, we consider the E_s/N_0 working points of $\mathrm{E}_s/N_0 = \{0, 4, 8\}$ dB. Moreover, a different unknown waveform is randomly selected for each Monte Carlo run. In total, 20000 different waveforms are generated for each E_s/N_0 working point. The plots in Figure 4.8 represent the cumulative probability of the NMSE when the observation interval is fixed to $L = 250$ symbols. Again, there is a significant gain by using the proposed waveform estimation technique. For instance, for the case of $\mathrm{E}_s/N_0 = 4$ dB, 20% of the estimated waveforms with the SS approach have a NMSE lower than 10dB. For the proposed technique, this percentage ranges from 55% up to 75% depending on the way the signal subspace dimension is determined.

Finally, the results in Figure 4.9 depict the increment in the cumulative probability of the NMSE when moving from $\mathrm{E}_s/N_0 = 0$ dB to $\mathrm{E}_s/N_0 = 4$ dB and when moving from $\mathrm{E}_s/N_0 = 4$ dB to $\mathrm{E}_s/N_0 = 8$ dB. That is, these are the difference curves between the ones in Figure 4.8. Thus, the results in Figure 4.9 are not in percentage but in absolute value from 0 to 100. The key feature of the increment cumulative plots in Figure 4.9 is that they reflect the degree of improvement of the NMSE as the E_s/N_0 increases. For instance, in the left-hand side plot of Figure 4.9 it

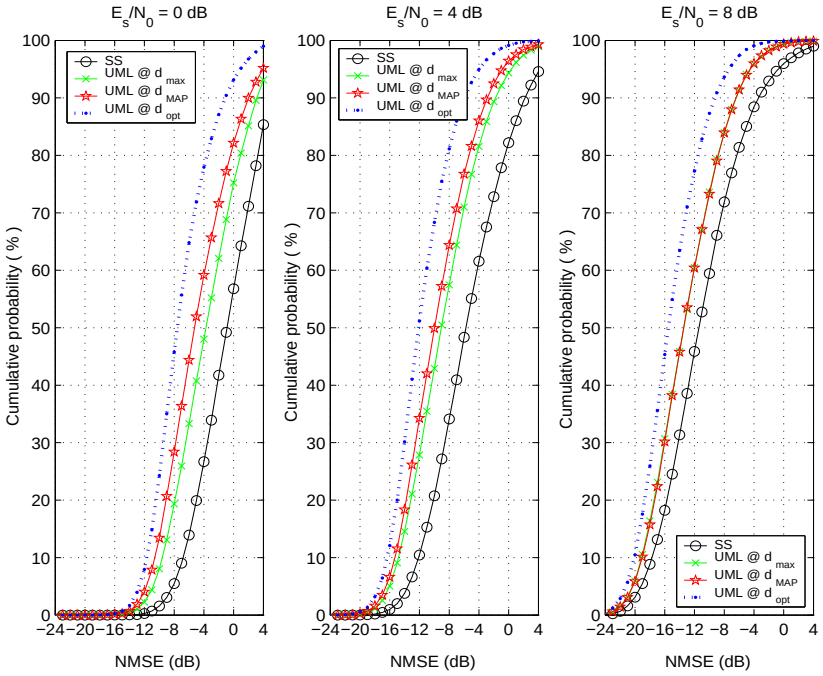

Figure 4.8: Cumulative distribution function (CDF) of the NMSE for $\mathrm{E}_s/N_0 = \{0, 4, 8\}$ dB.

is shown that the greatest improvement in NMSE is achieved by the population of waveform estimates with NMSE=-10 dB. In contrast, and for the SS approach, the greatest improvement in terms of NMSE is achieved by the population of waveform estimates with NMSE=-5 dB. This corresponds to the position of the peaks for the Gaussian-like curves appearing in Figure 4.9.

4.5.2 Simulation results for UWB signals with binary APPM modulation

The proposed waveform estimation technique is of special interest for application to coherent receivers with UWB signals, since they require robust channel state information for reliable symbol detection. The closed-form solution and the estimation of the whole received waveform (instead of just the propagation path delays and amplitudes) are the main features of the proposed technique with respect to previous contributions in channel estimation for UWB signals.

Some valuable contributions can be found in [Lot00], [Car03], [Xu03b] or [Wil03], among many other. However, most of these contributions do assume that the shape of the received pulse is known (e.g. [Lot00], [Xu03b], [Wil03]) and thus, channel estimation is restricted to the estimation of the time delays and amplitudes of the multipath rays through an iterative optimization (e.g. [Lot00], [Car03]). As already mentioned in Section 4.1, the assumption of known received pulse and a tapped-delay line model is not reasonable in practical UWB systems. Many studies on the propagation of UWB signals conclude that the severe frequency-selective and dispersive channel makes not possible for the receiver to know the shape of the received pulse

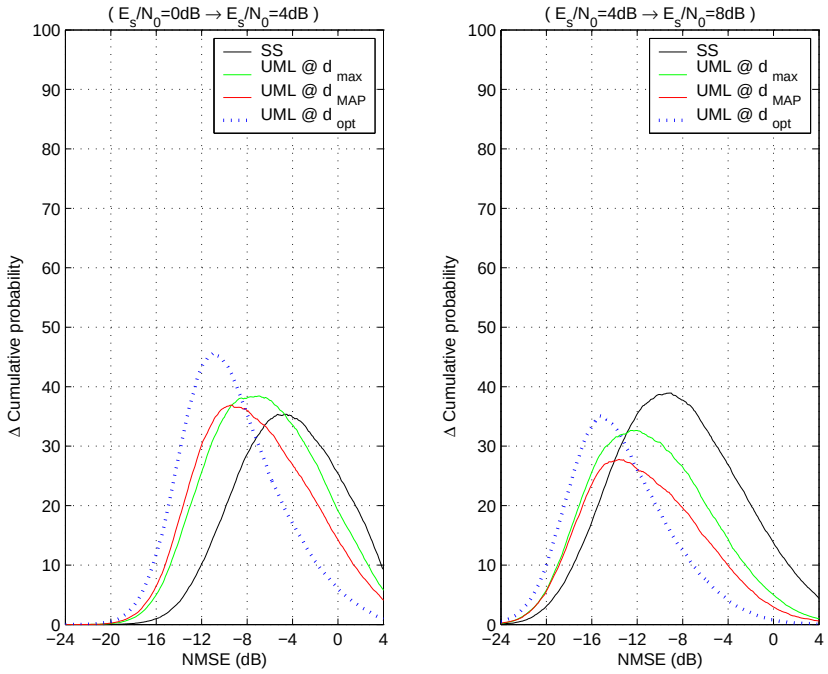

Figure 4.9: Incremental cumulative distribution of the NMSE from $\mathrm{E}_s/N_0 = 0$ dB to $\mathrm{E}_s/N_0 = 4$ dB (left) and from $\mathrm{E}_s/N_0 = 4$ dB to $\mathrm{E}_s/N_0 = 8$ dB (right).

in advance [Qiu02]. In addition to this, most approaches to channel estimation for UWB signals do not assume the received signal to incur in interframe interference. For many techniques, overlapping is not desired at the receiver, and thus, they space consecutive transmitted pulses such that the maximum delay spread of the channel does not incur in overlapping (e.g. [Lot00], [Car03]). In contrast, our closed-form approach to the waveform estimation problem allows the received waveforms to be overlapped with each other within the symbol interval, which in turn, determines the dimension of the signal subspace constraint.

In the simulation results to be presented herein, the simulation set-up comprises the transmission of ultra-short pulses corresponding to the second derivative of the Gaussian pulse with a total duration of 4 ns and modulated with binary APPM. The UWB channel is randomly generated according to the channel model CM1 proposed by Intel [Foe03] whose power profile is truncated to make the maximum delay spread of the multipath channel equal to 72 ns. The pulse-position modulation involves a time-shift of 8 ns and the frame duration is set to 94 ns. The transmission of a single information bearing symbol is carried out by the repetition of $N_f = 64$ frame intervals, and finally, the sampling period to $T_s = 2$ ns and the MAP model order rule is adopted for determining the signal subspace dimension.

Experiment 1B- Mean estimated waveform for different noise realizations. For a randomly selected received waveform, the results in Figure 4.10 depict the estimated waveform for 10 different noise realizations. For the sampling period and the channel model under consideration,

the maximum finite time support of the unknown received waveform is $N_g = 49$ samples. As shown in Figure 4.10, the estimates for the unknown waveform are pretty good for those initial samples with significant SNR. However, the last samples of the selected unknown waveform are close to zero, and thus, these samples are more difficult to estimate. A larger estimation variance is exhibited in this null-region since there is no signal but only noise.

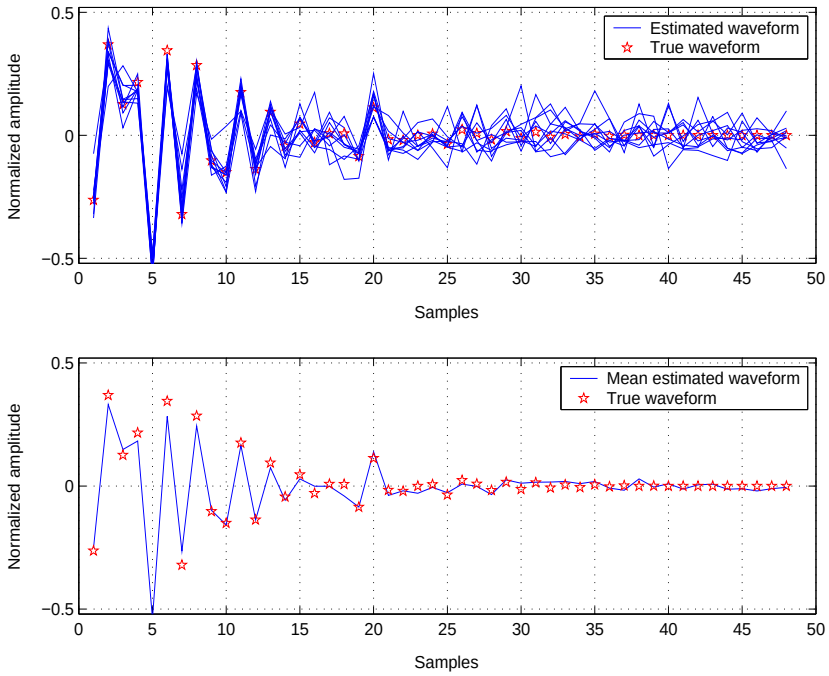

Figure 4.10: Example of waveform estimates for nonorthogonal binary-APPM transmission and 10 different noise realizations. The channel realization is fixed and generated from the channel model CM1 proposed by Intel [Foe03].

Experiment 2B- Cumulative probability of the NMSE. For the case of $N_g = 49$ samples as in Experiment 1B, the results in Figure 4.11 show the cumulative probability of the NMSE for a total of 10000 randomly selected waveforms from the channel model in [Foe03]. Note that the energy-per-frame to noise spectral density parameter E_f/N_0 is adopted, since the waveform estimation is performed on a frame-level basis (i.e. $N_r = N_{sf}$, with N_{sf} the number of samples per frame). Because of the frame repetition structure of UWB signals, $\mathrm{E}_f/N_0 = \frac{1}{N_f}\mathrm{E}_s/N_0$, so that the E_f/N_0 coincides with the E_s/N_0 when there is no repetition and $N_f = 1$. The evaluation of the NMSE is performed for different E_f/N_0 values from 0 to 5 dB. Again, the robustness of the proposed waveform estimation technique can be observed by noting that for $\mathrm{E}_f/N_0 = 5$ dB, 90 % of the received waveform estimates have a NMSE $\leq$ -20 dB.

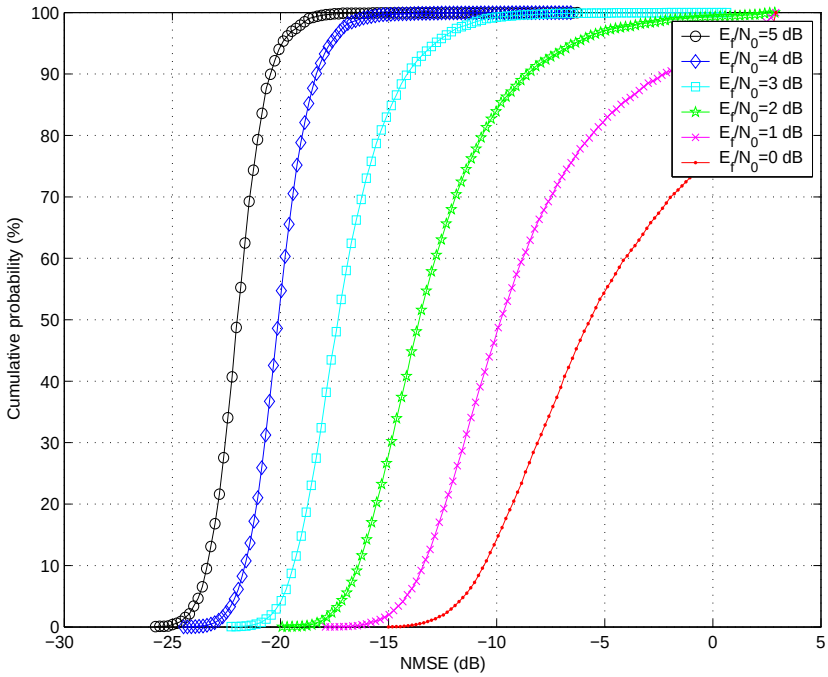

Figure 4.11: Cumulative distribution function (CDF) of the NMSE for different E_f/N_0 values.

4.6 Conclusions

A closed-form waveform estimation technique has been proposed based on the low-SNR UML criterion. By introducing a signal subspace constraint and the *vec* operator, a subspace-compressed low-SNR likelihood function is obtained which converts the nonlinear optimization problem into a linear least-squares problem on the second-order statistics of the received signal. The subspace-compressed approach can be understood as a principal component analysis, and thus, a significant reduction in the computational burden is obtained through a tradeoff between bias and variance. Another advantage of the subspace constraint is that it restricts the solution space and hence, it avoids many of the effects of ill-conditioning and local-maxima of traditional ML channel and waveform estimators. Finally, and for the low-SNR scenarios, simulation results show the superior performance of the proposed technique with respect to existing closed-form methods that are based on second-order statistics.

Appendix 4.A Derivation of the low-SNR log-likelihood UML cost function

Under the low-SNR assumption, the likelihood function in (4.12) can be approximated by its Taylor series expansion

$$\Lambda\left(\mathbf{r}|\mathbf{g};\mathbf{x}\right) \approx C_1 \left[1 + \frac{2}{\sigma_w^2}\chi\left(\mathbf{r};\mathbf{g};\mathbf{x}\right) + \frac{2}{\sigma_w^4}\chi^2\left(\mathbf{r};\mathbf{g};\mathbf{x}\right)\right] \tag{4.39}$$

with $\chi\left(\mathbf{r};\mathbf{g};\mathbf{x}\right) \doteq \sum_{p=0}^{P-1} \mathrm{Re}\left[\mathbf{x}_p^H \mathbf{A}_p^H \mathbf{r}\right] - \frac{1}{2}\sum_{p=0}^{P-1}\sum_{q=0}^{P-1} \mathbf{x}_q^H \mathbf{A}_q^H \mathbf{A}_p \mathbf{x}_p$. Next, since the transmitted symbols are assumed to be all random, the symbol-independent likelihood function $\Lambda\left(\mathbf{r}|\mathbf{g}\right)$ is obtained as $\Lambda\left(\mathbf{r}|\mathbf{g}\right) = \mathrm{E}_{\mathbf{x}}\left[\Lambda\left(\mathbf{r}|\mathbf{g};\mathbf{x}\right)\right]$. Thus, the expectations $\mathrm{E}_{\mathbf{x}}\left[\chi\left(\mathbf{r};\mathbf{g};\mathbf{x}\right)\right]$ and $\mathrm{E}_{\mathbf{x}}\left[\chi^2\left(\mathbf{r};\mathbf{g};\mathbf{x}\right)\right]$ are required. The first order moment of $\chi\left(\mathbf{r};\mathbf{g};\mathbf{x}\right)$ is rather simple to calculate,

$$\begin{aligned}
\mathrm{E}_{\mathbf{x}}\left[\chi\left(\mathbf{r};\mathbf{g};\mathbf{x}\right)\right] &= \sum_{p=0}^{P-1} \mathrm{Re}\left[\mathrm{E}_{\mathbf{x}}\left[\mathbf{x}_p^H\right]\mathbf{A}_p^H\mathbf{r}\right] - \frac{1}{2}\sum_{p=0}^{P-1}\sum_{q=0}^{P-1} Tr\left(\mathbf{A}_q^H\mathbf{A}_p\mathrm{E}_{\mathbf{x}}\left[\mathbf{x}_p\mathbf{x}_q^H\right]\right) && (4.40)\\
&= -\frac{1}{2P}Tr\left(\mathbf{M}\right) && (4.41)
\end{aligned}$$

where, for the sake of simplicity, the new matrix $\mathbf{M}$ is defined as

$$\mathbf{M} \doteq \sum_{p=0}^{P-1} \mathbf{A}_p\mathbf{A}_p^H = \sum_{p=0}^{P-1}\sum_{n=0}^{L-1} \mathbf{K}_{n,p}\mathbf{g}\mathbf{g}^H\mathbf{K}_{n,p}^H. \tag{4.42}$$

In the derivation of the first order moment of $\chi\left(\mathbf{r};\mathbf{g};\mathbf{x}\right)$ in (4.41) it has been taken into consideration that $\mathrm{E}_{\mathbf{x}}\left[\mathbf{x}_p\right] = \mathbf{0}$ and $\mathrm{E}_{\mathbf{x}}\left[\mathbf{x}_p\mathbf{x}_q^H\right] = \frac{1}{P}\mathbf{I}_L\delta_{pq}$. As for the second order moment of $\chi\left(\mathbf{r};\mathbf{g};\mathbf{x}\right)$, this requires further manipulation. As it is shown in Appendix 4.B, the second order moment of $\chi\left(\mathbf{r};\mathbf{g};\mathbf{x}\right)$ is found to be given by

$$\mathrm{E}_{\mathbf{x}}\left[\chi^2\left(\mathbf{r};\mathbf{g};\mathbf{x}\right)\right] = \frac{1}{2P}\mathbf{r}^H\mathbf{M}\mathbf{r} + \frac{1}{4P}\|\mathbf{M}\|_F^2 + \frac{\zeta}{4}, \tag{4.43}$$

with ζ a constant term. Then, the low-SNR UML likelihood function results in

$$\begin{aligned}
\Lambda\left(\mathbf{r}|\mathbf{g}\right) &\approx C_1\left[1 + \frac{1}{\sigma_w^4 P}\left[-\sigma_w^2 Tr\left(\mathbf{M}\right) + \mathbf{r}^H\mathbf{M}\mathbf{r} + \frac{1}{2}\|\mathbf{M}\|_F^2 + \frac{\zeta}{2}P\right]\right] && (4.44)\\
&= C_1\left[1 + \frac{1}{\sigma_w^4 P}\left[Tr\left(\mathbf{M}\left[\mathbf{r}\mathbf{r}^H - \sigma_w^2\mathbf{I}_N\right]\right) + \frac{1}{2}\|\mathbf{M}\|_F^2 + \frac{\zeta}{2}P\right]\right]. && (4.45)
\end{aligned}$$

Alternatively, the log-likelihood function $L\left(\mathbf{r}|\mathbf{g}\right) \doteq \ln\Lambda\left(\mathbf{r}|\mathbf{g}\right)$ can be adopted. This is just a formal consideration but it will allow us to relate the likelihood function in (4.45) with the information criteria for determining the dimension of the signal subspace of the received data. Thus, by taking into consideration that $\ln\left(1+x\right) \approx x$ when $x \to 0$, the low-SNR UML log-likelihood function can be expressed as

$$L\left(\mathbf{r}|\mathbf{g}\right) \approx C_2 + \frac{1}{\sigma_w^4 P}\left[Tr\left(\mathbf{M}\left[\mathbf{r}\mathbf{r}^H - \sigma_w^2\mathbf{I}_N\right]\right) + \frac{1}{2}\|\mathbf{M}\|_F^2 + \frac{\zeta}{2}P\right], \tag{4.46}$$

where $C_2 = \ln C_1$. For an asymptotically large observation interval, let us decompose the $(N \times 1)$ vector of received samples $\mathbf{r}$ into a set of small $(N_r \times 1)$ and N_{ss}-samples shifted vectors $\mathbf{r}_n$, with $\mathbf{r}_n \doteq [r(nN_{ss}), r(nN_{ss}+1), \ldots, r(nN_{ss}+N_r-1)]^T$ and $N_r = \max\{N_g, N_{ss}\}$. Note that by setting the reduced observation interval to $N_r = \max\{N_g, N_{ss}\}$, a significant computational complexity is saved while preserving the information regarding the unknown waveform. This is because with $N_r = \max\{N_g, N_{ss}\}$, we guarantee that, at least, one of the waveform replicas within the observation interval is not truncated. Finally, removing all the irrelevant constant terms in (4.46) results in an equivalent low-SNR UML log-likelihood function, namely $L'(\mathbf{r}|\mathbf{g})$, which is defined as follows,

$$L'(\mathbf{r}|\mathbf{g}) = Tr\left(\breve{\mathbf{M}}\left[\mathbf{R} - \sigma_w^2 \mathbf{I}_{N_r}\right]\right) + \frac{1}{2}\|\breve{\mathbf{M}}\|_F^2. \tag{4.47}$$

with $\breve{\mathbf{M}}$ the $(N_r \times N_r)$ truncated version of matrix $\mathbf{M}$ in (4.42). That is,

$$\breve{\mathbf{M}} \doteq \sum_{p=0}^{L_p-1} \sum_{n=-K_r}^{K_r} \breve{\mathbf{K}}_{n,p} \mathbf{g}\mathbf{g}^H \breve{\mathbf{K}}_{n,p}^H \tag{4.48}$$

with K_r the one-sided number of N_{ss}-samples shifted replicas of $\mathbf{g}$, and L_p the number of N_Δ-samples shifted replicas of $\mathbf{g}$, both within an observation interval of N_r samples. In addition, $\breve{\mathbf{K}}_{n,p}$ is the $(N_r \times N_g)$ truncated version of matrix $\mathbf{K}_{n,p}$. In Matlab notation, $\breve{\mathbf{K}}_{n,p} \doteq \mathbf{K}_{n,p}(1:N_r,:)$. Note that in (4.47), the initial observation interval of N samples has been asymptotically $(L \to \infty)$ folded into a smaller observation interval of N_r samples. Consequently, the $(N \times N)$ sample covariance matrix $\mathbf{r}\mathbf{r}^H$ in (4.46) is converted into the $(N_r \times N_r)$ synchronous autocorrelation matrix $\mathbf{R}$. Thus, the second-order statistics of the received signal become the sufficient statistics for the problem under consideration.

Appendix 4.B Derivation of the Second Order Moment of $\chi(\mathbf{r};\mathbf{g};\mathbf{x})$

From the definition of $\chi(\mathbf{r};\mathbf{g};\mathbf{x})$ in (4.13) it can be found that,

$$\chi^2(\mathbf{r};\mathbf{g};\mathbf{x}) = \underbrace{\left(\sum_{p=0}^{P-1} \mathrm{Re}\left[\mathbf{x}_p^H \mathbf{A}_p^H \mathbf{r}\right]\right)^2}_{B1} - \underbrace{\left(\sum_{p=0}^{P-1} \mathrm{Re}\left[\mathbf{x}_p^H \mathbf{A}_p^H \mathbf{r}\right]\right) \sum_{p=0}^{P-1}\sum_{q=0}^{P-1} \mathbf{x}_q^H \mathbf{A}_q^H \mathbf{A}_p \mathbf{x}_p}_{B2} \tag{4.49}$$

$$+ \underbrace{\frac{1}{4}\left(\sum_{p=0}^{P-1}\sum_{q=0}^{P-1} \mathbf{x}_q^H \mathbf{A}_q^H \mathbf{A}_p \mathbf{x}_p\right)^2}_{B3}. \tag{4.50}$$

Therefore, the evaluation of $\mathrm{E}_{\mathbf{x}}\left[\chi^2(\mathbf{r};\mathbf{g};\mathbf{x})\right]$ involves the expectation of B1, B2 and B3 in (4.50).

B1: This quadratic term can be first expanded, and then, by taking into consideration that $\mathrm{E}_{\mathbf{x}}\left[\mathbf{x}_p\mathbf{x}_q^H\right] = \frac{1}{P}\mathbf{I}_L\delta_{pq}$ it is found that,

$$\mathrm{E}_{\mathbf{x}}\left[\left(\sum_{p=0}^{P-1}\mathrm{Re}\left[\mathbf{x}_p^H\mathbf{A}_p^H\mathbf{r}\right]\right)^2\right] = \frac{1}{2P}\mathbf{r}^H\mathbf{M}\mathbf{r} \tag{4.51}$$

with $\mathbf{M}$ defined in (4.42).

B2: This term vanishes because it depends on the odd moments of the transmitted symbols.

B3: This term should be first expanded as,

$$\left(\sum_{p=0}^{P-1}\sum_{q=0}^{P-1}\mathbf{x}_q^H\mathbf{A}_q^H\mathbf{A}_p\mathbf{x}_p\right)^2 = \sum_{p=0}^{P-1}\sum_{q=0}^{P-1}\sum_{m=0}^{P-1}\sum_{n=0}^{P-1} Tr\left(\mathbf{A}_p^H\mathbf{A}_q\mathbf{x}_q\mathbf{x}_m^H\mathbf{A}_m^H\mathbf{A}_n\mathbf{x}_n\mathbf{x}_p^H\right) \tag{4.52}$$

$$= vec^T\left(\mathbf{x}_m^*\mathbf{x}_q^T\mathbf{A}_q^T\mathbf{A}_p^*\right)vec\left(\mathbf{A}_m^H\mathbf{A}_n\mathbf{x}_n\mathbf{x}_p^H\right), \tag{4.53}$$

where it has been used the property $Tr(\mathbf{BC}) = vec^T\left(\mathbf{B}^T\right)vec(\mathbf{C})$ for any $(n\times q)$ matrix $\mathbf{B}$ and any $(q\times p)$ matrix $\mathbf{C}$. In addition, and for any $(m\times n)$ matrix $\mathbf{A}$, it is found that $vec(\mathbf{ABC}) = \left(\mathbf{C}^T\otimes\mathbf{A}\right)vec(\mathbf{B})$ with $\otimes$ the Kronecker product [Har00, p.342]. Therefore,

$$\left(\sum_{p=0}^{P-1}\sum_{q=0}^{P-1}\mathbf{x}_q^H\mathbf{A}_q^H\mathbf{A}_p\mathbf{x}_p\right)^2 = vec^T\left(\mathbf{x}_m^*\mathbf{x}_q^T\right)\left[\left(\mathbf{A}_q^T\mathbf{A}_p^*\right)\otimes\mathbf{I}_L\right]\left[\mathbf{I}_L\otimes\left(\mathbf{A}_m^H\mathbf{A}_n\right)\right]vec\left(\mathbf{x}_n\mathbf{x}_p^H\right)$$

$$= vec^H\left(\mathbf{x}_m\mathbf{x}_q^H\right)\left[\left(\mathbf{A}_q^T\mathbf{A}_p^*\right)\otimes\left(\mathbf{A}_m^H\mathbf{A}_n\right)\right]vec\left(\mathbf{x}_n\mathbf{x}_p^H\right) \tag{4.54}$$

$$= Tr\left(\left[\left(\mathbf{A}_q^T\mathbf{A}_p^*\right)\otimes\left(\mathbf{A}_m^H\mathbf{A}_n\right)\right]vec\left(\mathbf{x}_n\mathbf{x}_p^H\right)vec^H\left(\mathbf{x}_m\mathbf{x}_q^H\right)\right) \tag{4.55}$$

At this point, the expectation with respect to the transmitted symbols can be introduced in (4.55). Then, the main focus of interest is the computation of the term $\mathrm{E}_{\mathbf{x}}\left[vec\left(\mathbf{x}_n\mathbf{x}_p^H\right)vec^H\left(\mathbf{x}_m\mathbf{x}_q^H\right)\right]$. The result for the particular case in which $n=p=m=q$ can be found in [Vil05], and with this help, the general expression can be found after tedious algebraic manipulations. As a result, the expectation with respect to the transmitted symbols of (4.55) can be summarized as follows,

$$\mathrm{E}_{\mathbf{x}}\left[\left(\sum_{p=0}^{P-1}\sum_{q=0}^{P-1}\mathbf{x}_q^H\mathbf{A}_q^H\mathbf{A}_p\mathbf{x}_p\right)^2\right] = \frac{1}{P}\|\mathbf{M}\|_F^2 + \zeta \tag{4.56}$$

with ζ a term that is asymptotically constant for large data records, and it just depends on the energy of the received waveform. In the derivation of (4.56) it has been taken into consideration that for $P>1$ (i.e. with PPM and APPM modulations) there is enough separation between consecutive pulses so as to avoid intersymbol interference, that is, $N_g \le N_{ss}$. Then, the product of matrices in the form $\mathbf{A}_q^H\mathbf{A}_p$ results in a diagonal matrix for any value of $\{p,q\}$.

From the above considerations, we finally have that

$$\mathrm{E}_{\mathbf{x}}\left[\chi^2\left(\mathbf{r};\mathbf{g};\mathbf{x}\right)\right] = \frac{1}{2P}\mathbf{r}^H\mathbf{M}\mathbf{r} + \frac{1}{4P}\|\mathbf{M}\|_F^2 + \frac{\zeta}{4}. \tag{4.57}$$

Appendix 4.C Application of the *vec* operator to the low-SNR UML log-likelihood cost function

By using the *vec* operator, the low-SNR UML cost function in (4.47) can be recast as,

$$L'\left(\mathbf{r}|\mathbf{g}\right) = vec^T\left(\breve{\mathbf{M}}^*\right) vec\left(\mathbf{R} - \sigma_w^2\mathbf{I}_{N_r}\right) + \frac{1}{2}vec^T\left(\breve{\mathbf{M}}^*\right) vec\left(\breve{\mathbf{M}}\right) \tag{4.58}$$

with $(\cdot)^*$ the complex conjugate. Let us further manipulate the terms involving $vec\left(\breve{\mathbf{M}}\right)$ by taking into consideration the subspace-constraint in (4.19) and the relationship $vec\left(\mathbf{ABC}\right) = \left(\mathbf{C}^T \otimes \mathbf{A}\right) vec\left(\mathbf{B}\right)$,

$$\begin{aligned} vec\left(\breve{\mathbf{M}}\right) &= vec\left(\sum_{n=-K_r}^{K_r}\sum_{p=0}^{L_p-1}\breve{\mathbf{K}}_{n,p}\mathbf{g}\mathbf{g}^H\breve{\mathbf{K}}_{n,p}^H\right) = \sum_{n=-K_r}^{K_r}\sum_{p=0}^{L_p-1} vec\left(\breve{\mathbf{K}}_{n,p}\mathbf{U}_{\mathrm{s}}\boldsymbol{\alpha}\boldsymbol{\alpha}^H\mathbf{U}_{\mathrm{s}}^H\breve{\mathbf{K}}_{n,p}^H\right) \\ &= \left(\sum_{n=-K_r}^{K_r}\sum_{p=0}^{L_p-1}\left(\breve{\mathbf{K}}_{n,p}\mathbf{U}_{\mathrm{s}}^*\right)\otimes\left(\breve{\mathbf{K}}_{n,p}\mathbf{U}_{\mathrm{s}}\right)\right) vec\left(\boldsymbol{\alpha}\boldsymbol{\alpha}^H\right). \end{aligned} \tag{4.59}$$

Next, let us define the $(N_r^2 \times 1)$ vector $\mathring{\mathbf{r}}_{\mathrm{v}}$, the $(N_r^2 \times d^2)$ matrix $\mathbf{Q}$ and the $(d^2 \times 1)$ vector $\boldsymbol{\alpha}_{\mathrm{v}}$ as,

$$\mathring{\mathbf{r}}_{\mathrm{v}} \doteq vec\left(\mathbf{R} - \sigma_w^2\mathbf{I}_{N_r}\right), \tag{4.60}$$

$$\mathbf{Q} \doteq \sum_{n=-K_r}^{K_r}\sum_{p=0}^{L_p-1}\left(\breve{\mathbf{K}}_{n,p}\mathbf{U}_{\mathrm{s}}^*\right)\otimes\left(\breve{\mathbf{K}}_{n,p}\mathbf{U}_{\mathrm{s}}\right), \tag{4.61}$$

$$\boldsymbol{\alpha}_{\mathrm{v}} \doteq vec\left(\boldsymbol{\alpha}\boldsymbol{\alpha}^H\right). \tag{4.62}$$

Then, the low-SNR UML cost function in (4.58) results in

$$L'\left(\mathbf{r}|\mathbf{g}\right) = \boldsymbol{\alpha}_{\mathrm{v}}^H\mathbf{Q}^H\mathring{\mathbf{r}}_{\mathrm{v}} + \frac{1}{2}\boldsymbol{\alpha}_{\mathrm{v}}^H\mathbf{Q}^H\mathbf{Q}\boldsymbol{\alpha}_{\mathrm{v}}. \tag{4.63}$$

Chapter 5

Non-Coherent Detection of Random UWB Signals

5.1 Introduction

One of the main problems with the transmission of UWB signals is that the received waveform has very little resemblance with the original transmitted pulse. As already mentioned in Section 2.4, some of the reasons for this behavior are the following. First, the solid state pulse generating devices exhibit implementation imperfections such as random timing jitter or asymmetric polarity rising times that prevent the transmitted pulses to be all exactly the same [Win02]. Second, the radiating elements are found to differentiate the transmitted pulse [Zio92], [Mir01] and a different distortion is experienced depending on the angle of radiation [Kon05], [Wan05]. Third, the propagation physics of UWB signals make the channel response to be terribly frequency-dependent and this causes a severe pulse distortion at the receiver [Qiu02], [Qiu05]. Fourth, experimental results show that the pulse distortion is also path-dependent and thus, different pulse distortions are experienced when propagating through different paths and through different materials [Cra02]. As a result of all these degradations, the end-to-end channel response can reasonably be assumed to be time-varying. This is particularly true when the propagation paths change as a result of the relative movement between transmitter and receiver. In addition, the paths can also change as a result of moving scatterers like moving persons in indoor scenarios [Sch05b] and thus it is reasonable to assume the received waveform as *random*.

Because of the above considerations, the adoption of coherent receivers (i.e the assumption of channel state information) is restricted to those applications where slow channel variations are experienced and significant computational complexity is available at the receiver. This is due to the fact that the large multipath resolution of UWB signals makes the computation of fast and accurate channel estimates a challenging and computationally demanding task. When

such a computational burden is not available, there is no choice but to resort to non-coherent receivers [Car06a].

At this point, note that many of the traditional signal processing techniques for narrowband communication systems cannot be adopted anymore. In particular, the popular receiver based on a filter matched to the transmitted pulse can no longer be considered since the received pulse has no resemblance with the transmitted one. However, many contributions on UWB communication systems ignore this problem and they still formulate the optimal receiver by applying the well-known matched filter principle to all the propagation paths (see, for instance, [Gez04], [Chu04], [Oh05] or [Tan05a] among many other).

Symbol detection for UWB signals when no channel state information is available is also considered in [D'A05], [Car06a] or [Fen03], among many other. Nevertheless, an *unknown deterministic* approach is considered where the received waveform is assumed to be unknown but constant during all the observation interval. Other approaches consider the problem of waveform time-variation by adopting transmitted reference (TR) signaling, which is based on the transmission of a reference pulse prior to each data modulated pulse [Rus64], [Hoc02], [Fra03], [Cha05]. In that way, noisy channel state information is provided by the received unmodulated pulses themselves. However, this comes at the expense of an efficiency loss due to the transmission of unmodulated pulses and at the end, a coherent receiver is required once again.

Contrary to the *deterministic* approach, herein the emphasis is placed on treating the received signal as *random*. Since no channel state information is assumed at the receiver, coherent detection cannot be applied and non-coherent techniques must be adopted based on the underlying statistics of the received data. Clearly, this is a problem of random signal detection, a topic that has received significant attention in the last decades with many important contributions in RADAR and SONAR applications [Van03], [Kay98], among many other.

In this sense, the goal of this chapter is to address the optimal non-coherent symbol detection problem of PPM modulated UWB signals when the received waveforms are assumed to be all random. For the sake of clarity, binary-PPM is considered but the extension to higher order constellations can be done in a straightforward manner. In particular, the symbol detection problem is formulated here within the framework of likelihood ratio testing for the low-SNR regime. The low-SNR assumption is an important part of this study since it can be considered as a realistic hypothesis to the real operating conditions of UWB systems. Once the optimal symbol decision statistics are derived, different practical cases of interest are further analyzed. For instance, an information theoretic based receiver is proposed as a tradeoff between performance and implementation complexity in the presence of correlated scattering. The result is a gradient based scheme which provides the best and simplest receiver filter for maximizing the divergence measure of the symbol decision problem. Simulation results are provided to evaluate the performance of the proposed receivers and insightful links are established with existing

contributions in the recent literature.

The chapter is organized as follows. The signal model and the problem statement are introduced in Section 5.2. The determination of the actual propagation conditions is presented in Section 5.3 by estimating the covariance matrix of the unknown random channel. Next, the optimal non-coherent symbol decision rule is derived in Section 5.4 for the low-SNR regime. The particularization of this symbol decision strategy to the case of uncorrelated and correlated scattering is analyzed in Section 5.5 and Section 5.6, respectively. Finally, simulation results are discussed in Section 5.7 and conclusions are drawn in Section 5.8.

5.2 Signal Model and Problem Statement

5.2.1 Modulation format

The signal model to be considered in this chapter assumes the transmission of ultra-short pulses with binary pulse-position modulation (2-PPM). It is important to recall that PAM cannot be considered since it does not allow non-coherent detection.

As it is standard in most UWB communication systems, the transmission of every single information bearing symbol is implemented by the repetition of N_f low-power pulses. Each of these pulses is confined within a frame duration of N_{sf} samples that must be long enough so as to avoid interframe interference between consecutive frames. Consequently, the frame duration must encompass the maximum delay spread of the channel and the maximum time-shift introduced by the PPM modulation and the time-hopping (TH) sequence. In this chapter, however, no TH sequence is assumed. The reason is that, since we focus on the symbol decision problem, the TH sequence is assumed to have been previously acquired in a prior stage of the receiver.

At the receiver, the transmitted pulses arrive in the form of distorted waveforms. The degradation is caused by the inherent distortion produced by the wideband radiating elements, but especially, because of the propagation physics of UWB signals. In this sense, and similarly to [Car06b], an *unstructured* approach is adopted for modeling the propagation of the transmitted signal. That is, we completely disregard the paths of the propagation channel and we just consider the received waveform as a whole. This received waveform is denoted by the discrete-time notation $g(k)$, and the received signal can be expressed as,

$$r(k) = \sum_{n=-\infty}^{\infty} c_n \sum_{i=0}^{N_f-1} g_{n,i}\left(k - d_n N_\Delta - iN_{sf} - nN_{ss}\right) + n(k) \tag{5.1}$$

with N_Δ the number of samples for the PPM time-shift, N_{sf} the number of samples per frame (i.e. the frame duration) and N_{ss} the number of samples per symbol (i.e. the symbol duration).

Because of the frame repetition within the symbol duration, the number of samples per symbol is $N_{ss} \doteq N_f N_{sf}$. Since binary PPM is adopted, pulse-position symbols are restricted to $d_n = \{0, 1\}$. Moreover, the sequence $c_n = \{-1, 1\}$ accounts for the polarity randomization code that is introduced in order to avoid the existence of spectral lines that may violate spectral regulations [Nak03]. Finally, $n(k)$ includes the contribution of both the thermal noise and the interference signal. That is, $n(k) = w(k) + i(k)$ with $w(k)$ the zero-mean Gaussian samples of the thermal noise with variance σ_w^2 and $i(k)$ the interference signal to be described in Section 5.2.2.

Regarding the received waveform, note that $g_{n,i}(k)$ in (5.1) stands for the received waveform corresponding to the n-th symbol and the i-th frame. The received waveforms $g_{n,i}(k)$ have a maximum finite time support of N_g samples and the indexation $\{n, i\}$ is consistent with the fact that the received waveform may differ from frame to frame. For instance, this variation of the received waveforms may be caused by the relative movement between transmitter and receiver but also because of moving scatterers like moving persons [Sch05b]. Moreover, the signal model in (5.1) assumes that the coarse frame-timing error has been previously acquired, a topic to be discussed in Chapter 6. As a result, the starting time of the symbol period is known up to a fraction of the frame duration and this frame-level residual timing error is incorporated in the shape of the unknown waveform.

At this point, let us express the signal model in (5.1) into a more compact matrix notation. To this end, let us divide the observation interval into a total of L segments $\mathbf{r}_n$, each with a length equal to the symbol duration N_{ss}. Thus, the observation interval assumes the transmission of L binary-PPM symbols. Similarly, let us divide each received symbol vector $\mathbf{r}_n$ into a total of N_f segments $\mathbf{r}_{n,i}$ corresponding to the N_f frames within a symbol duration. That is, $\mathbf{r}_n = \left[\mathbf{r}_{n,0}^T, \mathbf{r}_{n,1}^T, \ldots, \mathbf{r}_{n,N_f-1}^T\right]^T$ with $\mathbf{r}_{n,i}$ a $(N_{sf} \times 1)$ vector with the samples of the i-the frame of the n-th symbol. According to the structure of binary pulse position modulation, the received signal for each frame interval can be expressed as follows,

$$\mathbf{r}_{n,i} = \begin{cases} c_n \mathbf{\Pi} \mathbf{g}_{n,i} + \mathbf{n}_{n,i} & : \quad d_n = 0 \\ c_n \mathbf{J}_{N_\Delta} \mathbf{\Pi} \mathbf{g}_{n,i} + \mathbf{n}_{n,i} & : \quad d_n = 1 \ . \end{cases} \tag{5.2}$$

Matrices $\mathbf{\Pi}$ and $\mathbf{J}_{N_\Delta}$ in (5.2) are a $(N_{sf} \times N_g)$ zero-padding matrix and a $(N_{sf} \times N_{sf})$ N_Δ-samples time-shift matrix, respectively. Finally, the $(N_g \times 1)$ vector $\mathbf{g}_{n,i}$ incorporates the N_g samples of the received waveform for the n-th symbol and i-th frame, and $\mathbf{n}_{n,i}$ the corresponding samples of the noise and interference contribution.

5.2.2 Interference signal model

The two major characteristics of UWB communication systems are their very large spectral occupancy and their very low power spectral density. The spectral occupancy of UWB signals

is on the order of a few GHz and this forces UWB signals to coexist with most of the existing wireless communication systems. However, the very large spectral occupancy of UWB signals makes current wireless communication systems to be perceived as narrowband interferences by a UWB receiver. Since spectral regulations restrict the radiation of UWB signals within the band from 3 GHz to 10 GHz, it turns out that the most significant source of interference are IEEE 802.11a WLAN devices, whose central frequency is located around 5 GHz and the transmitted bandwidth is about 20 MHz. Moreover, these WLAN interference sources can also be considered to be high-power sources compared to UWB signals [Sah05]. For instance, the maximum transmitted power for IEEE 802.11a devices is about 17dBm/Mhz. For the case of UWB signals, the maximum allowed transmitted power is -41.3dB/MHz according to the FCC spectral regulations. Therefore, an IEEE 802.11a system with 20 MHz of bandwidth results in a total transmitted power of $\mathrm{P}_{\mathrm{max}}^{\mathrm{IEEE802.11a}} = 30$ dBm. In contrast, an UWB system with a maximum bandwidth of 7 GHz results in a total transmitted power of $\mathrm{P}_{\mathrm{max}}^{\mathrm{UWB}} = -2.85$ dBm. That is, the transmitted power of an IEEE 802.11a device is more than 30 dB higher than that of an UWB system.

In order to model the interfering signals arriving to an UWB receiver, the Gaussian signal model is assumed herein. Similarly to [Chu04] or [Ber02], the interference signals are assumed to be discrete-time zero-mean passband Gaussian random processes whose spectral density $S_{\mathrm{I}}(f)$ is characterized by the central frequency f_{I} and the bandwidth occupancy $\mathrm{BW_I}$ as follows,

$$S_{\mathrm{I}}(f) = \begin{cases} \frac{N_{\mathrm{I}}}{2}, & f_{\mathrm{I}} - \frac{\mathrm{BW_I}}{2} \leq |f| \leq f_{\mathrm{I}} + \frac{\mathrm{BW_I}}{2} \\ 0, & \text{otherwise.} \end{cases} \tag{5.3}$$

Consequently the interference $i(k)$ for $n(k) = w(k)+i(k)$ in (5.1) is characterized by a covariance matrix $\mathbf{C}_{\mathrm{I}}$ whose (i, j) entries are given by

$$[\mathbf{C}_{\mathrm{I}}]_{i,j} = \mathrm{P_I} sinc\left(\mathrm{BW_I}\left(i-j\right)\right) cos\left(2\pi f_{\mathrm{I}}\left(i-j\right)\right) \tag{5.4}$$

with $\mathrm{P_I} = \mathrm{N_I} \cdot \mathrm{BW_I}$ the interference power.

5.2.3 UWB channel model and operating conditions

The optimal design of a communication system must take into consideration the propagation conditions of the transmitted signal in the way to the receiver. However many issues related with the propagation conditions of UWB signals are still under study. The main reason is that, although UWB technology has been around since the 60s, most channel measurement campaigns are being performed in the recent years. Thus, there is still a lot to be learned about the propagation characteristics of UWB signals and more measurement campaigns are still required [Mol05].

The most common characteristic of UWB transmissions is the extremely frequency-, path-, and angle-dependent transfer function. From a stochastic point of the view, some authors indicate that the statistical modeling of the measured small-scale fading is related to the Nakagami distribution (e.g. [Cas02a]), or to the lognormal distribution (e.g. [Foe03]). These results are indeed included in the IEEE 802.15.3a channel models which are especially devoted to high data-rate UWB systems operating in residential and office environments [Foe03]. However, UWB channels measured by other authors are found to be not so different from traditional channels. Measurement campaigns were carried out with both moving and fixed terminals in open space environments such as a lobby (e.g. [Sch05b], [Sch05c]) and in industrial environments (e.g. [Kar04]). For these propagation environments, the small-scale fading statistics of the received waveforms were found to be closer to the traditional Rayleigh and Rice distributions rather than to the Nakagami and lognormal distributions assumed in the IEEE 802.15.3a channel models. Similarly to traditional wideband channels, the Rayleigh distribution was found to apply with moving terminals whereas the Rice distribution was found to apply with static terminals. This is somehow surprising because the very large bandwidth of UWB signals is often argued for not assuming the traditional Gaussian assumption for the tap amplitudes. These new results were included in the IEEE 802.15.4a channel models [Mol04] which were intended to cover the gap left by the IEEE 802.15.3a channel models and to focus on low data-rate applications that usually operate in industrial, outdoor or rural environments. See Figure 5.1 and Figure 5.2 to notice the difference between the statistical characterization of non-line-of-sight channels within the IEEE 802.15.3a/4 standards.

In the sequel, the Gaussian approach suggested by [Sch05b], [Sch05c] or [Kar04] is adopted for mathematical tractability. Consequently, the samples of the received waveforms are modeled by a zero-mean random Gaussian process driven by a $(N_g \times N_g)$ covariance matrix $\mathbf{C}_g$.

According to the signal model in Section 5.2, let us indicate the hypothesis of transmitting $d_n = 1$ by $\mathcal{H}_+$ and the hypothesis of transmitting $d_n = 0$ by $\mathcal{H}_-$. Under the hypothesis $\mathcal{H}_+$, the conditional probability density function for the n-th received symbol is given by the multivariate Gaussian probability density function as follows,

$$f\left(\mathbf{r}_n|\mathcal{H}_+;\mathbf{C_g}\right) = \prod_{i=0}^{N_f-1} \frac{1}{(2\pi)^{N_{sf}/2}\det^{1/2}\left(\mathbf{C}_+ + \mathbf{C}_{\mathrm{N}}\right)} \exp\left(-\frac{1}{2}\mathbf{r}_{n,i}^T\left(\mathbf{C}_+ + \mathbf{C}_{\mathrm{N}}\right)^{-1}\mathbf{r}_{n,i}\right) \quad (5.5)$$

with $\mathbf{C}_+ \doteq \mathbf{\Pi C_g \Pi}^T$ the covariance matrix for the signal received under $\mathcal{H}_+$ and $\mathbf{C}_{\mathrm{N}} \doteq \sigma_w^2\mathbf{I} + \mathbf{C}_{\mathrm{I}}$ the covariance matrix for the Gaussian contribution of both the thermal noise and the narrowband interference. Similarly, the probability density function under the hypothesis $\mathcal{H}_-$ is found by substituting $\mathbf{C}_+$ with $\mathbf{C}_- \doteq \mathbf{J}_{N_\Delta}\mathbf{\Pi C_g \Pi}^T\mathbf{J}_{N_\Delta}^T$ in (5.5).

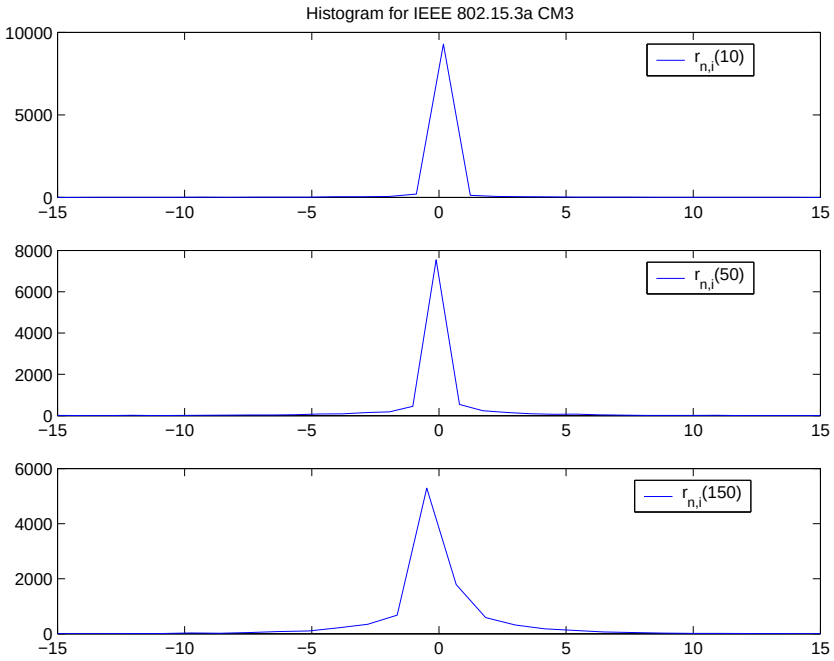

Figure 5.1: Histogram of received waveforms at the sample bins $k = \{10, 50, 150\}$ under the channel model IEEE 802.15.3a CM3 (non-line-of-sight) .

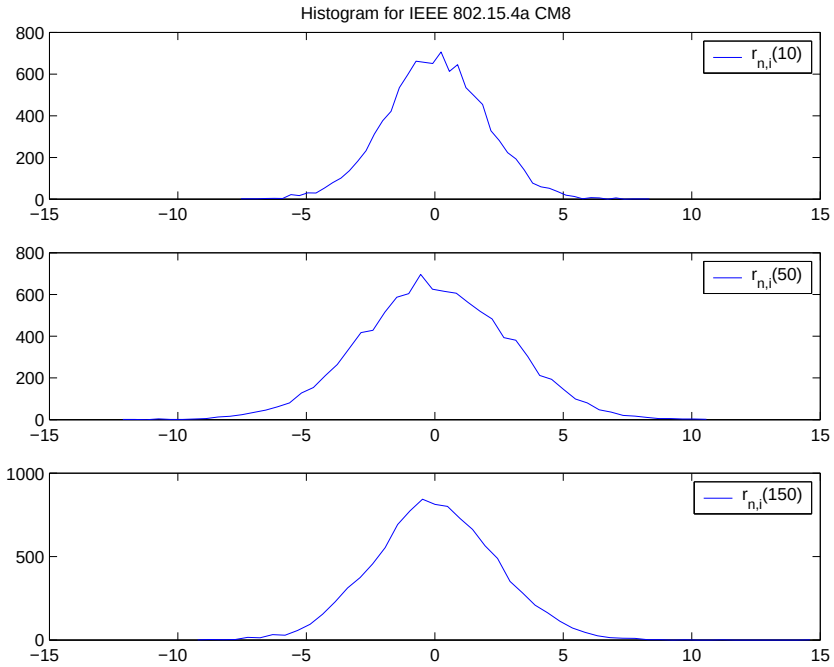

Figure 5.2: Histogram of received waveforms at the sample bins $k = \{10, 50, 150\}$ under the channel model IEEE 802.15.4 CM8 (industrial non-line-of-sight) .

It is important to note that the probability density function in (5.5) is conditioned on the covariance matrix $\mathbf{C_g}$. This covariance matrix $\mathbf{C_g}$ is unknown since it conveys the information regarding the second-order statistics of the actual received waveforms, which are usually unknown and depend on the particular transmission/reception set-up and propagation conditions. Therefore the covariance matrix $\mathbf{C_g}$ can be regarded as a nuisance parameter that has to be estimated. Replacing $\mathbf{C_g}$ with a suitable estimate leads to a compressed or conditional approach where the symbol decision statistics do not depend on $\mathbf{C_g}$ anymore. This conditional approach is presented in Section 5.5 and Section 5.6 whereas the estimate for $\mathbf{C_g}$ is to be presented next in Section 5.3.

5.2.4 Receiver architecture

The system architecture to be considered in this chapter is represented in the block diagram of Figure 5.3. It represents a fully digital non-coherent receiver where the incoming signal is synchronized at the frame-level in a non-coherent fashion. The purpose to include the frame-synchronization as the first step of this receiver is due to the fact that, for the subsequent analysis within this chapter, the signal to be considered for the symbol detection is assumed to be frame-synchronized. Frame-synchronization is possible to be performed prior to the channel characterization since the proposed non-coherent frame synchronization method is able to succeed in the absence of any channel knowledge. This will be discussed in more detailed in Chapter 6.

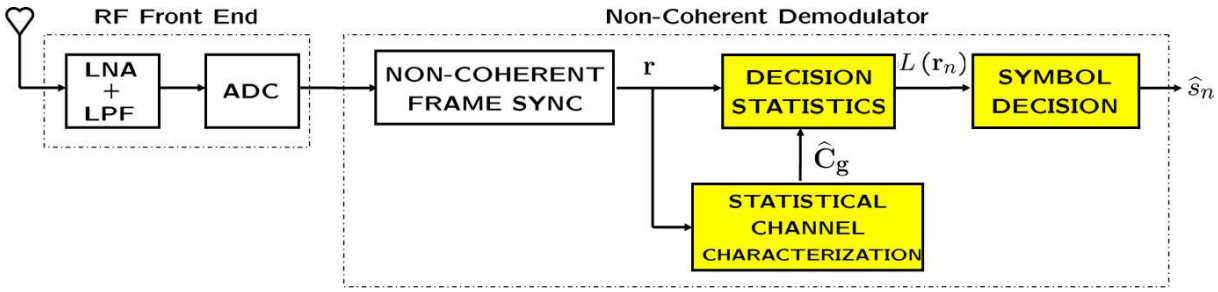

Figure 5.3: Block diagram of the receiver architecture to be considered in this chapter.

5.3 Estimation of the Unknown Channel Covariance Matrix

As a result of the unknown distortion suffered by the transmitted pulse, the covariance matrix $\mathbf{C_g}$ for the Gaussian random received waveform model is also unknown. However, this covariance matrix is ultimately required for the evaluation of the symbol decision statistics and it must be estimated from the received data. To this end, an estimate for $\mathbf{C_g}$ is presented herein which is based on the least-squares principle. The key point is to exploit the structure of the frame-level

synchronous autocorrelation matrix of the received data, a $(N_{sf} \times N_{sf})$ matrix indicated herein by $\mathbf{R}$. According to the signal model of the received random signal, $\mathbf{R}$ is given by

$$\mathbf{R} = \frac{1}{2}\left[\mathbf{C}_{+} + \mathbf{C}_{-}\right] + \mathbf{C}_{\mathrm{N}}. \tag{5.6}$$

The signal model in (5.6) assumes binary-PPM with equiprobable symbols. In this sense, the number of symbols L in the actual data record must be large enough so as to guarantee the equiprobability of the received symbols (e.g. $L > 100$). Since $\mathbf{C}_{+} \doteq \mathbf{\Pi}\mathbf{C}_{\mathbf{g}}\mathbf{\Pi}^{T}$ and $\mathbf{C}_{-} \doteq \mathbf{J}_{N_\Delta}\mathbf{\Pi}\mathbf{C}_{\mathbf{g}}\mathbf{\Pi}^{T}\mathbf{J}_{N_\Delta}^{T}$ according to Section 5.2.1, the following least-squares criterion can be formulated

$$\widehat{\mathbf{C}}_{\mathbf{g}} = \arg\max_{\mathbf{C}_{\mathbf{g}}} \left\| \widehat{\mathbf{R}} - \frac{1}{2}\left[\mathbf{\Pi}\mathbf{C}_{\mathbf{g}}\mathbf{\Pi}^{T} + \mathbf{J}_{N_\Delta}\mathbf{\Pi}\mathbf{C}_{\mathbf{g}}\mathbf{\Pi}^{T}\mathbf{J}_{N_\Delta}\right] - \mathbf{C}_{\mathrm{N}} \right\|_{F}^{2}. \tag{5.7}$$

In (5.7), $\widehat{\mathbf{R}}$ stands for the estimate of the synchronous autocorrelation matrix during the whole observation interval of L symbols,

$$\widehat{\mathbf{R}} = \frac{1}{LN_f}\sum_{n=0}^{L-1}\sum_{i=0}^{N_f-1}\mathbf{r}_{n,i}\mathbf{r}_{n,i}^{T} = \frac{1}{L}\sum_{n=0}^{L-1}\widehat{\mathbf{R}}_{n}. \tag{5.8}$$

The characterization of interferring signals on UWB receivers is indeed a whole problem itself, and it is out of the scope of this dissertation. For this reason, the covariance matrix of the interference contribution $\mathbf{C}_{\mathrm{I}}$ is assumed to be known in $\mathbf{C}_{\mathrm{N}} = \sigma_w^2\mathbf{I} + \mathbf{C}_{\mathrm{I}}$.

With the above considerations, the unique solution to the least-squares problem in (5.7) is given by,

$$\widehat{\mathbf{C}}_{\mathbf{g}} \;=\; \mathbf{\Pi}^{T} vec^{-1}\left(\left(\mathbf{A}_{\mathrm{S}}^{T}\mathbf{A}_{\mathrm{S}}\right)^{-1}\mathbf{A}_{\mathrm{S}}^{T} vec\left(\widehat{\mathbf{R}} - \mathbf{C}_{\mathrm{N}}\right)\right)\mathbf{\Pi} \tag{5.9}$$

with $\mathbf{A}_{\mathrm{S}} \doteq \mathbf{I} + \mathbf{J}_{N_\Delta} \otimes \mathbf{J}_{N_\Delta}$ the so-called *mixture* matrix, since it represents the linear mapping of the covariance matrix $\mathbf{C}_{\mathbf{g}}$ onto the synchronous autocorrelation matrix of the received data, $\mathbf{R}$. In addition, $vec^{-1}(\cdot)$ stands for the inverse of the column-stacking $vec(\cdot)$ operator [1]. Finally note that the mixture matrix $\mathbf{A}_{\mathrm{S}}$ is a constant matrix that can be calculated offline. This is because the matrix $\mathbf{A}_{\mathrm{S}}$ only depends on the time-shift N_Δ which is usually a priori known by the receiver.

5.4 Optimal Symbol Decision Statistics

In the sequel, optimal test statistics are presented for the symbol detection problem of random UWB signals with binary-PPM modulation. Moreover, the relationship with some previous contributions in the literature is also overviewed.

[1] The solution in (5.9) can also be formulated in terms of the $vech(\cdot)$ operator which eliminates the redundancy of symmetric matrices by just considering the entries on and below the main diagonal.

5.4.1 Log-GLRT for the binary-PPM decision problem

Since the received waveforms are assumed to be all random, the symbol detection problem must rely on the statistical properties of the received waveforms rather than on their particular shape. The optimal symbol decision statistics will be derived based on the generalized likelihood ratio test (GLRT) which maximizes the probability of detection for a given probability of false alarm [Kay98]. The GLRT just requires the knowledge of the probability density function of the signal hypothesis to be considered, and for the problem under consideration, two hypothesis must be decided depending on whether $d_n = 1$ or $d_n = 0$. Thus, the GLRT is obtained by evaluating the ratio

$$\Lambda(\mathbf{r}_n|\mathbf{C_g}) \doteq \frac{f\left(\mathbf{r}_n|\mathcal{H}_+;\mathbf{C_g}\right)}{f\left(\mathbf{r}_n|\mathcal{H}_-;\mathbf{C_g}\right)} \tag{5.10}$$

with $f\left(\mathbf{r}_n|\mathcal{H}_+;\mathbf{C_g}\right)$ defined in (5.5), and deciding $d_n = 1$ when $\Lambda(\mathbf{r}_n|\mathbf{C_g}) > 1$ or $d_n = 0$ when $\Lambda(\mathbf{r}_n|\mathbf{C_g}) < 1$. Alternatively, the logarithm can be taken in both sides of (5.10) resulting in the log-GLRT,

$$\begin{aligned} L\left(\mathbf{r}_n|\mathbf{C_g}\right) &\doteq \log\Lambda(\mathbf{r}_n|\mathbf{C_g}) && (5.11)\\ &= \log\frac{f\left(\mathbf{r}_n|\mathcal{H}_+;\mathbf{C_g}\right)}{f\left(\mathbf{r}_n|\mathcal{H}_-;\mathbf{C_g}\right)} && (5.12)\end{aligned}$$

from which a simple and compact decision metric can be obtained.

At this point, two important assumptions are considered. First, the low power of UWB signals allows us to assume that both the noise and the interference signals can be considered high power sources. Second, the very large bandwidth of UWB signals allows us to assume that existing wireless transmission systems are narrowband interferences. This second assumption is reasonable since the bandwidth of UWB signals is on the order of a few GHz whereas the bandwidth of existing wideband wireless systems is on the order of 10 to 20 MHz (e.g. IEEE802.11a/b/g wireless LAN devices).

With the above considerations, the optimal decision metric for random UWB signals with binary-PPM modulation is given by the log-GLRT,

$$L'(\mathbf{r}_n|\mathbf{C_g}) = Tr\left(\left[\mathbf{C}_+ - \mathbf{C}_-\right]\widehat{\mathbf{R}}_n\right) \tag{5.13}$$

where $\{\mathbf{C}_+, \mathbf{C}_-\}$ are the frame-level covariance matrices for the signal model under the hypothesis $\{\mathcal{H}_+, \mathcal{H}_-\}$, and $\widehat{\mathbf{R}}_n$ is the estimate of the frame-level synchronous autocorrelation matrix during the n-th received symbol duration. That is,

$$\widehat{\mathbf{R}}_n \doteq \frac{1}{N_f}\sum_{i=0}^{N_f-1}\mathbf{r}_{n,i}\mathbf{r}_{n,i}^T. \tag{5.14}$$

Moreover, $L'\left(\mathbf{r}_n|\mathbf{C_g}\right)$ in (5.13) is obtained from $L\left(\mathbf{r}_n|\mathbf{C_g}\right)$ in (5.12) by omitting all the irrelevant constant terms. All the analytic derivations to obtain (5.13) are omitted for clarity reasons but they are all given in Appendix 5.A and Appendix 5.B.

Finally, and with the above considerations, the symbol decision rule can be implemented as

$$\widehat{d}_n = \frac{1}{2}\left[1 + sign\left\{L'(\mathbf{r}_n|\mathbf{C_g})\right\}\right]. \tag{5.15}$$

An important point with respect to the result in (5.13) is that the log-GLRT in (5.13) depends on the covariance matrix of the random end-to-end channel response $\mathbf{C_g}$. This is due to the fact that both $\mathbf{C}_+$ and $\mathbf{C}_-$ are based on $\mathbf{C_g}$ according to Section 5.2.3. Since the covariance matrix $\mathbf{C_g}$ is unknown, it must be first estimated from the incoming data in order to evaluate the log-GLRT. At this point, the estimate for $\mathbf{C_g}$ already presented in (5.9) can be incorporated. By doing so, the log-GLRT is compressed with the information regarding the actual channel conditions, and this results in the contributions to be presented later on in Section 5.5 and Section 5.6 for the case of uncorrelated and correlated scattering, respectively.

5.4.2 Relationship of the proposed log-GLRT with existing literature

The log-GLRT presented in (5.13) is a rather general result for the symbol detection problem of binary-PPM UWB signals under the assumptions of low signal-to-noise ratio and low signal-to-interference ratio. In this sense, it is interesting to note that many of the receivers heuristically proposed in the existing literature are indeed particular cases of the more general result in (5.13).

First of all, the log-GLRT can be understood as a balanced second-order matched filter. Let us denote the difference matrix $\mathbf{C}_+ - \mathbf{C}_-$ in (5.13) by $\mathbf{P}$, that is, $\mathbf{P} \doteq \mathbf{C}_+ - \mathbf{C}_-$. Thus, matrix $\mathbf{P}$ becomes a correlation template for deciding between the hypothesis $\mathcal{H}_+$ and $\mathcal{H}_-$, similarly to what occurs for the binary symbol detection problem with deterministic signals. In fact, for the case of deterministic signals, the coherent receiver is based on a correlation template with impulse response $p(k) = g(k) - g(k - N_\Delta)$, being $g(k)$ the transmitted pulse [Win00]. This is indeed the coherent scalar version of the non-coherent second-order template $\mathbf{P}$.

Another important point to be highlighted is that no matrices are required to be inverted in the test statistics in (5.13). This is in contrast with traditional detectors for random signals, where the inverse of the involved covariance matrices is usually required [Van03]. In fact, this matrix inversion can be understood as a way of emphasizing the noise subspace since most of the traditional detectors are based on exploiting the deterministic structure of this subspace. Contrary to this approach, it is important to remark that the result obtained in (5.13) is indeed exploiting the signal subspace by projecting the received data onto the space defined by the signal covariance matrices. This is a consequence of the low SNR approach adopted herein and it is expected to provide a more robust performance in front of the noise at the expense of a limiting floor effect for the high SNR scenarios. This floor effect phenomenon is explained as the degradation resulting from the noise introduced by the algorithm itself [Gar80] and it is commonly exhibited by most low-SNR techniques.

As it will be shown later on, the result in (5.13) includes the energy-detector receiver [Rab04a], [Wei04]. This is a suboptimal receiver that can be obtained from (5.13) by forcing uncorrelated scattering with a constant power delay profile. The eigen-based receiver in [Zha05b] can also be obtained from (5.13) by taking just the principal eigenvector of $\mathbf{P}$, which is found to be the best deterministic template for linear filtering the random received data. Finally, the test statistic in (5.13) under the assumption of uncorrelated scattering will be shown to include the receiver proposed in [Wei05] where the power delay profile of the channel is assumed to be known.

5.5 Optimal Receiver under the Uncorrelated Scattering Assumption

In the presence of uncorrelated scattering (US) the covariance matrix of the received waveforms simplifies to a diagonal matrix. That is[2],

$$\mathbf{C_g} = diag\,(\boldsymbol{\gamma}) \tag{5.16}$$

with

$$\boldsymbol{\gamma} = [\gamma(0), \gamma(1), \ldots, \gamma(N_g - 1)]^T \tag{5.17}$$

the power-delay profile (PDP) of the end-to-end channel response (i.e. the PDP of the received waveforms). Consequently the frame-level covariance matrices for the hypothesis $\{\mathcal{H}_+, \mathcal{H}_-\}$ become

$$\mathbf{C}_+ = diag\,(\tilde{\boldsymbol{\gamma}})\,, \tag{5.18}$$

$$\mathbf{C}_- = diag\,(\mathbf{J}_{N_\Delta}\tilde{\boldsymbol{\gamma}})\,, \tag{5.19}$$

respectively. Note that $\tilde{\boldsymbol{\gamma}} \doteq \boldsymbol{\Pi}\boldsymbol{\gamma}$ is the $(N_{sf} \times 1)$ zero-padded version of the $(N_g \times 1)$ power-delay profile indicated by $\boldsymbol{\gamma}$ in (5.16).

It is first interesting to keep in mind the expression of the log-GLRT in (5.13) and assume for a while that the power-delay profile is a priori known at the receiver. By doing so, Section 5.5.1 provides insightful relationships with existing contributions in the current literature. In Section 5.5.2, however, the power-delay profile will be assumed to be unknown. In that case, a conditional log-GLRT will be presented by compressing the unknown parameter with the information available from the incoming data.

[2] $diag(\mathbf{X})$, when $\mathbf{X}$ is a matrix, returns a vector formed from the elements of the main diagonal of $\mathbf{X}$. Similarly, $diag(\mathbf{x})$, when $\mathbf{x}$ is a vector, returns a diagonal matrix formed from the elements of $\mathbf{x}$.

5.5.1 Log-GLRT under the assumption of known power-delay profile

Initially, let us assume that the power-delay profile is a priori known at the receiver. Then, the log-GLRT in (5.13) results in

$$L'(\mathbf{r}_n) = Tr\left(diag\left(\tilde{\boldsymbol{\gamma}} - \mathbf{J}_{N_\Delta}\tilde{\boldsymbol{\gamma}}\right)\widehat{\mathbf{R}}_n\right) = Tr\left(diag(\mathbf{w})\widehat{\mathbf{R}}_n\right) \quad (5.20)$$

$$= \sum_{k=0}^{N_{sf}-1} w(k) \sum_{i=0}^{N_f-1} r_{n,i}^2(k) \quad (5.21)$$

where the optimal correlation template $\mathbf{w}$ is defined as $\mathbf{w} \doteq \tilde{\boldsymbol{\gamma}} - \mathbf{J}_{N_\Delta}\tilde{\boldsymbol{\gamma}}$ and $r_{n,i}(k)$ stands for the k-th sample within vector $\mathbf{r}_{n,i}$. That is, $r_{n,i}(k) \doteq [\mathbf{r}_{n,i}]_k$. The receiver implementation for the test statistics in (5.21) is shown in Figure 5.4.

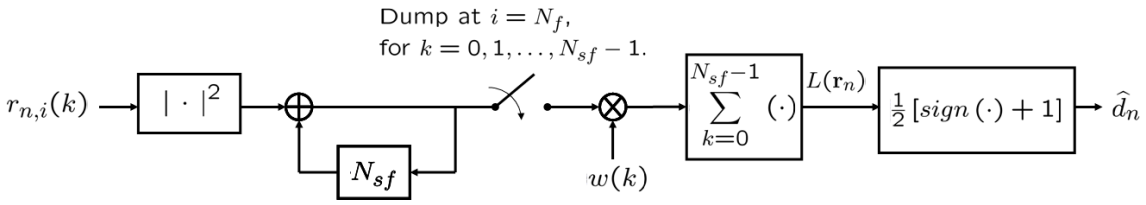

Figure 5.4: Optimal detector for random binary-PPM signals with uncorrelated scattering when the PDP is a priori known.

Next, the following relationships with existing contributions can be established. Firstly, the structure in (5.21) is similar to the MLRP receiver in [Wei05] where the received waveform was modeled as a continuous-time random process given by the product of a white Gaussian noise and a low-pass signal. However, the weighting function $w(k)$ for the MLRP receiver is found to depend on the inverse of the noise power and thus, it may be significantly more unstable. On the contrary, the result in (5.21) shows that the weighting function $w(k)$ does not depend on the noise power but just on the power-delay profile and thus, a more robust and stable performance is expected.

Secondly, the PDP-receiver proposed in (5.21) particularizes to the well-known energy-detector receiver [Rab04a] when the power-delay profile is constant. In this case, $\boldsymbol{\gamma} = \gamma\mathbf{1}_{N_g}$ for some positive constant γ and $\mathbf{1}_n$ an all ones $(n \times 1)$ vector[3]. Then the weighting function $w(k)$ becomes the difference of two noncoherent integrations of received samples.

5.5.2 Conditional log-GLRT

A possible approach when the power-delay profile $\boldsymbol{\gamma}$ is not a priori known is to consider that it is an unknown deterministic nuisance parameter that has to be estimated. In this sense, an

[3]When omitted, the dimensions of the all ones vector $\mathbf{1}$ and the identity matrix $\mathbf{I}$ are $(N_{sf} \times 1)$ and $(N_{sf} \times N_{sf})$, respectively, with N_{sf} the number of samples per frame.

estimate for the zero-padded power-delay profile $\tilde{\boldsymbol{\gamma}}$ is proposed here based on the least-squares criterion introduced in (5.7). For the case of uncorrelated scattering the cost function in (5.7) simplifies to

$$\widehat{\tilde{\boldsymbol{\gamma}}} = \arg\max_{\tilde{\boldsymbol{\gamma}}} \left\| diag(\widehat{\mathbf{R}}) - \frac{1}{2}\left(\mathbf{I} + \mathbf{J}_{N_\Delta}\right)\tilde{\boldsymbol{\gamma}} - \left(\sigma_w^2 + \mathrm{P_I}\right)\mathbf{1} \right\|^2. \tag{5.22}$$

Therefore, the least-squares estimate for the zero-padded power-delay profile $\tilde{\boldsymbol{\gamma}}$ is given by

$$\widehat{\tilde{\boldsymbol{\gamma}}} = \left(\mathbf{B}_{\mathrm{S}}^T\mathbf{B}_{\mathrm{S}}\right)^{-1}\mathbf{B}_{\mathrm{S}}^T diag\left(\widehat{\mathbf{R}} - \left(\sigma_w^2 + \mathrm{P_I}\right)\mathbf{I}\right) \tag{5.23}$$

with $\mathbf{B}_{\mathrm{S}} \doteq \mathbf{I} + \mathbf{J}_{N_\Delta}$ the *mixture* matrix representing the linear mapping of the power-delay profile onto the synchronous autocorrelation of the received data. Next, (5.23) is substituted into the log-GLRT in (5.13). As a result, and by taking into consideration the diagonal structure of $\widehat{\mathbf{R}}_n$ under the US assumption, the test statistics are given by

$$\begin{aligned} L'(\mathbf{r}_n) &= \left(\widehat{\tilde{\boldsymbol{\gamma}}} - \mathbf{J}_{N_\Delta}\widehat{\tilde{\boldsymbol{\gamma}}}\right)^T diag\left(\widehat{\mathbf{R}}_n\right) = \widehat{\tilde{\boldsymbol{\gamma}}}^T\left(\mathbf{I} - \mathbf{J}_{N_\Delta}\right)^T diag\left(\widehat{\mathbf{R}}_n\right) && (5.24)\\ &= diag^T\left(\widehat{\mathbf{R}} - \left(\sigma_w^2 + \mathrm{P_I}\right)\mathbf{I}\right)\mathbf{B}_{\mathrm{S}}\left(\mathbf{B}_{\mathrm{S}}^T\mathbf{B}_{\mathrm{S}}\right)^{-1}\mathbf{B}_{\mathrm{D}}^T diag\left(\widehat{\mathbf{R}}_n\right) && (5.25)\end{aligned}$$

with $\mathbf{B}_{\mathrm{D}} \doteq \mathbf{I} - \mathbf{J}_{N_\Delta}$ the *separation* matrix representing the linear mapping of the power-delay profile onto the weighting function $\mathbf{w}$ in (5.20). Since the mixture matrix $\mathbf{B}_{\mathrm{S}}$ is full rank then $\left(\mathbf{B}_{\mathrm{S}}^T\mathbf{B}_{\mathrm{S}}\right)^{-1} = \mathbf{B}_{\mathrm{S}}^{-1}\left(\mathbf{B}_{\mathrm{S}}^T\right)^{-1}$ and the log-GLRT in (5.25) can be recast as

$$L'(\mathbf{r}_n) = \underbrace{diag^T\left(\widehat{\mathbf{R}} - \left(\sigma_w^2 + \mathrm{P_I}\right)\mathbf{I}\right)\left(\mathbf{B}_{\mathrm{S}}^T\right)^{-1}\mathbf{B}_{\mathrm{D}}^T}_{\text{hypothesis testing template}} diag\left(\widehat{\mathbf{R}}_n\right). \tag{5.26}$$

At this point it is important to remark that, as indicated in (5.8), $\widehat{\mathbf{R}}$ is the estimate of the synchronous autocorrelation matrix during the whole observation interval of L symbols whereas $\widehat{\mathbf{R}}_n$ is the estimate restricted to a single symbol duration (i.e. the n-th symbol).

Another important remark is to note that the log-GLRT in (5.26) can be understood as a three-step procedure. First, the signal contributions corresponding to the $\mathcal{H}_+$ and $\mathcal{H}_-$ hypothesis are extracted from the estimate of the synchronous autocorrelation matrix $\widehat{\mathbf{R}}$. This is done by projecting the term $diag\left(\widehat{\mathbf{R}} - \left(\sigma_w^2 + \mathrm{P_I}\right)\mathbf{I}\right)$ onto the inverse of the mixture matrix $\mathbf{B}_{\mathrm{S}}$. Second, the result of this projection is used to built the hypothesis testing template. This is done by projecting onto the separation matrix $\mathbf{B}_{\mathrm{D}}$. Finally, the test statistics for the n-th received symbol are obtained by correlating the resulting hypothesis testing template with the data corresponding to the n-th symbol synchronous autocorrelation matrix $\widehat{\mathbf{R}}_n$. Note that both $\mathbf{B}_{\mathrm{S}}$ and $\mathbf{B}_{\mathrm{D}}$ are a-priori known at the receiver since they only depend on the time-shift N_Δ. Thus, the matrix product $\left(\mathbf{B}_{\mathrm{S}}^T\right)^{-1}\mathbf{B}_{\mathrm{D}}^T$ in (5.26) can be calculated offline.

5.6 Optimal Receiver under the Correlated Scattering Assumption

For the case of correlated scattering (CS), the only reasonable assumption that can be made is that the covariance matrix $\mathbf{C_g}$ is a symmetric positive semidefinite matrix with decreasing entries along the diagonals[4]. In Section 5.6.1, the conditional decision statistics for the CS assumption are first provided based on the compression of the log-GLRT with the full-rank estimation of $\mathbf{C_g}$. Later on, Section 5.6.2 presents a simplification of this decision rule that is based on selecting a single eigenmode of the covariance matrix $\mathbf{C_g}$ so as to implement a low-complexity rank-1 detector.

5.6.1 Conditional log-GLRT

In order to evaluate the symbol decision rule, the log-GLRT in (5.13) must be first compressed with the information regarding the unknown channel response. To this end, let us express the log-GLRT explicitly as a function of $\mathbf{C_g}$. Using the signal model in Section 5.2 we have that

$$L'(\mathbf{r}_n|\mathbf{C_g}) = Tr\left(\left[\mathbf{\Pi C_g \Pi}^T - \mathbf{J}_{N_\Delta}\mathbf{\Pi C_g \Pi}^T\mathbf{J}_{N_\Delta}^T\right]\widehat{\mathbf{R}}_n\right) \quad (5.27)$$

$$= vec^T\left(\mathbf{\Pi C_g \Pi}^T\right)\mathbf{A}_{\mathrm{D}}^T vec\,\widehat{\mathbf{R}}_n. \quad (5.28)$$

Similarly to the US assumption, the *separation* matrix $\mathbf{A}_{\mathrm{D}}$ in (5.28) is defined as $\mathbf{A}_{\mathrm{D}} \doteq \mathbf{I} - \mathbf{J}_{N_\Delta} \otimes \mathbf{J}_{N_\Delta}$. Next, let us substitute the covariance matrix $\mathbf{C_g}$ with the estimate $\widehat{\mathbf{C}}_{\mathbf{g}}$ proposed in (5.9). By doing so the log-GLRT results in

$$L'(\mathbf{r}_n) = vec^T\left(\widehat{\mathbf{R}} - \mathbf{C}_{\mathrm{N}}\right)\mathbf{A}_{\mathrm{S}}\left(\mathbf{A}_{\mathrm{S}}^T\mathbf{A}_{\mathrm{S}}\right)^{-1}\mathbf{A}_{\mathrm{D}}^T vec\,\widehat{\mathbf{R}}_n. \quad (5.29)$$

Since the mixture matrix $\mathbf{A}_{\mathrm{S}}$ is a full-rank matrix, then $\left(\mathbf{A}_{\mathrm{S}}^T\mathbf{A}_{\mathrm{S}}\right)^{-1} = \mathbf{A}_{\mathrm{S}}^{-1}\left(\mathbf{A}_{\mathrm{S}}^T\right)^{-1}$ and the log-GLRT in (5.29) can be equivalently expressed as

$$L'(\mathbf{r}_n) = \underbrace{vec^T\left(\widehat{\mathbf{R}} - \mathbf{C}_{\mathrm{N}}\right)\left(\mathbf{A}_{\mathrm{S}}^T\right)^{-1}\mathbf{A}_{\mathrm{D}}^T}_{\text{hypothesis testing template}} vec\,\widehat{\mathbf{R}}_n. \quad (5.30)$$

Similarly to (5.26), the log-GLRT in (5.30) can be also understood as a three-step procedure. First, the signal contributions corresponding to the $\mathcal{H}_+$ and $\mathcal{H}_-$ hypothesis are extracted from the estimate of the synchronous autocorrelation matrix $\widehat{\mathbf{R}}$. This is done by projecting the term $vec\left(\widehat{\mathbf{R}} - \mathbf{C}_{\mathrm{N}}\right)$ onto the inverse of the mixture matrix $\mathbf{A}_{\mathrm{S}}$. Second, the result of this projection is used to built the hypothesis testing template. This is done by projecting onto

[4]Note that the Toeplitz structure does not apply to this covariance matrix since the path-loss results in non-WSS random Gaussian waveforms.

the separation matrix $\mathbf{A}_{\mathrm{D}}$. Finally, the test statistics for the n-th received symbol are obtained by correlating the resulting hypothesis testing template with the data corresponding to the n-th symbol synchronous autocorrelation matrix $\widehat{\mathbf{R}}_n$. Note that both $\mathbf{A}_{\mathrm{S}}$ and $\mathbf{A}_{\mathrm{D}}$ are a-priori known at the receiver since they only depend on the time-shift N_Δ. Thus, the matrix product $\left(\mathbf{A}_{\mathrm{S}}^T\right)^{-1}\mathbf{A}_{\mathrm{D}}^T$ can be calculated offline.

5.6.2 Divergence maximizing rank-1 approach

The major drawback of the full-rank approach in (5.30) is that a relatively high computational burden is involved. Note that the $(N_{sf} \times N_{sf})$ matrix $\widehat{\mathbf{R}}_n$ is required and the number of samples per frame N_{sf} may be a large number because of the extremely fine time resolution of UWB signals. In order to reduce the required complexity, a practical alternative is to adopt a rank-1 approach, as shown in Figure 5.5. The problem can be stated as that of finding the best deterministic receiver filter for the incoming random signal. Rank-1 approaches for UWB signals have been previously addressed in the literature, for instance, in [Zha05b]. However, very specific constraints were imposed such as assuming the modulation format to be orthogonal PPM and forcing the optimal receiver to maximize the signal-to-noise ratio at the receiver output.

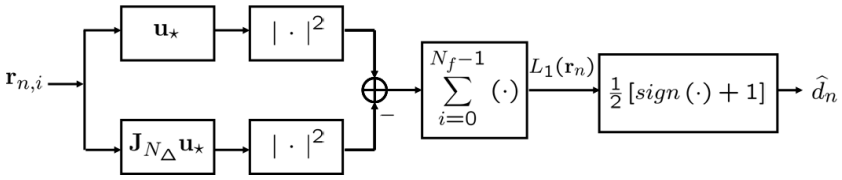

Figure 5.5: Optimal rank-1 detector for random binary-PPM signals with correlated scattering.

In this dissertation, there are two major contributions with respect to previous rank-1 approaches in the literature.

1. The proposed rank-1 detection criterion does not restrict the PPM modulation to be orthogonal. Thus the maximum delay spread of the end-to-end channel response is allowed to be larger than the PPM pulse spacing N_Δ, but smaller than the frame duration in order to avoid interframe (and intersymbol) interference.

2. The Jeffreys divergence between the hypothesis $\mathcal{H}_+$ and $\mathcal{H}_-$ is adopted here as a reference criterion for minimizing the bit error rate. The Jeffreys divergence or *J-divergence* is a symmetric measure of the difficulty in discriminating between two hypothesis [Jef46]. For the case of hypothesis $\mathcal{H}_+$ and $\mathcal{H}_-$ under consideration, and the received data $\mathbf{r}_n$, the J-divergence is defined similarly to the notation in [Kul97] as

$$J \doteq \mathrm{E}_{\mathbf{r}_n|\mathcal{H}_+}\left[L(\mathbf{r}_n)\right] - \mathrm{E}_{\mathbf{r}_n|\mathcal{H}_-}\left[L(\mathbf{r}_n)\right]. \tag{5.31}$$

An interesting property of the J-divergence measure in (5.31) is that it is closely related with the Kullback-Leibler pseudo-distance as follows,

$$J = D\left(\mathcal{H}_+ \| \mathcal{H}_-\right) + D\left(\mathcal{H}_- \| \mathcal{H}_+\right) \tag{5.32}$$

with $D\left(\mathcal{H}_+ \| \mathcal{H}_-\right)$ the Kullback-Leibler pseudo-distance between the probability density function for hypothesis $\mathcal{H}_+$ and the probability density function for hypothesis $\mathcal{H}_-$. That is[5],

$$D\left(\mathcal{H}_+ \| \mathcal{H}_-\right) \doteq \int_{\mathbf{r}_n} f\left(\mathbf{r}_n|\mathcal{H}_+\right) \log \frac{f\left(\mathbf{r}_n|\mathcal{H}_+\right)}{f\left(\mathbf{r}_n|\mathcal{H}_-\right)} d\mathbf{r}_n. \tag{5.33}$$

Note that, according to the GLRT definition in (5.12), the Kullback-Leibler pseudo-distance can also be expressed as

$$\begin{aligned} D\left(\mathcal{H}_+ \| \mathcal{H}_-\right) &= \int_{\mathbf{r}_n} f\left(\mathbf{r}_n|\mathcal{H}_+\right) \log \Lambda\left(\mathbf{r}_n\right) d\mathbf{r}_n & (5.34)\\ &= \int_{\mathbf{r}_n} f\left(\mathbf{r}_n|\mathcal{H}_+\right) L\left(\mathbf{r}_n\right) d\mathbf{r}_n & (5.35)\\ &= \mathrm{E}_{\mathbf{r}_n|\mathcal{H}_+}\left[L(\mathbf{r}_n)\right]. & (5.36) \end{aligned}$$

Similarly for the converse $D\left(\mathcal{H}_- \| \mathcal{H}_+\right)$,

$$\begin{aligned} D\left(\mathcal{H}_- \| \mathcal{H}_+\right) &= \int_{\mathbf{r}_n} f\left(\mathbf{r}_n|\mathcal{H}_-\right) \log \frac{f\left(\mathbf{r}_n|\mathcal{H}_-\right)}{f\left(\mathbf{r}_n|\mathcal{H}_+\right)} d\mathbf{r}_n & (5.37)\\ &= -\int_{\mathbf{r}_n} f\left(\mathbf{r}_n|\mathcal{H}_-\right) \log \Lambda\left(\mathbf{r}_n\right) d\mathbf{r}_n & (5.38)\\ &= -\int_{\mathbf{r}_n} f\left(\mathbf{r}_n|\mathcal{H}_-\right) L\left(\mathbf{r}_n\right) d\mathbf{r}_n & (5.39)\\ &= -\mathrm{E}_{\mathbf{r}_n|\mathcal{H}_-}\left[L(\mathbf{r}_n)\right]. & (5.40) \end{aligned}$$

Finally, we have that

$$J \doteq \mathrm{E}_{\mathbf{r}_n|\mathcal{H}_+}\left[L(\mathbf{r}_n)\right] - \mathrm{E}_{\mathbf{r}_n|\mathcal{H}_-}\left[L(\mathbf{r}_n)\right] = D\left(\mathcal{H}_+ \| \mathcal{H}_-\right) + D\left(\mathcal{H}_- \| \mathcal{H}_+\right). \tag{5.41}$$

With the above considerations, it seems reasonable to design the optimal low-rank detector by selecting those eigenmodes from $\mathbf{C_g}$ that maximize the J-divergence. By doing so, and from the interpretation in terms of Kullback-Leibler pseudo-distance, we are indeed maximizing the distance between hypothesis $\mathcal{H}_+$ and hypothesis $\mathcal{H}_-$. Consequently, the substitution with the log-GLRT test in (5.13) results in the J-divergence for the problem at hand to be given by

$$\begin{aligned} J &\propto Tr\left(\left[\mathbf{C}_+ - \mathbf{C}_-\right]\left[\mathrm{E}_{\mathbf{r}_n|\mathcal{H}_+}\left[\widehat{\mathbf{R}}_n\right] - \mathrm{E}_{\mathbf{r}_n|\mathcal{H}_-}\left[\widehat{\mathbf{R}}_n\right]\right]\right) & (5.42)\\ &= Tr\left(\left[\mathbf{C}_+ - \mathbf{C}_-\right]\left[\mathbf{C}_+ + \mathbf{C}_\mathrm{N} - \left(\mathbf{C}_- + \mathbf{C}_\mathrm{N}\right)\right]\right) & (5.43)\\ &= \|\mathbf{C}_+ - \mathbf{C}_-\|_F^2 & (5.44) \end{aligned}$$

[5]In the formal definition of the J-divergence and the Kullback-Leibler pseudo-distance, the dependence with the unknown waveform covariance matrix $\mathbf{C_g}$ is omitted for clarity.

where all the irrelevant constant terms have been omitted for simplicity.

The result in (5.44) indicates that the difficulty in discriminating between $\mathcal{H}_+$ and $\mathcal{H}_-$ is given by the *distance* between the corresponding signal covariance matrices $\{\mathbf{C}_+, \mathbf{C}_-\}$. This is a very important result since it can be used to evaluate the impact of the pulse-spacing N_Δ in the discrimination between $\mathcal{H}_+$ and $\mathcal{H}_-$. An example is shown in Figure 5.6 for different channel models of the IEEE 802.15.3a/4a standards.

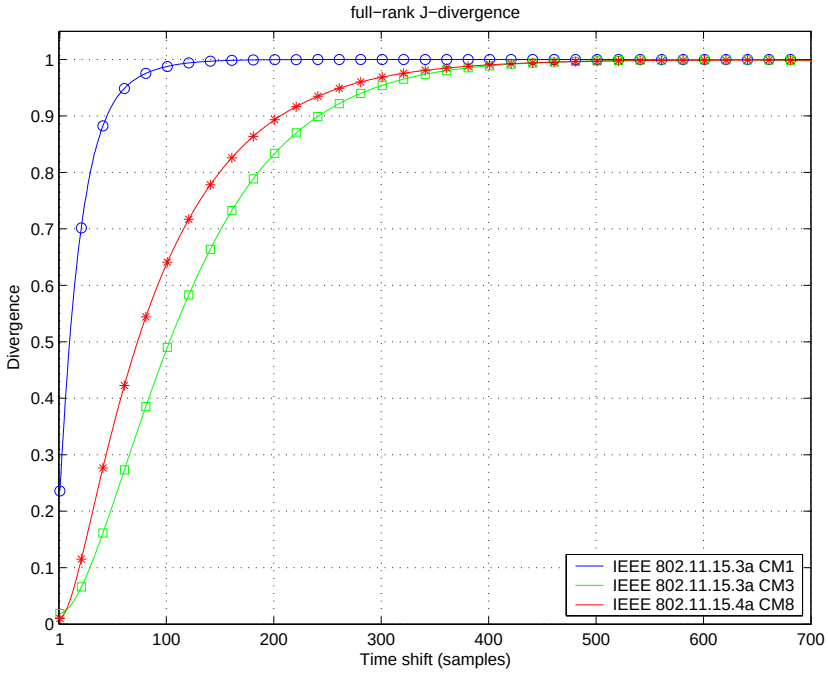

Figure 5.6: Normalized J-divergence as a function of the PPM time-shift N_Δ for different channel models. Sampling time 250 ps.

The rank-1 approach aims to provide the best deterministic receiving filter that maximizes the J-divergence in (5.44). To this end, let us express the signal covariance matrix under $\mathcal{H}_+$ as $\mathbf{C}_+ = \mathbf{U}\mathbf{D}\mathbf{U}^T$, with the $(N_{sf} \times N_{sf})$ matrix $\mathbf{U} = \left[\mathbf{u}_0, \mathbf{u}_1, \ldots, \mathbf{u}_{N_{sf}-1}\right]$ containing the eigenvectors of $\mathbf{C}_+$ and the diagonal matrix $\mathbf{D} = diag\left(\lambda_0, \lambda_1, \ldots, \lambda_{Nsf-1}\right)$ containing the corresponding eigenvalues. In this way, the log-GLRT in (5.13) and the J-divergence in (5.44) can equivalently be expressed as,

$$L'_d(\mathbf{r}_n|\mathbf{C}_\mathbf{g}) = \frac{1}{N_f}\sum_{m=0}^{d-1}\sum_{i=0}^{N_f-1}\lambda_m\left[\|\mathbf{u}_m^T\mathbf{r}_{n,i}\|^2 - \|\mathbf{u}_m^T\mathbf{J}_{N_\Delta}^T\mathbf{r}_{n,i}\|^2\right] \tag{5.45}$$

$$J_d = \frac{2}{N_f}\sum_{p=0}^{d-1}\sum_{q=0}^{d-1}\lambda_p\lambda_q\left[1 - \left(\mathbf{u}_p^T\mathbf{J}_{N_\Delta}\mathbf{u}_q\right)^2\right] \tag{5.46}$$

with d the dimension of the signal subspace, i.e., the number of significant eigenvalues. For the

case of $d = 1$, the rank-1 test statistics particularize to

$$L_1'(\mathbf{r}_n|\mathbf{C_g}) = \frac{1}{N_f}\sum_{i=0}^{N_f-1}\lambda_\star\left(\|\mathbf{u}_\star^T\mathbf{r}_{n,i}\|^2 - \|\mathbf{u}_\star^T\mathbf{J}_{N_\Delta}^T\mathbf{r}_{n,i}\|^2\right), \tag{5.47}$$

$$\lambda_\star = \frac{\mathbf{u}_\star^H\mathbf{C}_+\mathbf{u}_\star}{\mathbf{u}_\star^H\mathbf{u}_\star}, \tag{5.48}$$

$$\mathbf{u}_\star = \arg\max_{\mathbf{u}_m} J_1(\mathbf{u}_m) \tag{5.49}$$

where $\mathbf{u}_\star$ is the optimal receiver filter that maximizes the rank-1 J-divergence

$$J_1(\mathbf{u}_m) = \frac{2}{N_f}\lambda_m^2\left[1 - \left(\mathbf{u}_m^T\mathbf{J}_{N_\Delta}\mathbf{u}_m\right)^2\right]. \tag{5.50}$$

The rank-1 J-divergence cost function in (5.50) is very insightful. Firstly, the structure of the cost function resembles the well-known constant modulus algorithm (CMA) [Tre83], [Vee05]. Secondly, for each of the eigenvectors $\mathbf{u}_m$ of $\mathbf{C}_+$, both the energy contribution for $\mathcal{H}_+$ and the blocking capability for $\mathcal{H}_-$ are evaluated. This is done by the terms λ_m^2 and $\rho_m(N_\Delta) \doteq \mathbf{u}_m^T\mathbf{J}_{N_\Delta}\mathbf{u}_m$, respectively. Thus, the selection criterion for the optimal receiver filter is not only the energy it can extract from the incoming random signal but also the autocorrelation properties it has to block the random signals belonging to the opposite hypothesis .

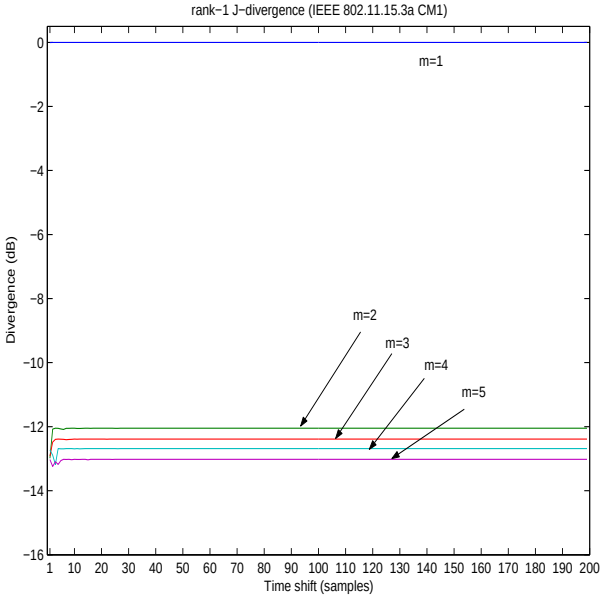

Figure 5.7: Evolution of the rank-1 J-divergence measure as a function of the PPM time-shift N_Δ for the IEEE802.15.3a channel model CM1 (line-of-sight).

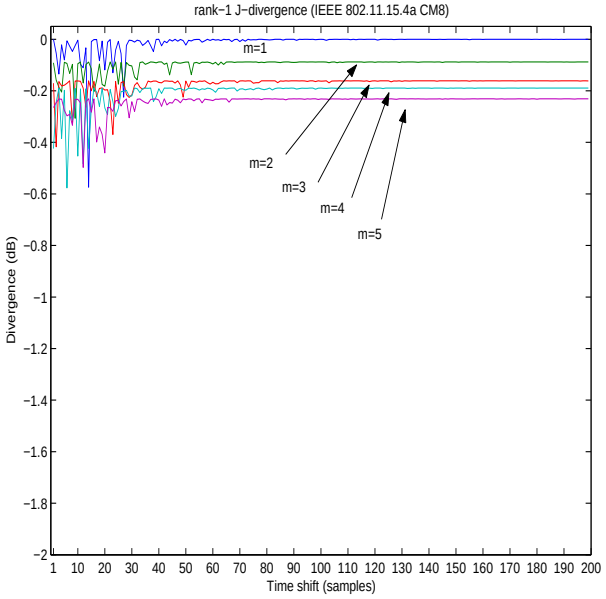

Figure 5.8: Evolution of the rank-1 J-divergence measure as a function of the PPM time-shift N_Δ for the IEEE802.15.4a channel model CM8 (industrial non line-of-sight)

5.6.3 Iterative solution for the divergence maximizing receiver filter

In this section an iterative procedure is proposed to circumvent the computationally demanding task of the complete eigendecomposition of $\mathbf{C_g}$ within $\mathbf{C}_+$. Apart from the computational savings, the iterative approach provides a more flexible design criterion where transitions between different propagation scenarios can be optimally tracked with an appropriate memory factor. This can be done by properly updating the estimated synchronous autocorrelation matrix $\widehat{\mathbf{R}}$ and feeding this information to the iterative criterion.

In the sequel the stochastic gradient descent method is adopted for addressing the iterative optimization in (5.49)-(5.50). The recursion is considered here to be given by

$$\mathbf{u}_\star^{(k+1)} = \mathbf{u}_\star^{(k)} + \mu \left[\nabla_{\mathbf{u}_m} \log J_1(\mathbf{u}_m)\right]_{\Big|_{\mathbf{u}_m=\mathbf{u}_\star^{(k)}}} \tag{5.51}$$

$$\nabla_{\mathbf{u}_m} \log J_1(\mathbf{u}_m) = \Big[\left(1-\rho_m^2(N_\Delta)\right)\left(\mathbf{C}_+ - \lambda_m \mathbf{I}\right) - \lambda_m \rho_m(N_\Delta)\mathbf{J}_{N_\Delta}\Big]\mathbf{u}_m. \tag{5.52}$$

with μ a fixed step size. Note that the gradient descent method in (5.51) is applied to the logarithm of the rank-1 divergence cost function. By doing so, the optimal solution remains the same but the expression for the gradient is simpler. Finally, the gradient in (5.52) is evaluated assuming that the eigenvalue λ_m and the autocorrelation $\rho_m(N_\Delta)$ are defined as

$$\lambda_m \doteq \frac{\mathbf{u}_m^T \mathbf{C}_+ \mathbf{u}_m}{\mathbf{u}_m^T \mathbf{u}_m} \tag{5.53}$$

$$\rho_m(N_\Delta) \doteq \mathbf{u}_m^T \mathbf{J}_{N_\Delta} \mathbf{u}_m. \tag{5.54}$$

In practice, an estimate for $\mathbf{C}_+$ can be obtained in a straightforward manner by properly zero-padding the estimate $\widehat{\mathbf{C}}_\mathbf{g}$ proposed in (5.9).

An example of the resulting waveform for the best deterministic rank-1 receiver filter $\mathbf{u}_\star$ is shown in Figure 5.9 for the case of the IEEE 802.15.4a CM8 channel model with a sampling time of $T_s = 0.25$ ns, a PPM time-shift of $N_\Delta = 100$ samples and a frame-interval of $N_{sf} = 1000$ samples. The optimal receiving filter is shown on the bottom left hand side of Figure 5.9 whereas the receiving filter obtained by using the gradient descent method in (5.51)-(5.52) is shown on the top left hand side. The resulting value of the rank-1 J-divergence is also depicted on the right hand side of Figure 5.9 as a function of the number of iterations.

It is important to remark that the proposed iterative approach resembles the well-known Rayleigh quotient iteration (RQI) which provides the maximum eigenvalue and the corresponding eigenvector of any symmetric matrix [Gol96]. The resemblance with the RQI is clear when orthogonal PPM is considered. In that case we have $\rho_m(n) = 0$ for all m when $n \geq N_\Delta$ as a result of the orthogonal transmission. Thus the gradient in (5.52) simplifies to

$$\nabla_{\mathbf{u}_m} \log J_1(\mathbf{u}_m)_{\Big|_{\text{orthogonal 2-PPM}}} = \left[\mathbf{C}_+ - \lambda_m \mathbf{I}\right]\mathbf{u}_m \tag{5.55}$$

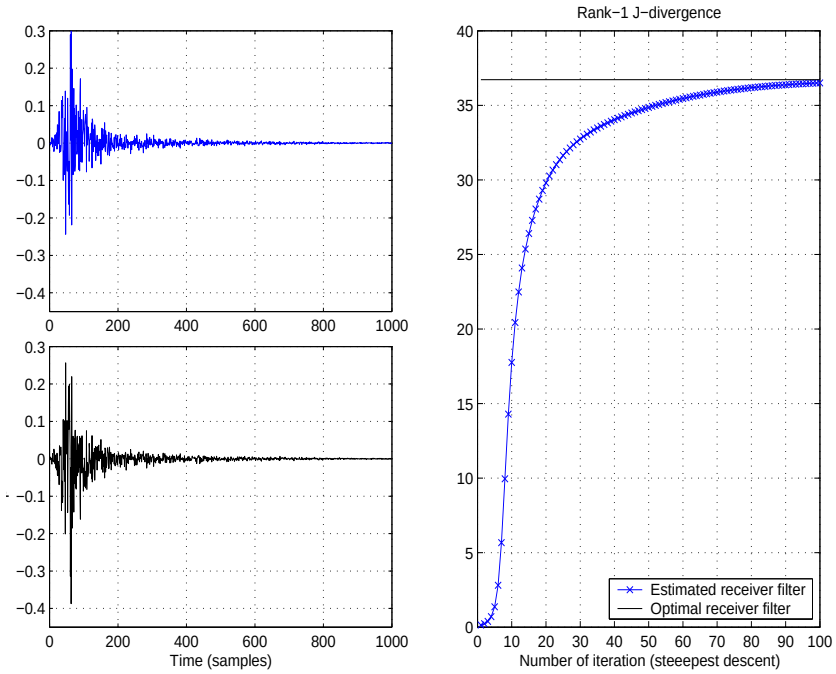

Figure 5.9: Best deterministic receiver filter for the IEEE 802.15.4a CM8 channel model according to the proposed iterative rank-1 J-divergence optimization. The estimated filter at the end of 100 iterations is shown in the top left hand side corner whereas the exact filter is shown in the bottom left hand side corner.

which coincides with the gradient of the RQI [Gol96]. Therefore, the best deterministic receiver filter for orthogonal PPM corresponds to the well-known result of being the maximum eigenvector of $\mathbf{C_g}$ (i.e. $\mathbf{C}_+$). This solution is also found to provide the maximum signal-to-noise ratio at the receiver output. For non-orthogonal PPM, however, the solution is not trivial and it must be determined based on the maximization of the rank-1 J-divergence cost function proposed in (5.50).

Finally, note that the proposed rank-1 receiver in Figure 5.5 can be extended to the case where a set of $d_0 > 1$ eigenmodes are considered. In that situation the receiver architecture can be generalized to the rank-d_0 architecture depicted in Figure 5.10. The receiver filters $\mathbf{u}_{\star|d}$ in Figure 5.10 are obtained in a sequential manner starting from $\mathbf{u}_{\star|d=1}$ and using (5.51). Once $\mathbf{u}_{\star|d=1}$ is obtained, the covariance matrix $\mathbf{C}_+$ must be updated as follows, $\mathbf{C}_{+|d} = \mathbf{C}_{+|d-1} - \mathbf{u}_{\star|d-1}\mathbf{u}_{\star|d-1}^T$ and the iterative procedure in (5.51) must be started again with the new covariance matrix.

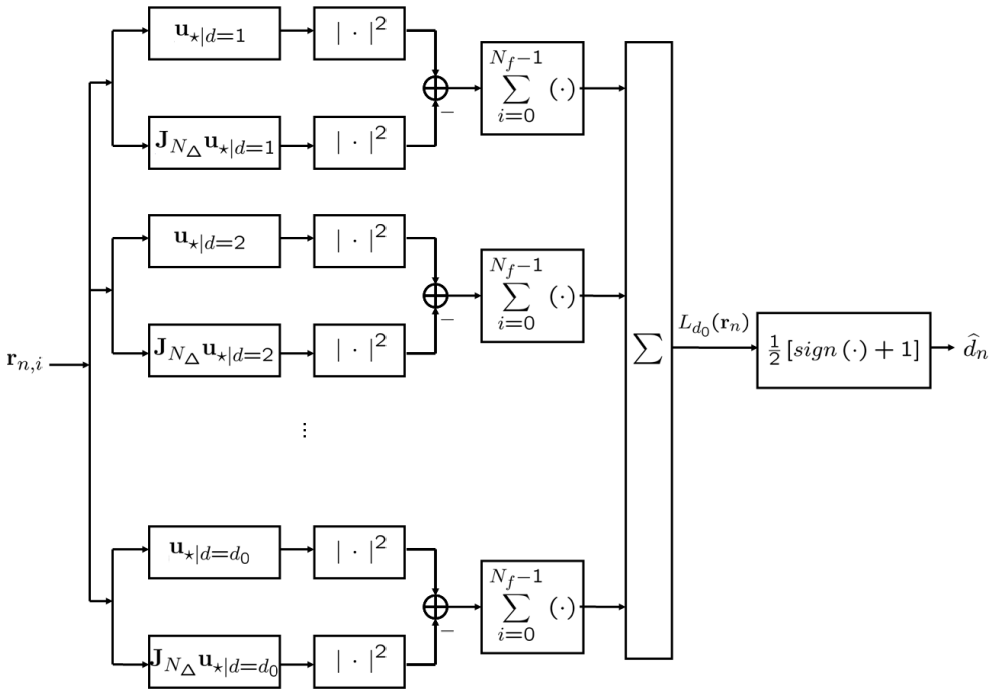

Figure 5.10: Extension of the rank-1 optimal detector in Figure 5.5 to the case $d = d_0$ with $d_0 > 1$.

5.7 Simulation Results

In this section, computer simulations are carried out in order to evaluate the performance of the proposed binary-PPM detectors. To this end, two different simulation scenarios are considered:

(A): *Random Gaussian waveforms.* The received waveforms are assumed to be zero-mean random Gaussian processes driven by a given covariance matrix $\mathbf{C_g}$. The processes are non wide-sense stationary with an exponentially decaying power delay profile as in [Cas02a]. Two distinctions are made among uncorrelated scattering (US) and correlated scattering (CS) depending on whether the covariance matrix $\mathbf{C_g}$ is diagonal or not.

(B): *IEEE 802.15.3a/4a waveforms.* The received waveforms are generated according to the IEEE 802.15.3a channel models for high data rate applications and the IEEE 802.15.4a channel models for low data rate applications.

For all the simulation scenarios, the sampling time is set to $T_s = 0.125$ ns. The frame duration extends over $N_{sf} = 2000$ samples ($T_f = 250$ ns) and a total of $N_f = 20$ frames are conveyed within a symbol period. The PPM time shift is set to $N_\Delta = 400$ samples ($T_\Delta = 50$ ns) unless otherwise specified. Finally, an observation interval of $L = 500$ symbols is considered for estimating the synchronous autocorrelation matrix $\mathbf{R}$. Note that the matrix $\mathbf{R}$ is the basis

for estimating the covariance matrices $\mathbf{C_g}$ or $\mathbf{C}_+$ as indicated in Section 5.3. The performance results for the proposed receivers are compared with the performance of the well-known energy-detector receiver (ED) [Rab04a], [Wei04] which is a simple but suboptimal receiver that assumes the power delay profile of the channel to be constant. For the simulation results with the ED receiver, the integration length is set to be equal to the time-shift N_Δ.

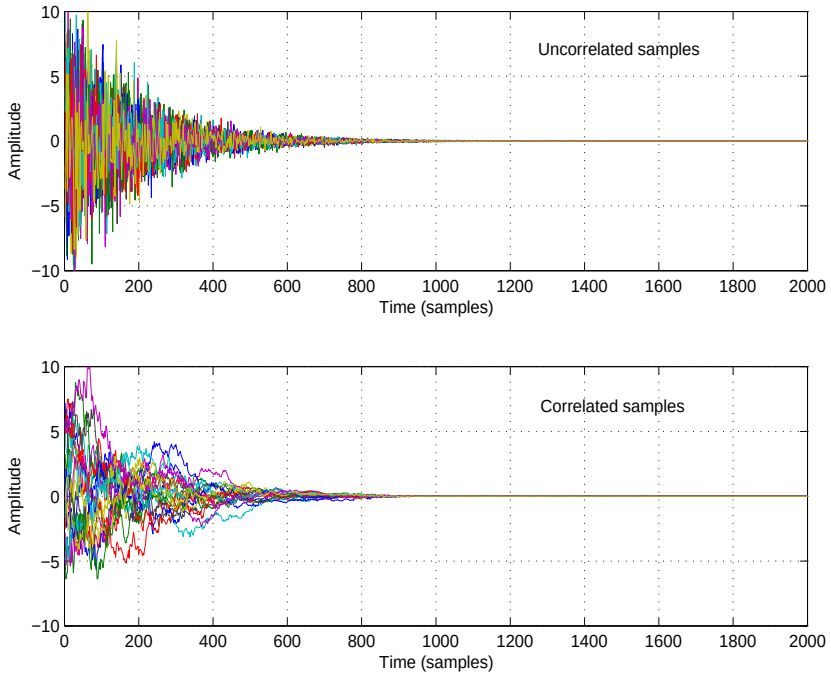

Figure 5.11: 1000 realizations of the Gaussian random received waveforms with uncorrelated samples (top) and correlated samples (bottom). The power delay profile is exponentially decaying with an average delay spread of 100 samples. For correlated samples, the time-lags of the autocorrelation are also exponentially decaying with an average spread of 200 samples.

5.7.1 Simulation results for random Gaussian waveforms

Experiment 1: Random waveforms with US. In this experiment the received waveforms are modeled as zero-mean Gaussian random processes with uncorrelated samples. The power-delay profile is exponentially decaying with an average delay spread of 100 samples (12.5 ns). A total of 1000 waveforms are depicted at the top of Figure 5.11 for illustrating the shape of the received waveforms. For this simulation set-up, two different PPM time-shifts are considered: $N_\Delta = 30$ samples (3.75 ns) and $N_\Delta = 400$ samples (50 ns).

The receiver performance is analyzed in terms of bit error rate (BER) and it is shown in Figure 5.12 as a function of the energy-per-symbol to noise spectral density E_s/N_0. As it is expected, the full-rank detector based on (5.30) and the PDP detector based on (5.26) do

coincide. Note that the PDP detector just considers the main diagonal of the covariance matrix $\mathbf{C_g}$ whereas the full-rank detector estimates the whole covariance matrix $\mathbf{C_g}$ and compresses this information into the likelihood ratio test statistics. However, in the presence of US scattering, $\mathbf{C_g}$ is diagonal and thus the full-rank detector is indeed a PDP detector.

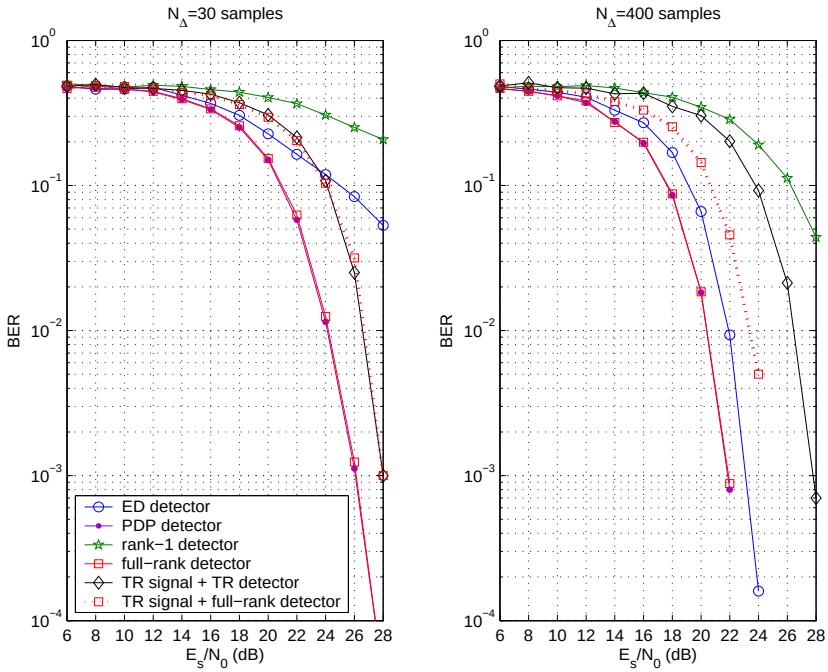

Figure 5.12: BER performance for random Gaussian UWB signals with uncorrelated scattering.

Contrary to the full-rank and the PDP detectors, the rank-1 detector provides the worst performance. This is because the uncorrelateness of the received samples expands the number of significant eigenmodes in the covariance matrix $\mathbf{C_g}$. As a result, the contribution of a rank-1 approximation is almost negligible compared with the large amount of significant eigenvalues.

Finally, the results in Figure 5.12 also incorporate the performance of a transmitted-reference (TR) scheme where an unmodulated pulse is transmitted prior to each data modulated pulse. In order to model rapid time variations of the propagation environment, the end-to-end channel response is assumed to change from frame to frame. As shown in Figure 5.12, this causes a severe degradation of the TR scheme. The reason is that each unmodulated pulse can only be used for one modulated pulse and thus, no coherent integration can be performed across multiple frames to combat the severe noise contribution. However, a significant improvement can be obtained when the TR signal is processed by the full rank detector. In that way, the optimal receiver for time-varying channels is adopted and there is just about 3 dB of performance loss due to the transmission of unmodulated pulses.

Experiment 2: Random waveforms with correlated samples. In this experiment, the received waveforms are modeled as Gaussian random processes with correlated samples. The power delay

profile is exponentially decaying with an average delay spread of 100 samples (12.5 ns) and the temporal lags of the autocorrelation are also set to be exponentially decaying with an average delay spread of 200 samples (25 ns). A total of 1000 waveforms are depicted at the bottom of Figure 5.11 for illustrating the shape of the received waveforms.

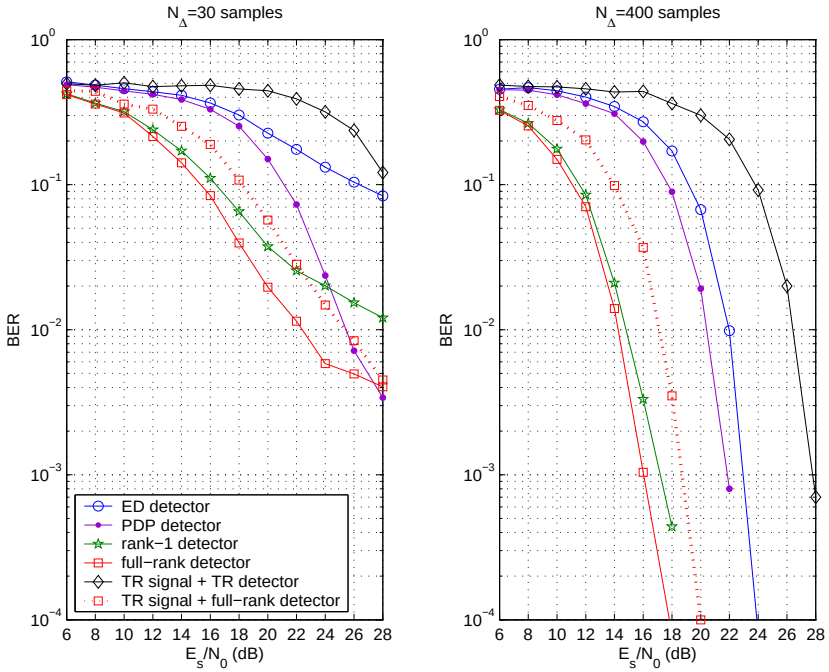

Figure 5.13: BER performance for random Gaussian UWB signals with correlated scattering.

The BER performance in terms of the energy-per-symbol to noise spectral density E_s/N_0 is presented in Figure 5.13. Again, the full-rank detector provides the best performance because it estimates the whole covariance matrix $\mathbf{C_g}$. However, the PDP detector degrades because it just considers the main diagonal of $\mathbf{C_g}$ and ignores the rest of the entries, many of them being different from zero when the scattering is correlated. The second best performance for the low-SNR regime is provided by the low-complexity rank-1 detector both for $N_\Delta = 30$ (3.75 ns) and $N_\Delta = 400$ samples (50 ns). The reason is that the correlation of the received waveforms reduces the number of significant eigenmodes in $\mathbf{C_g}$. In contrast, with the US case, the contribution of a rank-1 approximation is now significant compared with the total amount of eigenvalues.

Moreover, and as a general remark, note that the BER of CS simulations is usually lower than that of US simulations. The reason can be found in the fact that reducing the uncertainty in the received waveforms (i.e. introducing correlation between samples) makes the BER performance to be close to that of coherent receivers where perfect channel state information is available.

Finally, it should be noted that for the case of very small time-shifts N_Δ, the BER performance changes when entering the high-SNR region. For instance, this can be observed in the left-hand side of Figure 5.13 for $E_s/N_0 > 24$ dB. Beyond this E_s/N_0 value, the performance

of the rank-1 detector experiences a floor effect that is caused by the noise introduced by the detector itself. Similarly, a floor effect is also exhibited by the full-rank detector. However, the latter is mainly due to the finite observation interval when calculating the estimate for the synchronous autocorrelation matrix $\mathbf{R}$. For the high E_s/N_0 range, the PDP receiver outperforms the full-rank detector because the PDP receiver just considers the main diagonal of $\mathbf{R}$, and thus, it is more robust to the estimation errors in $\mathbf{R}$ due to the finite observation interval.

Experiment 3: Random waveforms in the presence of narrowband interferences. In this experiment, the BER performance is evaluated in the presence of interference from IEEE 802.11b WLAN devices. The central frequency for this interference is set to $f_{\mathrm{I}} = 2.4$ GHz with a bandwidth of $\mathrm{BW_I} = 20$ MHz. The simulation parameters are the same as for the previous experiments except for the PPM time-shift that is set here to $N_\Delta = 200$ samples (25 ns). The signal and noise powers are fixed to result in $E_s/N_0 = 20$ dB.

In Figure 5.14, the BER performance is evaluated as a function of the interference-to-noise ratio $\frac{\mathrm{P_I}}{\sigma_w^2}$. It is interesting to note that, for the case of correlated scattering (right hand side plot in Figure 5.14), the rank-1 detector becomes the optimal detector when increasing the interference power. This can be seen for $\frac{\mathrm{P_I}}{\sigma_w^2} > 6$ dB because the lower bound BER corresponding to the optimal full-rank detector coincides with the BER provided by the low-complexity rank-1 detector. Consequently, the rank-1 detector turns out to be the optimal detector for interference dominating scenarios.

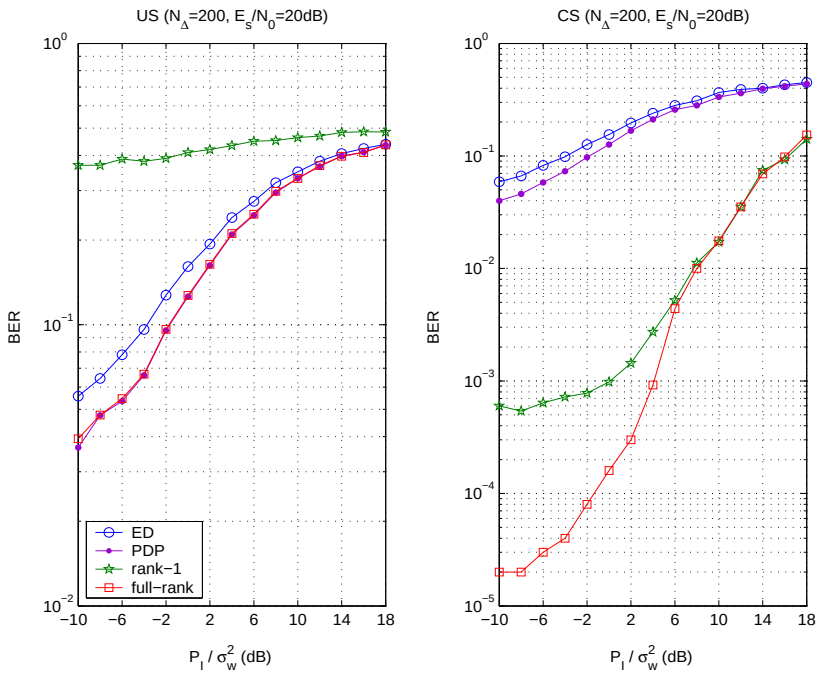

Figure 5.14: BER performance for random Gaussian UWB signals in the presence of narrowband interference.

Finally, it is found that the correlation between samples in the CS assumption allows a more robust performance against random Gaussian interferences. This can be seen by noting that the BER for US (left hand side of Figure 5.14) significantly degrades as compared with the BER for CS (right hand side 5.14).

5.7.2 Simulation results for the IEEE 802.15.3a/4a channel models

In this section simulation results are provided for the channel models considered in the IEEE 802.15.3a [Foe03] (high data rate) and the IEEE 802.15.4a (low data rate) standards [Mol04]. The simulation set-up is the same as for the case of random waveforms with the exception that only the PPM time-shift of $N_\Delta = 400$ (50 ns) is considered. The selected channel models include both line-of-sight (LOS) and non line-of-sight (NLOS) scenarios. As for LOS scenarios, the channel model CM1 from the IEEE 802.15.3a standard is considered. NLOS scenarios are herein represented by the channel model CM3 from the IEEE 802.15.3a standard and the channel model CM8 from the IEEE 802.15.4a standard. Finally, the channel model for body-area-networks (BAN) within the IEEE 802.15.4a is also considered. The simulation parameters for the BAN channel model assume a distance between transmitter and receiver of 0.1 meters and the floor material is concrete. This channel model allows the representation of measurements taken at the front, side or back of the body. Among these options, measurements in the back position of the body are considered for the simulation results to be presented herein.

An important issue to be taken into consideration is the path-dependent propagation of UWB signals. This path-dependent distortion is not considered in the current channel simulation software available from the IEEE 802.15.3a/4a working group. However, and according to the IEEE 802.15.4a final report, the path-dependent distortion can be incorporated by considering the generated taps of the tapped delay line model to be the discrete-time samples of a bandlimited random process (i.e. the random received waveform) [Mol04, p.35]. Therefore, the samples of the received waveforms considered herein are indeed the tap values generated by the standardized software provided by the IEEE working group.

The BER results are presented in Figure 5.15 and Figure 5.16 for the IEEE 802.15.3a and the IEEE 802.15.4a channel models, respectively. For all the channel models the full-rank detector based on (5.30) continues to provide the best performance. Moreover, the performance of the PDP receiver based on (5.26) is found to coincide with the full-rank detector for all the tested channel models except for the CM8. This indicates that the US assumption considered in the PDP detector applies to most of the tested IEEE channel models.

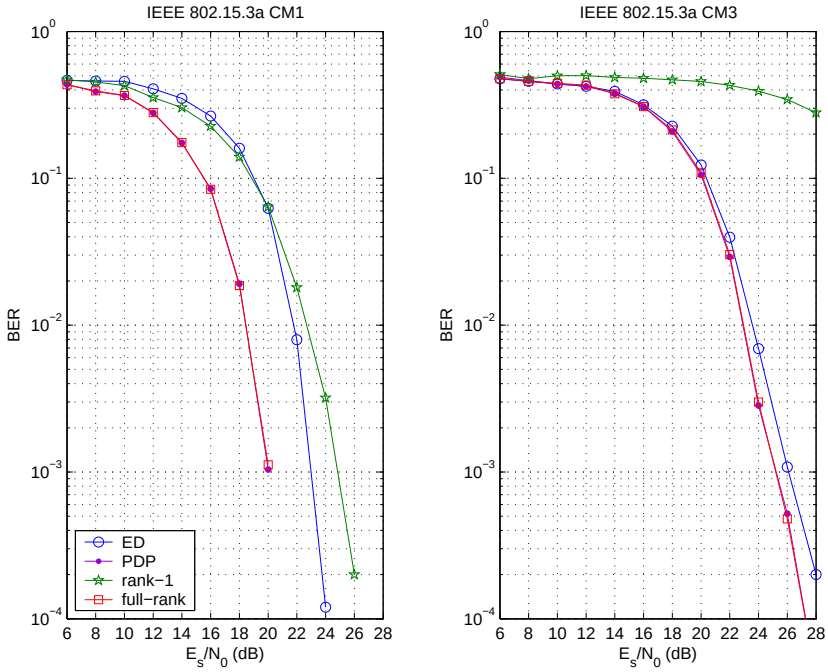

Figure 5.15: BER performance for the IEEE 802.15.3a CM1 channel model (line-of-sight) and the IEEE 802.15.3a CM3 channel model (non line-of-sight).

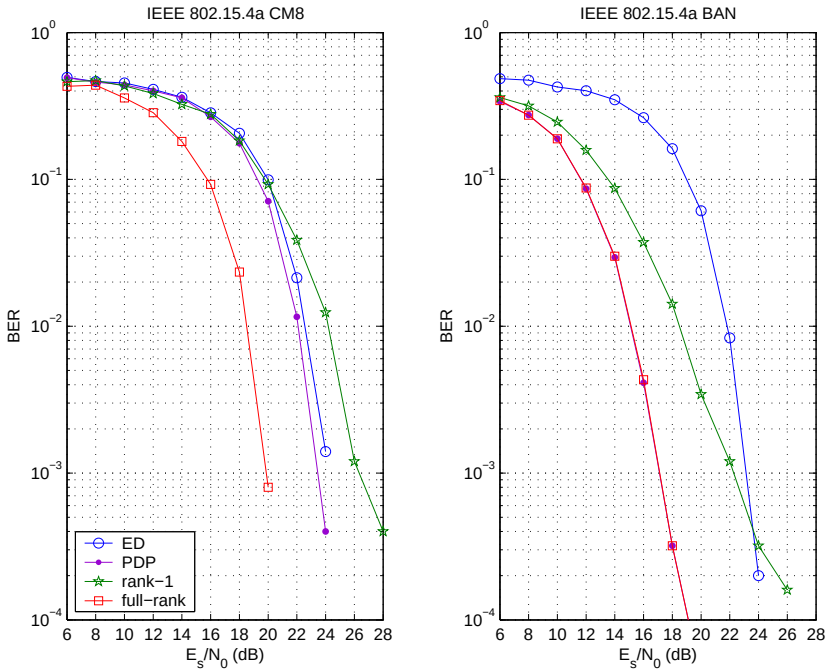

Figure 5.16: BER performance for the IEEE 802.15.4a CM8 channel model (industrial non line-of-sight) and the IEEE 802.15.4a BAN channel model (body area network).

Related with the above remark, note that the rank-1 detector usually provides the worst performance except for the BAN channel. This is due to the fact that the rank-1 detector is devoted to propagation environments where the amplitudes of the received samples (not the absolute values) are correlated and thus, the channel energy is only spread over a small number of eigenmodes.

The requirement of correlated received samples is not fulfilled in most of the considered channel models, as indicated in [Saa04], [Men05]. Thus the performance of the rank-1 detector seriously degrades. For the BAN channel, however, the reasonable performance of the rank-1 detector is in line with the correlated scattering results found in [For06].

5.8 Conclusions

The optimal framework for the symbol decision problem of binary-PPM with random UWB signals has been presented. The optimal symbol decision statistics are provided and the relationship with previous contributions in the current literature has been revised. Two different analyses for the symbol decision problem have been presented depending on whether the amplitudes of the received waveforms are correlated or not. The correlated scenario is of special interest since it is found to allow a low cost implementation of the optimal symbol detector. In this sense, an iterative algorithm is proposed for the design of the optimal receiver filter which is based on information-theoretic criteria and allow us to minimize the bit error probability.

Appendix 5.A Derivation of the Low-SNR Generalized Likelihood Ratio Test

The GLRT provides the optimal decision rule for deciding between the hypothesis $\mathcal{H}_+ : d_n = 1$ and $\mathcal{H}_- : d_n = 0$ based on the probability density function of the received data conditioned on the hypothesis to be tested. According to the channel model in Section 5.2, the conditioned probability density function for the n-th received symbol under $\mathcal{H}_+$ is given by the multivariate Gaussian probability density function,

$$f\left(\mathbf{r}_n|\mathcal{H}_+;\mathbf{C_g}\right) = \prod_{i=0}^{N_f-1} \frac{1}{(2\pi)^{N_{sf}/2}\det^{1/2}\left(\mathbf{C}_+ + \mathbf{C}_\mathrm{N}\right)} \exp\left(-\frac{1}{2}\mathbf{r}_{n,i}^T\left(\mathbf{C}_+ + \mathbf{C}_\mathrm{N}\right)^{-1}\mathbf{r}_{n,i}\right) \quad (5.56)$$

with $\mathbf{C}_+ \doteq \mathbf{\Pi C_g \Pi}^T$ the covariance matrix for the signal received under $\mathcal{H}_+$ and $\mathbf{C}_\mathrm{N} \doteq \sigma_w^2\mathbf{I} + \mathbf{C}_\mathrm{I}$ the covariance matrix for the Gaussian contribution of both the thermal noise and the narrowband interference.

Similarly to (5.56), the conditioned probability density function under the hypothesis $\mathcal{H}_-$ is found by substituting $\mathbf{C}_+$ in (5.56) with $\mathbf{C}_- \doteq \mathbf{J}_{N_\Delta}\mathbf{\Pi C_g \Pi}^T\mathbf{J}_{N_\Delta}$. When both $f(\mathbf{r}_n|\mathcal{H}_+;\mathbf{C_g})$ and $f(\mathbf{r}_n|\mathcal{H}_-;\mathbf{C_g})$ are available, the GLRT results in

$$\Lambda(\mathbf{r}_n|\mathbf{C_g}) = \frac{\det^{1/2}\left(\mathbf{C}_- + \mathbf{C}_\mathrm{N}\right)}{\det^{1/2}\left(\mathbf{C}_+ + \mathbf{C}_\mathrm{N}\right)} \prod_{i=0}^{N_f-1} \frac{\exp\left(-\frac{1}{2}\mathbf{r}_{n,i}^T\left(\mathbf{C}_+ + \mathbf{C}_\mathrm{N}\right)^{-1}\mathbf{r}_{n,i}\right)}{\exp\left(-\frac{1}{2}\mathbf{r}_{n,i}^T\left(\mathbf{C}_- + \mathbf{C}_\mathrm{N}\right)^{-1}\mathbf{r}_{n,i}\right)}. \quad (5.57)$$

The GLRT in (5.57) can be significantly simplified when both the noise and the interference are high-power sources compared with the UWB transmitter. The following assumptions can be done:

***(AS1) Assumption** 1:*

$$\frac{\det\left(\mathbf{C}_- + \mathbf{C}_\mathrm{N}\right)}{\det\left(\mathbf{C}_+ + \mathbf{C}_\mathrm{N}\right)} \approx 1. \quad (5.58)$$

Proof. Let us first expand the determinant $\det\left(\mathbf{C}_+ + \mathbf{C}_\mathrm{N}\right)$ as follows,

$$\det\left(\mathbf{C}_+ + \mathbf{C}_\mathrm{N}\right) = \det\left(\mathbf{C}_+ + \sigma_w^2\mathbf{I} + \mathbf{C}_\mathrm{I}\right) = \det\left(\sigma_w^2\left[\sigma_w^{-2}\mathbf{C}_+ + \mathbf{I} + \sigma_w^{-2}\mathbf{C}_\mathrm{I}\right]\right) \quad (5.59)$$

$$= \sigma_w^{2N_{sf}}\det\left(\sigma_w^{-2}\mathbf{C}_+ + \mathbf{I} + \sigma_w^{-2}\mathbf{C}_\mathrm{I}\right). \quad (5.60)$$

Since the noise is considered a high-power source compared to the UWB signal, it is reasonable to assume that $\sigma_w^{-2}\mathbf{C}_+ \approx \mathbf{0}$. Note that the same approximation cannot be applied to the term $\sigma_w^{-2}\mathbf{C}_\mathrm{I}$ since both the noise and the interference may have powers on the same order. Consequently,

$$\det\left(\mathbf{C}_+ + \mathbf{C}_\mathrm{N}\right) \approx \sigma_w^{2N_{sf}}\det\left(\mathbf{I} + \sigma_w^{-2}\mathbf{C}_\mathrm{I}\right). \quad (5.61)$$

The key point is to notice that the approximation in (5.61) does not depend on the signal covariance matrix $\mathbf{C}_+$. The same conclusion applies when expanding the determinant

$\det(\mathbf{C}_- + \mathbf{C}_\mathrm{N})$, which is also found to be independent of $\mathbf{C}_-$. As a result, it can be stated that $\det(\mathbf{C}_+ + \mathbf{C}_\mathrm{N}) \approx \det(\mathbf{C}_- + \mathbf{C}_\mathrm{N})$ which confirms the assumption in (5.58). ■

***(AS2) Assumption** 2:*

$$(\mathbf{C}_+ + \mathbf{C}_\mathrm{N})^{-1} \approx \mathbf{C}_\mathrm{N}^{-1} - \mathbf{C}_\mathrm{N}^{-1}\mathbf{C}_+\mathbf{C}_\mathrm{N}^{-1}, \tag{5.62}$$

$$(\mathbf{C}_- + \mathbf{C}_\mathrm{N})^{-1} \approx \mathbf{C}_\mathrm{N}^{-1} - \mathbf{C}_\mathrm{N}^{-1}\mathbf{C}_-\mathbf{C}_\mathrm{N}^{-1}. \tag{5.63}$$

Proof. Let us consider the proof for the assumption in (5.62). The same proof applies also to (5.63) by substituting $\mathbf{C}_+$ with $\mathbf{C}_-$. To proceed, the matrix inversion lemma is considered which states that $(\mathbf{A}+\mathbf{BCD})^{-1} = \mathbf{A}^{-1} - \mathbf{A}^{-1}\mathbf{B}\left(\mathbf{DA}^{-1}\mathbf{B} + \mathbf{C}^{-1}\right)^{-1}\mathbf{DA}^{-1}$, where $\mathbf{A}$ is $(n \times n)$, $\mathbf{B}$ is $(n \times m)$, $\mathbf{C}$ is $(m \times m)$, $\mathbf{D}$ is $(m \times n)$, and the required inverses exist. When applied to (5.62), the inversion lemma results in

$$(\mathbf{C}_+ + \mathbf{C}_\mathrm{N})^{-1} = \mathbf{C}_\mathrm{N}^{-1} - \mathbf{C}_\mathrm{N}^{-1}\mathbf{C}_+\left(\mathbf{C}_\mathrm{N}^{-1}\mathbf{C}_+ + \mathbf{I}\right)^{-1}\mathbf{C}_\mathrm{N}^{-1}. \tag{5.64}$$

Compared to the UWB transmitter, the aggregation of the noise and the interference contributions can be considered a single high-power source. Then it is reasonable to assume that $\mathbf{C}_\mathrm{N}^{-1}\mathbf{C}_+ + \mathbf{I} \approx \mathbf{I}$ in (5.64). Therefore, the result in (5.64) can be simplified to $(\mathbf{C}_+ + \mathbf{C}_\mathrm{N})^{-1} \approx \mathbf{C}_\mathrm{N}^{-1} - \mathbf{C}_\mathrm{N}^{-1}\mathbf{C}_+\mathbf{C}_\mathrm{N}^{-1}$ which concludes the proof. ■

With the above assumptions, the GLRT in (5.57) simplifies to

$$\Lambda(\mathbf{r}_n|\mathbf{C_g}) \approx \prod_{i=0}^{N_f-1} \frac{\exp\left(-\frac{1}{2}\mathbf{r}_{n,i}^T\left(\mathbf{C}_\mathrm{N}^{-1} - \mathbf{C}_\mathrm{N}^{-1}\mathbf{C}_+\mathbf{C}_\mathrm{N}^{-1}\right)\mathbf{r}_{n,i}\right)}{\exp\left(-\frac{1}{2}\mathbf{r}_{n,i}^T\left(\mathbf{C}_\mathrm{N}^{-1} - \mathbf{C}_\mathrm{N}^{-1}\mathbf{C}_-\mathbf{C}_\mathrm{N}^{-1}\right)\mathbf{r}_{n,i}\right)} \tag{5.65}$$

$$= \prod_{i=0}^{N_f-1} \frac{\exp\left(-\frac{1}{2}\mathbf{r}_{n,i}^T\mathbf{C}_\mathrm{N}^{-1}\mathbf{C}_+\mathbf{C}_\mathrm{N}^{-1}\mathbf{r}_{n,i}\right)}{\exp\left(-\frac{1}{2}\mathbf{r}_{n,i}^T\mathbf{C}_\mathrm{N}^{-1}\mathbf{C}_-\mathbf{C}_\mathrm{N}^{-1}\mathbf{r}_{n,i}\right)}. \tag{5.66}$$

Alternatively, the log-GLRT can be adopted with $L(\mathbf{r}_n|\mathbf{C_g}) \doteq \log\Lambda(\mathbf{r}_n|\mathbf{C_g})$. In this way, and except for some irrelevant constant terms, a more compact expression is obtained as follows,

$$L'(\mathbf{r}_n|\mathbf{C_g}) = Tr\left(\left[\mathbf{C}_+ - \mathbf{C}_-\right]\mathbf{C}_\mathrm{N}^{-1}\widehat{\mathbf{R}}_n\mathbf{C}_\mathrm{N}^{-1}\right). \tag{5.67}$$

In (5.67), the $(N_{sf} \times N_{sf})$ matrix $\widehat{\mathbf{R}}_n$ stands for the estimate of the synchronous autocorrelation matrix for the n-th received symbol, that is,

$$\widehat{\mathbf{R}}_n \doteq \frac{1}{N_f}\sum_{i=0}^{N_f-1}\mathbf{r}_{n,i}\mathbf{r}_{n,i}^T. \tag{5.68}$$

Finally, two important remarks must be made. First, note that the synchronous autocorrelation matrix $\widehat{\mathbf{R}}_n$ is the sufficient statistics for the symbol decision problem. Second, since the dimensions of $\widehat{\mathbf{R}}_n$ are $(N_{sf} \times N_{sf})$, the symbol decision problem can indeed be addressed on a frame-level basis.

Appendix 5.B Impact of narrowband interferences

This appendix presents some results on how the interference signals affect the symbol decision statistics. In particular, this involves the evaluation of $\mathbf{C}_{\mathrm{N}}^{-1}$ in (5.67), with $\mathbf{C}_{\mathrm{N}}$ the covariance matrix including both the thermal noise and the interference statistics. Let us assume that the frame duration of the UWB signal is small compared with the coherence time of the interference, defined as $T_{\mathrm{ci}} \doteq \frac{1}{\mathrm{BW_I}}$. Then the entries of the interference covariance matrix $\mathbf{C}_{\mathrm{I}}$ in (5.4) can be reasonably approximated by $[\mathbf{C}_{\mathrm{I}}]_{i,j} \approx \mathrm{P_I} cos\left(2\pi f_{\mathrm{I}}\left(i-j\right)\right)$. As a result, the whole covariance matrix $\mathbf{C}_{\mathrm{I}}$ can be approximated by

$$\mathbf{C}_{\mathrm{I}} \approx \mathrm{P_I Re}\left[\mathbf{e}_{f_{\mathrm{I}}}\mathbf{e}_{f_{\mathrm{I}}}^{H}\right] = \frac{\mathrm{P_I}}{2}\left[\mathbf{e}_{f_{\mathrm{I}}}\mathbf{e}_{f_{\mathrm{I}}}^{H} + \mathbf{e}_{f_{\mathrm{I}}}^{*}\mathbf{e}_{f_{\mathrm{I}}}^{T}\right] \tag{5.69}$$

with the phasor $\mathbf{e}_{f_{\mathrm{I}}} \doteq \left[1, e^{j2\pi f_{\mathrm{I}}}, \ldots, e^{j2\pi f_{\mathrm{I}}\left(N_{sf}-1\right)}\right]^{T}$. For an asymptotically large observation interval, the covariance matrix $\mathbf{C}_{\mathrm{I}}$ can be expressed in terms of the discrete-time Fourier transform matrix $\mathbf{F}$ as $\mathbf{C}_{\mathrm{I}} \approx \frac{\mathrm{P_I}}{2}\mathbf{F}\mathbf{\Lambda}_{f_{\mathrm{I}}}\mathbf{F}^{H}$. In this notation, the diagonal matrix $\mathbf{\Lambda}_{f_{\mathrm{I}}}$ has all its entries equal to zero except for the entries corresponding to discrete frequencies f_{I} and $(1-f_{\mathrm{I}})$ that are equal to 1. Basically, $\mathbf{\Lambda}_{f_{\mathrm{I}}}$ is a sparse matrix. With these considerations, the expression for $\mathbf{C}_{\mathrm{I}}$ in (5.69) allows us to express the noise plus interference covariance matrix $\mathbf{C}_{\mathrm{N}}$ as,

$$\mathbf{C}_{\mathrm{N}} = \sigma_w^2\mathbf{I} + \mathbf{C}_{\mathrm{I}} \approx \sigma_w^2\mathbf{I} + \frac{\mathrm{P_I}}{2}\mathbf{F}\mathbf{\Lambda}_{f_{\mathrm{I}}}\mathbf{F}^{H} = \mathbf{F}\left[\sigma_w^2\mathbf{I} + \frac{\mathrm{P_I}}{2}\mathbf{\Lambda}_{f_{\mathrm{I}}}\right]\mathbf{F}^{H}. \tag{5.70}$$

Since the covariance matrix $\mathbf{C}_{\mathrm{N}}$ is found to be diagonalized with the discrete Fourier transform matrix, the inverse of $\mathbf{C}_{\mathrm{N}}$ can be easily obtained as

$$\mathbf{C}_{\mathrm{N}}^{-1} = \mathbf{F}\left[\sigma_w^2\mathbf{I} + \frac{\mathrm{P_I}}{2}\mathbf{\Lambda}_{f_{\mathrm{I}}}\right]^{-1}\mathbf{F}^{H} \approx \sigma_w^{-2}\mathbf{I}. \tag{5.71}$$

The approximation in (5.71) is due to the fact that the number of non-zero entries in the diagonal of matrix $\mathbf{\Lambda}_{f_{\mathrm{I}}}$ is negligible compared to the number of elements in the diagonal of $\sigma_w^2\mathbf{I}$. Moreover, it is reasonable to consider that $\sigma_w^2 \gg \mathrm{P_I}$ because of the large bandwidth occupancy of UWB signals. Therefore, we can assume that $\left[\sigma_w^2\mathbf{I} + \frac{\mathrm{P_I}}{2}\mathbf{\Lambda}_{f_{\mathrm{I}}}\right]^{-1} \approx \sigma_w^{-2}\mathbf{I}$. Under this assumption, the log-GLRT in (5.67) simplifies to

$$L'(\mathbf{r}_n|\mathbf{C_g}) = Tr\left(\left[\mathbf{C}_{+} - \mathbf{C}_{-}\right]\widehat{\mathbf{R}}_n\right) \tag{5.72}$$

where all the irrelevant constant terms have been omitted for the sake of clarity.

Chapter 6

Non-Coherent Frame-Timing Acquisition

6.1 Introduction

The attractive features of UWB technology are based on its particular transmission format based on the emission of extremely-short and low-power pulses. However, although UWB technology has been around since the 1960s, it has been mainly used in the past for low data rate and non-communications applications because of the great difficulty in efficiently handling such a stream of sub-nanosecond pulses. It has not been until the recent years that the implementation of high data rate and reliable UWB communication systems has become feasible.

Nowadays, one of the most challenging issues is still concerned with the synchronization of UWB signals [Yan04b]. In particular, timing recovery becomes a critical issue because of the extremely-short time duration of the transmitted pulses. For both coherent and non-coherent receivers, timing recovery is required at the frame level to determine the starting point of each information-bearing symbol. For coherent receivers, timing recovery is also required at the pulse level to find where the pulse is located within the frame period. In that way, the optimal sampling time instant can be selected when correlating the received signal with the local replica of the received pulses [Win97], [Mir01]. In any case, proper alignment of the received signal is found to be essential for reliable communication.

In this chapter the problem of timing acquisition for UWB signals focuses on three major aspects:

- **Non-coherent receiver.** The non-coherent approach is inherited from Chapter 5 and it is motivated by the complex propagation physics of UWB signals that make fast and accurate channel estimation a challenging and computationally demanding task [Cra02], [Qiu02],

[Qiu05]. In these circumstances it is reasonable to assume that neither the transmitted pulse nor the channel response are known at the receiver. For this reason, the received waveform is considered here to be an unknown parameter in the mathematical formulation. Thus, the proposed techniques in this chapter can be thought of as *waveform-independent* techniques. By *waveform-independent* we mean that no effort is placed on estimating the channel response.

- **Nondata-aided synchronization.** The timing recovery is addressed under a nondata-aided perspective. In that way, the transmitted symbols are assumed to be unknown. Since no pilot symbols are required, nondata-aided techniques can operate with any piece of modulated data without any prior prealignment. In addition, by adopting a nondata-aided strategy, the effective transmitted throughput is maximized and the mean transmitted power is minimized.

- **Frame-level timing.** Similarly to traditional spread-spectrum communication systems, the timing recovery for UWB signals can be decomposed into two stages. Firstly, frame-level timing acquisition (i.e. coarse acquisition). Secondly, pulse-level timing acquisition (i.e. fine acquisition). This chapter focuses on the first stage of the timing recovery, that is, frame-timing acquisition. The second stage is not considered since the notion of fine timing error is always related to some reference pulse. Since a non-coherent receiver is adopted and thus, the received waveform is assumed to be unknown, the fine timing error is undefined and it is considered to be part of the shape of the unknown waveform.

Many contributions in the recent literature do address the problem of timing recovery for UWB signals. However, some kind of a priori knowledge is usually assumed at the receiver such as training symbols (e.g. [Yan03a], [Tia05d], [Tia05e], [Car06b]), or perfect channel state information. As for the latter, the frame-timing acquisition problem is often addressed in a rather heuristic or *ad-hoc* manner by adopting some kind of correlator-based receiver. That is, coherent receivers are adopted and a replica of the received waveform is assumed to be available at the receiver for matched filtering [Win98], [Zha03],[Blá03]. Usually, the output statistics are processed either by exploiting the cyclostationary properties of the transmitted signal [Tia02], by adopting search algorithms [Gez02], [Hom02] or by using parallel architectures [Lov02]. Interestingly, significant efforts are also being placed on addressing the acquisition problem under a more rigorous approach. To this end, the maximum likelihood formulation has already been proposed, for instance, in some valuable contributions such as the ones in [Lot00] and [Car04a].

Regarding the non-coherent approach to the problem, it is important to mention that recent contributions in the field of UWB timing acquisition are aware of the necessity to make the acquisition process a waveform-independent procedure. This is especially important in low

cost sensor networks, where energy collection is usually adopted as a simple and effective way to implement low-cost non-coherent receivers [Che05]. Another possible alternative to avoid channel estimation is to use a piece of the received signal as the correlating pattern. This is the idea behind the concept of *dirty template* which is presented in [Yan04a], [Yan05] and related to transmitted reference approaches in [Rus64], [Hoc02], [Cha03]. However, the main drawback of this approach is that a relatively high signal-to-noise ratio (SNR) is required for obtaining a valid timing estimate when dealing with modulated data. Other approaches can also be found in the literature such as transmitting nonzero mean amplitude modulating symbols [Luo05]. In this way, the received signal can be averaged on a symbol-by-symbol basis so as to obtain the received waveform at the expense of a degradation in spectral efficiency.

The work to be presented herein differs from previous contributions related to the timing acquisition of UWB signals. The reason is that the problem is addressed in a systematic and analytic manner under the well-known unconditional maximum likelihood criterion [Ott93], [Váz00]. By adopting a general nondata-aided approach, it is shown that optimal frame-level timing estimation is possible when neither the transmitted symbols nor the received waveform are known at the receiver. Indeed, the resulting estimator is reminiscent of the energy detection approach adopted in many radar signal detection techniques [Rab04a]. Finally, it is worth noting that the proposed method is not restricted to the modulation format of UWB signals and it can be applied to other spread spectrum communication systems.

The chapter is structured as follows. The optimal frame-timing acquisition approach is presented in Section 6.2 within the framework of unconditional maximum likelihood estimation. Because of the particular working conditions of UWB communication systems, particular emphasis is placed on the acquisition problem for the low-SNR regime. The derivation of the optimal frame-timing acquisition method is introduced in Section 6.2.4, the proposed implementation is presented in Section 6.2.6 and Section 6.2.7, and some simulation results are analyzed in Section 6.2.8. Moreover, a low complexity implementation of the proposed frame-timing acquisition approach is presented in Section 6.3 as a solution to a model-order detection problem. The proposed low-cost implementation is discussed in Section 6.3.4 and simulation results are also enclosed in Section 6.3.5. Finally, conclusions are drawn in Section 6.4.

6.2 Optimal Frame-Timing Acquisition in the low-SNR Regime

6.2.1 Signal Model in Scalar Notation

The signal model to be considered in this chapter assumes the transmission of ultra-short pulses with pulse-position modulation (PPM), pulse-amplitude modulation (PAM), or possibly both,

the so-called amplitude-pulse-position modulation (APPM)[1]. The discrete-time representation of the received signal is given by

$$r(k) = \sum_{n=-\infty}^{+\infty} s_n g_T \left(k - d_n N_\Delta - n N_{ss} - \tau\right) + w(k) \tag{6.1}$$

with d_n the pulse-position modulating symbols, N_Δ the PPM time-shift in samples, N_{ss} the number of samples per symbol (i.e. the symbol period), τ the symbol timing error and $w(k)$ the Gaussian contribution from the thermal noise and possible multiple user interference. The amplitude values represented by s_n have two different goals depending on whether amplitude modulation is implemented or not. On the one hand, s_n represents the amplitude modulating information-bearing symbols when PAM or APPM modulation is considered. On the other hand, $s_n = \{-1, +1\}$ represents a simple symbol-by-symbol polarity randomization code for avoiding the existence of spectral lines caused by PPM modulation [Nak03]. Thus, the sign of s_n is ignored by non-coherent PPM receivers since it does not bear any information.

The major difference between the signal model in (6.1) and the one adopted in Chapter 5 is the adoption of the *template waveform* $g_T(k)$ as the basis for the frame-timing acquisition problem. The template waveform collects the set of N_f repeated pulses that represent the transmission of a single information-bearing symbol, and it is given by

$$g_T(k) \doteq \sum_{i=0}^{N_f-1} g(k - i N_{sf} - u_i N_{sc}) \tag{6.2}$$

with N_{sf} the number of samples per frame (i.e. the frame duration) and $u_i = \{0, 1, \ldots, N_c - 1\}$ the time-hopping (TH) code with time resolution N_{sc} samples[2]. The length of the template waveform is $N_{ss} = N_f N_{sf}$ and the frame duration is assumed to be large enough so as to avoid interframe interference due to the channel delay spread, pulse-position modulation and time-hopping. Similarly to [Yan04a], the TH code is assumed to be periodic within the symbol duration. In contrast with Chapter 5, the received waveforms $g(k)$ in (6.2) are assumed to be unknown but not time-varying for the sake of simplicity. However, time-varying random waveforms can indeed be supported by the proposed timing acquisition technique as long as the coherence time is larger than the symbol period.

Finally, the symbol timing error τ is constrained within $\tau \in [0, N_{ss})$, and it can be decomposed as

$$\tau = N_\epsilon N_{sf} + \epsilon \tag{6.3}$$

[1]The combination of both PPM and PAM is an approach that has also been adopted in [Li00], [Zha05a], or in [Tan05a] for application to transmitted-reference systems.

[2]The problem of TH code acquisition is not considered here since it is a whole problem itself and shares many similarities with the problem of code acquisition for traditional spread-spectrum communication systems. However, some references about this topic can be found in [Hom02], [Gez02] and [Reg05], among many others.

with the integer $N_\epsilon = \{0, \ldots, N_f - 1\}$ being the frame-level timing error and $\epsilon \in [0, N_{sf})$ the pulse-level timing error. In the sequel, the goal is the estimation of the frame-level timing error N_ϵ which is an unknown deterministic parameter. The pulse-level timing error ϵ is left as a nuisance parameter that is part of the shape of the unknown received waveform $g(k)$.

6.2.2 Signal Model in Matrix Notation

The matrix notation to be presented herein is based on the fact that PPM modulation can be expressed as the sum of parallel independent linear modulations [Mar00]. To this end, let us take an observation interval comprising a total of $L \doteq 2K + 1$ symbols (i.e. L template waveforms) with K some positive integer number. Then, assuming $d_n = \{0, 1, \ldots, P - 1\}$, the signal model in (6.1) can be equivalently expressed in matrix notation as

$$\mathbf{r} = \sum_{p=0}^{P-1} \mathbf{A}_p(\tau, \mathbf{t})\mathbf{x}_p + \mathbf{w} \tag{6.4}$$

where $\mathbf{r}$ is an $(N \times 1)$ vector of real-valued received samples with $N \doteq N_{ss}L$. The transmitted symbols through the p-th PPM position are contained in the $(L \times 1)$ vector $\mathbf{x}_p$. Because just one PPM position can be active within the transmission of a symbol, the entries equal to zero in $\mathbf{x}_p$ indicate which of the p-th PPM positions are not active. Due to either amplitude modulation or polarity randomization, the symbols in $\mathbf{x}_p$ are assumed to be zero mean, $E_{\mathbf{x}}[\mathbf{x}_p] = \mathbf{0}$ for any p, and to have a covariance matrix given by[3] $E_{\mathbf{x}}\left[\mathbf{x}_p\mathbf{x}_q^T\right] = \frac{1}{P}\mathbf{I}_L\delta_{pq}$. Finally, the noise samples are incorporated in the $(N \times 1)$ vector $\mathbf{w}$ with covariance matrix $E\left[\mathbf{w}\mathbf{w}^T\right] = \sigma_w^2\mathbf{I}_N$.

The shaping matrix $\mathbf{A}_p(\tau, \mathbf{t})$, with $\mathbf{t}$ the vectorized stacking of the template waveform $g_T(k)$, is defined as follows:

$$\mathbf{A}_p(\tau, \mathbf{t}) \doteq [\mathbf{a}_{-K,p}(\tau, \mathbf{t}), \mathbf{a}_{-K+1,p}(\tau, \mathbf{t}), \ldots, \mathbf{a}_{K,p}(\tau, \mathbf{t})], \tag{6.5}$$

$$\mathbf{a}_{n,p}(\tau, \mathbf{t}) \doteq \mathbf{J}^{N_\epsilon}\mathbf{K}_n\mathbf{t}_p(\epsilon), \tag{6.6}$$

$$\mathbf{t}_p(\epsilon) \doteq [g_T(-pN_\Delta - \epsilon), g_T(1 - pN_\Delta - \epsilon), \ldots, g_T(N_{ss} - 1 - pN_\Delta - \epsilon)]^T. \tag{6.7}$$

Note that the vector $\mathbf{t}_p$ contains the samples of the template waveform for the p-th position of the PPM modulation. The subscript $_n$ in (6.6) refers to the n-th column of the shaping matrix $\mathbf{A}_p(\tau, \mathbf{t})$, and finally, the matrix $\mathbf{K}_n$ is an $(N \times N_{ss})$ zero-padding and N_{ss}-samples shifting matrix,

$$\mathbf{K}_n \doteq \mathbf{J}^{nN_f}\mathbf{\Pi}, \tag{6.8}$$

$$[\mathbf{J}]_{i,j} = \begin{cases} 1 & : \quad (j - i) = N_{sf} \\ 0 & : \quad (j - i) \neq N_{sf} \end{cases}, \tag{6.9}$$

$$\mathbf{\Pi} \doteq \left[\begin{array}{ccc} \mathbf{0}^T_{(N-N_{ss})/2\times N_{ss}} & \mathbf{I}_{N_{ss}} & \mathbf{0}^T_{(N-N_{ss})/2\times N_{ss}} \end{array}\right]^T. \tag{6.10}$$

[3] The notation δ_{ij} stands for the Kronecker delta.

In the above definitions, $\mathbf{I}_n$ stands for the $(n \times n)$ identity matrix and $\mathbf{0}_{n\times m}$ is an $(n \times m)$ all-zeros matrix.

6.2.3 Receiver architecture

The system architecture to be considered in this chapter is represented by the fully digital block diagram in Figure 6.1. The key point of this chapter is to focus on non-coherent frame-timing synchronization, a procedure that can be adopted by either coherent or non-coherent receivers. Under some circumstances, and especially for the case of coherent receivers, non-coherent synchronization is useful to be performed prior to channel estimation. The reason is that frame-level synchronization may significantly simplify the channel estimation procedure. For instance, waveform estimation can easily be performed by simply averaging the N_f repeated frames within a symbol duration provided that the number of repeated frames is sufficiently large. To this end, frame-level synchronization is required for coherent integration in order to avoid data modulation in the waveforms corresponding to adjacent symbols.

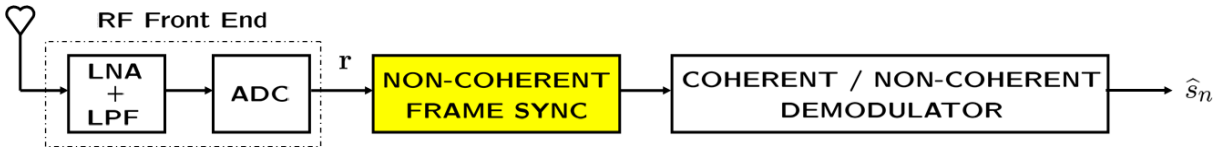

Figure 6.1: Block diagram of the receiver architecture to be considered in this chapter.

Nevertheless, we will forget for a moment about waveform estimation and symbol detection and we will concentrate purely on frame-level synchronization.

6.2.4 Unconditional Maximum Likelihood Cost Function for Frame-Timing Acquisition in the low-SNR Regime

The proposed frame-timing acquisition approach concentrates on the *Stochastic* or Unconditional Maximum Likelihood approach (UML) which considers that the nuisance parameters are all random. Therefore, not only the transmitted symbols but also the received waveform are assumed to be random. According to [Váz00], the analysis is started by formulating the likelihood function for the linear signal model under consideration. By doing so, the likelihood function is found to be based on the Gaussian noise probability density function as follows:

$$\Lambda\left(\mathbf{r}|\tau;\mathbf{t};\mathbf{x}\right) = C_0 \exp\left(-\frac{1}{\sigma_w^2}\left\|\mathbf{r} - \sum_{p=0}^{P-1}\mathbf{A}_p\left(\tau,\mathbf{t}\right)\mathbf{x}_p\right\|^2\right) \tag{6.11}$$

with C_0 an irrelevant positive constant. By expanding the quadratic norm in (6.11) and taking into consideration just those terms which depend on the parameters of interest, we have

$$\Lambda\left(\mathbf{r}|\tau;\mathbf{t};\mathbf{x}\right) = C_1 \exp\left(\frac{2}{\sigma_w^2}\chi\left(\mathbf{r};\tau;\mathbf{t};\mathbf{x}\right)\right), \tag{6.12}$$

$$\chi\left(\mathbf{r};\tau;\mathbf{t};\mathbf{x}\right) \doteq \sum_{p=0}^{P-1}\mathbf{x}_p^T\mathbf{A}_p^T\mathbf{r} - \frac{1}{2}\sum_{p=0}^{P-1}\sum_{q=0}^{P-1}\mathbf{x}_p^T\mathbf{A}_p^T\mathbf{A}_q\mathbf{x}_q, \tag{6.13}$$

with $C_1 = C_0 \exp\left(-\mathbf{r}^T\mathbf{r}/\sigma_w^2\right)$ and where the dependence of $\mathbf{A}_p$ on $(\tau;\mathbf{t})$ is omitted for the sake of simplicity. Assuming the SNR to be sufficiently low, the likelihood function presented so far can be importantly simplified. This is the reason why the low-SNR assumption is traditionally adopted in the derivation of many blind synchronizers within the ML estimation framework [Men97]. For the case of UWB signals, the application of the low-SNR assumption is completely justified by the extremely low power radiating conditions of the UWB transmission. A low-SNR analysis not only provides an easier manipulation of the likelihood function but also a realistic approach to the real working conditions. Under the low-SNR assumption, the likelihood function in (6.12)-(6.13) can be approximated by its second order Taylor series expansion as follows,

$$\Lambda\left(\mathbf{r}|\tau;\mathbf{t};\mathbf{x}\right) \approx C_1\left[1 + \frac{2}{\sigma_w^2}\chi\left(\mathbf{r};\tau;\mathbf{t};\mathbf{x}\right) + \frac{2}{\sigma_w^4}\chi^2\left(\mathbf{r};\tau;\mathbf{t};\mathbf{x}\right)\right]. \tag{6.14}$$

In order to obtain a likelihood function which does not depend on neither the transmitted symbols nor the received waveform, the next step is to eliminate the dependence on the set of nuisance parameters $\{\mathbf{t};\mathbf{x}\}$ from (6.14).

6.2.4.1 Marginal likelihood function with respect of the transmitted symbols

The dependence on the transmitted symbols can be avoided by adopting the marginal likelihood function

$$\Lambda\left(\mathbf{r}|\tau;\mathbf{t}\right) = \mathrm{E}_{\mathbf{x}}\left[\Lambda\left(\mathbf{r}|\tau;\mathbf{t};\mathbf{x}\right)\right]. \tag{6.15}$$

Therefore, and according to the results in Appendix 6.A and Appendix 6.B, it is found that

$$\mathrm{E}_{\mathbf{x}}\left[\chi\left(\mathbf{r};\tau;\mathbf{t};\mathbf{x}\right)\right] = \gamma_a\left(\mathbf{t}\right), \tag{6.16}$$

$$\mathrm{E}_{\mathbf{x}}\left[\chi^2\left(\mathbf{r};\tau;\mathbf{t};\mathbf{x}\right)\right] = \sum_{p=0}^{P-1}\mathbf{r}^T\mathbf{A}_p\mathbf{A}_p^T\mathbf{r} + \gamma_b\left(\mathbf{t}\right), \tag{6.17}$$

with $\{\gamma_a\left(\mathbf{t}\right), \gamma_b\left(\mathbf{t}\right)\}$ two constant terms with respect to the symbol timing error τ but with dependence on the template waveform $\mathbf{t}$. With these considerations, the likelihood function in (6.15) can be expressed as

$$\Lambda\left(\mathbf{r}|\tau;\mathbf{t}\right) \approx C_1\left[1 + \frac{2\gamma_a\left(\mathbf{t}\right)}{\sigma_w^2} + \frac{2\gamma_b\left(\mathbf{t}\right)}{\sigma_w^4} + \frac{2}{\sigma_w^4}\sum_{p=0}^{P-1}\mathbf{r}^T\mathbf{A}_p\mathbf{A}_p^T\mathbf{r}\right]. \tag{6.18}$$

Next, the expression of the shaping matrix $\mathbf{A}_p$ in (6.5)-(6.7) can be substituted into (6.18) resulting in

$$\begin{aligned}\Lambda\left(\mathbf{r}|\tau;\mathbf{t}\right) &\approx C_1\left[1+\frac{2\gamma_a\left(\mathbf{t}\right)}{\sigma_w^2}+\frac{2\gamma_b\left(\mathbf{t}\right)}{\sigma_w^4}+\frac{2}{\sigma_w^4}\sum_{p=0}^{P-1}\sum_{n=-K}^{K}Tr\left(\mathbf{t}_p\left(\epsilon\right)\mathbf{t}_p^T\left(\epsilon\right)\mathbf{K}_n^T\mathbf{J}^{-N_\epsilon}\mathbf{r}\mathbf{r}^T\mathbf{J}^{N_\epsilon}\mathbf{K}_n\right)\right] \\ &= C_1\left[1+\frac{2\gamma_a\left(\mathbf{t}\right)}{\sigma_w^2}+\frac{2\gamma_b\left(\mathbf{t}\right)}{\sigma_w^4}+\frac{2LP}{\sigma_w^4}Tr\left(\mathbf{T}(\epsilon)\mathbf{R}(N_\epsilon)\right)\right], \qquad (6.19)\end{aligned}$$

with

$$\mathbf{T}\left(\epsilon\right) \doteq \frac{1}{P}\sum_{p=0}^{P-1}\mathbf{t}_p\left(\epsilon\right)\mathbf{t}_p\left(\epsilon\right)=\mathrm{E}_{\mathbf{x}}\left[\mathbf{t}\left(\epsilon\right)\mathbf{t}^T\left(\epsilon\right)\right], \qquad (6.20)$$

$$\mathbf{R}\left(N_\epsilon\right) = \sum_{n=-K}^{K}\mathbf{K}_n^T\mathbf{J}^{-N_\epsilon}\mathbf{r}\mathbf{r}^T\mathbf{J}^{N_\epsilon}\mathbf{K}_n. \qquad (6.21)$$

Note that $\mathbf{R}(N_\epsilon)$ is the $(N_{ss}\times N_{ss})$ synchronous autocorrelation matrix of the received signal when a time shift correction of $N_\epsilon N_{sf}$ samples is applied on it. In this sense, the time-shifted synchronous autocorrelation matrix is defined as

$$\mathbf{R}\left(m\right)\doteq\lim_{L\to\infty}\frac{1}{L}\sum_{n=0}^{L-1}\mathbf{r}_n\left(m\right)\mathbf{r}_n^T\left(m\right) \qquad (6.22)$$

with

$$\mathbf{r}_n\left(m\right)\doteq\left[r(nN_{ss}+mN_{sf}),r(nN_{ss}+mN_{sf}+1),\ldots,r(nN_{ss}+mN_{sf}+N_{ss}-1)\right]^T. \qquad (6.23)$$

6.2.4.2 Marginal likelihood function with respect of the template waveform

In the current approach to the timing estimation problem for UWB signals, the received template waveform is assumed to be unknown. For this reason, the template waveform is considered a nuisance parameter in the subsequent formulation. Similarly, the residual pulse-level timing error ϵ can also be considered a nuisance parameter as well. This is similar to what happens in traditional timing estimation for non-coherent receivers at the output of an unknown frequency-selective channel [Git92, p.434]. In that case, the pulse-level timing error is not properly defined because it is always related to some reference pulse. Since the reference pulse is not available in non-coherent receivers, the pulse-level timing error is unknown and it can be incorporated as part of the shape of the unknown received waveform.

Since both the received waveform and the pulse-level timing error are assumed to be nuisance parameters, the marginal likelihood function from (6.15) depends only on the frame-level timing error N_ϵ,

$$\mathrm{E}_{\mathbf{t},\epsilon}\left[\Lambda\left(\mathbf{r}|\tau;\mathbf{t}\right)\right]=\Lambda\left(\mathbf{r}|N_\epsilon\right). \qquad (6.24)$$

In particular, it is found that

$$\Lambda\left(\mathbf{r}|N_\epsilon\right) \approx C_1 \left[1 + C_2 + C_3 + \frac{2LP}{\sigma_w^4} Tr\left(\mathbf{\Xi R}\left(N_\epsilon\right)\right)\right] \tag{6.25}$$

with

$$C_2 \doteq \frac{2}{\sigma_w^2} \mathrm{E}_{\mathbf{t}}\left[\gamma_a\left(\mathbf{t}\right)\right], \tag{6.26}$$

$$C_3 \doteq \frac{2}{\sigma_w^4} \mathrm{E}_{\mathbf{t}}\left[\gamma_b\left(\mathbf{t}\right)\right], \tag{6.27}$$

$$\mathbf{\Xi} \doteq \mathrm{E}_{\mathbf{t},\epsilon}\left[\mathbf{T}\left(\epsilon\right)\right] = \mathbf{1}_{N_f}\mathbf{1}_{N_f}^T \otimes \mathbf{M}. \tag{6.28}$$

In (6.28), the notation $\mathbf{1}_n$ stands for an $(n \times 1)$ all-ones vector and $\mathbf{M}$ is an unknown but non-zero $(N_{sf} \times N_{sf})$ matrix which resumes the statistical characterization of the frame-level waveform. The key point in (6.28) is not the particular structure of $\mathbf{M}$ but the repeated structure of $\mathbf{\Xi}$ because of the frame repetition within a symbol interval.

Finally, and in order to avoid all the irrelevant constant terms in (6.25), the equivalent likelihood function $\Lambda'\left(\mathbf{r}|N_\epsilon\right) = Tr\left(\mathbf{\Xi R}\left(N_\epsilon\right)\right)$ is adopted. Thus, the optimal frame-level timing estimation results in

$$\widehat{N}_\epsilon = \arg\max_{N_\epsilon} \Lambda'\left(\mathbf{r}|N_\epsilon\right) = \arg\max_{m} Tr\left(\mathbf{\Xi R}\left(m\right)\right). \tag{6.29}$$

The interpretation of (6.29) shows that the estimation of the frame-level timing error N_ϵ must be performed by choosing the time-shifted synchronous autocorrelation matrix $\mathbf{R}(m)$ that maximizes the projection onto $\mathbf{\Xi}$. It is true that this procedure may seem rather vague, especially with respect to the "unknown" matrix $\mathbf{M}$ within $\mathbf{\Xi}$. However, the clear conclusion is that the timing search becomes now a problem related to finding a regular structure for $\mathbf{R}(m)$ similar to the one in the right hand side of (6.28). Thus, we can forget about $\mathbf{\Xi}$ and concentrate on the analysis of the structure of $\mathbf{R}(m)$ itself. Further insights on the procedure to obtain the frame-level timing error from $\mathbf{R}(m)$ are presented in Section 6.2.6.

6.2.5 Analysis of the Time-Shifted Synchronous Autocorrelation Matrix

6.2.5.1 Structure of the time-shifted synchronous autocorrelation matrix

The estimation of the frame-level timing error is shown in Section 6.2.4.2 to be based on the exploitation of the structure of the time-shifted synchronous autocorrelation matrix $\mathbf{R}\left(m\right)$ in (6.22). The purpose is to analyze the structure of the transmitted signal within the received synchronous autocorrelation matrix. To this end, and in the presence of some frame-level timing error N_ϵ, the $(N_{ss} \times 1)$ segments of the received data $\mathbf{r}_n(m)$ in (6.23) are decomposed into an upper and a lower part as shown in Figure 6.2.

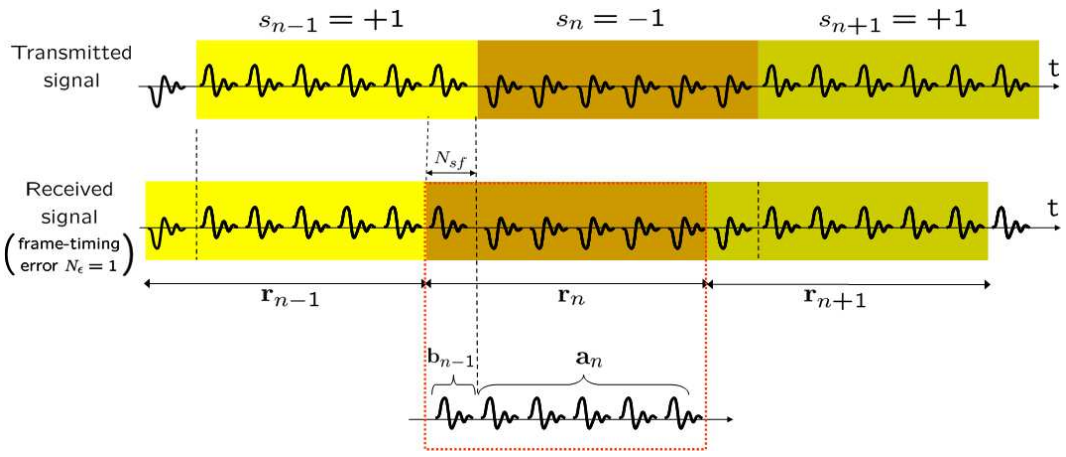

Figure 6.2: Structure of the received signal when some time delay is present. Note that each vector of received samples $\mathbf{r}_n$ is composed by an upper and lower part, $\mathbf{b}(n)$ and $\mathbf{a}(n)$ respectively, which correspond to segments of two consecutive transmitted templates.

More specifically, the lower part of $\mathbf{r}_n$ corresponds to the transmission of the current symbol. This lower part is indicated by an $((N_{ss} - (N_\epsilon - m)N_{sf}) \times 1)$ vector of samples $\mathbf{a}_n$. Similarly, the upper part of $\mathbf{r}_n$ corresponds to the transmission of the previous symbol. This upper part is indicated by an $((N_\epsilon - m)\, N_{sf} \times 1)$ vector of samples $\mathbf{b}_{n-1}$. According to these considerations,

$$\mathbf{r}_n(m) = \begin{bmatrix} s_{n-1}\mathbf{b}_{n-1} \\ s_n\mathbf{a}_n \end{bmatrix} + \mathbf{w}_n\,(m) \tag{6.30}$$

with

$$\mathbf{w}_n\,(m) \doteq [w(nN_{ss} + mN_{sf}), w(nN_{ss} + mN_{sf} + 1), \ldots, w(nN_{ss} + mN_{sf} + N_{ss} - 1)]^T\,. \tag{6.31}$$

Note that the amplitude modulating symbols $\{s_{n-1}, s_n\}$ are explicitly indicated in (6.30) whereas the possible position modulating symbols are implicitly incorporated within $\mathbf{b}_{n-1}$ and $\mathbf{a}_n$. Moreover, note that for $m = N_\epsilon$, the received signal is synchronized and thus $\mathbf{r}_n(N_\epsilon) = s_n\mathbf{a}_n + \mathbf{w}_n$ according to (6.30).

Then, by taking into consideration that $\mathrm{E}\,[s_i s_j] = \delta_{ij}$, the time-shifted synchronous autocorrelation matrix results in

$$\mathbf{R}\,(m)_{|N_\epsilon = i} = \begin{bmatrix} \mathbf{T}_b(i) & \mathbf{0}_{P(m;i)\times Q(m;i)} \\ \mathbf{0}_{Q(m;i)\times P(m;i)} & \mathbf{T}_a(i) \end{bmatrix} + \sigma_w^2 \mathbf{I}_{N_{ss}} \tag{6.32}$$

with $P(m;i) \doteq (i-m)\, N_{sf}$ and $Q(m;i) \doteq (N_{ss} - (i-m)\, N_{sf})$. Matrices $\mathbf{T}_a$ and $\mathbf{T}_b$ come from the definition of $\mathbf{T}$ in (6.20) but in its block-partitioned form,

$$\mathbf{T} = \begin{bmatrix} \mathbf{T}_a(i) & \mathbf{T}_c^T(i) \\ \mathbf{T}_c(i) & \mathbf{T}_b(i) \end{bmatrix} \tag{6.33}$$

for any $i = \{0, 1, \ldots, N_f - 1\}$, with

$$\mathbf{T}_a(i) \doteq \mathrm{E}\left[\mathbf{a}_n \mathbf{a}_n^T \mid N_\epsilon = i\right], \tag{6.34}$$

$$\mathbf{T}_b(i) \doteq \mathrm{E}\left[\mathbf{b}_n \mathbf{b}_n^T \mid N_\epsilon = i\right], \tag{6.35}$$

$$\mathbf{T}_c(i) \doteq \mathrm{E}\left[\mathbf{b}_n \mathbf{a}_n^T \mid N_\epsilon = i\right]. \tag{6.36}$$

At this point, there are two important remarks to be made. First, the fact that the particular structure of the synchronous autocorrelation matrix in (6.32) is due to the statistical independence of the amplitude modulating transmitted symbols. Therefore, the proposed frame-timing estimator requires the adoption of a signaling scheme with amplitude modulating symbols, either PAM or both PAM and PPM at the same time. Second, it is also important to note that the smaller the all-zeros matrices in $\mathbf{R}(m)$, the closer is $\mathbf{R}(m)$ to the regular structure of $\boldsymbol{\Xi}$ in (6.28)-(6.29). This will be the basis for the timing acquisition procedure to be presented in Section 6.2.6.

6.2.5.2 Timing search in the time-shifted synchronous autocorrelation matrix

According to (6.29), every trial value $\widehat{N}_\epsilon = m$ implies the computation of a new $(N_{ss} \times N_{ss})$ matrix $\mathbf{R}(m)$. However, this is clearly inefficient. A simple and straightforward alternative is based on computing the augmented $(2N_{ss} \times 2N_{ss})$ synchronous autocorrelation matrix once, and then extracting from it all the required matrices $\mathbf{R}(m)$.

Let us denote the augmented $(2N_{ss} \times 2N_{ss})$ synchronous autocorrelation by $\mathbf{R}_2(m)$. Then, similarly to Section 6.2.5.1, the structure of the $\mathbf{R}_2(m)$ is found to be given by

$$\mathbf{R}_2(m)_{|N_\epsilon = i} = \begin{bmatrix} \mathbf{T}_b(i) & \mathbf{0}_{P(m;i)\times N_{ss}} & \mathbf{0}_{P(m;i)\times Q(m;i)} \\ \mathbf{0}_{N_{ss}\times P(m;i)} & \mathbf{T} & \mathbf{0}_{N_{ss}\times Q(m;i)} \\ \mathbf{0}_{Q(m;i)\times P(m;i)} & \mathbf{0}_{Q(m;i)\times N_{ss}} & \mathbf{T}_a(i) \end{bmatrix} + \sigma_w^2 \mathbf{I}_{2N_{ss}}. \tag{6.37}$$

The key point in considering the $(2N_{ss} \times 2N_{ss})$ augmented synchronous autocorrelation matrix $\mathbf{R}_2(m)$ is that the $(N_{ss} \times N_{ss})$ synchronous autocorrelation matrix $\mathbf{R}(m)$ can be easily recovered from $\mathbf{R}_2(m)$ as follows,

$$\mathbf{R}(m) = \boldsymbol{\Pi}^T(m) \mathbf{R}_2(0) \boldsymbol{\Pi}(m) \tag{6.38}$$

where the selection matrix $\boldsymbol{\Pi}(m)$ is defined as

$$\boldsymbol{\Pi}(m)^T = \begin{bmatrix} \mathbf{0}_{N_{ss}\times mN_{sf}} & \mathbf{I}_{N_{ss}} & \mathbf{0}_{N_{ss}\times (N_{ss} - mN_{sf})} \end{bmatrix}. \tag{6.39}$$

Therefore, it is just required to compute $\mathbf{R}_2$ once, for instance, $\mathbf{R}_2(0)$, and all the subsequent time-shifted versions of $\mathbf{R}(m)$ can be obtained via (6.38).

6.2.6 Proposed Frame-Timing Acquisition Method

The derivation of the proposed frame-level timing estimator can be summarized as follows.

Lemma 1. *Without loss of generality, the frame-level timing estimate which maximizes the UML likelihood function in (6.29) can be obtained as,*

$$\widehat{N}_\epsilon = \arg\max_m \|\mathbf{\Pi}^T(m)\mathbf{R}_2(0)\mathbf{\Pi}(m)\|_F^2 \tag{6.40}$$

where $m = \{0, 1, \dots N_f - 1\}$ *and the residual timing error is constrained within* $|\widehat{\tau} - \tau| = \epsilon < N_{sf}$.

Proof. The maximization of the likelihood function in (6.29) can be understood as the inner product of matrices as follows,

$$\widehat{N}_\epsilon = \arg\max_m Tr\left(\mathbf{\Xi}\mathbf{R}\left(m\right)\right) = \arg\max_m \left\{\mathbf{\Xi}^T \bullet \mathbf{R}\left(m\right)\right\} \tag{6.41}$$

where $\bullet$ stands for the inner product operator. Similarly to the scalar case, the inner product of matrices is maximum when $\mathbf{\Xi} = \beta\mathbf{R}\left(m\right)$ for any positive constant β [Har00]. Thus, by taking into consideration the property $Tr\left(\mathbf{A}^T\mathbf{A}\right) = \|\mathbf{A}\|_F^2$, (6.41) can be rewritten as,

$$\widehat{N}_\epsilon = \arg\max_m \beta Tr\left(\mathbf{R}^T\left(m\right)\mathbf{R}\left(m\right)\right) = \arg\max_m \|\mathbf{R}\left(m\right)\|_F^2. \tag{6.42}$$

Finally, the substitution of (6.38) into (6.42) results in

$$\widehat{N}_\epsilon = \arg\max_m \|\mathbf{\Pi}^T(m)\mathbf{R}_2(0)\mathbf{\Pi}(m)\|_F^2. \tag{6.43}$$

■

Lemma 2. *The solution to the proposed timing acquisition method in Lemma 1 is unique.*

Proof. Let us define the cost function $J(m)$ as

$$J(m) \doteq \|\mathbf{\Pi}^T(m)\mathbf{R}_2(0)\mathbf{\Pi}(m)\|_F^2. \tag{6.44}$$

For the general case where the frame-timing $N_\epsilon = i$ but $m \neq i$, the argument of the Frobenius norm in (6.44) results in $\mathbf{\Pi}^T(m)\mathbf{R}_2(0)\mathbf{\Pi}(m) = \mathbf{R}(m)$. Thus, according to the definition of the synchronous autocorrelation matrix $\mathbf{R}(m)$ in (6.32) and to the definition of matrix $\mathbf{T}$ in (6.33), the cost function $J(m)$ results in

$$J(m)\Big|_{\substack{N_\epsilon = i \\ (m \neq i)}} = \|\mathbf{T}\|_F^2 - 2\|\mathbf{T}_c(i)\|_F^2 + \sigma_w^2\left(N_{ss}\sigma_w^2 + 2E_{g_T}\right), \tag{6.45}$$

with E_{g_T} the energy of the received template waveform, which is assumed to be constant. Note that, by definition, $\|\mathbf{T}_c(i)\|_F^2 > 0$ for $m \neq i$. Similarly, and for the case where $N_\epsilon = m$, it turns

out that $\mathbf{\Pi}^T(m)\mathbf{R}_2(0)\mathbf{\Pi}(m) = \mathbf{R}(N_\epsilon) = \mathbf{T} + \sigma_w^2\mathbf{I}_{N_{ss}}$. Therefore, the cost function $J(m)$ results in

$$J(m)_{|N_\epsilon=m} = \|\mathbf{T}\|_F^2 + \sigma_w^2\left(N_{ss}\sigma_w^2 + 2E_{g_T}\right) \tag{6.46}$$

From the results in (6.45) and (6.46), it is found that

$$J(m)_{|N_\epsilon=m} > J(m)_{|N_\epsilon\neq m} \tag{6.47}$$

which guarantees the uniqueness of the solution to (6.40). ■

It is important to note that the proposed frame-level timing estimation method in (6.40) is based on a frame-level search over the synchronous autocorrelation matrix of the received signal. This can be shown in Figure 6.3 both when timing error is absent or present.

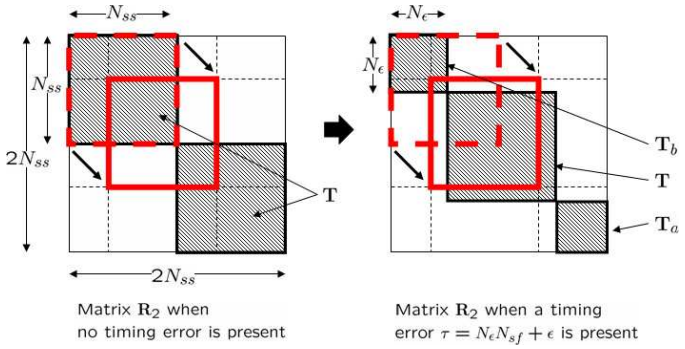

Figure 6.3: Illustration of the sliding matrix $\mathbf{\Pi}^T(m)\mathbf{R}_2\mathbf{\Pi}(m)$ (thick line) when $\mathbf{R}_2$ is computed from received samples with perfectly acquired timing (left) or with some timing error τ (right).

From the above considerations, the synchronous autocorrelation matrix becomes the sufficient statistics for the problem at hand. Contrary to [Yan04a], where a non-coherent integration of the noise is performed, an important advantage of the proposed method is that a coherent integration is addressed in the off-diagonal entries of the synchronous autocorrelation matrix. As a result, the proposed method is expected to be more robust to low signal-to-noise ratio scenarios than the one in [Yan04a].

6.2.7 Algorithm Implementation

An important issue when implementing the proposed method in Section 6.2.6 is to realize that it is not necessary to compute the Frobenius norm for every trial value m in (6.40). The reason is that, from $\widehat{N}_\epsilon = m-1$ to $\widehat{N}_\epsilon = m$, most of the entries in the associated Frobenius norm are the same, so they can be reused as indicated in Figure 6.4.

As a result, the Frobenius norm for $\widehat{N}_\epsilon = m$ can be computed from the Frobenius norm for $\widehat{N}_\epsilon = m-1$, resulting in the procedure shown in Table 6.1. In the algorithm description of

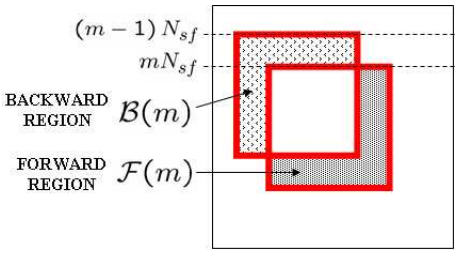

Figure 6.4: When the sliding matrix $\mathbf{\Pi}^T(m-1)\mathbf{R}_2\mathbf{\Pi}(m-1)$ is shifted to $\mathbf{\Pi}^T(m)\mathbf{R}_2\mathbf{\Pi}(m)$, the backward and the forward regions appear which allow an optimized computation of the Frobenius norm for $\mathbf{\Pi}^T(m)\mathbf{R}_2\mathbf{\Pi}(m)$.

Table 6.1, the Matlab® notation $\mathbf{R}_2\,(a:b, c:d)$ has been used to denote the elements of matrix $\mathbf{R}_2$ contained within the a-th to b-th rows and within the c-th to d-th columns, with $a < b$ and $c < d$. That is, the entries contained within the rectangular region which is bounded by the upper left hand corner (a, c) and the lower right hand corner (b, d).

Regarding the computational complexity, most of the required computational burden of the proposed algorithm is due to the computation of the $(2N_{ss} \times 2N_{ss})$ synchronous autocorrelation matrix in Step 1 of Table 6.1. In particular, the overall complexity of the proposed algorithm can be roughly approximated to $8N_f^2LN_{sf}^2$ flops (floating point operations). Note that the complexity of the proposed algorithm is quadratic on the number of samples per frame N_{sf}. This is in contrast with the timing acquisition algorithm in [Yan04a] which is adopted for comparison in the simulation results of Section 6.2.8. The algorithm in [Yan04a] is quite simple and it just requires approximately $N_f^2LN_{sf}$ flops. Thus, it has a linear dependence on the number of samples per frame N_{sf} in contrast with the quadratic dependence of the proposed algorithm.

However, the increase in complexity for the proposed method comes at the expense of a better performance. This can be observed in Section 6.2.8 where the proposed frame-timing acquisition method is found to clearly outperform the one in [Yan04a] for the low signal-to-noise ratio scenarios typically encountered in UWB communication systems.

6.2.8 Simulation Results

In this section, computer simulations are carried out to compare the performance of the proposed frame-timing acquisition method with existing techniques in the literature. To this end, only binary PAM modulation is considered for the sake of simplicity and two distinct simulation scenarios are evaluated:

(A): *Random Gaussian waveforms.* The received waveforms are considered to be zero-mean random Gaussian processes under the uncorrelated scattering (US) assumption. The re-

1) Calculate an estimate for $\mathbf{R}_2$ as, $\widehat{\mathbf{R}}_2 = \frac{1}{L}\sum_{n=0}^{L-1} \mathbf{r}_{2,n}\mathbf{r}_{2,n}^T$,
with $\mathbf{r}_{2,n} \doteq [r(nN_{ss}), r(nN_{ss}+1), \ldots, r(nN_{ss}+2N_{ss}-1)]^T$.

2) f(0)=$\|\mathbf{\Pi}^T(0)\widehat{\mathbf{R}}_2\mathbf{\Pi}(0)\|_F^2$

3) for m=1:(N_f-1),

- p = mN_{sf}.
- q = m$N_{sf} + N_{ss}$.
- t = (m-1)N_{sf}.
- Calculate $\|\mathcal{F}(m)\|_F^2$ with,
$$\mathcal{F}(m) = \mathbf{R}_2\left(q - N_{sf} + 1 : q, p+1 : q\right) \cup \mathbf{R}_2\left(p+1 : q - N_{sf}, q - N_{sf} + 1 : q\right).$$
- Calculate $\|\mathcal{B}(m)\|_F^2$ with,
$$\mathcal{B}(m) = \mathbf{R}_2\left(1+t : p, t+1 : t+N_{ss}\right) \cup \mathbf{R}_2\left(p+1 : t+N_{ss}, 1+t : p\right).$$
- f(m)=f(m-1)+$\|\mathcal{F}(m)\|_F^2 - \|\mathcal{B}(m)\|_F^2$

end

4) Decide $\widehat{N}_\epsilon$=$\max_m f(m)$

Table 6.1: Procedure for the low-SNR UML frame-timing acquisition method.

ceived waveform duration is $T_g = 10$ ns and the frame duration is $T_f = 14$ ns.

(B): *IEEE 802.15.3a waveforms.* The received waveforms are generated according to the IEEE 802.15.3a channel model CM1 proposed by Intel [Foe03]. The power delay profile of the channel is truncated to 74 ns and the frame duration is set to $T_f = 86$ ns to avoid inter-frame interference.

For all the simulation scenarios, the sampling period is set to $T_s = 2$ ns and the symbol duration involves the repetition of $N_f = 16$ frames. The symbol timing error τ is randomly generated and uniformly distributed within $\tau \in [0, N_{ss})$. Finally, waveforms are assumed to change from symbol to symbol.

In order to translate frame-timing acquisition performance into bit error rate (BER), it is important to isolate mistiming from channel uncertainty (i.e. uncertainty caused by the lack of knowledge about the received waveform). For this reason, the simulation results to be presented herein are obtained by placing a coherent receiver with perfect channel state information after the frame-timing acquisition stage. Note that this perfect channel state information must include the residual pulse-level timing error since this is an information that non-coherent receivers assume to be part of the channel uncertainty. The adoption of a coherent receiver with perfect channel state information allows us to separate the performance degradation due to the channel uncertainty from the performance degradation which is purely due to the frame-timing acquisition algorithm.

Finally, the results of the method proposed in Section 6.2.6 and Section 6.2.7 are compared with the popular dirty template (DT) method proposed in [Yan04a].

6.2.8.1 Simulation results for random Gaussian waveforms

Experiment 1: BER Performance as a function of E_s/N_0. Figure 6.5 shows the BER results for an observation interval of $L = 100$ symbols. Note that almost an error-free performance in terms of BER is experienced for $E_s/N_0 > 5$ dB, which is indeed a really low E_s/N_0 value. This is in contrast with the dirty template (DT) method, which requires a significantly higher E_s/N_0 for reliable frame-timing acquisition. As it was already mentioned, the poor low-SNR performance of the DT is caused by the non-coherent integration of the noise when evaluating the DT cost function in [Yan04a, Eq. (14)]. In that sense, the advantage of the proposed method is that a coherent integration of the noise terms is addressed in the off-diagonal entries of the synchronous autocorrelation matrix. As it is well-known in statistical estimation theory, the noise contribution in coherent integration converges faster to zero than when non-coherent integration is performed [Kay98, p. 251]. As a result, the proposed method is found to be more robust to low-SNR scenarios than the DT.

Experiment 2: Probability of correct frame acquisition. The results in Figure 6.6 show the probability of correct frame acquisition as a function of the observation interval L in symbols. The observation interval is important for the proposed method in the sense that enough data must be processed so as to obtain a reasonable estimate for the synchronous autocorrelation matrix of the received signals, which is the sufficient statistics for the problem at hand. For the proposed method, the simulation results indicate that the probability of correct acquisition rapidly improves as the observation interval increases. As a result, almost an error-free performance is achieved for $L > 80$ symbols at $E_s/N_0 = 7$ dB whereas the DT method fails 50 % of the times for the same working conditions.

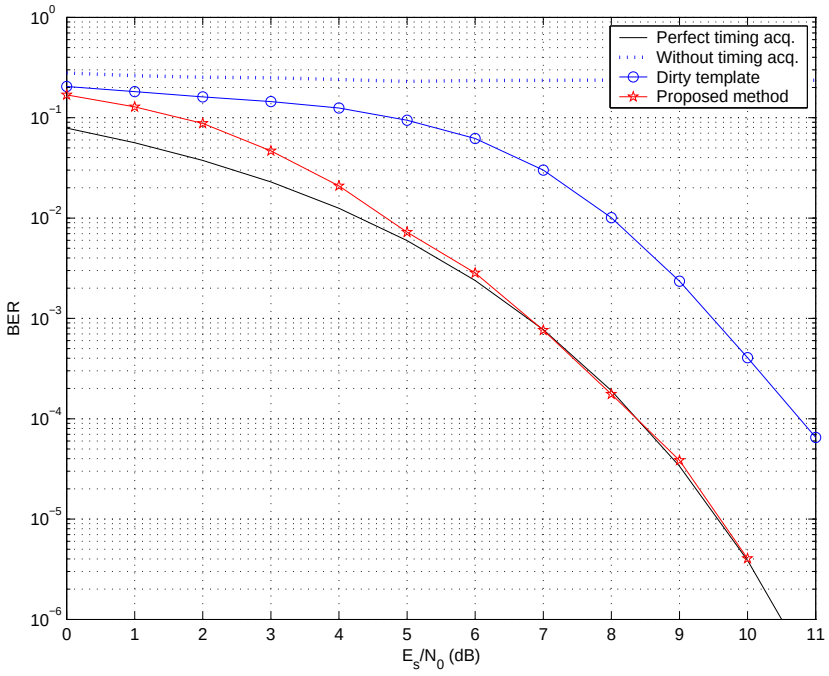

Figure 6.5: BER due to mistiming for an observation interval comprising $L = 100$ symbols with random Gaussian waveforms.

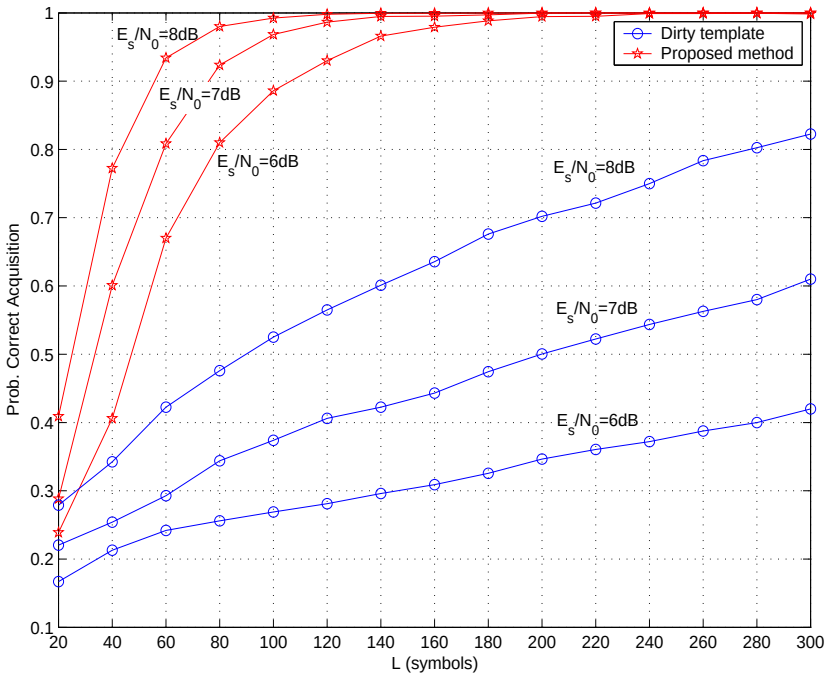

Figure 6.6: Probability of correct frame acquisition as a function of the observation interval L with random Gaussian waveforms.

Experiment 3: Degradation caused by inter-frame interference (IFI). It is important to remark that the proposed method has been derived under the assumption that no IFI was present in the received signal. However, it is also interesting to evaluate the performance when this assumption does not hold. Figure 6.7 presents the probability of correct frame-timing acquisition in the case of frame intervals with 28% and 57% overlap. The results are compared with the standard performance in the case of no IFI. For low-E_s/N_0 values, the proposed method is more sensitive to IFI than the dirty template. However, a superior performance is still obtained. For high-E_s/N_0 values, both methods degrade similarly and the probability of correct frame-timing acquisition degrades 15% to 20% compared to the IFI free results.

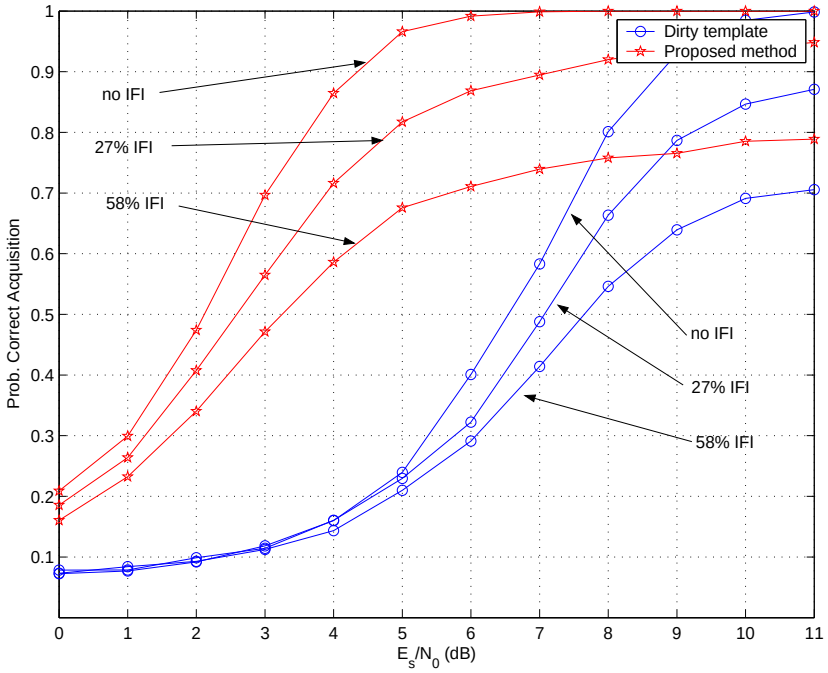

Figure 6.7: Impact of inter-frame interference on the probability of correct frame acquisition with $L = 100$ symbols and random Gaussian waveforms.

6.2.8.2 Simulation results for the IEEE 802.15.3a channel model

Experiment 1: BER Performance as a function of E_s/N_0. The BER results for an observation interval of $L = 100$ and $L = 200$ symbols are presented in Figure 6.8 and Figure 6.9, respectively. As it was already pointed out for the simulation results with random Gaussian waveforms, the BER is significantly reduced by using the proposed method when the observation interval is long enough so as to properly estimate the synchronous autocorrelation matrix. Finally, since the BER is degraded when the frame-timing error is not correctly acquired, Figure 6.10 evaluates this BER degradation. This is done by understanding the BER degradation as a loss in terms of E_s/N_0 with respect to the case with perfect timing acquisition.

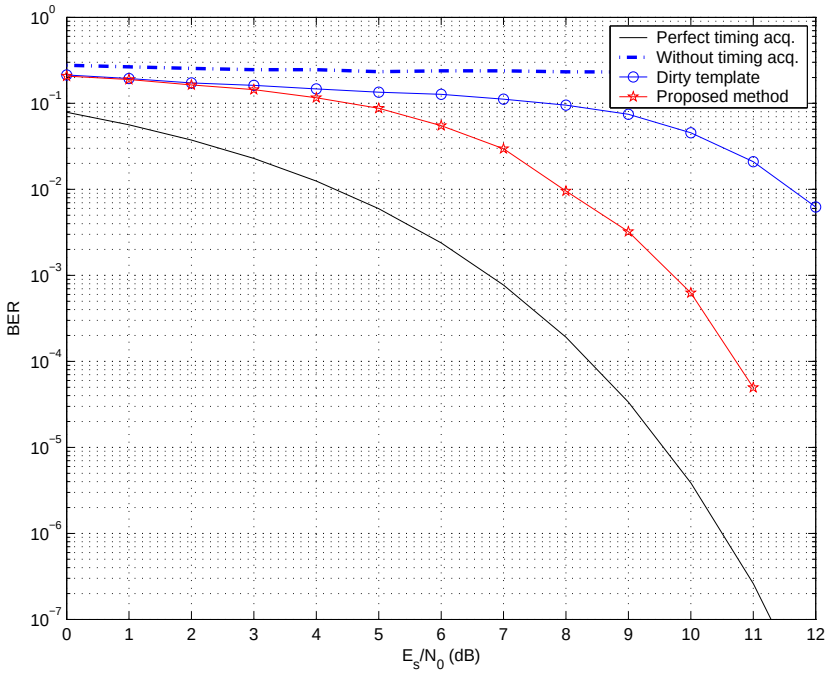

Figure 6.8: BER due to mistiming for an observation interval comprising $L = 100$ symbols with channel model CM1 from IEEE 802.15.3a.

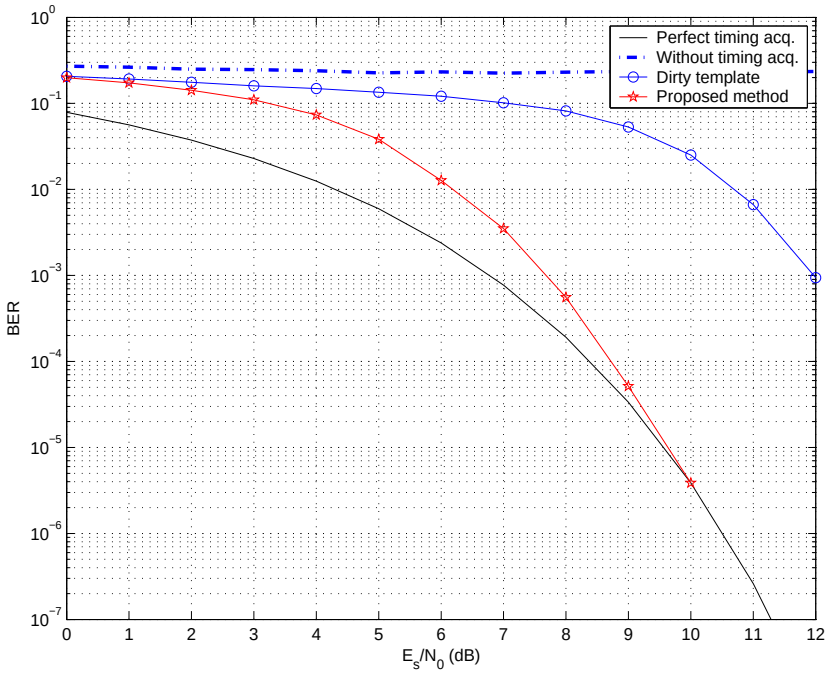

Figure 6.9: BER due to mistiming for an observation interval comprising $L = 200$ symbols with channel model CM1 from IEEE 802.15.3a.

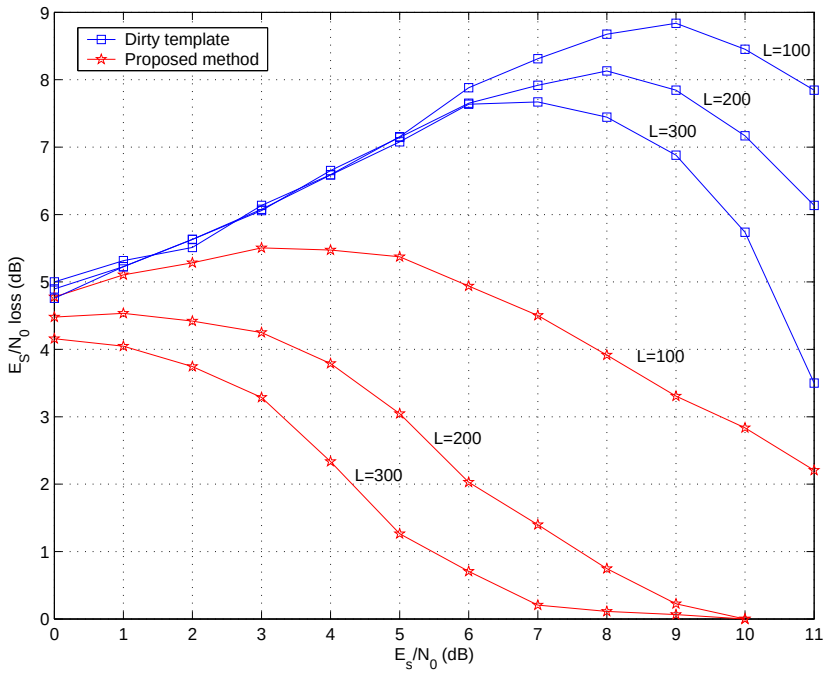

Figure 6.10: E_s/N_0 loss (dB) due to mistiming with respect to perfect frame acquisition for channel CM1 from IEEE 802.15.3a.

Experiment 2: Probability of correct frame acquisition. Figure 6.11 depicts the probability of correct frame-timing acquisition as a function of E_s/N_0. As for the case with random Gaussian waveforms, the proposed method is found to provide a significantly higher probability of correct frame-timing acquisition than the dirty template with the same simulation parameters. For the same number of transmitted symbols L, the coherent integration of the noise allows the proposed method to provide a more robust behavior in the low-SNR regime.

Moreover, the gain when increasing the observation interval is more significant in the proposed method. For instance, for all the working conditions in Figure 6.11, the most significant improvement in probability of correct frame acquisition is experienced at $E_s/N_0 = 6$ dB when increasing the observation interval from $L = 100$ to $L = 200$ for the proposed method. In this case, the probability of correct acquisition moves from 0.47 to 0.82 (almost improves 100%). In contrast, the most significant improvement for the DT method is at $E_s/N_0 = 10$ dB (4 dB later than for the proposed method) where the probability of correct frame acquisition moves from 0.44 to 0.65 (just 50%).

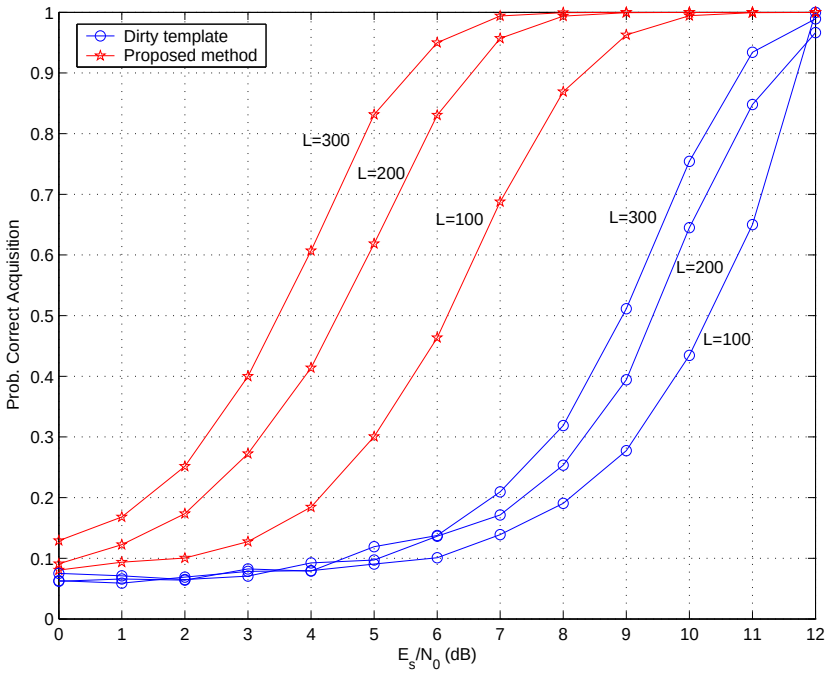

Figure 6.11: Probability of correct frame acquisition as a function of E_s/N_0 with channel model CM1 from IEEE 802.15.3a.

6.3 Frame-Timing Acquisition via the Multifamily Likelihood Ratio Test

The main contribution of this Section is the interpretation of the maximum likelihood cost function in Section 6.2.6 as a problem of model order selection. As a result, a reduced-complexity frame-timing estimator is proposed based on the multifamily likelihood ratio test [Kay05b]. While still outperforming existing frame-timing acquisition techniques, the proposed method provides a tradeoff between performance and implementation complexity with respect to the more complex and optimal maximum likelihood solution in Section 6.2.6.

6.3.1 Relationship with the optimal UML frame-timing acquisition approach

According to Section 6.2.6, the optimal frame-timing estimation in the UML sense is given by

$$\widehat{N}_\epsilon = \arg \max_{0 \leq m \leq N_f - 1} \|\mathbf{R}_0(m)\|_F^2 \tag{6.48}$$

where the general time-shifted synchronous cross-correlation matrix is defined here as,

$$\mathbf{R}_k(m) \doteq \mathrm{E}\left[\mathbf{r}_n(m)\, \mathbf{r}_{n+k}^T(m)\right] \tag{6.49}$$

with

$$\mathbf{r}_n(m) \doteq \left[r(nN_{ss}+mN_{sf}), r(nN_{ss}+mN_{sf}+1), \ldots, r(nN_{ss}+mN_{sf}+N_{ss}-1)\right]^T \quad (6.50)$$

for $m = \{0, 1, \ldots, N_f - 1\}$. Note that for $k = 0$, the matrix in (6.49) becomes the synchronous *autocorrelation* matrix in (6.22).

From the general expression in (6.48), several maximization strategies can be devised to obtain the desired frame-timing estimate $\widehat{N}_\epsilon$. The straightforward solution to (6.48) is presented in Section 6.2.6 and Section 6.2.7 and it makes use of the augmented $(2N_{ss} \times 2N_{ss})$ time-shifted synchronous autocorrelation matrix, and a sliding window for non-coherent detection once the synchronous autocorrelation matrix has been computed. Alternatively, the main purpose of this section is to show that the optimization involving $\mathbf{R}_0(m)$ in (6.48) can be reformulated in terms of the synchronous *cross-correlation* matrix $\mathbf{R}_1(m)$. By doing so, an equivalent optimization criterion can be obtained at the expense of a significant reduction in complexity.

To prove the above statement, let us take into consideration the signal model in (6.30). Moreover, and without loss of generality, let us assume in general $m = 0$ so that $\mathbf{R}_k \doteq \mathbf{R}_k(0)$ unless otherwise specified. In the presence of frame-timing error we have $N_\epsilon = i$ for some $i = \{1, \ldots, N_f - 1\}$. Similarly, in the absence of frame-timing error we have $N_\epsilon = 0$. Therefore, the corresponding synchronous autocorrelation matrices can be expressed as follows,

$$\mathbf{R}_{0\big|_{N_\epsilon=i}} = \begin{bmatrix} \mathbf{T}_b(i) & \mathbf{0}_{P(i)\times Q(i)} \\ \mathbf{0}_{Q(i)\times P(i)} & \mathbf{T}_a(i) \end{bmatrix} + \sigma_w^2 \mathbf{I}_{N_{ss}} \quad (6.51)$$

$$\mathbf{R}_{0\big|_{N_\epsilon=0}} = \begin{bmatrix} \mathbf{T}_a(i) & \mathbf{T}_c^T(i) \\ \mathbf{T}_c(i) & \mathbf{T}_b(i) \end{bmatrix} + \sigma_w^2 \mathbf{I}_{N_{ss}}, \quad (6.52)$$

with $P(i) \doteq iN_{sf}$ and $Q(i) \doteq N_{ss} - iN_{sf}$. As already defined in (6.34), (6.35) and (6.36), $\mathbf{T}_a(i) \doteq \mathrm{E}\left[\mathbf{a}\mathbf{a}^T | N_\epsilon = i\right]$, $\mathbf{T}_b(i) \doteq \mathrm{E}\left[\mathbf{b}\mathbf{b}^T | N_\epsilon = i\right]$ and $\mathbf{T}_c(i) \doteq \mathrm{E}\left[\mathbf{b}\mathbf{a}^T | N_\epsilon = i\right]$, respectively. Note that the conditional expectations are taken with respect to the samples of the received waveform, since the waveform is considered an unknown nuisance parameter. In addition, the key point is to notice that $\mathbf{R}_{0\big|_{N_\epsilon=0}}$ can always be expressed as a function of $\mathbf{T}_a(i)$, $\mathbf{T}_b(i)$ and $\mathbf{T}_c(i)$, which are indeed matrices defined for $N_\epsilon = i \neq 0$. Then, the corresponding Frobenius norms to (6.51)-(6.52) are given by,

$$\|\mathbf{R}_{0\big|_{N_\epsilon=i}}\|_F^2 = \|\mathbf{T}_b(i)\|_F^2 + \|\mathbf{T}_a(i)\|_F^2 + \sigma_w^2\left(N_{ss}\sigma_w^2 + 2E_{g_T}\right), \quad (6.53)$$

$$\|\mathbf{R}_{0\big|_{N_\epsilon=0}}\|_F^2 = \|\mathbf{T}_b(i)\|_F^2 + \|\mathbf{T}_a(i)\|_F^2 + 2\|\mathbf{T}_c(i)\|_F^2 + \sigma_w^2\left(N_{ss}\sigma_w^2 + 2E_{g_T}\right), \quad (6.54)$$

with E_{g_T} the energy of the received waveform, which is assumed a constant term. As a result of (6.53)-(6.54), it is possible to establish the following and very important relationship,

$$\|\mathbf{R}_{0\big|_{N_\epsilon=i}}\|_F^2 = \|\mathbf{R}_{0\big|_{N_\epsilon=0}}\|_F^2 - 2\|\mathbf{T}_c(i)\|_F^2. \quad (6.55)$$

The first important point is to notice that $\|\mathbf{R}_{0}\big|_{N_\epsilon=0}\|_F^2$ is by definition, a constant term which depends on the energy of the received waveform but not on the frame-timing error. This is because $\mathbf{R}_{0}\big|_{N_\epsilon=0}$ assumes by definition no frame-timing error. Therefore, the information regarding the frame-timing error must be contained within the matrix $\mathbf{T}_c(i)$, according to (6.55). The second important point is to notice that the structure of the synchronous cross-correlation matrix is,

$$\mathbf{R}_{1}\big|_{N_\epsilon=i} = \begin{bmatrix} \mathbf{0}_{P(i)\times P(i)} & \mathbf{0}_{P(i)\times Q(i)} \\ \mathbf{T}_c(i) & \mathbf{0}_{Q(i)\times Q(i)} \end{bmatrix}. \tag{6.56}$$

That is, the synchronous cross-correlation matrix of the received signal is based on the matrix $\mathbf{T}_c(i)$, which indeed contains the information regarding the frame-timing error. Thus, $\mathbf{R}_1$ is a sufficient statistic for the recovery of the frame-timing error. In fact, the dimensions of the unknown but non-zero matrix $\mathbf{T}_c(i)$ are $Q(i) \times P(i)$, so they are directly related to the frame-timing error $N_\epsilon = i$. Consequently, the optimization criterion in (6.48) can be recast as,

$$\widehat{N}_\epsilon \;=\; \arg \max_{0\leq m\leq N_f-1} \|\mathbf{R}_0(m)\|_F^2 \equiv \arg \min_{0\leq m\leq N_f-1} \|\mathbf{R}_1(m)\|_F^2. \tag{6.57}$$

Based on (6.57), the synchronous cross-correlation matrix $\mathbf{R}_1$ allows an alternative strategy for the frame-timing error acquisition. The advantage of this approach is that it makes use of the $(N_{ss} \times N_{ss})$ matrix $\mathbf{R}_1$ instead of the augmented $(2N_{ss} \times 2N_{ss})$ matrix $\mathbf{R}_0$ used in Section 6.2.6. As a result, the computational burden is significantly reduced, especially by taking into consideration that the number of samples per symbol may be a very large number when dealing with UWB signals.

However, it should be pointed out that it is not straightforward to determine the dimensions of the matrix $\mathbf{T}_c(i)$ from $\mathbf{R}_1$. Since the matrix $\mathbf{T}_c(i)$ exists only when $N_\epsilon = i \neq 0$, the detection of the case in which $N_\epsilon = 0$ should be done by evaluating a signal detection threshold. When the threshold is exceeded, the dimensions of $\mathbf{T}_c(i)$ would be determined to get the frame-timing error. When the threshold is not exceeded, then the frame-timing error would be directly set to $N_\epsilon = 0$. This strategy is very unpleasant, since it involves a two-step procedure and the signal detection threshold depends on the working point of the scenario under consideration. In order to circumvent this limitation, a simpler approach is proposed next by considering the synchronous *overlapped* cross-correlation matrix.

6.3.2 Synchronous overlapped cross-correlation matrix for the frame-timing acquisition problem

The synchronous overlapped cross-correlation (SOCC) matrix is a particular case of the generalized cross-correlation matrix in (6.49) and it is defined as,

$$\mathbf{R}_k\,(m,l) \doteq \mathrm{E}\left[\mathbf{r}_n\,(m)\,\mathbf{r}_{n+k}^T\,(m+l)\right] \tag{6.58}$$

where $k \neq 0$, $m = \{0, 1, \ldots, N_f - 1\}$, and $|l| = \{1, \ldots, N_f - 1\}$. Note that $k \neq 0$ is the responsible for the *cross*-correlation whereas $l \neq 0$ makes the expectation to be performed on cyclostationary-overlapped pieces of data.

For the proposed frame-timing acquisition method, we focus on the case of the SOCC matrix with $k = 1$ and $l = -1$, that is, $\mathbf{R}_1(0, -1)$. It its interesting to note that the $(N_{ss} \times N_{ss})$ SOCC matrix $\mathbf{R}_1(0, -1)$ contains the smaller $((N_{ss} - N_{sf}) \times (N_{ss} - N_{sf}))$ cross-correlation matrix $\mathbf{R}_1(0, 0)$ in its top right-hand corner. Therefore, the SOCC matrix contains the matrix $\mathbf{T}_c(i)$ when $N_\epsilon = i \neq 0$. In addition, and contrary to what happened with the traditional cross-correlation matrix, the SOCC matrix also presents a non-null signal contribution when $N_\epsilon = 0$. Thus, no signal detection threshold is required since there is always a signal contribution within $\mathbf{R}_1(0, -1)$. For this reason, the SOCC can safely be adopted to determine the unique frame-timing error N_ϵ that minimizes the optimization criterion in (6.57).

6.3.3 Frame-timing acquisition and model order detection

As previously mentioned, the main contribution of this Section 6.3 is that by using the SOCC matrix, the frame-timing acquisition can be understood as a problem of determining the length of an unknown signal.

In order to prove this statement, let us decompose the SOCC matrix $\mathbf{R}_1(0, -1)$ into a grid of small $(N_{sf} \times N_{sf})$ matrices called *frame-cells*, as shown in the top left-hand corner of Figure 6.12. In this way, the unknown signal will be given by the frame-cell *vech* stacking of $\mathbf{R}_1(0, -1)$. That is, the stacking of frame-cell columns of $\mathbf{R}_1(0, -1)$ by eliminating the frame-cells above the diagonal. The result is a tall matrix denoted by $\boldsymbol{\mathcal{R}}$ that contains a total of $N_{fc} = N_f(N_f + 1)/2$ frame-cells. As it is shown in Figure 6.12,

$$\boldsymbol{\mathcal{R}} \doteq \left[\boldsymbol{\mathcal{R}}(0)^T, \boldsymbol{\mathcal{R}}(1)^T, \ldots, \boldsymbol{\mathcal{R}}(N_f - 1)^T\right]^T \tag{6.59}$$

where $\boldsymbol{\mathcal{R}}(i)$ is a matrix that stands for the i-th frame-cell vech-column of $\mathbf{R}_1(0, -1)$, and it contains a total of $(N_f - i)$ frame-cells.

For the purpose of model order detection, each $\boldsymbol{\mathcal{R}}(i)$ matrix is considered as a whole. When $\boldsymbol{\mathcal{R}}(i)$ is not a null matrix, the signal model is $\boldsymbol{\mathcal{R}}(i) = \boldsymbol{\mathcal{S}}(i) + \boldsymbol{\mathcal{V}}(i)$, where $\boldsymbol{\mathcal{S}}(i)$ stands for an unknown but non-zero signal matrix. When $\boldsymbol{\mathcal{R}}(i)$ is a null matrix, the signal model is $\boldsymbol{\mathcal{R}}(i) = \boldsymbol{\mathcal{V}}(i)$ where $\boldsymbol{\mathcal{V}}(i)$ incorporates the corresponding noise samples. These noise samples are asymptotically Gaussian distributed with zero mean and variance $\sigma_v^2 = \sigma_w^4/L$. This assumption is particularly true when L, the number of transmitted symbols within the observation interval, becomes large (i.e. $L \gg 2$). In addition, and because of the overlapped approach in $\mathbf{R}_1(0, -1)$, the diagonal entries of the last frame-cell within $\boldsymbol{\mathcal{V}}(0)$ are not zero but equal to σ_w^2. This single frame-cell can be eliminated to avoid the frame-timing acquisition to become biased when σ_w^2 is

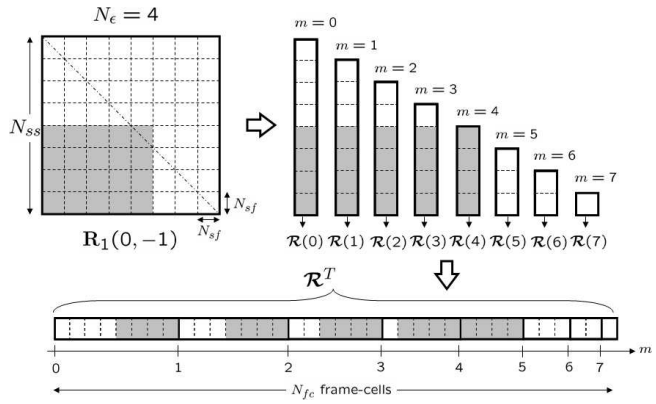

Figure 6.12: Set of $\boldsymbol{\mathcal{R}}(i)$ matrices resulting from the frame-cell vech-stacking of $\mathbf{R}_1(0,-1)$. This example assumes $N_\epsilon = 4$.

large. Finally, the frame-timing acquisition problem is addressed by evaluating the hypothesis $\mathcal{H}_m$ for $m = \{0, 1, \ldots N_f - 1\}$ as follows,

$$\mathcal{H}_m \quad : \quad \begin{cases} \boldsymbol{\mathcal{R}}(i) = \boldsymbol{\mathcal{S}}(i) + \boldsymbol{\mathcal{V}}(i), & i = 0, \ldots, m, \\ \boldsymbol{\mathcal{R}}(i) = \boldsymbol{\mathcal{V}}(i), & i = m+1, \ldots, N_f - 1, \end{cases} \tag{6.60}$$

The decision $\widehat{N}_\epsilon = m$ is taken when $\mathcal{H}_m$ is the most likely hypothesis. In other words, the frame-timing error is related to the number of non-null matrices $\boldsymbol{\mathcal{S}}(i)$ within $\mathbf{R}_1(0,-1)$, similarly to what occurs in the scalar case of determining the length of an unknown signal [Kay05b].

6.3.4 Multifamily likelihood ratio test for frame-timing acquisition

Certainly, the frame-timing acquisition can be thought to be equivalent to a problem of model order detection involving the evaluation of a multiple hypotheses testing. However, a major issue for the multiple hypotheses testing is that the problem of frame-timing acquisition involves an unknown set of unknown parameters. This is because neither the number of non-null matrices $\boldsymbol{\mathcal{S}}(i)$ is known nor the signal values they contain. Consequently, the multiple hypotheses are found to be nested and this prevents traditional detectors to succeed [Kay05b]. Under these circumstances, the adoption of the multifamily likelihood ratio test (MLRT) is proposed in [Kay05b]. Indeed, the MLRT can be understood as an extension of the well-known generalized likelihood ratio test (GLRT) [Kay98]. For the problem at hand, the decision rule is

$$\widehat{N}_\epsilon = \arg \max_{0 \leq m \leq \left(N_f - 1\right)} T_m(\boldsymbol{\mathcal{R}}) \tag{6.61}$$

where the MLRT test statistic is given by

$$T_m\left(\boldsymbol{\mathcal{R}}\right) \quad = \quad \left[L_m\left(\boldsymbol{\mathcal{R}}\right) - N_u(m)\left(\ln\left(\frac{L_m\left(\boldsymbol{\mathcal{R}}\right)}{N_u(m)}\right) + 1\right)\right] u\left(\frac{L_m\left(\boldsymbol{\mathcal{R}}\right)}{N_u(m)} - 1\right). \tag{6.62}$$

1) Calculate an estimate for the SOCC matrix $\mathbf{R}_1(0,-1)$ as,

$$\widehat{\mathbf{R}}_1(0,-1) = \frac{1}{L}\sum_{n=0}^{L-1} \mathbf{r}_n(0)\mathbf{r}_{n+1}(-1)$$

with $\mathbf{r}_n(m) \doteq \left[r(nN_{ss}+mN_{sf}), r(nN_{ss}+mN_{sf}+1), \ldots, r(nN_{ss}+mN_{sf}+N_{ss}-1)\right]^T$.

2) for $m = 0 : (N_f - 1)$,

- Evaluate the GLRT for the problem at hand,

$$L_m(\boldsymbol{\mathcal{R}}) = \frac{1}{\sigma_v^2}\sum_{n=0}^{m} \|\boldsymbol{\mathcal{R}}(n)\|_F^2$$

- Calculate the total number of samples (unknowns) considered in $L_m(\boldsymbol{\mathcal{R}})$

$$N_u(m) = (m+1)\left(N_f - \frac{m}{2}\right)$$

- Evaluate the MLRT test statistic $T_m(\boldsymbol{\mathcal{R}})$ according to (6.62).

$$T_m(\boldsymbol{\mathcal{R}}) = \left[L_m(\boldsymbol{\mathcal{R}}) - N_u(m)\left(\ln\left(\frac{L_m(\boldsymbol{\mathcal{R}})}{N_u(m)}\right)+1\right)\right] u\left(\frac{L_m(\boldsymbol{\mathcal{R}})}{N_u(m)} - 1\right).$$

end

4) Decide $\widehat{N}_\epsilon = \arg\max_m T_m(\boldsymbol{\mathcal{R}})$

Table 6.2: Procedure for the proposed frame-timing acquisition method based on the multifamily likelihood ratio test (MLRT).

In (6.62), the term $N_u(m)$ stands for the total number of unknowns when $\mathcal{H}_m$ is evaluated, whereas $u(x)$ denotes the unit step function. It is important to note that $L_m(\boldsymbol{\mathcal{R}})$ is the GLRT under the hypothesis $\mathcal{H}_m$, that is, by assuming that $\widehat{N}_\epsilon = m$. Therefore, the MLRT first computes the GLRT for each hypothesis and then it applies a nonlinear transformation that penalizes the GLRT as the model order increases. As a consequence, the MLRT provides a better performance than the simple GLRT and is able to implement a detector/estimator scheme in the presence of nested signal models. For a more detailed and comprehensive presentation of the MLRT, the reader is referred to [Kay05b] and [Kay05a].

From the above considerations, the procedure in Table 6.2 is proposed to determine the frame-timing error by evaluating the MLRT test statistic.

6.3.5 Simulation results

Computer simulations have been carried out to validate the performance of the proposed frame-timing acquisition method. The results are compared with the dirty template (DT) technique in [Yan04a] and the low-SNR unconditional maximum likelihood (lowSNR-UML) technique in Section 6.2.6 - 6.2.7. The simulated scenario considers the transmission of ultra-short pulses corresponding to the second derivative of the Gaussian pulse with a total duration of 4ns. The UWB channel is randomly generated according to the channel model CM1 proposed by Intel [Foe03] whose maximum delay spread is set to be in the order of 78ns. To test the robustness

in front of inter-frame interference, the frame duration is set to 46ns. The number of repeated frames per symbol is $N_f = 8$ and the sampling period is set to $T_s = 2$ns. Finally, the frame-timing error N_ϵ is uniformly random generated and the pulse timing error is set to $\epsilon = 0$. By doing so, we are preserving a waveform independent scenario by ignoring the autocorrelation properties of the received waveform that come into action when $\epsilon \neq 0$.

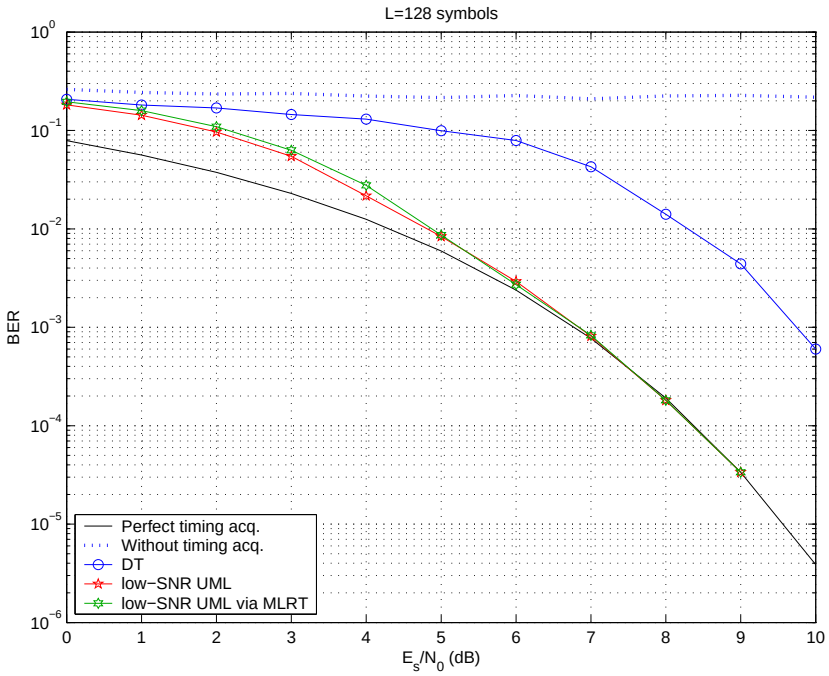

Figure 6.13: BER as a function of E_s/N_0 for an observation interval of $L = 128$ symbols.

As shown in Figure 6.13, the BER performance of the proposed method based on the multifamily likelihood ratio (MLRT) test almost coincides with the one of the optimal scheme in Section 6.2.6. However, the complexity of the MLRT method is approximately 25 % of the one required in 6.2.6. The results for the probability of correct frame-acquisition are presented in Figure 6.14. As it is shown, for the MLRT method there is a slight degradation of the probability of correct frame-acquisition with respect to the optimal approach. However, this degradation is not found to significantly alter the BER performance.

6.4 Conclusions

A nondata-aided and waveform-independent frame-level timing acquisition method has been proposed for UWB signals. The derivation of the proposed method has been performed under the systematic framework of unconditional maximum likelihood estimation for which the low-SNR assumption has been adopted. The major advantage of the proposed technique is that it is able to succeed regardless of the transmitted symbols and the received waveform. Therefore,

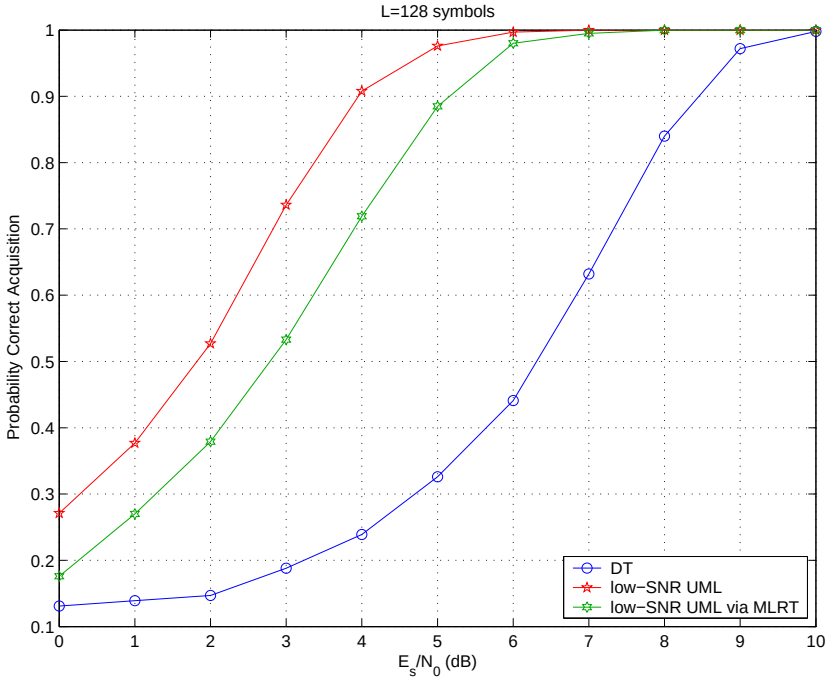

Figure 6.14: Probability of correct frame-acquisition as a function of E_s/N_0 for an observation interval of $L = 128$ symbols.

the problem of timing acquisition is solved without requiring any prior channel estimation. The algorithm implementation is based on a timing-search over the synchronous autocorrelation matrix of the received signal, and the low-SNR UML approach provides a robust performance in the presence of a severe noise degradation. In particular, and for low-SNR scenarios, the proposed method is found to outperform existing acquisition methods in the literature. A low-complexity implementation has also been presented by analyzing the frame-timing acquisition as a problem of model order detection. Finally, it should be noticed that the proposed method whose application has been demonstrated for the case of UWB signals, is also valid for blind acquisition of other spread-spectrum signaling schemes.

Appendix 6.A Derivation of the First Order Moment of $\chi(\mathbf{r};\tau;\mathbf{t};\mathbf{x})$ with Respect to x

This appendix is devoted to the derivation of $E_{\mathbf{x}}[\chi(\mathbf{r};\tau;\mathbf{t};\mathbf{x})]$ as required in (6.15). For this purpose, and from the definition of $\chi(\mathbf{r};\tau;\mathbf{t};\mathbf{x})$ in (6.13) we have,

$$E_{\mathbf{x}}[\chi(\mathbf{r};\tau;\mathbf{t};\mathbf{x})] = \sum_{p=0}^{P-1} E_{\mathbf{x}}\left[\mathbf{x}_p^T\right]\mathbf{A}_p^T\mathbf{r} - \frac{1}{2}\sum_{p=0}^{P-1}\sum_{q=0}^{P-1} E_{\mathbf{x}}\left[\mathbf{x}_p^T\mathbf{A}_p^T\mathbf{A}_q\mathbf{x}_q\right] \tag{6.63}$$

$$= -\frac{1}{2}\sum_{p=0}^{P-1}\sum_{q=0}^{P-1} Tr\left(\mathbf{A}_p^T\mathbf{A}_q E_{\mathbf{x}}\left[\mathbf{x}_q\mathbf{x}_p^T\right]\right) \tag{6.64}$$

$$= -\frac{1}{2P}\sum_{p=0}^{P-1} Tr\left(\mathbf{A}_p^T\mathbf{A}_p\right) \tag{6.65}$$

$$= -\frac{1}{2P}\sum_{p=0}^{P-1}\sum_{n=-K}^{K} \mathbf{a}_{n,p}^T\mathbf{a}_{n,p} \tag{6.66}$$

$$= -\frac{L}{2}E_t \doteq \gamma_a(\mathbf{t}). \tag{6.67}$$

As indicated in Section 6.2.1, the fact that $E_{\mathbf{x}}[\mathbf{x}_p] = \mathbf{0}$ for any p, and $E_{\mathbf{x}}\left[\mathbf{x}_p\mathbf{x}_q^T\right] = \frac{1}{P}\mathbf{I}\delta_{pq}$, has been used in (6.64) and (6.65) respectively. Moreover, it is important to note that the first order moment of $\chi(\mathbf{r};\tau;\mathbf{t};\mathbf{x})$ with respect to $\mathbf{x}$ does not depend on the timing error τ but just on the energy of the template waveform $E_t \doteq \|\mathbf{a}_{n,p}\|^2 = \|\mathbf{t}\|^2$, which is a constant term.

Appendix 6.B Derivation of the Second Order Moment of $\chi(\mathbf{r};\tau;\mathbf{t};\mathbf{x})$ with Respect to $\mathbf{x}$

The derivation of the second order moment of $\chi(\mathbf{r};\tau;\mathbf{t};\mathbf{x})$ with respect to $\mathbf{x}$ involves the evaluation of $E_{\mathbf{x}}\left[\chi^2(\mathbf{r};\tau;\mathbf{t};\mathbf{x})\right]$. From the definition of $\chi(\mathbf{r};\tau;\mathbf{t};\mathbf{x})$ in (6.13),

$$\begin{aligned}\chi^2(\mathbf{r};\tau;\mathbf{t};\mathbf{x}) &= \underbrace{\sum_{p=0}^{P-1}\sum_{q=0}^{P-1}\mathbf{r}^T\mathbf{A}_p\mathbf{x}_p\mathbf{x}_q^T\mathbf{A}_q^T\mathbf{r}}_{B1} - \underbrace{\left(\sum_{p=0}^{P-1}\mathbf{x}_p^T\mathbf{A}_p^T\mathbf{r}\right)\sum_{p=0}^{P-1}\sum_{q=0}^{P-1}\mathbf{x}_p^T\mathbf{A}_p^T\mathbf{A}_q\mathbf{x}_q}_{B2} \\ &+ \underbrace{\frac{1}{4}\sum_{p=0}^{P-1}\sum_{q=0}^{P-1}\sum_{m=0}^{P-1}\sum_{n=0}^{P-1}Tr\left(\mathbf{A}_p^T\mathbf{A}_q\mathbf{x}_q\mathbf{x}_m^T\mathbf{A}_m^T\mathbf{A}_n\mathbf{x}_n\mathbf{x}_p^T\right)}_{B3}. \end{aligned} \tag{6.68}$$

Therefore, the second order moment of $\chi(\mathbf{r};\tau;\mathbf{t};\mathbf{x})$ with respect to $\mathbf{x}$ involves the expectation of the terms B1, B2 and B3 in (6.68).

B1: The expectation of this term can be easily obtained by recalling that $E_{\mathbf{x}}\left[\mathbf{x}_p\mathbf{x}_q^T\right] = \frac{1}{P}\mathbf{I}\delta_{pq}$. Therefore,

$$E_{\mathbf{x}}\left[\sum_{p=0}^{P-1}\sum_{q=0}^{P-1}\mathbf{r}^T\mathbf{A}_p\mathbf{x}_p\mathbf{x}_q^T\mathbf{A}_q^T\mathbf{r}\right] = \sum_{p=0}^{P-1}\mathbf{r}^T\mathbf{A}_p\mathbf{A}_p^T\mathbf{r}. \tag{6.69}$$

B2: This term vanishes as it depends on the odd moments of the transmitted symbols.

B3: This term should be further manipulated by taking into consideration the relationship between the trace operator and the *vec* operator [Har00],

$$Tr\left(\mathbf{A}_p^T\mathbf{A}_q\mathbf{x}_q\mathbf{x}_m^T\mathbf{A}_m^T\mathbf{A}_n\mathbf{x}_n\mathbf{x}_p^T\right) = Tr\left(\left[\left(\mathbf{A}_q^T\mathbf{A}_p\right)\otimes\left(\mathbf{A}_m^T\mathbf{A}_n\right)\right]vec\left(\mathbf{x}_n\mathbf{x}_p^T\right)vec^T\left(\mathbf{x}_m\mathbf{x}_q^T\right)\right). \tag{6.70}$$

However, note that the products $\mathbf{A}_i^T\mathbf{A}_j$ in (6.70) do not depend on the timing error τ because all the waveforms within the column vectors of $\mathbf{A}$ do have the same delay τ. Indeed,

$$\mathbf{A}_i^T\mathbf{A}_j = N_f R_g\Big((i-j)N_\Delta\Big)\mathbf{I}_L, \tag{6.71}$$

for any $\{i,j\} = \{0,1,\ldots,P-1\}$ and with $R_g(n) = \sum_{m=0}^{N_g-1} g(m)g(n-m)$ the autocorrelation function of the received waveform $g(k)$. Hence, it is found that

$$E_{\mathbf{x}}\left[Tr\left(\mathbf{A}_p^T\mathbf{A}_q\mathbf{x}_q\mathbf{x}_m^T\mathbf{A}_m^T\mathbf{A}_n\mathbf{x}_n\mathbf{x}_p^T\right)\right] = \gamma_b(\mathbf{t}) \tag{6.72}$$

where $\gamma_b(\mathbf{t})$ is a term which only depends on the received template waveform.

Finally,

$$E_{\mathbf{x}}\left[\chi^2(\mathbf{r};\tau;\mathbf{t};\mathbf{x})\right] = \sum_{p=0}^{P-1}\mathbf{r}^T\mathbf{A}_p\mathbf{A}_p^T\mathbf{r} + \gamma_b(\mathbf{t}). \tag{6.73}$$

Chapter 7

Conclusions and Future Work

This thesis has analyzed the problem of coherent and non-coherent communication based on ultra-wideband signaling. Because of the very large bandwidth occupancy of UWB signals, the topic addressed in this dissertation has been placed within the framework of communication under the *wideband regime*. However, and under a given fixed power constraint, wideband regime has been shown to be equivalent to *low-SNR* working conditions. Thus, both wideband regime and low-SNR have become the key elements in our analysis of digital ultra-wideband receivers. This can be shown in Figure 7.1, where wideband regime and low-SNR are the starting points of the subsequent discussions. The topics where contributions have been presented are highlighted in this figure for the sake of clarity.

Let us first consider the topic of communication under the wideband regime. This topic has been shown to result in the distinction between coherent and non-coherent receivers depending on whether channel state information is available or not. This is an important issue because, unlike traditional narrowband communication systems, the severe propagation conditions of UWB signals involve a high complexity at the receiver side when coherent reception is adopted. In this way, the goal of Chapter 3 has been to determine the performance bounds for both coherent and non-coherent receivers so that the expected performance loss incurred by non-coherent receivers can be evaluated. This has constituted the first part of this dissertation.

Once the theoretical analysis of coherent and non-coherent receivers has been addressed, the next step has been to move forward into the receiver design. This has constituted the second part of this dissertation. The basic tasks to be considered at the receiver are signal synchronization, symbol detection and channel estimation (when required). For the case of coherent UWB receivers, Chapter 4 has shown that the major problem is related with waveform estimation. However, once the received waveform is identified, both synchronization and symbol detection can be done in a standard manner as for traditional narrowband receivers. For this reason only waveform estimation has been addressed when referring to the receiver design for coherent com-

munications. For the case of non-coherent UWB receivers, second-order cyclostationarity has been shown to be essential to compensate the lack of knowledge about the received waveform. With the aid of second-order statistics, Chapter 5 and Chapter 6 have dealt with the symbol detection strategy and synchronization techniques, respectively.

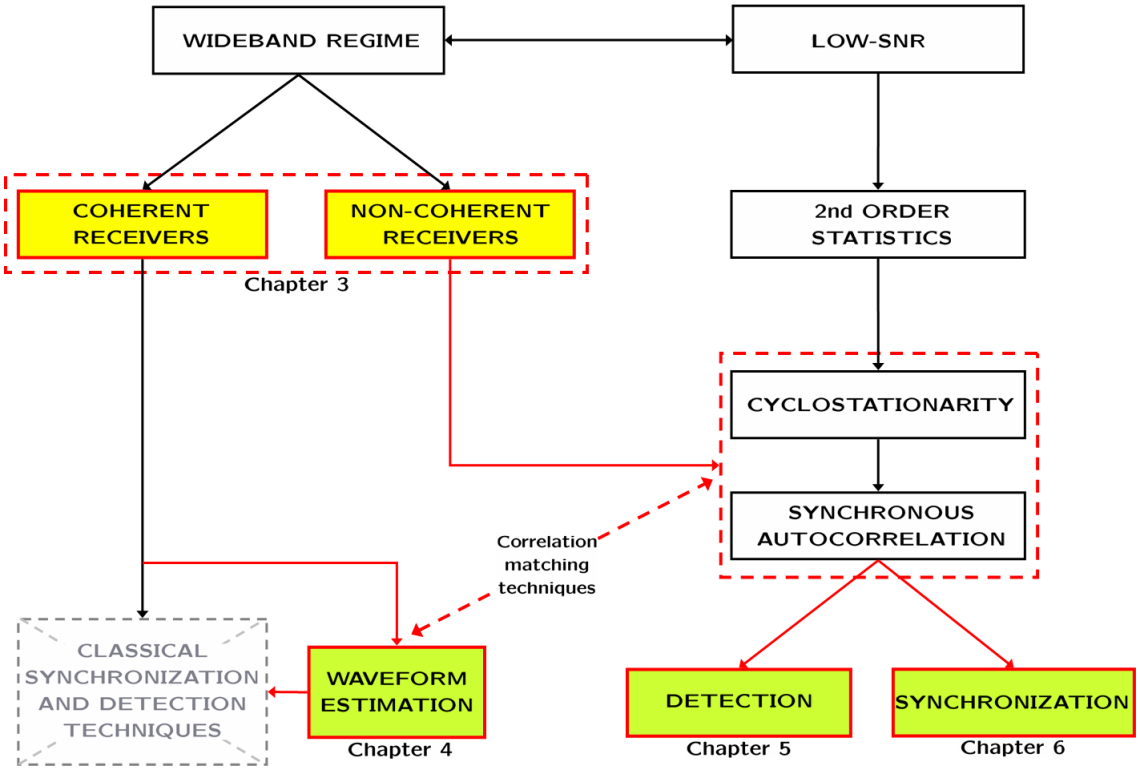

Figure 7.1: Schematic overview of the topics covered within the present dissertation.

Next, we summarize the contributions and future research lines for each of the topics addressed in this dissertation.

Coherent vs. Non-Coherent Communications

The discussion on coherent versus non-coherent receivers is addressed in Chapter 3 under an information theoretic approach. The main goal has been to characterize in an analytical manner the asymptotic behavior when operating under the wideband regime. To this end, the notion of *constellation-constrained* capacity provides an insightful measure on the achievable data rates for an arbitrarily small error probability. Contrary to the traditional measure of capacity, constellation-constrained capacity has been adopted to model the fact that we are dealing with digital communication systems. That is, to model the fact that we are dealing with discrete input distributions.

In the recent literature, most of the results dealing with achievable data rates for UWB

systems are based on numerical evaluations to overcome the difficulty in providing a closed-form expression for capacity. In this part of the dissertation, however, one of the most important contributions is that closed-form expressions are provided to upper-bound the constellation-constrained capacity for both coherent and non-coherent UWB systems. The proposed closed-form upper bounds have been compared with the exact (i.e. numerically evaluated) results and a tight match has been found.

In a second step, the analysis of the results for constellation-constrained capacity of UWB systems has led to an important conclusion. There exists the traditional belief that capacity in the AWGN channel can also be achieved in the presence of unknown fading provided that bandwidth is sufficiently large. This statement led to the assumption that UWB systems (i.e. very large bandwidth signaling) would achieve the same capacity as in the AWGN channel when propagating in the presence of unknown multipath fading channels. This was expected to be a very attractive result since it suggests that channel estimation would not be necessary for UWB systems. However, one of the most important results from the theory of spectral efficiency in the wideband regime is that capacity for the AWGN cannot be achieved in the presence of unknown fading when bandwidth is very large but finite, and when peakiness constraints are introduced. Peakiness constraints become necessary because UWB systems must co-exist with existing wireless communication systems and thus, harmful interference must be avoided. However, peakiness constraints come at the expense of a degradation loss in the achievable data rates of non-coherent receivers when compared to coherent receivers.

When operating under the wideband regime, capacity results shown in Figure 3.8 suggest a performance degradation from 9 to 10 dB. This degradation is experienced in terms of E_b/N_0 when non-coherent UWB reception is implemented instead of coherent UWB reception. However, high data rates can still be provided due to the very large bandwidth of UWB signals. This has been shown in Figure 3.9, where the achievable data rates for non-coherent UWB systems are also found to be more sensitive to changes in E_b/N_0 than the achievable data rates for coherent UWB systems.

Some of the topics that have not been addressed in this dissertation but may be subject to further investigation are the following:

- It would be interesting to extend the capacity analysis presented herein to the case where cognitive radio is implemented. Cognitive radio is an attractive paradigm for UWB communications since it allows to dynamically adapt the transmission and radiation parameters so as to exploit available spectral resources without interfering licensed users[1]. In that way, it is possible to exceed the allowable radiation limits of standard UWB systems by shaping the spectrum so as to incorporate inactive frequency bands. That is, by using

[1] The interested reader may found an excellent presentation on cognitive radio in [Hay05].

frequency bands of licensed users when these users are not inactive. The analysis of this new approach would involve the assumption of colored noise in our signal model. With some prior information about the licensed services that are supposed to be operated in a specific time and geographical location, the noise spectral mask of the received data provides information on active and not active users and services. This information can be represented in terms of a given noise correlation matrix whose impact in terms of capacity should be evaluated.

- A pending issue to be further analyzed is the relationship between capacity and likelihood ratio testing according to Eq. (3.23). This is an important issue since the meaning of Eq. (3.23) suggests that a clear link may be established between information theory and detection theory.

- Closed-form expressions have been provided for upper-bounding the constellation-constrained capacity of both coherent and non-coherent UWB communications. However, it would be interesting to further analyze the behavior of these upper-bounds in the limit of infinite bandwidth and to compare the results with the exact infinite-bandwidth capacity of Gaussian inputs in Eq. (3.9).

- Since tight upper-bounds have been derived for constellation-constrained capacity, tight lower-bounds are also required to restrict the region where capacity may range.

- In a context of random time variations of the propagation channel, and because of the particular signaling structure of UWB communication systems, it is reasonable to consider the transmission of random waveforms from a given waveform distribution. In that case, it is important to determine the optimal waveform distribution to maximize capacity for a given characterization of the propagation channel. Note that this approach is in contrast with the traditional implementation of UWB systems, where a deterministic pulse is usually transmitted.

- Possible extensions of the work presented herein includes the adoption of multiple-input multiple-output schemes and the impact of multi-user interference.

Waveform Estimation for Coherent Receivers

Coherent receivers assume perfect knowledge of the propagation conditions between transmitter and receiver. As indicated in Figure 7.1, coherent receivers require side information in the form of waveform or channel state information in order to proceed with their basic tasks (e.g. synchronization and symbol detection). The provision of channel state information has been shown to be a critical and computationally demanding problem in UWB receivers due to the severe and unique distortion of the UWB propagation channel.

In this dissertation, the waveform estimation problem has been approached from the low-SNR perspective. In this sense, the second-order statistics of the received signal have been shown to become the sufficient statistics for the problem at hand. As already indicated in the pioneering work by Tong et al., channel estimation is possible from second-order statistics when more than one sample per symbol is considered. Following this approach, the proposed waveform estimation technique is aimed at exploiting the cyclostationary properties of the second-order statistics of the received UWB signal. This has been shown to be possible by considering the synchronous autocorrelation matrix of the received signal, and by properly defining a precise signal model to represent the finite-length structure of the UWB received signal. Based on the above considerations, a waveform estimation technique has been derived in Chapter 4 which differs in many aspects with traditional approaches. Some of the most important features of the proposed method are listed below:

1. The aggregated channel response and not the individual paths and amplitudes is proposed to be estimated. This constitutes an unstructured approach where the paths of the propagation channel are completely disregarded and the received waveform for a single transmitted pulse is considered as a whole.

2. The unconditional maximum likelihood criterion is considered. As a result, the *unconditional* approach leads to a nondata-aided implementation of the waveform estimation technique whereas the maximum likelihood perspective allows an asymptotically unbiased and efficient performance.

3. The low-SNR approximation of the unconditional maximum likelihood criterion is adopted. Therefore, the resulting estimator is especially designed to cope with the low-SNR conditions of actual UWB receivers.

4. The likelihood criterion is compressed with information regarding the signal subspace. This restricts the solution space around the true value in order to avoid any possible ill-conditioning or local-maxima. This subspace-compressed approach can be understood as a principal component analysis, and thus, a significant reduction in the computational burden is obtained through a tradeoff between bias and variance.

5. The proposed solution can be understood as a correlation matching method. That is, it performs a matching between the synchronous autocorrelation of the received signal and the synchronous autocorrelation of the signal model. Indeed, correlation matching methods have been previously proposed in the literature for nondata-aided channel estimation, but the problem has been found to be nonlinear and the solution is usually obtained in a rather heuristic manner by numerical evaluation or gradient-based search.

6. Contrary to most of the traditional approaches, a closed-form expression for the proposed waveform estimator is provided. This is done by converting the nonlinear optimization

problem into a linear least-squares problem on the second-order statistics of the received signal.

Simulation results have been obtained for the proposed waveform estimation technique and a superior performance is observed when compared to existing methods based on second-order statistics. However, there are still some pending issues to be further investigated,

- Some research is still required to determine the identifiability conditions for the proposed closed-form waveform estimation technique. This issue was already discussed in Section 4.4.1 and the main problem was to find a formal proof to guarantee the full column rank condition of matrix $\mathbf{Q}$ in (4.24). This matrix can be thought to be the system matrix in a traditional least squares problem and thus, its full column rank condition is essential to guarantee the uniqueness of the solution.

- Extensive simulation results should also be obtained with different channel models within the IEEE 802.15.3a/4 standards. This would provide a more robust characterization of the proposed waveform estimation technique under different working conditions.

- Since a wide range of channel estimation methods have already been proposed in the literature, it is interesting to perform a more exhaustive comparison to assess the performance of the proposed technique.

- Finally, another pending issue is the one related with the extension of the current formulation to accommodate multi-user scenarios.

Symbol Detection for Non-Coherent Receivers

It has been shown that the adoption of coherent receivers (i.e the assumption of perfect channel state information) is restricted to those applications where slow channel variations are experienced and significant computational complexity is available at the receiver. This is due to the fact that the large multipath resolution of UWB signals makes the computation of fast and accurate channel estimates a challenging and computationally demanding task. When such a computational burden is not available, there is no choice but to resort to non-coherent receivers.

Non-coherent receivers have been previously addressed in the literature. However, most of the times an unknown deterministic approach is considered by assuming the received waveform to be unknown but constant during all the observation interval. Alternatively, other approaches consider the problem of waveform time-variation by adopting transmitted reference (TR) signaling, which is based on the transmission of a reference pulse prior to each data modulated pulse. In that way, noisy channel state information is provided by the received unmodulated pulses

themselves. However, this comes at the expense of an efficiency loss due to the transmission of unmodulated pulses and at the end, a coherent receiver is required once again.

Contrary to previous contributions, the problem of symbol detection for non-coherent receivers has been addressed in this dissertation by assuming the received signal to be random. The low-SNR maximum likelihood criterion has also been adopted for deriving the optimal framework for the symbol detection problem of binary-PPM. Two different analyses for this problem have been presented depending on whether the amplitudes of the received waveforms are correlated or not. For uncorrelated scenarios, the optimal symbol detector has been shown to be based on the exploitation of the power delay profile of the channel. For correlated scenarios, the optimal symbol detector has been found to result in a rather intricate expression. In that case, however, significant simplifications can be introduced by allowing the implementation of a rank-1 receiver. This low cost alternative can be implemented by adopting an information theoretic criterion for deciding the optimal deterministic linear receiver to be selected among the set of signal subspace eigenvectors. In particular, this criterion has been shown to be based on the minimization of the system bit error rate through the maximization of the Jeffreys' divergence between the two symbol hypotheses to be decided.

Some of the topics that have not been addressed in this dissertation but may be subject to further investigation are the following:

- As already mentioned in Chapter 5, the proposed symbol detection techniques are based on the assumption that the received signal is Gaussian distributed. This allows the symbol detection problem to be mathematically tractable but, fortunately, it also corresponds to some realistic scenarios such as the one encountered in the propagation of UWB signals in industrial environments [Sch05b], [Sch05c]. For other scenarios such as office or residential environments, the statistics of UWB received signals cannot be properly modeled as Gaussian. Instead, Nakagami or log-normal distributions are found to provide a closer match. Consequently, it would be interesting to evaluate the performance of the proposed detectors in those scenarios where the received statistics are not Gaussian.

- A practical issue to be considered is the one related with reducing the complexity of the proposed detectors. As shown in Chapter 5, a relatively high computational burden is required to obtain the optimal symbol decision statistics. This is especially true for the case of correlated scattering scenarios where a simple rank one approach was suggested to alleviate the required complexity. However, suboptimal approaches to the problem of symbol detection in non-coherent receivers should be investigated.

- Again, and similarly to the waveform estimation problem, another pending issue is the one related with the extension of the current formulation to accommodate multi-user scenarios.

Synchronization for Non-Coherent Receivers

In the absence of any prior knowledge about the propagation conditions, the synchronization problem for non-coherent receivers has been addressed through the exploitation of the cyclostationary properties of the received signal. The formal procedure is similar to the one adopted for the non-coherent detection of UWB signals in the sense that the proposed method is based on the analysis of the synchronous autocorrelation of the received signal. Moreover, since carrierless UWB is considered along the present dissertation, synchronization reduces to timing acquisition.

As indicated in Chapter 6, synchronization of UWB receivers is similar to what happens in traditional spread-spectrum communication systems. That is, timing acquisition is divided into two different stages. First, coarse timing acquisition (i.e. frame-timing acquisition) and second, fine timing acquisition (i.e. pulse-timing acquisition). The second stage has not been considered for the case of non-coherent receivers because the notion of fine timing error is always related to a reference pulse. Since no channel information is available in non-coherent receivers, the reference waveform is unknown and thus fine timing error becomes part of the unknown waveform.

There are two main contributions to be highlighted in the topic of timing synchronization of UWB signals.

1. The problem of frame-timing acquisition has been formulated in a rigorous and analytical manner by using the low-SNR approximation of the unconditional maximum likelihood criterion. This is in contrast with many of the existing contributions on this topic, where most of the techniques are obtained in a rather ad-hoc or heuristic manner. The major advantage of the proposed technique is that it is able to succeed regardless of the transmitted symbols and the received waveform. Therefore, the problem of frame-timing acquisition can be solved in the absence of pilot symbols and without requiring any prior channel estimation. Finally, it has been shown that the optimal formulation of the problem leads to a simple strategy where frame-timing error is obtained as a result of an energy detection search over the synchronous autocorrelation matrix of the received signal.

2. A reduced complexity implementation has been proposed based on the principle of multifamily likelihood ratio testing. By doing so, the synchronization problem can be understood as a model order detection problem. Compared to the optimal approach, the major advantage of this low-cost solution is that at least 75 % of the computational complexity can be saved at no cost in terms of performance.

In both cases, the performance results of the proposed frame-timing acquisition techniques outperform existing contributions in the literature. However, some of the research lines that still remain open are the following:

- The proposed frame-timing acquisition methods are based on the assumption that the transmitted symbols are amplitude modulated. It would be interesting to extend the results to the case where no amplitude modulation but only pulse position modulation is being transmitted.

- Similarly to the symbol detection problem, low complexity receivers are strongly required for UWB systems. For this reason, one of the pending issues in this part of the dissertation is the investigation of suboptimal techniques that involve low-complexity and provide rapid acquisition.

Bibliography

[Aie03] G. R. Aiello, G. D. Rogerson, "Ultra-Wideband Wireless Systems", *IEEE Microwave*, Vol. 4, nº 2, pags. 36–47, June 2003.

[And05] C. R. Anderson, A. Annamalai et al., *Introduction to Ultra Wideband Communication Systems*, Prentice Hall Communications Engineering and Emerging Technologies Series, Prentice Hall, 2005.

[Ara03] F. E. Aranda, N. Brown, H. Arslan, "RAKE Receiver Finger Assignment for Ultra-Wideband Radio", *Proc. 4th IEEE Workshop on Signal Processing Advances in Wireless Communications (SPAWC)*, pags. 239–243, 15-18 June 2003.

[Bar00] T. W. Barrett, "History of UltraWideband (UWB) Radar & Communications: Pioneers and Innovators", *Proc. Progress in Electromagnetics Symposium*, 2000.

[Bel94] J. S. Belrose, "The Sounds of a Spark Transmitter: Telegraphy and Telephony", *Radioscientist*, 22 December 1994, available online at: http://www.physics.otago.ac.nz/ursi/belrose/spark.html.

[Ben78] C. L. Benett, G. F. Ross, "Time-Domain Electromagnetics and Its Application", *Proceedings of the IEEE*, Vol. 66, pags. 299–318, 1978.

[Ben06] M. Di Benedetto, T. Kaiser, A. F. Molisch, I. Oppermann, C. Politano, D. Porcino (eds.), *UWB Communication Systems. A Comprehensive Overview*, EURASIP Book Series on Signal Processing and Communications, Hindawi Publising Corporation, 2006.

[Ber02] I. Bergel, E. Fishler, H. Messer, "Narrow-band Interference Suppression in Time-Hopping Impulse-Radio Systems", *Proc. IEEE Conference on Ultra Wideband Systems and Technologies*, pags. 303–308, 2002.

[Blá03] R. Blázquez, P. Newaskar, A. Chandrakasan, "Coarse Acquisition for Ultra Wideband Digital Receivers", *Proc. IEEE International Conference on Acoustics, Speech and Signal Processing (ICASSP)*, Vol. 4, pags. 137–140, 6-10 April 2003.

[Bla87] R. E. Blahut, *Principles and Practice of Information Theory*, Addison-Wesley, 1987.

[Brz06] G. Brzezina, L. Roy, L. MacEachern, "Planar Antennas in LTCC Technology with Transceiver Integration Capability for Ultra-Wideband Applications", *IEEE Trans. Microwave Theory Tech.*, Vol. 54, nº 6, pags. 2830–2839, June 2006, part 2.

[Bue04] R. M. Buehrer, W. A. Davis, A. Safaai-Jazi, D. Sweeney, "Ultra-Wideband Propagation Measurements and Modeling - Final Report to DARPA NETEX

Program", Tech. rep., Virginia Tech. Antenna Group, 2004, Available at: http://www.mprg.org/people/buehrer/ultra/darpa%5Fnetex.shtml.

[Car01] M. Cardoza, et al., *Final Report Data Collection Campaign for Measuring UWB/GPS Compatibility Effects*, Center for Ultra-Wideband Research and Engineering, University of Austin Texas, TL-SG-01-01, 26 February 2001.

[Car03] C. Carbonelli, U. Mengali, U. Mitra, "Synchronization and Channel Estimation for UWB Signals", *Proc. IEEE Global Conference on Communications (GLOBECOM)*, Vol. 2, pags. 764–768, 1-5 December 2003.

[Car04a] C. Carbonelli, S. Franz, U. Mengali, U. Mitra, "Semi-Blind ML Synchronization for UWB Transmitted Reference Systems", *Conference Record of the Thirty-Eigth Asilomar Conference on Signals, Systems and Computers*, Vol. 2, pags. 1491–1495, 7-10 November 2004.

[Car04b] C. Carbonelli, U. Mitra, "Clustered Channel Estimation for UWB Signals", *Proc. International Conference on Communications (ICC)*, Vol. 4, pags. 2432–2436, 20-24 June 2004.

[Car06a] C. Carbonelli, U. Mengali, "M-PPM Noncoherent Receivers for UWB Applications", *IEEE Trans. Wireless Commun.*, Vol. 5, nº 8, pags. 2285 – 2294, August 2006.

[Car06b] C. Carbonelli, U. Mengali, "Synchronization Algorithms for UWB Signals", *IEEE Trans. Commun.*, Vol. 54, nº 2, pags. 329–338, February 2006.

[Cas02a] D. Cassioli, M. Z. Win, A. F. Molisch, "The Ultra-Wide Bandwidth Indoor Channel: From Statistical Model to Simulations", *IEEE J. Select. Areas Commun.*, Vol. 20, nº 6, pags. 1247–1257, August 2002.

[Cas02b] D. Cassioli, M. Z. Win, F. Vatalaro, A. F. Molisch, "Performance of Low-Complexity RAKE Reception in a Realistic UWB channel", *Proc. IEEE International Conference on Communications*, Vol. 2, pags. 763–767, 28 April - 2 May 2002.

[CEP06] *ECC Decision of 24 March 2006 on the harmonised conditions for devices using Ultra-Wideband (UWB) technology iin bands below 10.6 GHz*, 24 March 2006, eCC/DEC/(06)04.

[Cha03] Y. Chao, R. A. Scholtz, "Optimal and Suboptimal Receivers for Ultra-Wideband Transmitted Reference Systems", *IEEE Global Conference on Communications (GLOBECOM)*, Vol. 2, pags. 759–763, 1-5 December 2003.

[Cha05] Y.-L. Chao, R. A. Scholtz, "Ultra-wideband transmitted reference systems", *IEEE Trans. Veh. Commun.*, Vol. 54, nº 5, pags. 1556–1569, September 2005.

[Che05] P. Cheong, A. Rabbachin, J.-P. Montillet, K. Yu, I. Opperman, "Synchronization, TOA and Position Estimation for Low-Complexity LDR UWB Devices", *IEEE International Conference on Ultra-Wideband*, pags. 480–484, 2005.

[Chu04] X. Chu, R. D. Murch, "The Effect of NBI on UWB Time-Hopping Systems", *IEEE Trans. Wireless Commun.*, Vol. 3, nº 5, pags. 1431–1436, September 2004.

[Chu05] W. C. Chung, N. J. August, D. S. Ha, "Signaling and Multiple Access Techniques for Ultra Wideband 4G Wireless Communication Systems", *IEEE Wireless Commun. Mag.*, Vol. 12, nº 2, pags. 46–55, April 2005.

[Con06] M. Converse, E. J. Bond, B. D. Veen, S. C. Hagness, "A Computational Study of Ultra-Wideband versus Narrowband Microwave Hyperthermia for Breast Cancer Treatment", *IEEE Trans. Microwave Theory Tech.*, Vol. 54, nº 5, pags. 2169–2180, May 2006.

[Cov91] T. M. Cover, J. A. Thomas, *Elements of Information Theory*, John Wiley & Sons, 1991.

[Cra98a] R. J.-M. Cramer, M. Z. Win, R. A. Scholtz, "Evaluation of the Multipath Characteristics of the Impulse Radio Channel", *Proc. 9th IEEE International Symposium on Personal, Indoor and Mobile Radio Communications*, Vol. 2, pags. 864–868, 8 - 11 September 1998.

[Cra98b] R. J.-M. Cramer, M. Z. Win, R. A. Scholtz, "Impulse Radio Multipath Characteristics and Diversity Reception", *Proc. IEEE International Conference on Communications (ICC)*, Vol. 3, pags. 1650–1654, 7-11 June 1998.

[Cra02] R. J.-M. Cramer, R. A.Scholtz, M. Z. Win, "Evaluation of an Ultra-Wide-Band Propagation Channel", *IEEE Trans. Antennas Propagat.*, Vol. 50, pags. 561–570, May 2002.

[D'A05] A. A. D'Amico, U. Mengali, "GLRT Receivers for UWB Systems", *IEEE Commun. Lett.*, Vol. 9, nº 6, pags. 487–489, June 2005.

[DAR90] *Assessment of Ultra-Wideband (UWB) Technology*, 13 July 1990, OSD/DARPA Ultra-Wideband Radar Review Panel, Battelle Tactical Technology Center, Contract No. DAAH01-88-C-0131, ARPA Order 6049.

[Dav79] J. R. Davis, D. J. Baker, J. P. Shelton, W. S. Ament, "Some Physical Constraints on the Use of "Carrier-Free" Waveforms in Radio-Wave Transmission Systems", *Proc. IEEE*, Vol. 67, nº 6, pags. 884–890, June 1979.

[Dju98] P. Djuric, "Asymptotic MAP Criteria for Model Selection", *IEEE Trans. Signal Processing*, Vol. 46, pags. 2726–2735, October 1998.

[Dol00] S. Dolinar, D. Divsalar, J. Hamkins, F. Pollara, "Capacity of Pulse-Position Modulation (PPM) on Gaussian and Webb Channels", Tech. rep., Jet Propulsion Laboratory (JPL), National Aeronautics and Space Administration (NASA), 2000, LPL TMO Progress Report.

[ECC05] *The Protection Requirements of Radiocommunications Systems Below 10.6 GHz from Generic UWB Applications*, February 2005, Electronics Communication Committee (ECC), CEPT, Report 64.

[Ett77] P. Van Etten, "The Present Technology of Impulse Radars", *Proc. International Radar Conference*, pags. 535–539, October 1977.

[FCC02] *First Report and Order, Revision of Part 15 of the Commission's Rules Regarding Ultra-Wideband Transmission Systems*, April 2002, FCC, Washington, DC. ET Docket 98-153, FCC 02-48.

[Fen03] L. Feng, W. Namgoong, "Joint Estimation and Detection of UWB Signals with Timing Offset Error and Unknown Channel", *Proc. IEEE Conference on Ultra Wideband Systems and Technologies*, pags. 152–156, 16-19 November 2003.

[Foe03] J. Foerster, *Channel Modeling Sub-Committee Report (Final)*, IEEE P802.15 Working Group for Wireless Personal Area Networks (WPANs), February 2003.

[For06] A. Fort, J. Ryckaert, C. Desset, P. De Doncker, P. Wambacq, L. Van Biesen, "Ultra-Wideband Channel Model for Communications Around the Human Body", *IEEE J. Select. Areas Commun.*, Vol. 24, nº 4, pags. 927–933, April 2006.

[Fra03] S. Franz, U. Mitra, "On Optimal Data Detection for UWB Transmitted Reference Systems", *Proceedings IEEE Global Conference on Communications (GLOBECOM)*, Vol. 2, pags. 744–748, 1-5 December 2003.

[Gal68] R. G. Gallager, *Information Theory and Reliable Communication*, John Wiley and Sons, New York, NY, 1968.

[Gar80] F. M. Gardner, "Self-Noise in Synchronizers", *IEEE Trans. Commun.*, Vol. 28, pags. 1159–1163, August 1980.

[Gar88] F. M. Gardner, *Demodulator Reference Recovery Techniques Suited for Digital Implementation*, Final Report: ESTEC Contract No. 6847/86/NL/DG, European Space Agency, 1988.

[Gee06] D. Geer, "UWB Standardization Efforts Ends in Controversy", *IEEE Computer*, Vol. 39, nº 7, pags. 13–16, July 2006.

[Gez02] S. Gezici, E. Fishler, H. Kobayashi, H. V. Poor, A. F. Molisch, "A Rapid Acquisition Technique for Impulse Radio", *Proc. Pacific Communications, Computers and Signal Processing*, Vol. 2, pags. 627–630, 28-30 August 2002.

[Gez04] S. Gezici, H. Kobayashi, H. V. Poor, A. F. Molisch, "Optimal and Suboptimal Linear Receivers for Time-Hopping Impulse Radio Systems", *Proc. International Workshop on Ultra Wideband Systems (IWUWBS) Joint with Conference on Ultra Wideband Systems and Technologies (UWBST)*, pags. 11–15, 18-21 May 2004.

[Gez05] S. Gezici, Z. Tian, G. B. Giannakis, H. Kobayashi, A. F. Molisch, H. V. Poor, Z. Sahinoglu, "Localization via Ultra-Wideband Radios: A Look at Positioning Aspects for Future Sensor Networks", *IEEE Signal Processing Mag.*, Vol. 22, nº 4, pags. 70–84, July 2005.

[Gha04] M. Ghavami, L. B. Michael, R. Kohno, *Ultra Wideband Signals and Systems in Communication Engineering*, John Wiley & Sons, 2004.

[Gia97] G. B. Giannakis, S. D. Halford, "Asymptotically Optimal Blind Fractionally Spaced Channel Estimation and Performance Analysis", *IEEE Trans. Signal Processing*, Vol. 45, pags. 1815–1830, July 1997.

[Git92] R. D. Gitlin, J. F. Hayes, S. B. Weinstein, *Data Communications Principles*, Plenum Press, 1992.

[Gol49] M. J. Golay, "Note on the Theoretical Efficiency of Information Reception with PPM", *Proceedings of the IRE*, Vol. 37, pags. 1031, 1949.

[Gol96] G. H. Golub, C. F. Van Loan, *Matrix Computations*, Johns Hopkins University Press, 1996.

[Gué05] E. Guéguen, F. Thudor, P. Chambelin, "A Low Cost UWB Printed Dipole Antenna with High Performance", *Proc. IEEE International Conference on Ultra-Wideband*, pags. 89–92, 5-8 September 2005.

[Gur05a] M. C. Gursoy, H. V. Poor, S. Verdú, "The Noncoherent Rician Fading Channel. Part I: Structure of the Capacity-Achieving Input", *IEEE Trans. Wireless Commun.*, Vol. 4, nº 5, pags. 2193–2206, September 2005.

[Gur05b] M. C. Gursoy, H. V. Poor, S. Verdú, "The Noncoherent Rician Fading Channel. Part II: Spectral Efficiency in the Low-Power Regime", *IEEE Trans. Wireless Commun.*, Vol. 4, nº 5, pags. 2207–2221, September 2005.

[Ham04] J. Hamkins, B. Moision, "Selection of Modulation and Codes for Deep Space Optical Communications", *Proc. of SPIE, Free-Space Laser Communication Technologies XIV*, Vol. 5338, pags. 123–130, 2004.

[Har68] H. F: Harmuth, "A generalized concept of frequency and some applications", *IEEE Trans. Inform. Theory*, Vol. 14, nº 3, pags. 375–381, May 1968.

[Har69a] H. F. Harmuth, "Applications of Walsh Functions in Communications", *IEEE Spectr.*, pags. 82–91, November 1969.

[Har69b] H. F. Harmuth, *Transmission of Information by Orthogonal Functions*, Springer Verlag, 1969.

[Har79] H. F. Harmuth, "Comments on "Some Physical Constraints on the Use of "Carrier-Free" Waveforms in Radio-Wave Transmission Systems"", *Proc. IEEE*, Vol. 67, nº 6, pags. 890–891, June 1979.

[Har00] D. A. Harville, *Matrix Algebra from a Statistician's Perspective*, Springer, 2000.

[Har04] R. Harjani, J. Harvey, R. Sainati, "Analog/RF Physical Layer Issues for UWB Systems", *Proc. 17th International Conference on VLSI Design*, pags. 941–948, 2004.

[Hay05] S. Haykin, "Cognitive Radio: Brain-Empowered Wireless Communications", *IEEE J. Select. Areas Commun.*, Vol. 23, nº 2, pags. 201–220, February 2005.

[Hoc02] R. T. Hoctor, H. W. Tomlinson, *An Overview of Delay-Hopped, Transmitted-Reference RF Communications*, January 2002, G. E. Research and Development Center, Technical Information Series, pp. 1-29.

[Hoe61] C. H. Hoeppner, *Pulse Communication System*, 5 September 1961, U.S. Patent 2.999.128.

[Hom02] E. A. Homier, R. A. Scholtz, "Rapid Acquisition of Ultra-Wideband Signals in the Dense Multipath Channel", *Proc. IEEE Conf. on Ultra Wideband Systems and Technologies*, pags. 105–109, 21-23 May 2002.

[hop01] "Final Report, UWB-GPS Compatibility Analysis Project", 8 March 2001, John Hopkins University, Applied Physics Laboratory.

[Hoy03] S. Hoyos, B. M. Sadler, G. R. Arce, "Dithering and Sigma-Delta Modulation in Monobit Digital Receivers for Ultra-Wideband Communications", *Proc. IEEE Conf. on Ultra Wideband Systems and Technologies*, pags. 71–75, 16-19 November 2003.

[Hoy04] S. Hoyos, B. Sadler, G. R. Arce, "High-Speed A/D Conversion for Ultra-Wideband Signals Based on Signal Projection over Basis Functions", *Proc. IEEE International Conference on Acoustics, Speech and Signal Processing (ICASSP)*, Vol. 4, pags. 537–540, 17-21 May 2004.

[Hoy05] S. Hoyos, B. Sadler, G. R. Arce, "Monobit Digital Receivers for Ultrawideband Communications", *IEEE Trans. Wireless Commun.*, Vol. 4, nº 4, pags. 1337–1344, July 2005.

[Hua96a] Y. Hua, "Fast Maximum Likelihood for Blind Identification of Multiple FIR Channels", *IEEE Trans. Signal Processing*, Vol. 44, nº 3, pags. 661–672, March 1996.

[Hua96b] Y. Hua, M. Waz, "Strict Identifiability of Multiple FIR Channels Driven by an Unknown Arbitrary Sequence", *IEEE Trans. Signal Processing*, Vol. 44, nº 3, pags. 756–759, March 1996.

[Hua02] Y. Huang, J. Benesty, "Adaptive Blind Channel Identification: Multi-Channel Least Mean Square and Newton Algorithms", *Proc. International Conference on Acoustics, Speech and Signal Processing (ICASSP)*, Vol. 2, pags. 1637–1640, 2002.

[Int04] Intel, *Ultra-Wideband (UWB Technology). Enabling High-Speed Wireless Personal Area Networks*, Intel Corporation, 2004, Available at: http://www.intel.com/technology/ultrawideband/downloads/Ultra-Wideband.pdf.

[Int05a] Intel, *Ultra-Wideband (UWB Technology). One Step Closer to Wireless Freedom*, Intel Corporation, 2005, Available at: http://www.intel.com/technology/comms/uwb/download/wireless%5Fpb.pdf.

[Int05b] Intel, *Wireless USB. The First High-Speed Personal Wireless Interconnect*, Intel Corporation, 2005, Available at: http://www.intel.com/technology/comms/wusb/download/wirelessUSB.pdf.

[Jac63] I. Jacobs, "The Asymptotic Behavior of Incoherent M-ary Communication Systems", *Proceedings of the IRE*, Vol. 51, nº 1, pags. 251–252, 1963.

[Jef46] H. Jeffreys, "An Invariant Form for the Prior Probability in Estimation Problems", *Proc. Roy. Soc. Lon.*, A, pags. 453–461, 1946.

[Kar04] J. Karedal, S. Wyne, P. Almers, F. Tufvesson, A. F. Molisch, "Statistical Analysis of the UWB Channel in an Industrial Environment", *Proc. IEEE Vehicular Technology Conference (VTC-Fall)*, pags. 81–85, 2004.

[Kay93] S. M. Kay, *Fundamentals of Statistical Signal Processing. Estimation Theory*, Vol. I, Prentice Hall, 1993.

[Kay98] S. M. Kay, *Fundamentals of Statistical Signal Processing. Detection Theory*, Vol. II, Prentice Hall, 1998.

[Kay05a] S. M. Kay, "Exponentially Embedded Families-New Approaches to Model Order Estimation", *IEEE Trans. Aerosp. Electron. Syst.*, Vol. 41, nº 1, pags. 333–345, January 2005.

[Kay05b] S. M. Kay, "The Multifamily Likelihood Ratio Test for Multiple Signal Model Detection", *IEEE Signal Processing Lett.*, Vol. 12, nº 5, pags. 369–371, May 2005.

[Ken69] R. S. Kennedy, *Fading Dispersive Communication Channels*, John Wiley and Sons, New York, NY, 1969.

[Kol04] R. Kolic, "Ultra Wideband - The Next-Generation Wireless Connection", *Technology @ Intel Magazine*, pags. 1–6, February/March 2004, Available at: http://www.intel.com/technology/magazine/communications/wi02042.pdf.

[Kon05] W. Kong, Y. Zhu, G. Wang, "Effects of Pulse Distortion in UWB Radiation on UWB Impulse Communications", *Proc. International Conference on Wireless Communications, Networking and Mobile Computing (WCNM)*, Vol. 1, pags. 344–347, Sept. 23-26 2005.

[Kul97] S. Kullback, *Information Theory and Statistics*, Dover Publications, 1997.

[Lam10] H. Lamb, "The Diffraction of a Solitary Wave", *Proceedings of the London Mathematical Society*, Vol. 2, nº 8, pags. 422–437, 1910.

[Le05] B. Le, T. W. Rondeau, J. H. Reed, C. W. Bostian, "Analog-to-Digital Converters", *IEEE Signal Processing Mag.*, Vol. 22, nº 6, pags. 69–77, November 2005.

[Lee04] J.-Y. Lee, S. Choi, "Through-Material Propagation Characteristic and Time Resolution of UWB Signal", *Proc. International Workshop on Ultra Wideband Systems (IWUWBS) Joint with Conference on Ultra Wideband Systems and Technologies (UWBST)*, pags. 71–75, 18-21 May 2004.

[Li00] Y. Li, X. Huang, "The Spectral Evaluation and Comparison for Ultra-Wideband Signals with Different Modulation Schemes", *Proc. World Multiconf. on Systemics, Cybernetics and Informatics (SCI)*, pags. 277–282, July 2000.

[Li05] X. Li, E. J. Bond, B. D. Veen, C. S. Hagness, "An overview of ultra-wideband microwave imaging via space-time beamforming for early-stage breast-cancer detection", *IEEE Antennas Propagat. Mag.*, Vol. 47, nº 1, pags. 19–34, February 2005.

[Liu94] H. Liu, G. Xu, L. Tong, "A Deterministic Approach to Blind Identification of Multichannel FIR Systems", *Proc. IEEE International Conference on Acoustics, Speech and Signal Processing (ICASSP)*, Vol. IV, pags. 581–584, 19-22 April 1994.

[Liu96] H. Liu, G. Xu, L. Tong, T. Kailath, "Recent Developments in Blind Channel Equalization: From Cyclostationarity to Subspaces", *Signal Processing, Elsevier*, Vol. 50, pags. 83–99, 1996.

[Lot00] V. Lottici, A. D'Andrea, U. Mengali, "Channel estimation for ultra-wideband communications", *IEEE J. Select. Areas Commun.*, Vol. 20, nº 9, pags. 1638–1645, December 2000.

[Lou00] P. Loubaton, E. Moulines, P. Regalia, *Signal Processing Advances in Wireles and Mobile Communications*, Vol. 1, Prentice-Hall, 2000, Chapter 3: Subspace Method for Blind Identification and Deconvolution.

[Lov02] W. M. Lovelace, J. K. Townsend, "The Effects of Timing Jitter and Tracking on the Performance of Impulse Radio", *IEEE J. Select. Areas Commun.*, Vol. 20, nº 9, pags. 1646–1651, December 2002.

[Low05] Z. N. Low, J. H. Cheong, C. L. Law, "Low-Cost PCB Antenna for UWB Applications", *IEEE Antennas Wireless Propagat. Lett.*, Vol. 4, pags. 237–239, 2005.

[LS04] J. A. López-Salcedo, G. Vázquez, "Frequency Domain Iterative Pulse Shape Estimation Based on Second Order Statistics", *Proc. 5th IEEE Workshop on Signal Processing Advances in Wireless Communications (SPAWC)*, Lisbon, Portugal, 11-14 July 2004.

[Luo00] M. Luo, D. Akos, S. Pullen, P. Enge, *Potential Interference to GPS from UWB Transmitters, Test Results. Phase 1A: Accuracy and Loss-of-Lock Testing for Aviation Receivers*, Stanford University, 26 October 2000.

[Luo02] C. Luo, M. Médard, "Frequency-Shift Keying for Ultrawideband. Achieving Rates on the Order of Capacity", *Proc. 40th Annual Allerton Conference on Communication, Control and Computing*, Monticello, Illinois (USA), October 2002.

[Luo05] X. Luo, G. B. Giannakis, "Blind Timing Acquisition for Ultra-Wideband Multi-User Ad-Hoc Access", *Proc. IEEE International Conference on Acoustics, Speech and Signal Processing (ICASSP)*, Vol. III, pags. 313–316, 18-23 March 2005.

[Mar00] C. J. Le Martret, G. B. Giannakis, "All-Digital PAM Impulse Radio for Multiple-Access Through Frequency-Selective Multipath", *IEEE Global Conference on Communications (GLOBECOM)*, Vol. 1, pags. 77–81, 27 Nov. - 1 Dec. 2000.

[Mas76] J. L. Massey, "All Signal Sets Centered About the Origin are Optimal at Low Energy-to-Noise Ratios on the AWGN Channel", *Proc. IEEE International Symposium on Information Theory (ISIT)*, pags. 80–81, June 1976.

[Men97] U. Mengali, A. N. D'Andrea, *Synchronization Techniques for Digital Receivers*, Plenum Press, 1997.

[Men05] A. Menouni, R. Knopp, R. Saadane, "Subspace Analysis of Indoor UWB Channels", *EURASIP Journal on Applied Signal Processing*, Vol. 3, pags. 287–295, 2005.

[Mie03] B. Mielczarek, M. O. Wessman, A. Svensson, "Performance of Coherent UWB RAKE Receivers with Channel Estimators", *Proc. IEEE Vehicular Technology Conference Fall*, Vol. 3, pags. 1880–1884, 6-9 October 2003.

[Mir01] F. Ramirez Mireles, "On the Performance of Ultra-Wide-Band Signals in Gaussian Noise and Dense Multipath", *IEEE Trans. Veh. Technol.*, Vol. 50, nº 1, pags. 244–249, January 2001.

[Mof76] D. L. Moffatt, R. J. Puskar, "A Subsurface Electromagnetic Pulse Radar", *Geophysics*, , nº 41, pags. 506–518, 1976.

[Mol04] A. F. Molisch, *IEEE 802.15.4a Channel Model Final Report*, IEEE P802.15 Working Group for Wireless Personal Area Networks (WPANs), November 2004.

[Mol05] A. F. Molisch, "Ultrawideband Propagation Channels-Theory, Measurement and Modeling", *IEEE Trans. Veh. Technol.*, Vol. 54, nº 5, pags. 1528–1545, September 2005.

[Mor74] R. N. Moray, *Geophysical Survey System Employing Electromagnetic Pulses*, April 1974, U.S. Patent 3.806.795.

[Mou95] E. Moulines, P. Duhamel, J.-F. Cardoso, S. Mayrargue, "Subspace Methods for the Blind Identification of Multichannel FIR Filters", *IEEE Trans. Signal Processing*, Vol. 43, nº 2, pags. 516–525, February 1995.

[Nak03] Y.-P. Nakache, A. F. Molisch, "Spectral Shape of UWB Signals - Influence of Modulation Format, Multiple Access Scheme and Pulse Shape", *Proc. 57th IEEE Semiannual Conference on Vehicular Technology (VTC-Spring)*, Vol. 4, pags. 2510–2514, 22-25 April 2003.

[Nam03] W. Namgoong, "A Channelized Digital Ultrawideband Receiver", *IEEE Trans. Wireless Commun.*, Vol. 2, nº 3, pags. 502–510, May 2003.

[Nos04] H. Nosaka, M. Nakamura, M. Ida, K. Kurishima, T. Shibata, M. Tokumitsu, M. Muraguchi, "A 24-Gsps 3-bit Nyquist ADC using InP HBTs for Electronic Dispersion Compensation", *Proc. IEEE MTT-S International Microwave Symposium*, Vol. 1, pags. 101–104, 6-11 June 2004.

[Oh05] M.-K. Oh, B. Jung, R. Harjani, D.J. Park, "A New Noncoherent UWB Impulse Radio Receiver", *IEEE Commun. Lett.*, Vol. 9, nº 2, pags. 151–153, February 2005.

[Ott93] B. Ottersten, M. Viberg, P. Stoica, A. Nehorai, *Radar Array Processing*, Springer-Verlag, 1993, Chapter 4: Maximum Likelihood Techniques for Parameter Estimation.

[Par03] B. Parr, B. Cho, K. Wallace, Z. Ding, "A Novel Ultra-Wideband Pulse Design Algorithm", *IEEE Commun. Lett.*, Vol. 7, nº 4, pags. 219–221, Mayy 2003.

[Pie66] J. R. Pierce, "Ultimate Performance of M-ary Transmissions on Fading Channels", *IEEE Trans. Inform. Theory*, Vol. 12, nº 1, pags. 2–5, 1966.

[Por05] D. Porrat, "Information Theory of Wideband Communications. A Tutorial", 2005, http://www.cs.huji.ac.il/ dporrat/WidebandTutorial.pdf.

[Pri58] R. Price, P. E. Green, "A Communication Technique for Multipath Channels", *Proceedings of the IRE*, Vol. 46, pags. 555–570, March 1958.

[Pro94] J. G. Proakis, M. Salehi, *Communication Systems Engineering*, Prentice-Hall International Editions, 1994.

[Pro01] J. G. Proakis, *Digital Communications*, McGraw-Hill, 4th Edition, international edition ed., 2001.

[Qiu95] R. C. Qiu, *Time/Frequency Dispersion of Digital Transmission Media*, PhD Thesis, Polytechnic University, Brooklyn, New York, 1995.

[Qiu96] R. C. Qiu, "Wideband Wireless Multipath Channel Modeling with Path Frequency Dependence", *Proc. IEEE International Conference on Communications (ICC)*, Vol. 1, pags. 277–281, Dallas, Texas, USA, 23-27 June 1996.

[Qiu02] R. C. Qiu, "A Study of the Ultra-Wideband Wireless Propagation Channel and Optimum UWB Receiver Design", *IEEE J. Select. Areas Commun.*, Vol. 20, nº 9, pags. 1628–1637, December 2002.

[Qiu04] R. C. Qiu, "A Generalized Time Domain Multipath Channel and Optimal Receiver Design - Part II: Physics-Based System Analysis", *IEEE Trans. Wireless Commun.*, Vol. 3, nº 6, pags. 2312–2324, November 2004.

[Qiu05] R. C. Qiu, C. Zhou, Q. Liu, "Physics-Based Pulse Distortion for Ultra-Wideband Signals", *IEEE Trans. Veh. Technol.*, Vol. 54, nº 5, pags. 1546–1555, September 2005.

[Rab04a] A. Rabbachin, I. Oppermann, "Synchronization Analysis for UWB Systems with a Low-Complexity Energy Collection Receiver", *2004 International Workshop on Ultra Wideband Systems (IWUWBS) Joint with Conference on Ultra Wideband Systems and Technologies (UWBST)*, pags. 288–292, Kyoto, Japan, May 2004.

[Rab04b] A. Rabbachin, L. Stoica, S. Tiuraniemi, I. Oppermann, "A Low Cost, Low Power UWB Based Sensor Network", *Proc. International Workshop on Wireless Ad-Hoc Networks*, pags. 84–88, 31 May - 3 June 2004.

[Rao04] C. Rao, B. Hassibi, "Analysis of Multiple-Antenna Wireless Links at Low SNR", *IEEE Trans. Inform. Theory*, Vol. 50, nº 9, pags. 2123–2130, September 2004.

[Reg05] L. Reggiani, G. M. Maggio, "Rapid Search Algorithms for Code Acquisition in UWB Impulse Radio Communications", *IEEE J. Select. Areas Commun.*, Vol. 23, nº 5, pags. 898–908, May 2005.

[Ros54] L. A. De Rosa, *Random Impulse System*, 9 March 1954, U.S. Patent 2.671.896.

[Ros73] G. F. Ross, K. W. Robbins, *Base-Band Radiation and Reception System*, 12 June 1973, U.S. Patent 3.739.392.

[Ros86] G. F. Ross, *Early Developments and Motivations for Time-Domain Analysis and Applications. Time-Domain Measurements in Electromagnetics*, Van Nostrand Reinhold, 1986.

[Rus64] C. K. Rushforth, "Transmitted-Reference Techniques for Random or Unknown Channels", *IEEE Trans. Inform. Theory*, Vol. 10, nº 1, pags. 39–42, January 1964.

[Saa04] R. Saadane, A. Menouni, R. Knopp, D. Aboutajdine, "Empirical Eigenanalysis of Indoor UWB Propagation Channels", *Proc. IEEE Global Conference on Communications (GLOBECOM)*, pags. 3215–3219, December 2004.

[Sah05] M. E. Sahin, H. Arslan, "Narrowband Interference Identification Approach for UWB Systems", *Proc. IEEE Military Communications Conference (MILCOM)*, Vol. 3, pags. 1404–1408, 17-20 October 2005.

[Sal87] A. Saleh, R. Valenzuela, "A Statistical Model for Indoor Multipath Propagation", *IEEE J. Select. Areas Commun.*, Vol. 5, nº 2, pags. 128–137, February 1987.

[Sch93] R. A. Scholtz, "Multiple Access with Time-Hopping Impulse Modulation", *Proc. IEEE Conference on Military Communications (MILCOM)*, Vol. 2, pags. 447–450, October 1993.

[Sch05a] R. A. Scholtz, D. M. Pozar, W. Namgoong, "Ultra-Wideband Radio", *EURASIP Journal on Applied Signal Processing*, Vol. 2005, nº 3, pags. 252–272, 2005.

[Sch05b] U. G. Schuster, H. Bölcskei, "How Different are UWB Channels from Conventional Wideband Channels?", *Proc. International Workshop on Convergent Technologies*, Oulu, Finland, June 2005.

[Sch05c] U. G. Schuster, H. Bölcskei, "Ultra-Wideband Channel Modeling on the Basis of Information-Theoretic Criteria", *Proc. International Symposium on Information Theory (ISIT)*, pags. 97–101, 4-9 September 2005.

[Sch06] B. Schechner, *Ultrawideband Shipments to Reach Nearly 300 Million in 2011 Despite Apparent Barriers*, ABI Research, 15 May 2006, Available at: http://www.abiresearch.com/abiprdisplay.jsp?pressid=648.

[Sha48] C. E. Shannon, "A Mathematical Theory of Communication", *Bell Syst. Tech. J.*, Vol. 27, July-Oct. 1948.

[She03] H. Sheng, A. M. Haimovich, A. F. Molisch, J. Zhang, "Optimum Combining for Time Hopping Impulse Radio UWB RAKE Receivers", *Proc. IEEE Conference on Ultra Wideband Systems and Technologies*, pags. 224–228, 16-19 November 2003.

[Slo94] D. Slock, "Blind Factionally-Spaced Equalization, Perfect Reconstruction, Filterbanks, and Multilinear Prediction", *Proc. IEEE International Conference on Acoustics, Speech and Signal Processing (ICASSP)*, Vol. 4, pags. 585–588, April 1994.

[Som01] A. Sommerfield, "Theoretisches Uber die Beugung der Roentgenstrahlen", *Zeitschrift für Mathematik und Physik*, Vol. 46, pags. 11–97, 1901.

[Sou03] Y. Souilmi, R. Knopp, "On the Achievable Rates of Ultra-Wideband PPM with Non-Coherent Detection in Multipath Environments", *Proc. IEEE International Conference on Communications (ICC)*, Vol. 5, pags. 3530–3534, Anchorage, Alaska, USA, 11-15 May 2003.

[Sto04] L. Stoica, S. Tiuraniemi, H. Repo, A. Rabbachin, I. Oppermann, "Low Complexity UWB Circuit Transceiver Architecture for Low Cost Sensor Tag Systems", *Proc. IEEE International Symposium on Personal, Indoor and Mobile Radio Communications (PIMRC)*, Vol. 1, pags. 196–200, 5-8 September 2004.

[Sun93] F. W. Sun, H. C. Van Tilborg, "Approaching Capacity by Equiprobable Signaling on the Gaussian Channel", *IEEE Trans. Inform. Theory*, Vol. 39, pags. 1714–1716, September 1993.

[Tan05a] J. Tang, Z. Xu, "A Novel Modulation Diversity Assisted Ultra-Wideband Communication System", *Proc. IEEE International Conference on Acoustics, Speech and Signal Processing (ICASSP)*, Vol. 3, pags. 309–312, Philadelphia, USA, March 2005.

[Tan05b] J. Tang, Z. Xu, B. M. Sadler, "Digital Receiver for TR-UWB Systems with Inter-Pulse Interference", *Proc. 6th IEEE Workshop on Signal Processing Advances in Wireless Communications (SPAWC)*, pags. 420–424, 5-8 June 2005.

[Tay94] J. D. Taylor, *Introduction to Ultra-Wideband Radar Systems*, CRC Press, 1994.

[Tel00] I. E. Telatar, D. N. Tse, "Capacity and Mutual Information of Wideband Multipath Fading Channels", *IEEE Trans. Inform. Theory*, Vol. 46, nº 4, pags. 1384–1400, 2000.

[Tia02] Z. Tian, L. Yang, G. B. Giannakis, "Symbol Timing Estimation in Ultra Wideband Communications", *Proc. 36th Asilomar Conference on Signals, Systems and Computers*, Vol. 2, pags. 1924–1928, Pacific Grove, California, USA, 3-6 November 2002.

[Tia05a] Z. Tian, H. Ge, L. L. Scharf, "Low-Complexity Multiuser Detection and Reduced-Rank Wiener Filters for Ultra-Wideband Multiple Access", *Proc. IEEE International Conference on Acoustics, Speech and Signal Processing (ICASSP)*, Vol. 3, pags. 621–624, 18-23 March 2005.

[Tia05b] Z. Tian, G. B. Giannakis, "BER Sensitivity to Mistiming in Ultra-Wideband Impulse Radios - Part I: Nonrandom Channels", *IEEE Trans. Signal Processing*, Vol. 53, nº 4, pags. 1550–1560, April 2005.

[Tia05c] Z. Tian, G. B. Giannakis, "BER Sensitivity to Mistiming in Ultra-Wideband Impulse Radios - Part II: Fading Channels", *IEEE Trans. Signal Processing*, Vol. 53, nº 5, pags. 1897–1907, May 2005.

[Tia05d] Z. Tian, G. B. Giannakis, "A GLRT Approach to Data-Aided Timing Acquisition in UWB Radios - Part I: Algorithms", *IEEE Trans. Wireless Commun.*, Vol. 4, nº 6, pags. 2956–2967, November 2005.

[Tia05e] Z. Tian, G. B. Giannakis, "A GLRT Approach to Data-Aided Timing Acquisition in UWB Radios - Part II: Training Sequence Design", *IEEE Trans. Wireless Commun.*, Vol. 4, nº 6, pags. 2994–3004, November 2005.

[Ton91] L. Tong, G. Xu, T. Kailath, "A New Approach to Blind Identification and Equalization of Multipath Channels", *Proc. 25th Asilomar Conference on Signals, Systems and Computers*, Vol. 2, pags. 856–860, Pacific Grove, California, USA, 4-6 November 1991.

[Ton94] L. Tong, G. Xu, T. Kailath, "Blind Identification and Equalization Based on Second-order Statistics: A Time Domain Approach", *IEEE Trans. Inform. Theory*, Vol. 40, nº 2, pags. 340–349, March 1994.

[Ton98] L. Tong, S. Perreau, "Multichannel Blind Identification: From Subspace Methods to Maximum Likelihood Methods", *Proc. IEEE*, Vol. 86, nº 10, pags. 1951–1968, October 1998.

[Tre83] J. R. Treichler, B. G. Agee, "A New Approach to Multipath Correction of Constant Modulus Signals", *IEEE Trans. Acoust., Speech, Signal Processing*, Vol. 31, pags. 459–472, April 1983.

[Tur59] G. L. Turin, "The Asymptotic Behavior of Ideal M-ary Systems", *Proceedings of the IRE*, Vol. 47, pags. 93–94, 1959.

[Ung82] G. Ungerboeck, "Channel Coding with Multilevel/Phase Signals", *IEEE Trans. Inform. Theory*, Vol. 28, nº 1, pags. 55–67, January 1982.

[Van03] H. L. VanTrees, *Detection, Estimation, and Modulation Theory*, Vol. I, John Wiley and Sons, 2001-2003.

[Vee05] A. J. van der Veen, A. Leshem, *Robust Adaptive Beamforming*, Wiley Interscience, 2005, Chapter 6: Constant Modulus Beamforming.

[Ver02a] S. Verdú, "Recent Results on the Capacity of Wideband Channels in the Low-Power Regime", *IEEE Wireless Commun. Mag.*, Vol. 9, nº 4, pags. 40–45, August 2002.

[Ver02b] S. Verdú, "Spectral Efficiency in the Wideband Regime", *IEEE Trans. Inform. Theory*, Vol. 48, nº 6, pags. 1319–1343, June 2002.

[Vil05] J. Villares, G. Vazquez, "Second-Order Parameter Estimation", *IEEE Trans. Signal Processing*, Vol. 53, pags. 2408–2420, July 2005.

[Váz00] G. Vázquez, J. Riba, *Signal Processing Advances in Wireless and Mobile Communications*, Vol. 2, Prentice-Hall, 2000, Chapter 9: Non-Data-Aided Digital Synchronization.

[Wal99] R. H. Walden, "Analog-to-digital converter survey and analysis", *IEEE J. Select. Areas Commun.*, Vol. 17, nº 4, pags. 539–550, April 1999.

[Wan05] S. B.-T. Wang, *Design of Ultra-Wideband RF Front-End*, PhD Thesis, University of California, Berkeley, 2005, Available at: http://bwrc.eecs.berkeley.edu/Publications/2005/THESES/S. Wang/S. BoTing Wang Thesis.pdf.

[Wei04] M. Weisenhorn, W. Hirt, "Robust Noncoherent Receiver Exploiting UWB Channel Properties", *Proc. International Workshop on Ultra Wideband Systems (IWUWBS) Joint with Conference on Ultra Wideband Systems and Technologies (UWBST)*, pags. 156–160, Kyoto, Japan, May 2004 2004.

[Wei05] M. Weisenhorn, W. Hirt, "ML Receiver for Pulsed UWB Signals and Partial Channel State Information", *Proc. IEEE International Conference on Ultra-Wideband*, pags. 180–185, 5-8 September 2005.

[Wil03] R. D. Wilson, R. A. Scholtz, "Template Estimation in Ultra-Wideband Radio", *Proc. 37th Asilomar Conference on Signals, Systems and Computers*, Vol. 2, pags. 1244–1248, 9-12 November 2003.

[Win97] M. Z. Win, R. A. Scholtz, "Energy Capture vs. Correlator Resources in Ultra-Wide Bandwidth Indoor Wireless Communications Systems", *Proc. IEEE Conference on Military Communications (MILCOM)*, Vol. 3, pags. 1277–1281, 2-5 November 1997.

[Win98] M. Z. Win, R. A. Scholtz, "Impulse Radio: How It Works", *IEEE Commun. Lett.*, Vol. 2, nº 2, pags. 36–38, February 1998.

[Win00] M. Z. Win, R. A. Scholtz, "Ultra-Wide Bandwidth Time-Hopping Spread-Spectrum Impulse Radio for Wireless Multiple-Access Communications", *IEEE Trans. Commun.*, Vol. 48, nº 4, pags. 679–691, April 2000.

[Win02] M. Z. Win, "Spectral Density of Random UWB Signals", *IEEE Commun. Lett.*, Vol. 6, nº 12, pags. 526–528, December 2002.

[Woo00] J. P. Woodard, "Comparative Study of Turbo Decoding Techniques: An Overview", *IEEE Trans. Veh. Commun.*, Vol. 49, nº 6, pags. 2208–2233, November 2000.

[Woz65] J. M. Wozencraft, I. M. Jacobs, *Principles of Communications Engineering*, Waveland Press, 1965.

[Wu04] X. Wu, Z. Tian, T. N. Davidson, G. B. Giannakis, "Orthogonal waveform design for uwb radios", *Proc. 5th IEEE Workshop on Signal Processing Advances in Wireless Communications (SPAWC)*, pags. 150–154, 11-14 July 2004.

[Wu06] J.-Y. Wu, T.-S. Lee, "Periodic-Modulation-Based Blind Channel Identification for Single-Carrier Block Transmission with Frequency-Domain Equalization", *IEEE Trans. Signal Processing*, Vol. 54, nº 3, pags. 1114–1130, March 2006.

[Xu95] G. Xu, H. Liu, L. Tong, T. Kailath, "A Least-Squares Approach to the Blind Channel Identification", *IEEE Trans. Signal Processing*, Vol. 43, nº 12, pags. 2982–2993, December 1995.

[Xu01] Z. Xu, "Asymptotically Near-Optimal Blind Estimation of Multipath CDMA Channels", *IEEE Trans. Signal Processing*, Vol. 49, nº 9, pags. 2003–2017, September 2001.

[Xu03a] Z. Xu, "Blind Channel Estimation via Subspace Approximation", *Proc. 37th Asilomar Conference on Signals, Systems and Computers*, Vol. 2, pags. 1653–1657, 9-12 November 2003.

[Xu03b] Z. Xu, J. Tang, P. Liu, "Blind Channel Estimation for Multiple Access UWB Communications Based on Periodic Time Hopping and Pulse-Rate Modeling", *Proc. IEEE Topical Conference on Wireless Communication Technology*, pags. 453–454, 15-17 October 2003.

[Yan03a] L. Yang, G. B. Giannakis, "Low-Complexity Training for Rapid Timing Acquisition in Ultra Wideband Communications", *Proc. IEEE Global Conference on Communications (GLOBECOM)*, Vol. 2, pags. 769–773, 1-5 December 2003.

[Yan03b] L. Yang, Z. Tian, G. B. Giannakis, "Non-Data Aided Timing Acquisition of Ultra-Wideband Transmissions Using Cyclostationarity", *Proc. International Conference on Acoustics, Speech and Signal Processing*, Vol. 4, pags. 121–124, 6-10 April 2003.

[Yan04a] L. Yang, G. B. Giannakis, "Blind UWB Timing with a Dirty Template", *Proc. IEEE International Conference on Acoustics, Speech and Signal Processing (ICASSP)*, Vol. IV, pags. 509–512, Montreal (Canada), 17-21 May 2004.

[Yan04b] L. Yang, G. B. Giannakis, "Ultra-Wideband Communications: An Idea Whose Time Has Come", *IEEE Signal Processing Mag.*, Vol. 21, nº 6, pags. 26–54, November 2004.

[Yan04c] L. Yang, G. B. Giannakis, A. Swami, "Noncoherent Ultra-Wideband Radios", *Proc. IEEE Conference on Military Communications (MILCOM)*, Vol. 2, pags. 786–791, Monterey, California, USA, 31 October - 3 November 2004.

[Yan05] L. Yang, G. B. Giannakis, "Timing Ultra-Wideband Signals with Dirty Templates", *IEEE Trans. Commun.*, Vol. 53, nº 11, pags. 1952–1963, November 2005.

[Yan06] L. Yang, A. Swami, "Noncoherent Demodulator for PPM-UWB Radios", *Proc. IEEE International Conference on Acoustics, Speech and Signal Processing (ICASSP)*, Vol. 4, pags. 501–504, 14-19 May 2006.

[Yao04] W. Yao, Y. Wang, "Direct Antenna Modulation - A Promise for Ultra-Wideband (UWB) Transmitting", *Proc. IEEE MTT-S International Microwave Symposium*, Vol. 2, pags. 1273–1276, 6-11 June 2004.

[Yaz04] K. Y. Yazdandoost, R. Kohno, "Ultra Wideband Antenna", *IEEE Commun. Mag.*, Vol. 42, nº 6, pags. 29–32, June 2004.

[Yaz05] K. Y. Yazdandoost, R. Kohno, "Slot Antenna for Ultra Wideband System", *Proc. IEEE/ACES International Conference on Wireless Communications and Applied Computational Electromagnetics*, pags. 212–216, 3-7 April 2005.

[Yin04] Z. Ying, J. Andersson, "An Ultra Wideband "Cobra" Patch Antenna", *IEE Proceedings in Microwaves, Antennas and Propagation*, Vol. 151, nº 6, pags. 486–490, December 2004.

[Zar05] K. Zarifi, A. B. Gershman, "Enhanced Blind Subspace-Based Signature Waveform Estimation in CDMA Systems with Circular Noise", *Proc. IEEE International Conference on Acoustics, Speech and Signal Processing (ICASSP)*, Vol. 3, pags. 937–940, 18-23 March 2005.

[Zen97a] H. H. Zeng, L. Tong, "Blind Channel Estimation Using the Second-Order Statistics: Asymptotic Performance and Limitations", *IEEE Trans. Signal Processing*, Vol. 45, nº 8, pags. 2060–2071, August 1997.

[Zen97b] H. H. Zeng, L. Tong, "Blind Channel Estimation Using the Second-Order Statistics: Algorithms", *IEEE Trans. Signal Processing*, Vol. 45, nº 8, pags. 1919–1930, August 1997.

[Zha01] L. Zhao, A. M. Haimovich, "Capacity of M-ary PPM Ultra-Wideband Communications over AWGN Channels", *Proc. IEEE Vehicular Technology Conference (VTC)*, Vol. 2, pags. 1191–1195, 2001.

[Zha03] J. Zhang, T. D. Abhayapala, R. A. Kennedy, "Performance of Ultra-Wideband Correlator Receiver Using Gaussian Monocycles", *Proc. IEEE International Conference on Communications (ICC)*, Vol. 3, pags. 2192–2196, Anchorage, Alaska (USA), 11-15 May 2003.

[Zha05a] H. Zhang, W. Li, T. A. Gulliver, "Pulse Position Amplitude Modulation for Time-Hopping Multiple-Access UWB Communications", *IEEE Trans. Commun.*, Vol. 53, nº 8, pags. 1269–1273, August 2005.

[Zha05b] Q. T. Zhang, S. H. Song, "UWB Signal Detection Using Eigen-Based Receiver", *Proc. IEEE International Conference on Communications (ICC)*, Vol. 5, pags. 2867–2871, 16-20 May 2005.

[Zio92] R. W. Ziolkowski, "Properties of Electromagnetic Beams Generated by Ultra-Wide Bandwidth Pulse-Driven Arrays", *IEEE Trans. Antennas Propagat.*, Vol. 40, nº 8, pags. 888–905, August 1992.